

Copyright is owned by the Author of the thesis. Permission is given for a copy to be downloaded by an individual for the purpose of research and private study only. The thesis may not be reproduced elsewhere without the permission of the Author.

# **Structuring and Functionalisation of Titania**

A thesis presented in partial fulfillment of the requirements for  
the degree of

Doctor of Philosophy  
in  
Chemistry

at Massey University, Palmerston North, New Zealand.

**Yvonne PeeYee TING**

2008



## ***ABSTRACT***

Grätzel cells are liquid-electrolyte photoelectrochemical cells that contain dye-sensitised titania electrodes. The sensitiser is typically an organic species that absorbs visible light and increases the spectral region in which Grätzel cells may produce electricity. A key feature in the success of Grätzel cells is the high surface area of nanostructured titania electrodes. In this study, the nanostructuring of titania has been explored by two complementary methods: templation and self-assembly.

The templation of silica colloidal crystals (opals) was chosen as an inverse opal of titania would display a porous, bicontinuous structure in addition to a photonic band-gap. A diverse variety of titania inverse opals was produced, ranging from ideal 'honeycomb' to non-ideal 'grape-like' morphologies. However, the fragility of the material and difficulties in reproduction meant that the testing of such electrodes within Grätzel cells was limited.

Study towards the formation of a nanoparticle superlattice of titania via chemically-assisted self-assembly involved the investigation of both nanostructured titania surfaces and dye adsorption. The mode of dye binding to titania and the stability of adsorbed dyes was studied to aid work toward the design of a self-assembled titania superlattice, as well as to assist in the analysis of dye performance in Grätzel cells. Crystalline, aggregated titania and amorphous, dispersible titania was produced for dye binding studies of small organic carboxylic acid dyes. It was found that while dyes are adsorbed and intimately associated with titania, the mode of dye binding is different on a dry electrode than upon dispersed and solvated titania. The dyes appear to be bound to titania in a carboxylate form in the dry state, but in a mode that closer resembles that of the native dye upon dispersed titania.

## ***ACKNOWLEDGEMENTS***

I would like to thank all of the people who have helped me over the past four years and who have helped to make my doctoral experience a wonderful one. A tremendous “Thank you!” to David L. Officer and Mark R. Waterland for their supervision of my studies with great foresight and guidance!

Thanks also to the past and present members of the Nanomaterials Research Center (NRC) and the Institute of Fundamental Sciences at Massey University, all of who have been generous with their professional advice and time.

I would like to give a huge “Cheers!” to my husband David, my parents (Kooi Hong and Song Bong) and sisters (Valeska, Caroline & Edwina) for their support and confidence in my abilities – all without losing the plot! %:)

The support given by the MacDiarmid Institute for Advanced Materials and Nanotechnology in the form of my scholarship is also gratefully acknowledged.

### ***Acknowledgments for technical help:***

**AFM and STM:** Richard Haverkamp, Anita Sharma and Aaron Marshall of the Institute of Technology and Engineering, Massey University for training.

**Dynamic Light Scattering:** Reza Mozafari of the Riddet Centre, Massey University for training.

**Electron Microscopy:** Douglas Hopcroft and Raymond Bennett of the Electron Micrography Suite, Massey University (ex-HortResearch) for collection of SEM images, energy dispersive X-ray analysis and for training on the TEM. David Flynn and Richard Tilley of the Electron Microscopy suite, Victoria University of Wellington for the acquisition of TEM and SEM images. Aaron Hicks of the Institute of Veterinary Animal and Biomedical Sciences, Massey University for training on the techniques of embedding and sectioning samples for TEM.

**Nuclear Magnetic Resonance Spectroscopy:** Patrick Edwards of the Institute of Fundamental Sciences, Massey University for collection of  $^1\text{H}$  spin-echo and diffusion experiments.

**Optical Microscopy:** Elizabeth Nickless of the Institute of Molecular & Biological Sciences, Massey University, for training on the 100x Olympus microscope.

**Profilometer:** Andrea Bubendorfer of the Materials Physics Team, Industrial Research Limited for training and use of the equipment.

**Raman Spectroscopy:** Mark Waterland and Adam Swanson of the Institute of Fundamental Sciences, Massey University for training and help in using the apparatus. Geoff Waterhouse of the University of Auckland for the collection of backscattered resonance Raman spectra of titania films.

**Solar Cell Testing:** Wayne Campbell of the Nanomaterials Research Centre, Massey University for training on how to assemble and test dye-sensitised solar-cells.

**Voltammetry:** Klaudia Wagner of the Nanomaterials Research Centre, Massey University for training.

**X-ray Diffraction:** Gordon Heeley of the School of Physical and Chemical Sciences, Victoria University of Wellington and Robert Stewart of the Soil & Earth Sciences Group, Institute of Natural Resources, Massey University for training and use of the equipment. Tim Kemmit of the Materials Physics Team and Ian Brown of the Ceramics Team, Industrial Research Ltd for collection of grazing incidence XRD data.

**For help with Chemistry and in the General Prevention of Insanity during the course of my doctoral studies:** the past and present members of the NRC!

Amy Ballantyne, Warrick Belcher, Robert Breukers, Shannon Bullock, Wayne Campbell, Loretta Crowe, Beatrice Eccles, Sonja Ensink, Daina Grant, Sanjeev Ghambir, Sun Hao, Fabio Lodato, Donna Royal, Adam Stephenson, Mark Vigniswaran, Pawel & Klaudia Wagner, Amy Watson.



## **TABLE OF CONTENTS**

<i>Structuring and Functionalisation of Titania</i>	<i>i</i>
<i>Abstract</i>	<i>iii</i>
<i>Acknowledgments</i>	<i>iv</i>
<i>Table of Contents</i>	<i>vii</i>
<i>List of Tables, Figures and Equations</i>	<i>xi</i>
<i>Abbreviations</i>	<i>xxii</i>
<i>Definitions and Synonyms</i>	<i>xxiii</i>
<i>Pictorial Tables of Organic Species</i>	<i>xxvi</i>
<b>1. INTRODUCTION</b>	<b>1</b>
1.1. <i>Titania</i>	<i>1</i>
1.2. <i>Applications of Titania</i>	<i>3</i>
1.3. <i>Solar Cells</i>	<i>4</i>
1.3.1. <i>Fully Inorganic Devices</i>	<i>5</i>
1.3.2. <i>Organic Heterojunction Devices</i>	<i>6</i>
1.3.3. <i>The Grätzel Cell</i>	<i>8</i>
1.3.4. <i>Titania for Grätzel Cells</i>	<i>11</i>
1.4. <i>The Nanostructuring of Materials</i>	<i>12</i>
1.4.1. <i>Templated Nanostructures</i>	<i>12</i>
1.4.2. <i>Template-less Nanostructures</i>	<i>14</i>
1.5. <i>The Nanostructuring of Titania</i>	<i>15</i>
1.5.1. <i>Templated Nanostructures of Titania</i>	<i>16</i>
1.5.2. <i>Inverse Opals of Titania</i>	<i>18</i>
1.5.3. <i>Template-less Nanostructures of Titania</i>	<i>19</i>
1.5.4. <i>Self-Assembly of Titania using Small Molecules</i>	<i>21</i>
1.6. <i>Sensitiser Binding to Titania for Grätzel Cells</i>	<i>25</i>
1.6.1. <i>The Binding of Dye to Titania</i>	<i>26</i>
1.7. <i>Opportunities for Novel Research in Nanostructured and Functionalised Titania</i>	<i>29</i>
1.8. <i>Objectives and Hypotheses</i>	<i>30</i>
1.9. <i>References</i>	<i>31</i>

2.	<i>SYNTHESES OF TITANIA, MOLECULES FOR ITS SELF-ASSEMBLY, DYEING AND EXPERIMENTAL TECHNIQUES</i>	43
2.1.	<i>Materials</i>	43
2.2.	<i>Techniques</i>	43
2.3.	<i>Nanostructured Titania: Inverse Opals</i>	48
2.3.1.	<i>Colloid Synthesis</i>	48
2.3.2.	<i>Opal Formation</i>	48
2.3.3.	<i>Inverse Opals of Titania</i>	49
2.4.	<i>Nanostructured Titania for Binding Studies</i>	50
2.4.1.	<i>Thin and Non-porous Titania</i>	50
2.4.2.	<i>Aggregated and Sintered Titania</i>	51
2.4.3.	<i>Dispersible Titania</i>	52
2.5.	<i>Towards the Self-Assembly of Titania using Small Molecules</i>	52
2.5.1.	<i>The Functionalisation of ITO Electrodes</i>	54
2.5.2.	<i>Towards Chemically-Assisted Self-Assembled Titania Arrays</i>	58
2.6.	<i>The Binding of Dye to Titania</i>	58
2.6.1.	<i>UV-Vis Spectroscopy</i>	59
2.6.2.	<i>FTIR Spectroscopy</i>	59
2.6.3.	<i>Raman and Fluorescence Spectroscopy</i>	60
2.6.4.	<i>NMR Spectroscopy</i>	60
2.7.	<i>Solar Cell Testing</i>	61
2.8.	<i>References</i>	64
3.	<i>NANOSTRUCTURED TITANIA: INVERSE OPALS</i>	67
3.1.	<i>Introduction</i>	67
3.2.	<i>Opals</i>	68
3.3.	<i>Inverse Opals</i>	69
3.4.	<i>Opaline Templates of Silica</i>	70
3.5.	<i>Titania Inverse Opals</i>	73
3.6.	<i>Conclusions</i>	85
3.7.	<i>References</i>	87
4.	<i>NANOSTRUCTURED TITANIA FOR BINDING STUDIES</i>	91
4.1.	<i>Introduction</i>	91
4.2.	<i>Thin and Non-porous Titania</i>	92
4.3.	<i>Aggregated and Sintered Titania</i>	95

4.4.	<i>Dispersible Titania</i>	100
4.5.	<i>Conclusions</i>	102
4.6.	<i>References</i>	104
5.	<i>TOWARDS THE SELF-ASSEMBLY OF TITANIA USING SMALL MOLECULES</i>	109
5.1.	<i>Introduction</i>	109
5.2.	<i>Surface Functionalisation and Particle Binding</i>	110
5.3.	<i>The Functionalisation of ITO Electrodes</i>	113
5.4.	<i>The Binding of Amines and Carboxylic Acids to ITO</i>	116
5.5.	<i>The Adsorption of Small Aromatic Molecules</i>	119
5.6.	<i>The Adsorption of Ferrocene Derivatives</i>	125
	5.6.1. <i>UV-Vis Spectroscopy</i>	125
	5.6.2. <i>Voltammetry</i>	130
	5.6.3. <i>Surface Coverage Estimates</i>	139
5.7.	<i>Towards Chemically-Assisted Self-Assembled Titania Arrays</i>	140
5.8.	<i>Conclusions</i>	141
5.9.	<i>References</i>	143
6.	<i>THE BINDING OF DYE TO TITANIA</i>	149
6.1.	<i>Introduction</i>	149
6.2.	<i>Dye Adsorption on Titania for Grätzel Cells</i>	149
	6.2.1. <i>The Binding of Carboxylic Acids to Titania</i>	150
6.3.	<i>Dye Aggregation, Solvent and Concentration Effects</i>	152
6.4.	<i>Carboxylic Acid Probe Dyes</i>	156
6.5.	<i>Spectroscopic Analysis of Adsorbed Dyes &amp; Dye Adsorption</i>	157
	6.5.1. <i>UV-Vis Spectroscopy</i>	163
	6.5.1.1. <i>Dye Loading on Titania</i>	163
	6.5.1.2. <i>Aggregation Studies</i>	166
	6.5.1.2.1. <i>Introduction</i>	166
	6.5.1.2.2. <i>Overview of UV-Vis Signal Shifts</i>	167
	6.5.1.2.3. <i>Probe Dyes on Sol-Gel Titania</i>	168
	6.5.1.2.4. <i>Probe Dyes on Dyesol Titania</i>	169
	6.5.1.2.5. <i>Solvent Effects</i>	171
	6.5.1.2.6. <i>Support for Equilibrium Dye Binding</i>	173
	6.5.1.2.7. <i>Impact of Structure on Dye Aggregation</i>	175
	6.5.1.2.8. <i>Aggregation of Porphyrinic Dyes</i>	184
	6.5.1.2.9. <i>Summary</i>	189

6.5.3.	<i>FTIR Spectroscopy</i>	189
	6.5.3.1. <i>Introduction</i>	189
	6.5.3.2. <i>Computer Modelling and Experimental Results</i>	190
	6.5.3.3. <i>Summary</i>	205
6.5.4.	<i>Raman and Fluorescence Spectroscopy</i>	205
	6.5.4.1. <i>Experimental Results</i>	205
	6.5.4.2. <i>Summary</i>	209
6.5.5.	<i>NMR Spectroscopy</i>	210
	6.5.5.1. <i>Introduction</i>	210
	6.5.5.2. <i>Preliminary Experiments</i>	211
	6.5.5.3. <i>Adsorption of Dye 6.1 on Sol-Gel Titania</i>	218
	6.5.5.4. <i>Summary</i>	228
6.6.	<i>Section Summary</i>	229
6.7.	<i>References</i>	231
7.	<i>CONCLUSIONS</i>	237
7.1.	<i>Overview</i>	237
7.2.	<i>Key Findings</i>	237
7.3.	<i>Discussion</i>	239
7.4.	<i>Future Directions</i>	241
7.5.	<i>References</i>	243
8.	<i>SUPPLEMENTARY DATA</i>	245
8.1.	<i>Chapter 4</i>	245
8.2.	<i>Chapter 6</i>	245

## ***LIST OF TABLES, FIGURES AND EQUATIONS***

### *Section 1.1.*

- Table 1.1. Physical properties of the low-temperature titania polymorphs.  
Figure 1.1. Representations of the crystal unit cells for rutile, anatase and brookite.  
Figure 1.2. Phase diagram for anatase and rutile and two alternative forms of titania. Data from three different sources are plotted.

### *Section 1.2.*

- Equation 1.1. The tilanol and tiloxane equilibrium.

### *Section 1.3.1.*

- Figure 1.3. Schematic of a multi-junction, tandem GaAs/GaInP<sub>2</sub> solar cell, as described by S. K. Deb, 1998.

### *Section 1.3.2.*

- Figure 1.4. Cartoon of a solar cell using MEH-PPV and buckminsterfullerene. The associated energy level diagram is shown, as described by A. Moliton, 2004.

### *Section 1.3.3.*

- Figure 1.5. Chlorophyll a.  
Figure 1.6. Cartoon of a Grätzel cell with the associated energy level diagram for an anatase titania electrode sensitised by dye WMC-299b, 4-(2'-(5',10',15',20'-tetraoxylporphyrinatozinc(II)yl)butadienylmalonic acid, an iodine/triiodide electrolyte and a platinum counter electrode. 'CB' is the conduction band energy of titania, 'I<sub>3</sub><sup>-</sup>/I<sup>-</sup>' is the energy level of the iodide/triiodide couple.

### *Section 1.4.1.*

- Figure 1.7. A cartoon representation of a binary opal composed of large polystyrene spheres and smaller silica spheres (a) and the resulting array of sintered silica spheres (b).

### *Section 1.5.1.*

- Figure 1.8. A representation of the patterning of titania upon gold via the sacrificial organic intermediary of polystyrene.

### *Section 1.5.2.*

- Figure 1.9. A cartoon of a binary opal (a) and the resulting inverse opal (b).

### *Section 1.5.4.*

- Figure 1.10. Potential strategies for forming the first particulate layer of a titania array upon indium-doped tin oxide (ITO). a) A diacid linker binding titania directly to ITO. b) Pre-treatment of ITO with a diamine with binding of acid-functionalised titania via salt-formation. c) Pre-treatment of ITO with an amphiprotic linker and binding of pre-sensitised titania without an intervening salt layer.

Figure 1.11. A schematic of the porphyrin dyad assembly studied by Y.-J Cho *et al.* 2005.

Figure 1.12. A schematic of the ‘quaternary structure’ studied by H. Imahori *et al.* 2004.

### Section 1.6.

Figure 1.13. a) The “green” zinc porphyrin dye, 2-cyano-3-(2’-(5’,10’,15’,20’-tetraphenylporphyrinato zinc(II)yl)acrylic acid. b) The ruthenium “N3” dye, di(thiocyanato)-bis(2,2’-bipyridyl-4,4’-dicarboxylate) ruthenate(II) di-anion. c) The “Black” dye, tri(thiocyanato)-2,2’,2’’-terpyridyl-4,4’,4’’-tricarboxylate ruthenate(II) di-anion.

### Section 1.6.1.

Figure 1.14. Ru(II)LL’CN. L is 4’-phosphonic acid-2,2’:6’2’’-terpyridine and L’ is 1,2-bis(4’-methyl-2,2’-bipyridyl-4-yl)ethane.

### Section 2.5.1.

Figure 2.1. Chem3D<sup>®</sup> representations of 5.4 with estimates of the maximum and minimum rectangular footprint area. For clarity, only one cyclopentadiene ring of the ferrocenyl group is shown.

### Section 2.7.

Figure 2.2. A sample holder containing a DSSC with a green porphyrin dye on a nanocrystalline, mesoporous titania electrode.

### Section 3.1.

Figure 3.1. A schematic of the concept of Bragg diffraction of light from a regular, periodic array.

### Section 3.4.

Figure 3.2. SEM image of a silica opal deposited upon glass. The scale bar is for 1  $\mu\text{m}$ .

Figure 3.3. a) The opal composed of 250 nm silica spheres displays the Bragg diffraction of green light, while the opal made of 350 nm spheres diffracts orange light. b) Detail of silica colloids, with titania nanocrystals. Square and hexagonal close-packing is highlighted. The scale bar is for 100 nm.

Figure 3.4. a) A typical, fractured silica opal. b) The same opal at a higher magnification. The scale bars are for 1  $\mu\text{m}$ .

### Section 3.5.

Figure 3.5. a) An inverse opal that resembles sealed ‘honeycomb’. b) An inverse opal exhibiting a ‘grape’-like morphology. The scale bars are for 100 nm.

Figure 3.6. a) The desired ‘honeycomb’ morphology. Note that windows connect adjacent air-spheres and that the interstices appear to be completely filled. b) Partial, almost ‘skeletal’ inverse opals. The scale bars are for 100 nm.

Figure 3.7. a) Granular and fibrillar titania nanoparticles may be observed on lightly-templated silica colloids, particularly where colloids meet. b)

Titania inverse opal formed by six cycles of infiltration and rinsing, with two treatments with water, then sintered at 500°C. c) An inverse opal displaying a 'coral'-like morphology was displayed, perhaps due to sintering. The sample was treated twice with: three cycles of infiltration and rinsing, a treatment with water and sintering at 500°C. Both samples used 1 : 40 : 0.6 infiltrate and 1 : 120 : 0.6 rinsing solutions. The scale bars are for 100 nm.

- Table 3.1. The typical treatment protocol to form inverse opals of titania.
- Figure 3.8. a) Disordered, fragmented material from a sample that was not treated with water. b) Condensed matter that resulted from two cycles of infiltration and rinsing, without treatment with water. The scale bars are for 1  $\mu$ m.
- Figure 3.9. a) TEM image of a cross-section of a titania inverse opal, illustrating open fractures and a sealed top-face. The scale bar is for 200  $\mu$ m. b) SEM image of sample which was treated with rinsing steps. Colloids at the crack faces were cleanly templated, without excess titania occupying the crevice. The scale bar is for 100 nm.
- Figure 3.10. a) Titania film contracted away from the inverse opal below. This sample had six infiltrations and a treatment with water. The scale bar is for 1  $\mu$ m. b) The 'honeycomb' morphology, which is composed of thin titania shells. This sample was infiltrated five times and treated once with water. The scale bar is for 100 nm.
- Figure 3.11. These samples used an infiltrate with a mole ratio of 1 : 20 : 0.6 and a rinsing solution with 1 : 80 : 0.6 of titanium isopropoxide to dry ethanol to diethanol amine. The scale bar is for 1  $\mu$ m. a) A 'basement' layer of inverse opal that exhibited practically no shrinkage. The opal had two cycles of infiltration, rinsing and treatment with water. b) Significant warpage and shrinkage was observed for this sample that was infiltrated six times and air-dried, before sintering. The scale bar is for 100 nm.
- Figure 3.12. a) Titania-silica composite formed by six cycles of infiltration and rinsing, with two treatments with water, then sintered at 500°C. Mole ratios of 1 : 40 : 0.6 and 1 : 120 : 0.6 for reactants were used for infiltration and rinsing, respectively. The scale bar is for 100 nm. b) The resulting inverse opal displays a 'grape-like' morphology. The scale bar is for 1  $\mu$ m.
- Figure 3.13. a) Inverse opaline titania, with long-range structure. Twelve cycles of infiltration with centrifugation, then rinsing was followed by one treatment with water before sintering at 500°C. Mole ratios of 1 : 40 : 0.6 and 1 : 120 : 0.6 for reactants were used for the infiltration and rinsing solutions, respectively. The scale bar is for 1  $\mu$ m. b) A structure that resembles 'grapes'. Six cycles of infiltration were followed with two treatments with water. Solutions with mole ratios of 1 : 20 : 0.6 for both the infiltrate and rinsing solutions were used. The scale bar is for 100 nm.
- Figure 3.14. The difficulty of obtaining reproducible inverse opals is illustrated. Both of these samples were treated by twelve cycles of infiltration with centrifugation and rinsing. This was followed by one treatment with water before sintering at 500°C. Molar ratios of 1 : 40 : 0.6 and 1 : 120 : 0.6 for reactants were used for the infiltration and rinsing

solutions, respectively. a) The desired ‘honeycomb’ structure is displayed with filled interstices and windows to adjacent air-spheres. Fractures such as these were common. The scale bar is for 1  $\mu\text{m}$ . b) Open-face ‘honeycomb’ material was received, but with extensive cracking and large variation in film thickness. The scale bar is for 10  $\mu\text{m}$ .

#### Section 4.2.

Figure 4.1.

a) A SEM image of flat and dense titania with two coats. b) A contact mode AFM image of thin and non-porous titania formed by two sequential dip-coats into a solution of with a 1 : 40 : 0.6 molar ratio of titanium isopropoxide : dry ethanol : diethanolamine. A 40  $\text{mm min}^{-1}$  dip speed was used to produce a film with a RMS roughness of 10 nm.

Figure 4.2.

Cyclic voltammetry of blank ITO and ITO dip-coated with thin and non-porous titania in a 1 mM hexacyanoferrate solution. Redox activity is suppressed with increasing coats of thin and non-porous titania. Voltage is given with respect to a Ag/AgNO<sub>3</sub> pseudo-reference electrode. The electrolyte was 0.1 M tetrabutylammonium perchlorate in acetonitrile. The scan rate was 100  $\text{mV s}^{-1}$ .

#### Section 4.3.

Figure 4.3.

a) Dyesol opaque titania plate, 12  $\mu\text{m}$  thick. b) Screen-printed Dyesol transparent paste, 4  $\mu\text{m}$  thick. c) Screen-printed Degussa P25, 4  $\mu\text{m}$  thick. d) Spin-thinned sol-gel titania, 1  $\mu\text{m}$  thick.

Figure 4.4.

a) Titania of the Dyesol screen-printing paste for transparent films. b) Degussa P25 hydrophilic fumed titania. c) Sintered sol-gel titania.

#### Section 5.2.

Figure 5.1.

A cartoon of the base unit of the composite material described by R. Frantz *et al.* 2004.

Figure 5.2.

A dye used in the sol-gel preparation of a composite material for testing within Grätzel cells, as described by C. L. Lin *et al.* 2006.

#### Section 5.3.

Figure 5.3.

Di(3-aminopropyl)viologen, as described by K. H. Hyung, 2003.

Figure 5.4.

4,4'-bis(*N*-naph-1-yl-*N*-phenylamine)-1,1'-biphenyl, as described by Q. T. Lee *et al.* 2000.

#### Section 5.4.

Figure 5.5.

a) 1,4-benzenedicarboxylic acid. b) 2,6-naphthalenedicarboxylic acid.

Figure 5.6

The coordination compound of 4-(*trans*-2-(4-pyridinyl)ethenyl)benzoic acid and carbonyl(5',10',15',20'-tetraphenylporphyrinato)ruthenium(II).

Figure 5.7.

In order to receive useful UV-Vis spectra, it is essential to subtract the blank (reference) spectrum of the same piece of ITO glass as used for each adsorption experiment. The spectrum of piece 1, after subtraction of an earlier scan of the same piece of ITO produces the expected, featureless resultant. However, the spectrum of piece 1, after subtraction of a scan of a different piece of ITO creates an artificial result.

### Section 5.5.

- Table 5.1. UV-Vis absorption of aromatic species used in absorption studies.
- Figure 5.8. UV-Vis spectra of ITO glass with drop-dried: 4-nitroaniline, 4-phenylenediamine.
- Figure 5.9. UV-Vis spectra of species adsorbed onto ITO glass from 1 mM solutions in 1,4-dioxane: 4-phenylenediamine, 4-nitroaniline and 4-aminobenzoic acid. Glass absorbs below 300 nm, which produces a marked effect in subtracted spectra.
- Figure 5.10. UV-Vis absorption for fresh 1,4-dioxane and for 1,4-dioxane heated at 80°C for two days.
- Figure 5.11. UV-Vis solution spectra of 4-phenylenediamine kept within 1,4-dioxane, at 80°C. Shown are spectra corresponding to the initial solution and the solution after 21 hours and 4 days.
- Table 5.2. UV-Vis absorbance peaks for polymeric material related to the probe species.

### Section 5.6.1.

- Table 5.3. UV-Vis absorption of solution spectra of ferrocene derivatives.
- Figure 5.12. The effect of solvent on the deposition of 5.3 onto ITO glass: 1,4-dioxane, acetonitrile.
- Figure 5.13. UV-Vis spectra of the imine 5.3 in methanol, drop-dried upon ITO glass and ITO glass treated by immersion from a 2 mM solution in 2,2-dimethoxypropane.
- Figure 5.14. UV-Vis absorption spectra of ITO glass treated with 4-phenylenediamine, then with 5.2 to yield the overgrafted sample.
- Figure 5.15. UV-Vis spectra of 5.4 in solution, drop-dried upon ITO glass and ITO glass treated by immersion from a 2 mM solution.
- Figure 5.16. UV-Vis spectra of ITO glass treated by immersion within a 10 mM solution of 5.4 and a 5 mM solution of 5.1.

### Section 5.6.2.

- Figure 5.17. Cyclic voltammetry of within ITO glass was treated by immersion for an hour within a 2.5 mM solution in a 6% v/v solution of dry ethanol in hexane of either 5.1 or ferrocene. The sample was rinsed in a 5% v/v solution of 1,4-dioxane in hexane prior to voltammetry. The scans were done at 50 mV s<sup>-1</sup> in acetonitrile.
- Figure 5.18. The diffusion or degradation of adsorbed 5.1 off ITO glass over sequential cyclic voltammetry scans. The scans were done at 50 mV s<sup>-1</sup> in acetonitrile.
- Figure 5.19. Voltammetric plots of 5.3 in solution and adsorbed onto ITO glass. The scans were done at 100 mV s<sup>-1</sup> in acetonitrile.
- Figure 5.20. Cyclic voltammetry showing 5.3 deposited onto ITO glass by immersion within a 0.1 mM solution in 1,4-dioxane, at 85°C for three days. The scans were done at 50 mV s<sup>-1</sup> in acetonitrile.
- Figure 5.21. Cyclic voltammetry showing the irreversible oxidation of 5.4 from a 10 mM solution results in a contamination of the electrode, as evidenced by the decreased current. The scans were done at 50 mV s<sup>-1</sup> in acetonitrile.
- Figure 5.22. Cyclic voltammetry scans of a 10 mM solution of 5.4. The half-wave potential for the reversible ferrocene/ferrocenium redox couple is

- 0.196 V<sub>SCE</sub>. The scans were done at 50 mV s<sup>-1</sup> in acetonitrile.
- Figure 5.23. Cyclic voltammetry of 5.4 adsorbed upon ITO glass by immersion within a 2.3 mM solution, using 6% v/v 1,4-dioxane in hexane as the solvent. The scans were done at 50 mV s<sup>-1</sup> in acetonitrile.
- Figure 5.24. a) An ethenylferrocene and b) an ethynylferrocene, where ‘Ar’ represents aryl functionality, as described by L. Cuffe *et al.* 2005.
- Figure 5.25. 2-ferrocenylmethylideneimino-5-methyl-benzoic acid (a) and 2-ferrocenylmethylamino-5-methylbenzoic acid (b), as described by J. Cano *et al.* 1995.

### Section 5.6.3.

- Figure 5.26. a) Bare ITO glass cleaned by washing with detergent, then ultrasonication within acetone, water, then ethanol. b) ITO glass treated with 4-aminobenzoic acid and Degussa P25 titania. A central area was swept clear of titania nanoparticles by the force of contact mode AFM.

### Section 6.2.1.

- Figure 6.1. Plausible binding modes of an adsorbate via carboxylic acid functionality to titania. Monodentate forms: a) pseudo-ester; b) carboxylate; c) bridging carboxylate. Bidentate forms: d) chelating; e) bridging; f) chelating and bridging.

### Section 6.3.

- Figure 6.2. A cartoon of a) H-aggregation and b) J-aggregation of di(thienylenevinylene)thiophene.
- Figure 6.3. The origin of blue and red shifts in absorption on the formation of H- and J-aggregates as described by Mishra *et al.* 2000. The interaction between the electronic transition dipole moments of associated molecules results in additional excited states. Only one of the excited states is permitted, which for H-aggregates is that of higher energy and for J-aggregates is of lower energy.
- Figure 6.4. Coumarin dyes as described by Z. S. Wang *et al.* 2005. a) Cyano(5,5-dimethyl-3-[2-(1,1,6,6-tetramethyl-10-oxo-2,3,5,6-tetrahydro-1*H*,4*H*,10*H*-11-oxa-3*a*-aza-benzo[de]anthracen-9-yl)vinyl]cyclohex-2-enylidene)acetic acid which bears a side ring on the alkene chain, which prevents aggregation. b) The analogous material, which is without a side ring and forms H-aggregates.
- Figure 6.5. Hemin, the Fe<sup>3+</sup> analogue of heme.
- Figure 6.6. Glutamic acid as described by A. D. Roddick-Lanzilotta *et al.* 2000. Glutamic acid bound to titania by a) a single acid group and b) both acid functionalities.

### Section 6.4.

- Table 6.1. Spectral properties of carboxylic acid probe dyes.

### Section 6.5

- Figure 6.7. Chem3D<sup>®</sup> representations of 6.1 to 6.6 with estimates of the rectangular footprint area for dyes bound by only one carboxylic group.

- Figure 6.8. Chem3D<sup>®</sup> representations of 6.1 to 6.6 with estimates of the rectangular footprint area for bound dye with potential binding groups towards the surface.
- Table 6.2. Surface area of titania from nitrogen sorption data, unless otherwise stated.
- Table 6.3. Range of the rectangular footprint areas of probe dyes (Figs 6.7, 6.8) and monolayer coverage values for dye upon sintered transparent Dyesol titania and native sol-gel titania.

Section 6.5.1.1.

- Figure 6.9. UV-Vis absorbance over time for the 410 nm peak of 6.3 adsorbed onto sintered Dyesol titania plates from a 2 mM solution in tetrahydrofuran. The x-axis error bars are for  $\pm 1$  minute, the y-axis error bars are for  $\pm 0.001$  absorbance units.
- Figure 6.10. Adsorption of 6.2 onto sintered Dyesol titania powder from a 2.3 mM methanolic solution and desorption in dry methanol. Data was collected for the UV-Vis maximum at 330 nm, the error bars are for conservative values of a  $\pm 10\%$  uncertainty for the calculated number of moles of 6.2 and  $\pm 2$  minutes of time. Similar data was obtained for 6.1.

Section 6.5.1.2.

- Table 6.4. FWHM values for UV-Vis absorption signals of the probe dyes in tetrahydrofuran (THF) and on both dispersed sol-gel and sintered Dyesol titania.
- Table 6.5. UV-Vis absorption of pure dyes in THF and on both dispersed sol-gel and sintered Dyesol titania.
- Figure 6.11. UV-Vis spectra of a 1 : 1 and a 2 : 1 molar ratio of tetra-*n*-butylammonium hydroxide to 6.1 in methanol.
- Table 6.6. UV-Vis absorption of pure dyes and dyed titania in solvent A.
- Figure 6.12. UV-Vis spectra of 6.5 in tetrahydrofuran in a 1 : 5 v/v solution of tetrahydrofuran to 95% ethanol and adsorbed onto sintered titania plates.
- Figure 6.13. A red shift of UV-Vis absorbance is observed when a titania plate dyed with 6.5 is wet with tetrahydrofuran is dried. The effect is reproducible as shown by further immersion of the plate in a solution of 6.5 and subsequent drying. The spectra are not subtracted for the titania blank in order to show that the wet plate is more transparent than the dry plate.
- Figure 6.14. UV-Vis spectra of 6.4 in methanol, tetrahydrofuran, in a 1 : 5 v/v solution of tetrahydrofuran to 95% ethanol (solvent A) and with sol-gel titania in methanol, tetrahydrofuran and solvent A.
- Equation 6.1. Equilibrium dye binding involving free and bound dye, only.
- Equation 6.2. Equilibrium dye binding involving the available binding sites of titania and both free and bound dye.
- Figure 6.15. UV-Vis spectra of 6.4, showing an absence of signal shoulders on titration with sol-gel titania in ethanol. Pure dye, a 339 : 1, a 21 : 1, and a 1 : 1 mole ratio of dye to titania. The FWHM values are 99 nm, 109 nm, 114 nm and 113 nm, respectively, with an uncertainty of 3%.
- Figure 6.16. UV-Vis spectra of 6.1 in tetrahydrofuran, in acidic solution, in

- solution with acidic-sol-gel titania. The mole ratio of sol-gel titania spheres 2 nm in diameter to dye was 1 : 5.
- Figure 6.17. UV-Vis spectra of 6.2 in tetrahydrofuran, in acidic solution, in solution with acidic-sol-gel titania. The mole ratio of sol-gel titania spheres 2 nm in diameter to dye was 1 : 4.
- Figure 6.18. UV-Vis spectra of 6.3 in tetrahydrofuran, in acidic solution, in solution with acidic-sol-gel titania and adsorbed onto sintered titania plates. The mole ratio of sol-gel titania spheres 2 nm in diameter to dye was 4 : 1.
- Figure 6.19. UV-Vis spectra of 6.4 in tetrahydrofuran, in acidic solution, in solution with acidic-sol-gel titania and adsorbed on sintered titania plates. The mole ratio of sol-gel titania spheres 2 nm in diameter to dye was 4 : 1.
- Figure 6.20. UV-Vis spectra of terthienylcyanoacrylic acid in tetrahydrofuran, in acidic solution, in solution with acidic-sol-gel titania and adsorbed on sintered titania plates. n(sol-gel titania spheres 2 nm in diameter) : n(dye) of 3 : 1.
- Figure 6.21. UV-Vis spectra of terthienylvinylemalonic acid in tetrahydrofuran, in acidic solution, in solution with acidic-sol-gel titania and adsorbed on sintered titania plates. n(sol-gel titania 2 nm in diameter) : n(dye) of 3 : 1.
- Figure 6.22. A cartoon of possible aggregation and packing of a) 6.4 and b) 6.3 upon titania.
- Figure 6.23. A depiction of the packing of a malonic acid with the binding groups a) parallel and b) staggered with respect to each other. The carbon atom labelled 'R' denotes the rest of the molecule.
- Figure 6.24. UV-Vis spectra of 6.6 in tetrahydrofuran (507 nm), in acidic solution (514 nm), in solution with acidic-sol-gel titania (522 nm) and adsorbed onto sintered titania plates (510 nm). The mole ratio of sol-gel titania spheres 2 nm in diameter to dye was 4 : 1.
- Figure 6.25. UV-Vis spectra of 6.5 in tetrahydrofuran, in acidic solution, in solution with acidic-sol-gel titania and adsorbed onto sintered titania plates. The mole ratio of sol-gel titania spheres 2 nm in diameter to dye was 4 : 1.
- Figure 6.26. An extreme conformation of 6.6, where the ter(thienylenevinylene) group lies parallel to the surface.
- Table 6.7. Porphyrin-based dyes used in dye aggregation studies.
- Figure 6.27. UV-Vis spectra of sintered Dyesol titania dyed with 6.7 from a 0.2 mM solution in tetrahydrofuran. The dye absorbance increases with progressive immersion times of 2 min, 4 min, 12 min and 99 min.
- Figure 6.28. UV-Vis spectra of sintered Dyesol titania dyed with 6.9 from a 0.2 mM solution in tetrahydrofuran. The dye absorbance increases with progressive immersion times of 2 min, 4 min, 8 min and 50 min.
- Figure 6.29. UV-Vis spectra of sintered Dyesol titania dyed with 6.11 from a 0.2 mM solution in tetrahydrofuran. The dye absorbance increases with progressive immersion times of 2 min, 4 min, 10 min and 60 min.
- Figure 6.30. UV-Vis spectra of sintered Dyesol titania dyed with 6.8 from a 0.2 mM solution in tetrahydrofuran. The dye absorbance increases with progressive immersion times of 2 min, 4 min, 13 min and 90 min.
- Figure 6.31. UV-Vis spectra of sintered Dyesol titania dyed with 6.10 from a 0.2

mM solution in tetrahydrofuran. The dye absorbance increases with progressive immersion times of 2 min, 4 min, 12 min and 99 min.

### Section 6.5.3.

- Figure 6.32. ATR-FTIR spectra of native sol-gel titania and a sintered Dyesol titania plate. The fine structure in the spectra at 3700 and 1606  $\text{cm}^{-1}$  are due to residual water.
- Figure 6.33. Illustration of the two configurations (a) and (b) of 6.2 that were modelled for *ab initio* calculations.
- Figure 6.34. Calculated vibrational data for configuration (a) of 6.2.
- Figure 6.35. Calculated vibrational data for configuration (b) of 6.2.
- Figure 6.36. Calculated vibrational data for configuration (c) of 6.2.
- Figure 6.37. Calculated FTIR spectra for configuration (a) of 6.2 *in vacuo*.
- Figure 6.38. Calculated FTIR spectra for configuration (b) of 6.2 *in vacuo*.
- Figure 6.39. Calculated FTIR spectra for configuration (c) of 6.2 *in vacuo*.
- Figure 6.40. Experimental ATR-FTIR data for pure 6.1.
- Figure 6.41. Experimental ATR-FTIR data for pure 6.2.
- Figure 6.42. The minimised conformation of the doubly-deprotonated forms (a) to (c) of 6.2.
- Figure 6.43. Calculated vibrational data for the doubly-deprotonated form of 6.2.
- Figure 6.44. Calculated FTIR spectra of the doubly-deprotonated form of 6.2 *in vacuo*.
- Figure 6.45. ATR-FTIR spectra of pure 6.1 and the acid adsorbed onto native sol-gel titania in a 29 : 1 mole ratio of dye to 2 nm titania particles.
- Figure 6.46. An expansion of Figure 6.43, of pure 6.1 and the acid adsorbed onto native sol-gel titania in a 29 : 1 mole ratio of dye to 2 nm titania particles.
- Figure 6.47. Experimental ATR-FTIR data for pure 6.2 and the dye adsorbed onto sol-gel titania in a 15 : 1 mole ratio of dye to 2 nm titania particles.
- Figure 6.48. ATR-FTIR spectrum of pure 6.3 and upon sol-gel titania in an 18 : 1 mole ratio of dye to titania 2 nm in diameter.
- Figure 6.49. ATR-FTIR spectra of pure 6.4 and the acid bound to sol-gel titania in an 18 : 1 and in a 21 : 1 mole ratio of dye to titania 2 nm in diameter.

### Section 6.5.4.

- Figure 6.50. Fluorescence of 6.4 in methanol and with a calculated mole ratio of dye to titania 2 nm in diameter of 39 : 1, 20 : 1, 10 : 1 and 1 : 1. The excitation wavelength was 455 nm.
- Figure 6.51. Fluorescence maximum of 6.4 in methanol versus the mole ratio of dye to titania particles 2 nm in diameter. The fluorescence maximum of pure 6.4 is 592 nm. The excitation wavelength was 455 nm. The error bars are for an uncertainty of  $\pm 0.5$  nm of the fluorescence signal and approximately  $\pm 7\%$  for the mole ratio of dye to 2 nm diameter titania.
- Figure 6.52. Raman spectra of a methanolic solution with a 12 : 1, a 6 : 1, a 4 : 1 and a 1 : 3 mole ratio of acidic, amorphous 2 nm sol-gel titania to dye 6.4. The non-linear background has not been subtracted.

### Section 6.5.5.2.

- Figure 6.53.  $^1\text{H-NMR}$  spectrum of 6.1 in  $\text{CD}_3\text{OD}$ .

- Figure 6.54.  $^1\text{H-NMR}$  spectrum of 6.2 in  $\text{CD}_3\text{OD}$ .  
 Figure 6.55.  $^1\text{H-NMR}$  spectrum of 6.4 in  $\text{CD}_3\text{OD}$ .  
 Figure 6.56.  $^1\text{H-NMR}$  spectrum of the tetramethylammonium salt of 6.1 in  $\text{CD}_3\text{OD}$ . Pure 6.1, a 1 : 1 mole ratio and a 2 : 1 mole ratio of 6.1 to tetramethylammonium hydroxide.  
 Figure 6.57.  $^1\text{H-NMR}$  spectra of a 12 M solution of 6.2 in  $\text{CD}_3\text{OD}$ , titrated with hydrochloric acid. A mole ratio of dye to hydrochloric acid of 1 : 0, 1 : 45, 1 : 89 and 1 : 116.  
 Figure 6.58.  $^1\text{H-NMR}$  spectra of 6.3 in  $\text{CD}_3\text{OD}$ , with a mole ratio of dye to hydrochloric acid of 1 : 124 and with a mole ratio of dye to titania particles 2 nm in diameter of 19 : 1.

### Section 6.5.5.3.

- Figure 6.59. A cartoon of the solvent partition method. a) Sol-gel titania solvated in  $\text{D}_2\text{O}$  is added to a saturated solution of dye in  $\text{CDCl}_3$ . b) Dye diffuses through the solvent-solvent interface and binds to titania in the  $\text{D}_2\text{O}$  layer. c) The  $\text{D}_2\text{O}$  layer was removed by pipette for analysis by NMR spectroscopy.  
 Figure 6.60.  $^1\text{H-NMR}$  spectra of the titration of 6.1 with acidic, amorphous, sol-gel titania in  $\text{CD}_3\text{OD}$ . An 8 : 1, 12 : 1 and a 17 : 1 mole ratio of 6.1 to titania particles 2 nm in diameter.  
 Figure 6.61.  $^1\text{H-NMR}$  spectrum of the methanol-soluble portion of a titania resuspension experiment. The mole ratio of 6.1 to 2 nm titania particles was 18 : 1. A crude indication of the position of sharp overlaid signals due to free dye.  
 Figure 6.62.  $^1\text{H-NMR}$  spectrum of a 2 mM solution of 6.1 in  $\text{D}_2\text{O-DSS}$ .  
 Figure 6.63. Representations of: (a) the *cis*- and (b) the *trans*- mono-salt forms and (c) the di-salt of 6.1.  
 Figure 6.64.  $^1\text{H-NMR}$  spectrum of a saturated solution of 6.1 in  $\text{D}_2\text{O}$ .  
 Figure 6.65.  $^1\text{H-NMR}$  spectrum of an initial 12 : 1 mole ratio of 6.1 to 2 nm titania particles in  $\text{D}_2\text{O-DSS}$ .  
 Figure 6.66.  $^1\text{H-NMR}$  spectrum of the  $\text{D}_2\text{O}$  layer of a partition experiment that used an initial 17 : 1 mole ratio of 6.1 to 2 nm titania particles.  
 Figure 6.67.  $^1\text{H-NMR}$  spectra of the  $\text{D}_2\text{O}$  layer of a solvent partition experiment which used an initial 12 : 1 mole ratio of 6.1 to 2 nm titania particles. A 3x and a 10x dilution in  $\text{CD}_3\text{OD}$ .  
 Equation 6.3. The Einstein-Stokes equation, using methanol at 298K.

### Section 8.1.

- Table 8.1. Analysis of the  $\text{TiO}_2$ , water, solvent and acid content of sol-gel titania.

### Section 8.2.

- Table 8.2. Experimental extinction coefficients of probe dyes in tetrahydrofuran.  
 Table 8.3. Theoretical ratios of dye to titania, using estimated surface area for non-sintered native sol-gel titania 2 nm in diameter, with a surface area of  $12.57 \text{ nm}^2$  per particle and a molar mass of  $10847 \text{ g mol}^{-1}$ .  
 Table 8.4. Theoretical ratios of dye to titania, using estimated surface area for non-sintered native sol-gel titania 3 nm in diameter, with a surface area of  $28.27 \text{ nm}^2$  per particle and a molar mass of  $36607 \text{ g mol}^{-1}$ .

- Table 8.5. Theoretical ratios of dye to titania, using estimated surface area for non-sintered native sol-gel titania 4 nm in diameter, with a surface area of 50.27 nm<sup>2</sup> per particle and a molar mass of 86771 g mol<sup>-1</sup>.
- Table 8.6. The amount of dye required for monolayer coverage of sintered Dyesol titania, using the footprint areas shown in Table 8.3.
- Table 8.7. The amount of dye required for monolayer coverage of sintered sol-gel titania, using the footprint areas shown in Table 8.3.
- Table 8.8. If the surface area of sintered 'native' sol-gel titania is 187 m<sup>2</sup> g<sup>-1</sup>, if the footprint area of 6.1 is 4.5 x 10<sup>-19</sup>, a monolayer dye loading is 6.9 x 10<sup>-4</sup> mol g<sup>-1</sup>. Supposing that the sintered material was still composed of discrete spheres, then the mole ratio between dye and titania spheres is given by n(dye) : n(TiO<sub>2</sub>). The percentage dye loading of sintered titania over that of native sol-gel titania gives an indication of the degree of particle aggregation introduced by sintering.
- Table 8.9. UV-Vis absorption of dyes on sintered titania.
- Figure 8.1. The integrated area of the UV-Vis absorption of sintered Dyesol titania dyed with 6.5. The red shift in dye absorbance is due to rearrangement of dye on titania due to the loss of solvent, rather than to a decrease in the amount of dye present. The integrated region was 390 to 700 nm. Data is shown for samples immersed in a 0.2 mM solution of 6.5 in tetrahydrofuran for: a) 3 minutes, wet and dried; b) 6 minutes, wet and dried.
- Figure 8.2. The fluorescence intensity of 6.4, in methanol, normalised to absorbance. Two sets of data are displayed. The error bars are for conservative uncertainties of ± 50 counts of intensity and ± 10% of concentration.

## ***ABBREVIATIONS***

AFM	Atomic force microscopy, a type of scanning probe microscopy.
AM 1.5	Air mass 1.5. 'One Sun'. Equivalent to $100 \text{ mW cm}^{-2}$ , the intensity of solar light when the sun is $48.2^\circ$ from zenith. <sup>1-3</sup>
ATR-FTIR	Attenuated total internal reflectance Fourier transform infra-red spectroscopy.
CVD	Chemical vapour deposition.
DSSC	Dye-sensitised solar cell; Grätzel cell..
ITO	Indium-doped tin oxide. Commonly used to coat glass for a conductive surface.
SEM	Scanning electron microscopy.
SPM	Scanning probe microscopy.
STM	Scanning tunnelling microscopy, which is a type of scanning probe microscopy.
TEM	Transmission electron microscopy.
UV-Vis	Ultra-violet and visible light.
XRD	X-ray diffraction

## ***DEFINITIONS AND SYNONYMS***

### *Aqua Regia*

1 : 3 v/v concentrated (fuming) nitric acid to concentrated (1.18 g mL<sup>-1</sup>) hydrochloric acid. If the solution is to be stored, include 1 volume of water.<sup>4</sup>

### *Bohr radius*

The Bohr radius is unique for each substance and is the distance between the electron and hole of a Mott-Wannier pair, or ‘exciton’.

### *Dyesol Limited*

Previously known as Sustainable Technologies Australia (STA), then as Sustainable Technologies International Pty Ltd (STI).

### *External Quantum Efficiency (EQE)*

Of a solar cell: also known as the incident photon conversion efficiency, which is the number of electrons generated per incident photon.<sup>5</sup>  $EQE = n_e/n_{h\nu} = (I_{sc} \cdot hc)/(P_o \cdot \lambda_e)$

### *Fill-Factor (ff)*

Of a solar cell: the maximum electrical power generated divided by the product of the short-circuit current and the open circuit voltage. The maximum power generated is the product of the short circuit current (maximum) and the open circuit voltage (maximum).

$$ff = (I_{max} \cdot V_{max}) / (I_{sc} \cdot V_{oc})$$

### *Global conversion efficiency ( $\eta_{global}$ )*

Of a solar cell: the maximum electrical power generated divided by the intensity of the incident light.  $\eta_{global} = (I_{max} \cdot V_{max}) / I_s$

### *Grätzel Cell*

A liquid heterojunction DSSC which employs a mesoporous and nanocrystalline titania electrode that has been sensitised to absorb visible light.

### *Inverse Opal*

Inverse colloidal crystal, reverse-contrast colloidal crystal, air-sphere colloidal crystal.

### *Macrostructure*

A structure with dimensions larger than 100 nm.

### *Nanocrystalline*

A material that is crystalline with dimensions on the order of nanometres. The term is often used in reference to particulate material which may be composed of smaller particles.

### *Nanoparticles*

Particles with a size on the order of nanometres.

### *Nanostructure*

The structuring of materials such that at least one dimension that is less than a hundred nanometres wide.

### *Opal*

A colloidal crystal. Specifically, opal refers to a colloidal crystal of silica.

### *Polydispersity Index*

Equals the weight-average molecular weight divided by the number-average molecular weight. The number-average is never greater than the weight-average and the larger the index, the wider is the distribution.

### *Power Conversion Efficiency ( $\eta_{eff}$ )*

Of solar cells: the maximum electrical power generated divided by the incident optical power.  $\eta_{eff} = (I_{max} \cdot V_{max})/P_o$

### *Polyelectrolyte*

A polymer in which the degree of ionisation is dependent on the pH of the environment.<sup>6</sup>

### *Piranha Solution*

Either a 2 : 1 v/v, a 3 : 1 v/v or a 4 : 1 solution of concentrated (96%) sulfuric acid to 30% aqueous hydrogen peroxide.<sup>7-9</sup>

### *Quantum dot*

A material that is quantum-confined in three-dimensions.

### *Relative Centrifugal Force (rcf)*

Calculated from the rotations per minute (rpm) and the swing radius of the centrifuge. The units of measure are 'g', for gravitational acceleration.

### *Root Mean Square (RMS)*

Quadratic mean.  $RMS = ((\sum x_i)^2/n)^{1/2}$

### *Screen-printing*

Equivalent to tape-casting of material by pressing material through a mesh screen. The paste viscosity, mesh size, thread thickness and the tension of the screen determine the film thickness.

### *Sol; Sol-gel*

A suspension of tiny particles, which may be stabilised; a gel formed of a sol.

### *Superlattice*

An arrangement of material which recalls the ordering found within ionic lattices.

### *Tape-casting*

Doctor-blading, where a film is cast onto a substrate by application of a blade along guide rails or a mask. The paste viscosity and the height of the mask or guide determines the film thickness.

### $V_{Ag/Ag^+}$

Potential with respect to a pseudo-reference electrode of silver/silver ion.

$V_{SCE}$

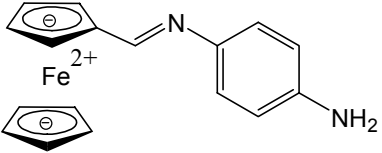
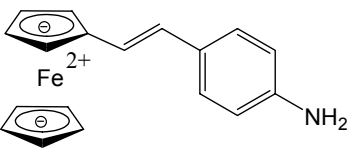
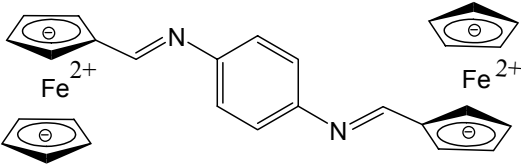
Potential with respect to a standard calomel electrode.

### **References**

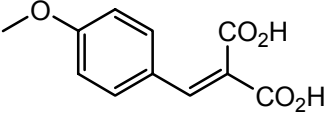
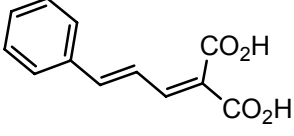
1. Green, M A; Emery, K; King, D L; Igari, S; Warta, W. Solar Cell Efficiency Tables (Version 24). *Progress in Photovoltaics: Research and Applications* **2004**, 12, 365-372.
2. Sun, S-S; Sariciftci, N S. *Organic Photovoltaics. Mechanisms, Materials and Devices*. Taylor & Francis Group, Florida, USA: **2005**.
3. Grätzel, M. Mesoscopic Solar Cells for Electricity and Hydrogen Production from Sunlight. *Chemistry Letters* **2005**, 34, 8-13.
4. Weast, R C; Lide, D R; Astle, M J; Beyer, W H. *CRC Handbook of Chemistry and Physics*. 70<sup>th</sup> ed, CRC Press Inc.: Boca Raton, Florida, **1989**.
5. Sun, S-S; Sariciftci, N S. *Organic Photovoltaics: Mechanisms, Materials and Devices*. Taylor & Francis Group: Florida, USA, **2005**.
6. Yap, H P; Quinn, J F; Ng, S M; Cho, J; Caruso, F. Colloid Surface Engineering via Deposition of Multilayered Thin Films from Polyelectrolyte Blend Solutions. *Langmuir* **2005**, 21, 4328-4333.
7. Wang, M; Leichti, K M; Wang, Q; White, J M. Self-Assembled Silane Monolayers: Fabrication with Monoscale Uniformity. *Langmuir* **2005**, 21, 1848-1857.
8. Bocking, T; Salomon, A; Cahen, D; Gooding, J J. Thiol-Terminated Monolayers on Oxide-Free Si: Assembly of Semiconductor-Alkyl-S-Metal Junctions. *Langmuir* **2007**, 23, 3236-3241.
9. Armstrong, N R; Carter, C; Donley, C; Simmonds, A; Lee, P; Brumbach, M; Kippelen, B; Domercq, B; Yoo, S. Interface Modification of ITO Thin Films: Organic Photovoltaic Cells. *Thin Solid Films* **2003**, 445, 342-352.

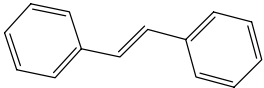
**PICTORIAL TABLES OF ORGANIC SPECIES**

***Ferrocenyl compounds for the functionalisation of ITO***

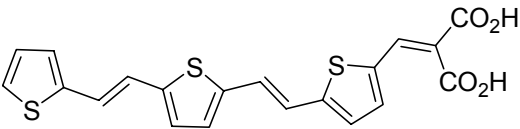
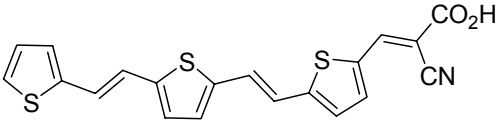
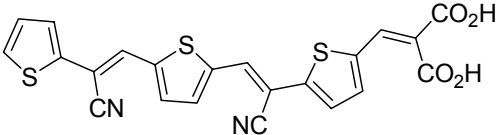
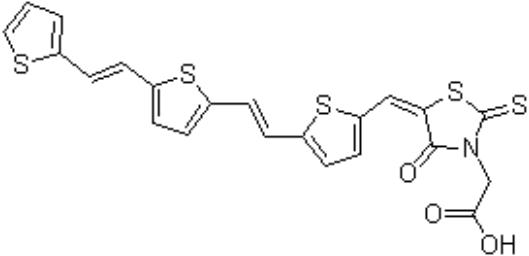
	<p><b>Compound 5.3</b>  <i>N</i>-(ferrocenylmethylidene)-4-phenylenediamine  <i>N</i>-(ferrocenylmethylidene)-<i>p</i>-phenylenediamine</p> <p>Mono-Schiff Base. 304 g mol<sup>-1</sup>.  <i>Synthesised by Ms. Yvonne Ting</i></p>
	<p><b>Compound 5.4</b>            2-(4-aminophenyl)ethenylferrocene            2-(<i>p</i>-aminophenyl)ethenylferrocene</p> <p>RJD-99-3. 303 g mol<sup>-1</sup>.  <i>Synthesised by Mr. Ross Davidson.</i></p>
	<p><i>N,N'</i>-di(ferrocenylmethylidene)-4-phenylenediamine  <i>N,N'</i>-di(ferrocenylmethylidene)-<i>p</i>-phenylenediamine</p> <p>Di-Schiff Base. 500 g mol<sup>-1</sup>.  <i>Synthesised by Ms. Yvonne Ting.</i></p>

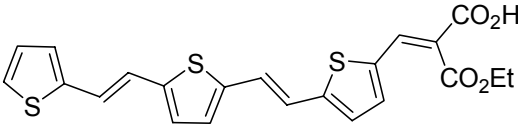
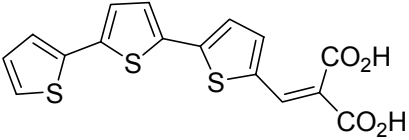
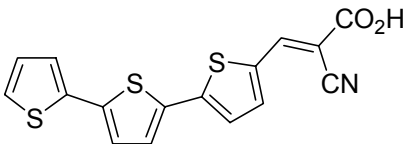
***Small organic dyes for binding to titania***

	<p><b>Compound 6.1</b>            4-methoxybenzylidenemalonic acid            4-methoxyphenylmethylene propanedioic acid  <i>p</i>-methoxybenzylidene malonic acid  <i>p</i>-methoxybenzal malonic acid</p> <p>060720. 222 g mol<sup>-1</sup>.  <i>Synthesised by Ms. Yvonne Ting.</i></p>
	<p><b>Compound 6.2</b>            Cinnamylidenemalonic acid.            (3-phenyl-2-propenylidene)-propanedioic acid            3-phenyl-2-propenylidene propanedioic acid</p> <p>AWIS-126. 218 g mol<sup>-1</sup>.  <i>Synthesised by Mr. Adam Stephenson.</i></p>

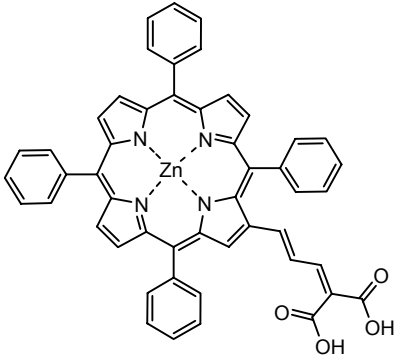
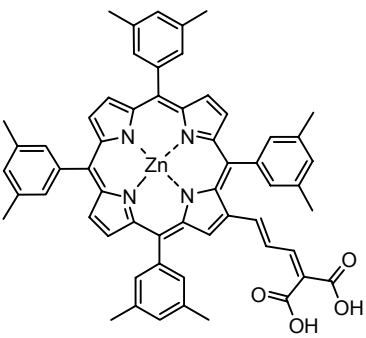
	<p><i>Trans</i>-stilbene. <i>Trans</i>-1,2-diphenyl-1-ethene</p> <p>180 g mol<sup>-1</sup>.</p>
---	---

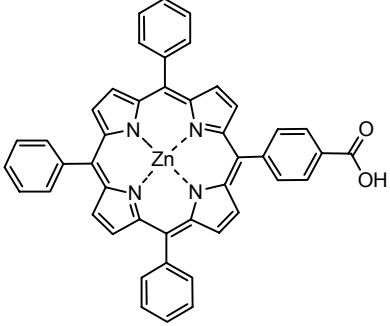
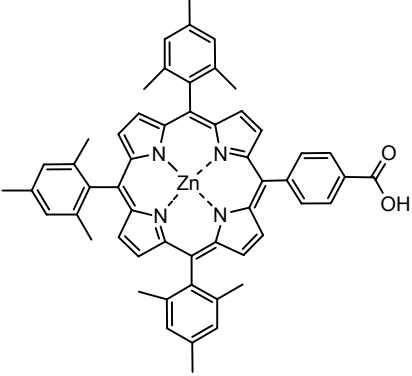
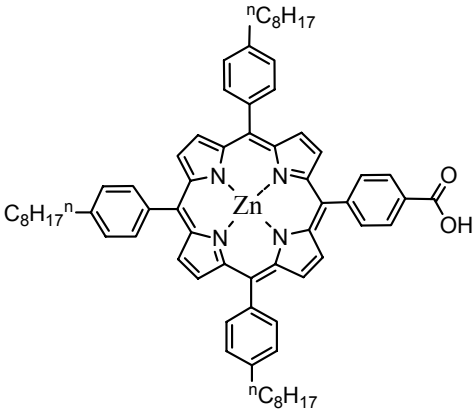
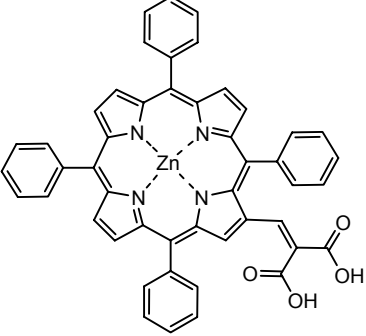
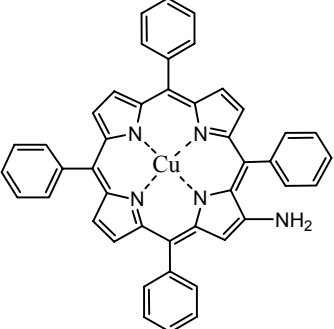
***Ter(thienylenevinylene) and ter(thienylvinylene) dyes for binding to titania***

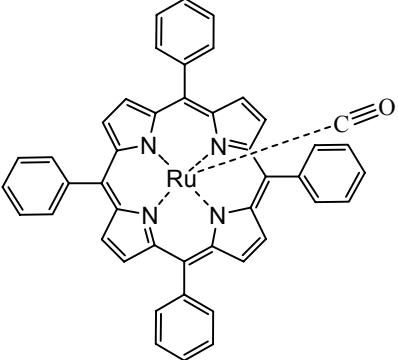
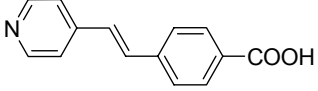
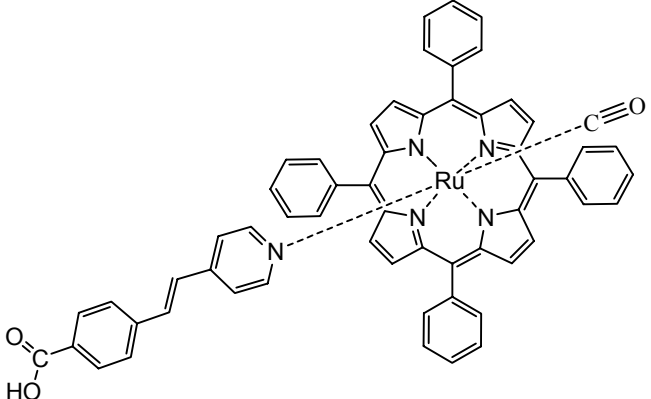
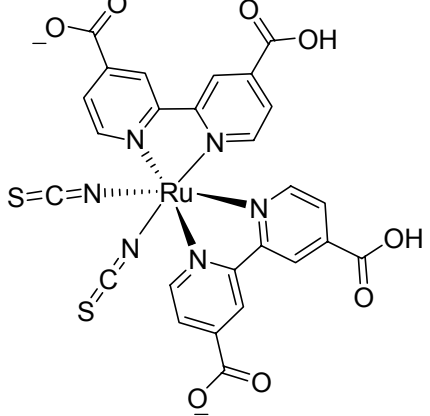
	<p><b>Compound 6.3</b>  Ter(thienylenevinylene)malonic acid  Ter(thiophene-2,5-diyl)vinylene malonic acid  (<i>E,E</i>)-(2-(5-(2-(5-(2-(2-thienyl)vinyl)-2-thienyl)vinyl)thiophenevinyl)malonic acid  5-((5-(2-thien-2-ylethenyl)thien-2-ylethenyl)thien-2-yl malonic acid</p> <p>E-491. 414.5 g mol<sup>-1</sup>.  Synthesised by Dr. Pawel Wagner.</p>
	<p><b>Compound 6.4</b>  Ter(thienylenevinylene)cianoacetic acid  2-cyano-3[2,2',5',2'']terthiophen-5-yl acrylic acid  5-((5-(2-thien-2-ylethenyl)thien-2-ylethenyl)thien-2-yl cyanoacetic acid</p> <p>E-490. 395.5 g mol<sup>-1</sup>.  Synthesised by Dr. Pawel Wagner.</p>
	<p><b>Compound 6.5</b>  8,15-dicyanoter(thienylenevinylene)-malonic acid  2-(5-(1-cyano-2-(5-(2(thiophen-2-yl)ethenyl)thiophen-2-yl)ethenyl)-thiophen-2-ylmethylene)malonic acid</p> <p>E-513. 464.5 g mol<sup>-1</sup>.  Synthesised by Dr. Pawel Wagner.</p>
	<p><b>Compound 6.6</b>  Ter(thienylenevinylene)rhodanine acetic acid</p> <p>EM-59. 503 g mol<sup>-1</sup>.  Synthesised by Dr. Pawel Wagner.</p>

	<p>Ter(thiénylenevinylene)malonate monoethyl ester</p> <p>EM-50. 442.5 g mol<sup>-1</sup>. Synthesised by Dr. Pawel Wagner.</p>
	<p>Terthiénylvinylene malonic acid 3-((2,2':5',2'')terthiophen-5-yl)malonic acid</p> <p>SG-72/5. 362.4 g mol<sup>-1</sup>. Synthesised by Dr. Sanjeev Ghambir.</p>
	<p>Terthiénylcynoacrylic acid 2-cyano-3-((2,2':5',2'')terthiophen-5-yl)acrylic acid</p> <p>SG-74/5. 343.4 g mol<sup>-1</sup>. Synthesised by Dr. Sanjeev Ghambir.</p>

***Porphyrin dyes and coordination compounds for binding to titania***

	<p>Compound <b>6.7</b> 4-(2'-(5',10',15',20'- tetraphenylporphyrinato zinc(II)yl)butadienylmalonic acid 4-(2'-(5',10',15',20'- tetraphenylporphyrinato zinc(II)yl)allylidene malonic acid</p> <p>WMC-236. Zn-2a. 818.2 g mol<sup>-1</sup>. Synthesised by Dr. Wayne Campbell.</p>
	<p>Compound <b>6.8</b> 4-(2'-(5',10',15',20'- tetraxylylporphyrinato zinc(II)yl)butadienylmalonic acid 4-(2'-(5',10',15',20'- tetraxylylporphyrinato zinc(II)yl)allylidene malonic acid</p> <p>WMC-299B. Zn-2g. 930.4 g mol<sup>-1</sup>. Synthesised by Dr. Wayne Campbell.</p>

	<p><b>Compound 6.9</b>  (5'-(10',15',20'-  triphenylporphyrinato zinc(II))-4-  benzoic acid</p> <p>EM-95. 722.12 g mol<sup>-1</sup>.  Synthesised by Dr. Pawel Wagner.</p>
	<p><b>Compound 6.10</b>  (5'-(10',15',20'-  trimesitylporphyrinato zinc(II))-4-  benzoic acid  5-(4-carboxyphenyl)-10,15,20-  trimesitylporphyrinato zinc(II)</p> <p>EM-55. 848.4 g mol<sup>-1</sup>.  Synthesised by Dr. Pawel Wagner.</p>
	<p><b>Compound 6.11</b>  (5'-(10',15',20'-tri-(4-<i>n</i>-  octylphenyl)porphyrinato zinc(II))-  4-benzoic acid</p> <p>EM-84. 1058.8 g mol<sup>-1</sup>.  Synthesised by Dr. Pawel Wagner.</p>
	<p><b>4-(2'-(5',10',15',20'-  tetraphenylporphyrinato  zinc(II)yl)ethenylmalonic acid</b></p> <p>WMC-221. Zn-1a. 792.2 g mol<sup>-1</sup>.  Synthesised by Dr. Wayne Campbell.</p>
	<p><b>2-(5'-(10',15',20'-  tetraphenylporphyrinato zinc(II))-  amine</b></p> <p>EM-428. 690.6 g mol<sup>-1</sup>.  Synthesised by Dr. Pawel Wagner.</p>

	<p>Carbonyl(5',10',15',20'-tetraphenylporphyrinato) ruthenium(II) Carbonyl(tetraphenylporphyrinato) ruthenium(II)</p> <p>RuTPPCO. 742.2 g mol<sup>-1</sup>. Synthesised by Dr. Sanjeev Ghambir.</p>
	<p><math>\gamma</math>-stilbazole-4'-carboxylic acid 4-[<i>trans</i>-2-(pyrid-4-yl-vinyl)]-benzoic acid 4-(<i>trans</i>-2-(4-pyridinyl)ethenyl)-benzoic acid</p> <p>060306. 225 g mol<sup>-1</sup>. Synthesised by Ms. Yvonne Ting.</p>
	<p>Carbonyl(5',10',15',20'-tetraphenylporphyrinato) ruthenium(II) with 4-(<i>trans</i>-2-(4-pyridinyl)ethenyl)benzoic acid.</p> <p>060327. 967 g mol<sup>-1</sup>. Synthesised by Ms. Yvonne Ting.</p>
	<p><i>Cis</i>-bis(isothiocyanato)bis(2,2'-bipyridyl-4,4'-dicarboxylato)-ruthenium(II) bis-tetrabutylammonium</p> <p>Ru 'N3' dye, Ru-535 bis-TBA, DyeSol B2/N719. 1188.5 g mol<sup>-1</sup>. 1260.5 g mol<sup>-1</sup> with 4H<sub>2</sub>O. Purchased from DyeSol, Australia.</p>

## 1. INTRODUCTION

### 1.1. Titania

Titania (titanium dioxide,  $\text{TiO}_2$ ) is an abundant and commercially available n-type semiconducting transition metal oxide and may be sourced as an ore or by extraction from ironsands.<sup>1, 2</sup> Crystalline titania has three major low-temperature polymorphic forms: anatase, rutile and brookite (Table 1.1, Fig. 1.1).

**Table 1.1.** Physical properties of the low-temperature titania polymorphs.

Crystalline phase	Anatase	Rutile	Brookite
Band gap energy (eV)	3.2 <sup>3</sup>	3.0 <sup>4</sup>	3.2 to 3.8 <sup>5</sup>
Refractive index <sup>6</sup>	2.49	2.61	2.58
Unit cell <sup>6</sup>	Tetragonal	Tetragonal	Orthorhombic

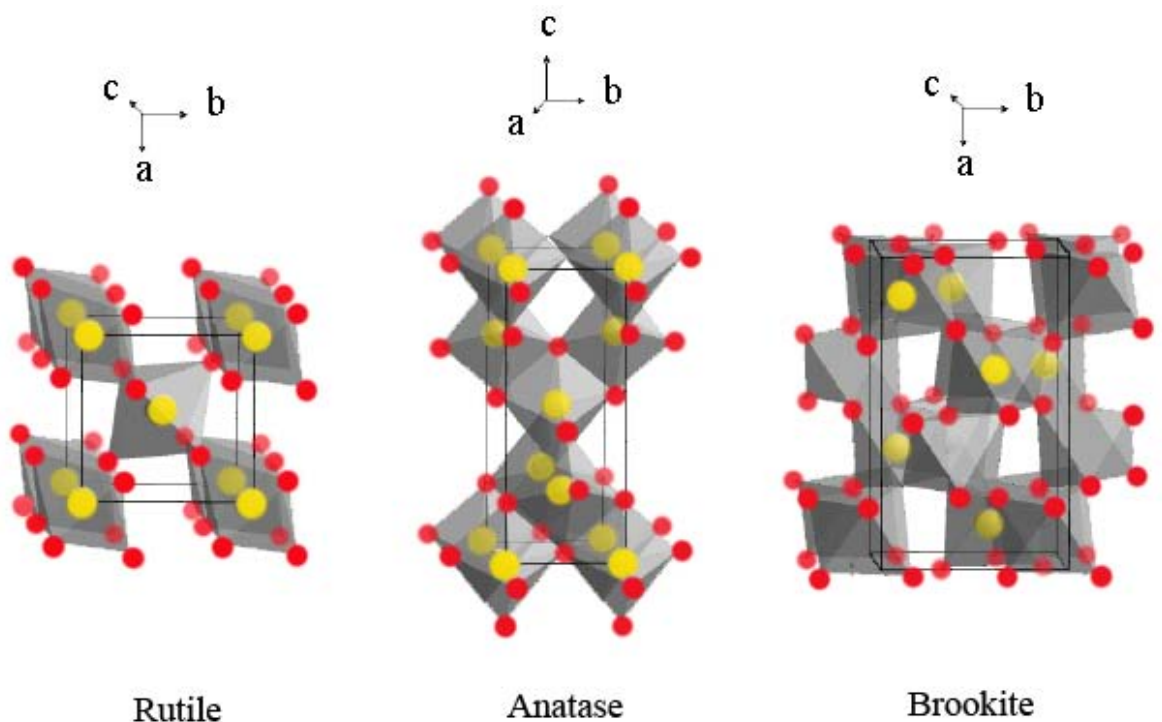


**Figure 1.1.** Representations of the crystal unit cells for rutile, anatase and brookite.

Rutile is the thermodynamically stable phase, which may be produced from anatase and brookite by heating at 750 to 800°C and at approximately 915°C, respectively (Fig. 1.2). The conversion to rutile is irreversible and is highly dependent upon the method of preparation and particle size, particularly when the material is nanoparticulate.<sup>7, 8</sup> As a result, phase transition boundaries have been reported at different positions. An alternative conversion method is to use mineral acids under ambient conditions to transform anatase to rutile *via* dissolution, then recrystallisation.<sup>9, 10</sup> Brookite is not shown on the phase diagram as it is the rarest and least characterised form, which is often a by-product in the synthesis of anatase and rutile.<sup>11</sup> The transition of brookite to rutile has been observed to occur both directly and *via* anatase.<sup>12, 13</sup>

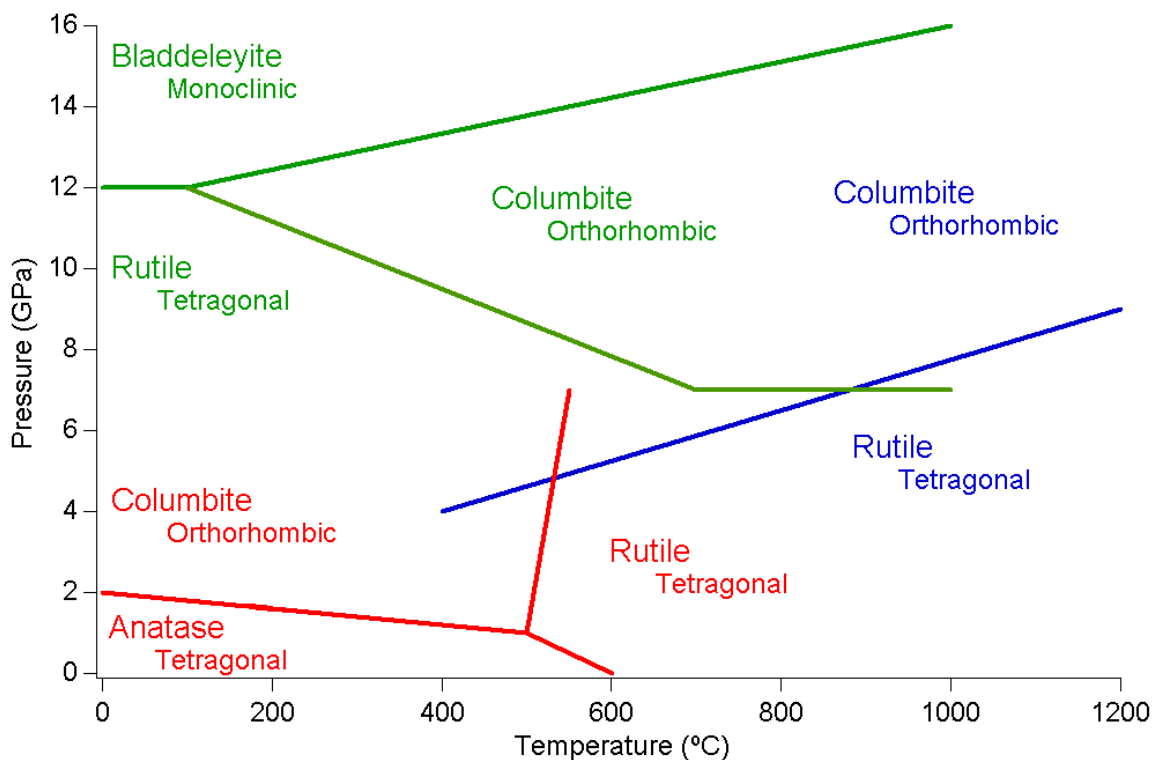


**Figure 1.2.** Phase diagram for anatase, rutile and two alternative forms of titania. Data from three different sources are plotted.<sup>5, 14, 15</sup>

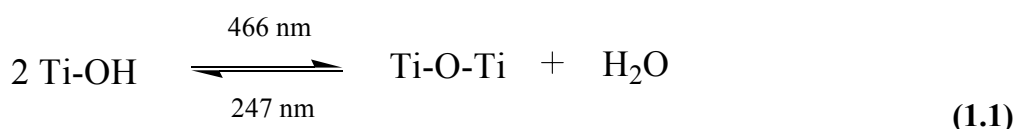
The properties of titania may be modified by doping with elements or organic species. Dopants of titania include iodine, calcium, sulphur and nitrogen, which are introduced during synthesis as salts or organic species.<sup>16, 17</sup> For example, titanium alkoxides may

be hydrolysed in the presence of species such as ammonium chloride, triethylamine, alkylammonium salts, thiourea and triethanolamine to form nitrogen-doped titania.<sup>18-20</sup> In the case of titania doped with nitrogen or sulphur, the material is able to absorb visible light. This is due in part to mixing between the p orbitals of the dopant with oxygen and to lattice substitution of oxygen, which reduces Ti<sup>4+</sup> to Ti<sup>3+</sup>/Ti<sup>2+</sup>. The strain of the O-Ti-O bond is increased, decreasing the electronic band-gap of forbidden states, which then permits the absorption of visible light. Lattice doping has produced titania electrodes with improved cell efficiencies in comparison to virgin titania. However, the improvement is likely to be a product of both an increased surface area and doping.<sup>21</sup> It has been noted that materials intended for use as dopants may bind chemically to the titania lattice without alteration of the titania conduction band energy, effectively producing surface-sensitised titania.<sup>22</sup> The formation of ‘core-shell’ materials has been shown to modify the properties of titania. In the case of titania dip-coated with strontium titanate the conduction band is shifted, while with niobium pentoxide there is an expansion of the titania conduction band.<sup>23, 24</sup>

## 1.2. *Applications of Titania*

The bulk material is a non-toxic, inexpensive white solid that is currently used in consumer goods such as paint, cosmetics, toothpaste and sunscreen. The role of titania within these products is as a light-scattering agent to improve opacity, whiteness and ultra-violet (UV) light absorption.<sup>25</sup> Titania has also been applied in self-cleaning surfaces, anti-reflective coatings, chemical sensors, photonic crystals, photocatalysis and photoelectrical generation.<sup>26-32</sup>

In the application of self-cleaning surfaces, photocatalysis is enhanced by the superhydrophilic activity of titania. Superhydrophilicity results from a light- or voltage-catalysed equilibrium between tilanol (Ti-OH) and tiloxane (Ti-O-Ti) functionalities (eq. 1.1).



As this is fully reversible, superhydrophilicity is a separate phenomenon to the photocatalytic oxidation of organic adsorbates.<sup>33, 34</sup> Photocatalytic degradation is improved upon a hydrophilic surface, as oxidation of contaminants may occur either through direct reduction with photoexcited titania or by indirect reaction with radicals of oxygen and peroxide from water.<sup>35</sup>

Photocatalysis using titania has been used to reduce buckminsterfullerene *via* colloidal gold.<sup>36</sup> Evidence has been found for a synergistic effect when using photocatalysts composed of a mixture of rutile and anatase. Energy transfer from rutile to anatase effectively improves the spectral range over which light is harvested.<sup>3, 6, 37</sup> Visible light absorption by a dense fluorite-type polymorph of titania at 570 nm has been predicted, due to a calculated band-gap energy of 2.18 eV.<sup>4</sup> For catalysis and for use in solar cells, titania has been doped and surface-sensitised to extend light absorption from the UV to the visible region. Extension of the region of light harvesting is advantageous as visible light conveys 45% of the Sun's energy, while only 8% is from UV light.<sup>19</sup>

Photoelectrical generation *via* chemical reactions in devices such as dye-sensitised solar cells (DSSCs) employ titania electrodes. The preferred form of titania is anatase, because of the large electronic band-gap and the suitable energy levels of the conduction and valence bands. In addition, titania is a non-toxic and relatively inexpensive material from which nanostructured DSSC electrodes may be produced.

### **1.3. Solar Cells**

Solar cells, together with bio-diesel, water- and wind-turbine technologies, provide a means for sustainable power generation. Photovoltaic generation of electricity already supplements society's demand for fossilised fuels. The modern economy is energy-intensive and has a heavy reliance upon the limited resource of fossil fuels: 80 million barrels of petroleum is used daily, of which 66% is used in transportation.<sup>38</sup> A current economic motive to burn fossil fuels, which accounts for 80% of global energy use,<sup>39</sup> is that coal- and gas-fired electricity plants have a cost per unit of 4 to 7 cents per kilowatt-hour. In comparison, crystalline solar cells currently cost 20 to 25 cents per kilowatt-hour.<sup>40</sup> However, the incentive for investment in solar cell technologies is that

while global energy usage is in excess of 13 TW, the sun bombards the Earth with more than that in a single hour.<sup>41</sup> Solar cells may be classed either as fully inorganic or as organic heterojunction devices.

### ***1.3.1. Fully Inorganic Devices***

Fully inorganic solar cells include devices based on Schottky-defects and on heterojunctions. Irrespective of type, as the doping ratio is critical to cell performance, the metals and alloys must be of the highest purity. Schottky-type solar cells have been made of single-, multicrystalline and amorphous silicon, all of which require precise doping of high-purity material to produce n- and p-doped silicon alloys. Incident light is absorbed and transmuted into separated charge carriers, which are then collected by the external circuit. Such Schottky-type devices depend on the presence of in-built electrical fields between n-doped and p-doped materials in order to suppress recombination between the photogenerated electron and hole. Heterojunction devices therefore rely on favourable kinetics to restrict the degree of charge recombination.<sup>42</sup> Inorganic heterojunction devices include thin-film chalcogenides (CIGS), group III-V and multi-junction (layered) cells. CIGS devices typically contain a layer of Cu(In, Ga)Se<sub>2</sub>, may be n- or p-doped and are more tolerant of defects than silicon-based devices. Group III-V devices include a multi-junction, tandem cell containing GaAs and GaInP<sub>2</sub>. Both alloys absorb visible light due to a direct band-gap energy of 1.4 eV (885 nm) and 1.9 eV (652 nm), respectively (Fig. 1.3).<sup>43, 44</sup>

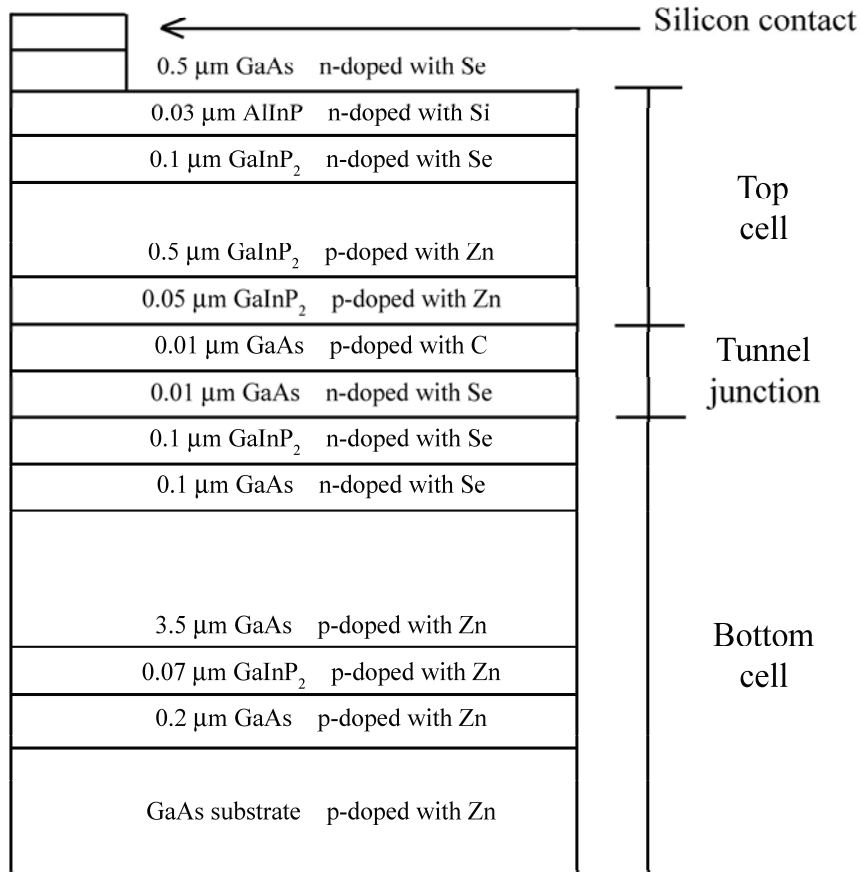


**Figure 1.3.** Schematic of a multi-junction, tandem GaAs/GaInP<sub>2</sub> solar cell, as described by S. K. Deb, 1998.<sup>43</sup>

The power conversion efficiencies of Schottky-type solar cells range from 10% for amorphous, 20% for multicrystalline and 25% for single crystal silicon cells under a light intensity of 100 mW cm<sup>-2</sup> ('one sun', Air Mass 1.5). Current inorganic heterojunction cell efficiencies are at 25% for a crystalline GaAs group III-V cell, 19% for a CIGS device and 32% for multi-junction GaInP/GaAs/Ge cells.<sup>45</sup>

### 1.3.2. Organic Heterojunction Devices

Heterojunction solar cells contain an interface at which the energy absorbed from incident light is dissociated into free charge carriers. Included in this category are organic polymer and photoelectrochemical solar cells. In the case of organic polymer cells, incident photons convey energy to the polymer in the form of excitons (electron-

hole pairs), which are dissociated into free holes and electrons at the interface of hole- and electron-conducting polymers. Bilayer heterojunction devices are formed by layering of hole- and electron-conducting materials. Bulk heterojunction devices are designed to have an intimate interpenetration of hole-acceptor and electron-donating materials. Bulk heterojunctions have a greater interfacial area at which excitons are dissociated than in a bilayer device, giving rise to an improvement in current production.<sup>46</sup> Polymeric heterojunction devices are typically formed by methods such as spin-coating or tape-casting and so require soluble or finely dispersible materials. Examples of nanostructured polymer-based cells includes one which contains poly(2-methoxy-5-(2-ethyl-hexoxy)-1,4-phenylenevinylene) (MEH-PPV) and buckminsterfullerene (Fig. 1.4) and another which uses poly(3-hexylthiophene) and [6,6]-phenyl-C61 butyric acid methyl ester. The polymeric materials act as hole-conductors, while the fullerene species are excellent electron-acceptors.<sup>47, 48</sup> Functionalisation of buckminsterfullerene with organic species gifts the electron-acceptor with an improved solubility and thus processability in organic solvents, such as chlorobenzene.<sup>49</sup>

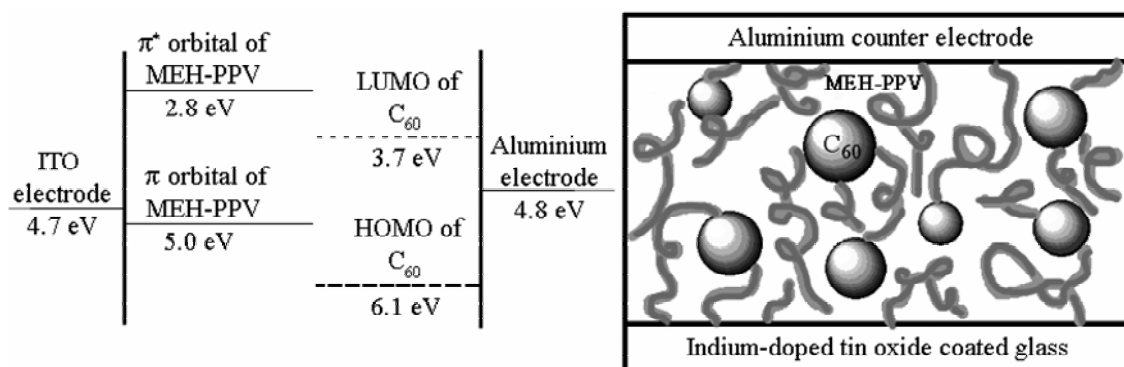


**Figure 1.4.** Cartoon of a solar cell using MEH-PPV and buckminsterfullerene. The associated energy level diagram is shown, as described by A. Moliton *et al*, 2004.<sup>47</sup>

The current record for bulk heterojunction devices is 5% efficiency for polymeric cells containing buckminsterfullerene. In comparison, photoelectrochemical Grätzel-type DSSCs have attained a 11% power conversion efficiency.<sup>45, 50</sup> DSSCs use

nanocrystalline and mesoporous electrodes, such as titania or zinc oxide, sensitised with dyes in order to absorb visible light. The sensitiser dyes absorb the energy of incident photons to produce separated charge: electrons are then shunted to the external circuit, while either electrolyte or a conducting polymer accepts the holes. Grätzel cells are a subclass of DSSCs, which use titania electrodes and a liquid electrolyte.<sup>43</sup>

### 1.3.3. The Grätzel Cell

Part of the appeal in researching Grätzel cells is the opportunity to mimic the efficient process of natural photosynthetic systems, most of which use chlorophylls to harvest light up to 700 nm (1.77 eV), though a few can absorb the entire visible spectrum and the near infra-red up to 1000 nm (1.24 eV).<sup>51</sup> A porphyrin-type core is featured in chlorophyll (Fig. 1.5) with coordinated magnesium, though zinc may also be coordinated. As a biomimetic, Grätzel cells substitute sensitiser dyes for chlorophyll arrays and a titania electrode for the electron-transfer chain of natural photosynthetic systems.<sup>42</sup> In terms of a biomimetic dye, porphyrin-based molecules are often used as they are easier to synthesise and more stable than chlorophylls, yet also are strong absorbers of blue light.<sup>52</sup> An advantage that Grätzel cells have over other families of solar cells is that though sensitisers are photobleached by titania at a faster rate under high light intensities, at lower intensities cells produce higher efficiencies.<sup>53, 54</sup>

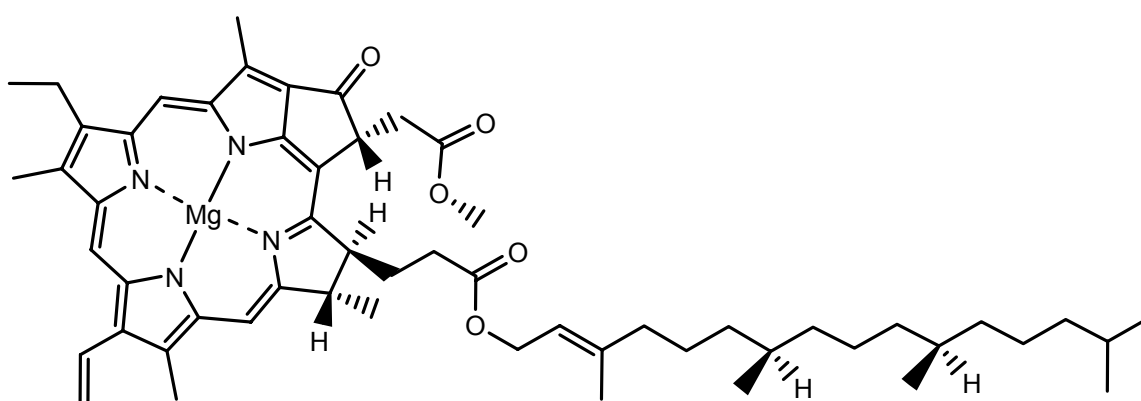
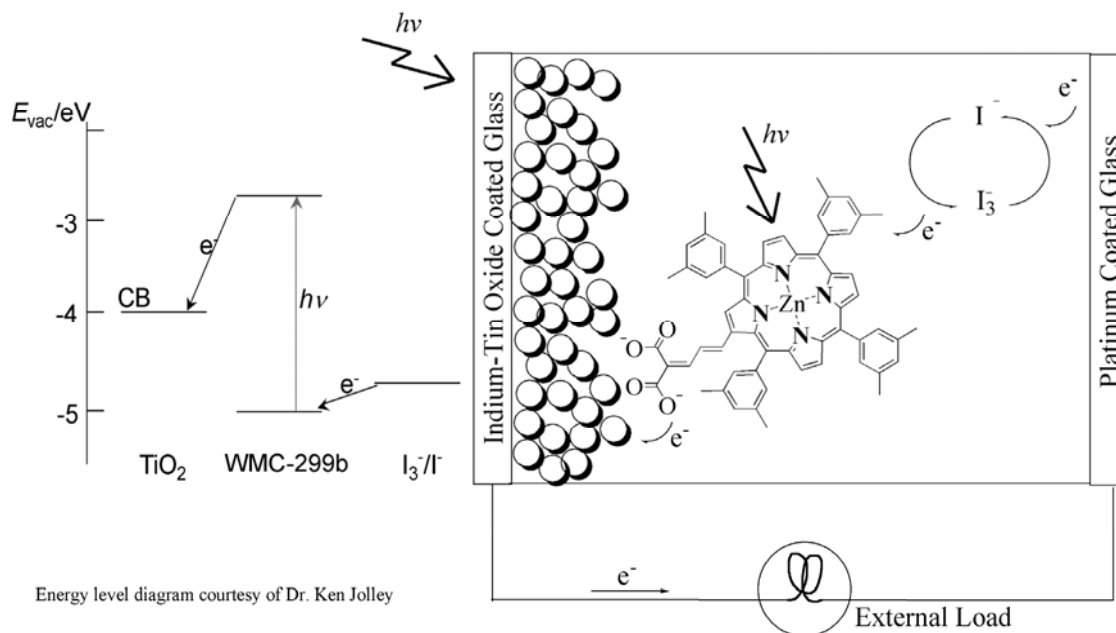


Figure 1.5. Chlorophyll a.

A typical Grätzel cell consists of a transparent electrode, such as glass coated with indium tin oxide (ITO), supporting a layer of nanocrystalline, mesoporous titania (Fig. 1.6). The titania surface is sensitised with a dye, typically a conjugated coordination compound, such as a porphyrinic species. The circuit is completed with a counter electrode of platinum on ITO glass and a redox-active electrolyte, typically containing an iodide/triiodide redox couple. Incident light excites the adsorbed dye, which then injects an electron into the conduction band of titania. The oxidised dye is regenerated by the iodide anion, while the corresponding hole is transferred to the counter electrode.<sup>55</sup> Titania is used as electron injection is facilitated by a close energy match between the conduction band and the excited state of a variety of adsorbed dyes. Anatase is preferred over rutile due to a larger band-gap energy of 3.2 eV (387 nm) and a suitable conduction band energy.<sup>3, 37</sup> The purity of the anatase phase may not be a critical issue as studies comparing the performance of rutile, brookite and anatase within solar cells have shown that differences may owe more to morphology, than to the structure of the unit cell.<sup>56, 57</sup> Alternative electrode materials include zinc oxide, zinc stannate and also tin oxide coated with colloidal zinc oxide. However, energy conversion efficiencies were found to be similar to that of titania electrodes.<sup>58-60</sup>



**Figure 1.6.** Cartoon of a Grätzel cell with the associated energy level diagram for an anatase titania electrode sensitised by dye WMC-299b, 4-(2'-(5',10',15',20'-tetraxyl)porphyrinato zinc(II)yl)butadienylmalonic acid, an iodine/triiodide electrolyte and a platinum counter electrode. 'CB' is the conduction band energy of titania, 'I<sub>3</sub><sup>-</sup>/I<sup>-</sup>' is the energy level of the iodide/triiodide couple.

The sensitiser dye absorbs energy from incident light, reaches an excited state, then may produce completely separated holes and electrons (polarons and bipolarons) or loosely associated electron-hole pairs (excitons or Mott-Wannier pairs). If the charge-carriers do not reach the external circuit, it is likely that recombination of the separated charges have occurred or that the charges have been trapped by the semiconductor.<sup>61</sup>

Grätzel cell efficiencies show strong variation with the composition of the cell, particularly with the type of electrolyte. Various electrolytes that have been investigated include ionic liquids and gels, such as 1-hexyl-3-methylimidazolium iodide with an organic gelator and 1-butyl-3-methylimidazolium tetrafluoroborate upon silica nanoparticles.<sup>62-64</sup> The replacement of the electrolyte with solid-state hole-conducting polymers such as polythiophene and spiro-containing species has also been studied.<sup>65, 66</sup> A number of alternate redox-active mediators have been investigated, including complexes of cobalt(II), in addition to studies on the effect of cationic additives. The complicated nature and role of the electrolyte is illustrated by the action of cationic additives. While larger cations such as tetrabutylammonium are more effective at screening the surface charge of titania from the triiodide ion than cations such as lithium, use of the lithium cation improves cell performance.<sup>67-69</sup> In addition, species such as 4-*t*-butylpyridine which improve dye adsorption by deprotonation of the titania surface, also shield titania from charge recombination with the triiodide species. However, this effect is heavily dependent upon the solvent of the electrolyte.<sup>70</sup>

The iodide/triiodide couple remains the favoured redox couple to regenerate sensitiser dyes in Grätzel cells due to differential kinetics; the diffusive transport of electrons within nanoparticulate titania is much slower than that of bulk titania. The result is that the rate of recombination between electrons injected into the conduction band of titania with the triiodide ion is significantly slower than that of the redox reaction at the platinum counter-electrode.<sup>71</sup> Also, for high light intensities and a closed circuit, the rate of charge recombination between titania and the triiodide anion is low, though under these conditions recombination with the diiodide ion is favoured over the triiodide ion.<sup>72, 73</sup> A coincident reason to use the iodide/triiodide couple is that the rate of recombination between ITO and the electrolyte is negligible.<sup>74</sup>

#### 1.3.4. *Titania for Grätzel Cells*

Titania electrodes have been treated to improve Grätzel cell efficiency by reducing the already low rate of charge recombination between the electrode and the electrolyte. Efforts include the use of co-adsorbents and the formation of ‘core-shell’ materials. Co-adsorbents such as quantum-confined gold and 4-guanidinobutyric acid inhibit the transfer of electrons to the electrolyte and suppress titania surface trap states.<sup>62, 75</sup> ‘Core-shell’ structures are formed either by deposition of the ‘shell’ material atop a pre-formed electrode or upon particles of the ‘core’ material prior to electrode fabrication. Examples of the first technique include dip-coating pre-formed titania electrodes with calcium acetate or aluminium nitrate, followed by sintering to produce thin coatings of insulating calcium carbonate and alumina. Titania electrodes have also been encased with nanoparticulate niobium pentoxide and lead sulfide by dip-coating methods.<sup>76</sup> Similarly, exposed regions of conductive ITO substrates have been insulated from the electrolyte by deposition of a thin and dense titania film.<sup>72</sup> The second technique for making ‘core-shell’ electrodes is illustrated by the adsorption of zinc cations onto colloidal titania, followed by tape-casting and sintering at 500°C for an hour in air. The resulting electrodes are coated with amorphous zinc oxide.<sup>77</sup> Improvement in performance arises from the retardation of charge recombination between the underlying electrode material and the electrolyte. With calcium carbonate as the blocking material, performance is also improved by provision of a more basic surface for the binding of acidic dyes.<sup>78</sup>

The key property of the Grätzel cell is the nanostructured titania electrode. The remarkably high surface area allows for a high concentration of sensitizers to be adsorbed, while the energy of photoexcited dyes is sufficient to allow injection into the titania conduction band (Fig. 1.6).<sup>79</sup> A typical Grätzel cell uses a nanocrystalline and mesoporous titania electrode which may be 1 to 20  $\mu\text{m}$  thick.<sup>80</sup> The thickness of the semiconducting layer, coupled with small, irregular particles and a high refractive index of 2.5 for anatase<sup>6</sup> results in a material that scatters light well and is anti-reflective.<sup>29</sup> Consequently, both the average path-length of incident light and the probability of a photon exciting the light-harvesting centre of a sensitizer dye are increased, contributing to an improved device efficiency.<sup>81</sup> The titania films used for electrodes are generally produced by hydrothermal techniques, sol-gel methods or a combination of both. For

use as an electrode, larger particles of titania, 100 to 400 nm in diameter, are often added to improve the light-scattering and efficiency of Grätzel cells.<sup>82</sup> In efforts to increase the amount of scattered light within Grätzel cells, electrodes have been treated with solutions of titanium tetrachloride or hexafluorotitanate to form a fine shell of nanocrystalline titania. However, the resulting improvement in performance is due to an increase in surface area and a drop of the titania conduction band potential.<sup>83, 84</sup> The benefit of nanostructuring titania for use within Grätzel cells is then two-fold: to increase the surface area available for binding sensitizer dyes and to increase the scattering of incident light within the device.

#### ***1.4. The Nanostructuring of Materials***

Nanostructures, with some dimension on the scale of nanometres, may involve dispersed or aggregated nanoparticles upon a substrate or as a self-supporting material. The particles may be amorphous, single- or multi-crystalline. Nanostructures can be formed either by physically directing material into position or by relying upon chemical interactions. It is possible to obtain the nanocrystalline, disordered and mesoporous titania of Grätzel cells by both routes. Templatation may produce porous material with predetermined and ordered morphology, while template-less, self-assembly may allow for a more intimate association of materials.

##### ***1.4.1. Templated Nanostructures***

The templatation of nanostructures may involve either the stamping, etching or moulding of the target material. For example, polymers have been stamped into patterns and also moulded by techniques such as electrospinning into non-woven mats.<sup>85, 86</sup>

Lithographic techniques have been applied to directly and indirectly form nanostructured material. For instance, techniques such as stamping, etching and by degradation using UV radiation have given monolayers of masking polymers.<sup>87</sup> Photolithography upon a hydrophobic, alkylsilane monolayer has been used to reduce the exposed area to hydrophilic silanol groups, allowing the subsequent accrual of silica

spheres upon the bare substrate.<sup>88</sup> Similarly, thin and dense titania films can be converted to a hydrophobic surface by functionalisation with fluoroalkylsilane. Subsequent UV photolithography of selected areas then removed the organic film by photooxidation upon titania, leaving a hydrophilic surface for the deposition of silica beads.<sup>89</sup>

Physical templates, such as colloidal crystals (opals), have been employed as a substrate for the deposition of other materials. Binary crystals of polystyrene spheres and smaller silica colloids have been used to form non-close-packed arrays of conjoined silica particles, after the removal of polystyrene by calcination (Fig. 1.7).<sup>90</sup> Organic templates can also direct the formation of nanostructures. For instance, the hydrothermal treatment of tetramethylammoniumsilicate with cetyltrimethylammonium chloride results in zeolites with pores on the order of 5 nm. A hexagonal, cubic or lamellar morphology is observed, depending on the ratio of silicate to cationic surfactant.<sup>91</sup> A bicontinuous system of the cubic phase of sodium dodecylsulfonate in water has also been used to form mesoporous zinc sulfide.<sup>92, 93</sup> Techniques which use the air-solvent or solvent-solvent interface of micelles, inverse micelles and droplets have been reported to produce rings, two dimensional opals and inverse opals. Nanostructures of titania rods, silica opals, and inverse opals of nanoparticulate gold have been formed in this manner.<sup>94-96</sup>

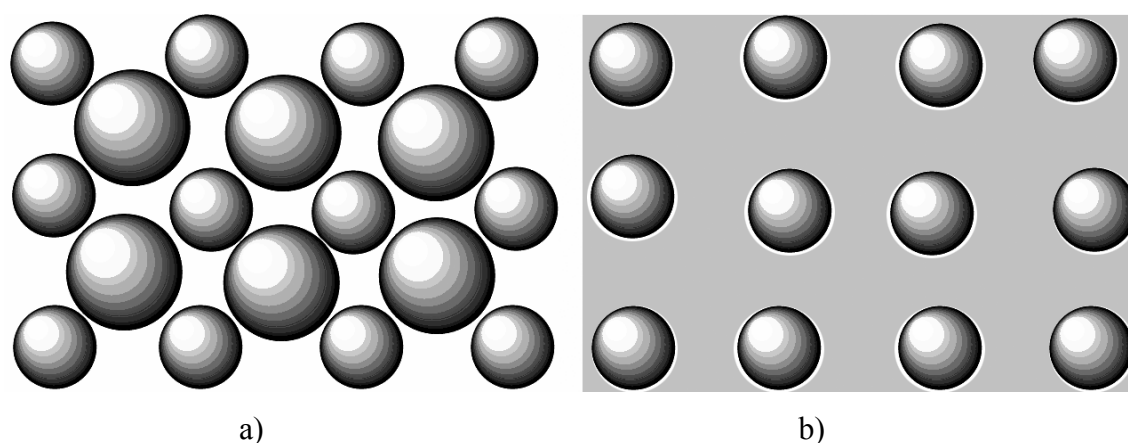


**Figure 1.7.** A cartoon representation of a binary opal composed of large polystyrene spheres and smaller silica spheres (a) and the resulting array of sintered silica spheres (b).

### 1.4.2. *Template-less Nanostructures*

Template-less nanostructures have been formed by methods such as laser ablation, chemical vapour deposition (CVD) and self-assembly. For instance, laser ablation of platinum foil in the presence of a surfactant produces nanoparticles and electro-spray CVD of organometallic species gives both cadmium selenide films and zinc sulfide quantum dots.<sup>97, 98</sup> Self-assembled close-packed photonic crystals have been reported with colloidal silica and with micelles of polymer/quantum dot composites.<sup>99, 100</sup> As mentioned earlier, colloidal material may form nanostructures with or without the aid of a lithographically-defined substrate to give close- or non-close-packed particles. Methods such as laser ablation, the use of electric arcs and thermal decomposition of organic materials in the presence of metal catalysts have produced complex nanostructures, such as single- and multi-walled carbon nanotubes, as well as iron- and molybdenum-doped fullerenes and fullerene-stuffed nanotubes.<sup>101-104</sup> In addition, the thermal decomposition of different precursor materials has been noted to influence nanoparticle morphology. For example, the respective decomposition of titania isopropoxide and titanium tetrachloride results in spherical and polyhedral particles.<sup>105</sup>

Nanostructured material may be formed with the aid of polymers, oligomers or small molecules to introduce porosity or to produce a charged surface. Such structure-directing agents have been used to nanostructure materials by the chemical modification of surfaces, without the use of lithographic techniques. The deposition of ionic polymers, 'polyelectrolytes' or monomers upon a substrate can direct the assembly of particulate matter by covalent, ionic, electrostatic or hydrogen-bonding interactions. For instance, cotton has been functionalised by alternating dip-coating with the anionic and cationic polyelectrolytes poly(sodium-4-styrenesulfonate) and poly(allylamine hydrochloride).<sup>106</sup> The extension of this technique is to embed particles between layers of organic species, while the direct functionalisation of particulate matter offers greater flexibility over how materials may be layered. For instance, the deposition of alternating layers of colloidal cadmium sulfate capped by mercaptoethanol and of cationic titania was facilitated by the use of intervening layers of anionic poly(styrenesulfonate) and cationic poly(diallyldimethyl ammonium chloride). Similarly, lamellar structures of gold functionalised by poly(4-vinylpyridine) or 4-mercaptobenzoic acid have been formed using polyelectrolytes, as have lamellae of

titania-coated silica beads.<sup>28, 107, 108</sup> Nanoparticle surfaces have been chemically modified by organic species that chelate, ligate and perhaps form a protective shell to aid dispersion and self-assembly. The simplest methods are sol-gel techniques that provide colloids with electrostatic or steric stabilisation, while the particle diameter depends on the number of nucleation sites and the rate of condensation.<sup>109</sup> For example, in the base-catalysed hydrolysis of tetraethylorthosilicate, colloids are electrostatically stabilised by a negatively-charged surface, while colloidal gold and cadmium sulfide gain steric stabilisation from ligation by citrate and tri-*n*-octylphosphine, respectively.<sup>110-112</sup>

The formation of nanostructures using the self-assembly of nanoparticles with the aid of small molecules has the potential to offer greater control over particle packing. For example, gold nanoparticles capped by tetraoctylammonium bromide have been assembled into spherical clusters of monodispersed size by the use of a multidentate thiol species as a 'linker' material.<sup>113</sup> The chemically-assisted self-assembly of particles by the functionalisation of both the substrate and particulate matter is a technique that has been used in the formation of arrays. An illustration is the microcontact printing of 16-mercaptohexadecanoic acid upon gold, to bind hydrophilic colloids of cadmium selenide chelated with 4-mercaptobenzoic acid. Alternatively, gold printed with 1-dodecanthiol was used to pattern hydrophobic colloids of cadmium selenide chelated with tri-*n*-octylphosphine oxide.<sup>114</sup> Less rigid networks have been formed using core/shell CdSe/ZnS nanoparticles and colloidal gold. The two inorganic materials are ligated to complementary strands of deoxyribonucleic acid (DNA), which on mixing form duplex-strand DNA which interlink the nanoparticles.<sup>115</sup> Similarly, gold nanoparticles have been bound to substrates functionalised with amino-, cyano- or mercaptosilanes. Subsequent layers of gold were then tethered together with intervening layers of molecular dithiols.<sup>116</sup>

### **1.5. *The Nanostructuring of Titania***

Titania may be nanostructured by a variety of techniques and from a range of sources, including bulk titania, inorganic and coordination compounds. For example, colloidal titania may be formed from reactive precursors such as titanium alkoxides or chlorides,

which readily hydrolyse with water to form titania by the respective elimination of alcohol or hydrochloric acid gas. Due to an increased surface area, porosity and number of defects, the chemical reactivity and physical characteristics of nanostructured titania often vary significantly in comparison to bulk titania. For instance, while the refractive index of bulk anatase is 2.5, the estimated indices for a film of amorphous, colloidal titania and for inverse opaline titania are 1.5 and 2.3, respectively.<sup>3, 6, 117</sup> It has been shown that in comparison to the bulk material, nanoparticulate titania displays a higher photocatalytic activity and is more sensitive to environmental factors.<sup>118-121</sup> The ideal would be to produce titania with a high degree of order within the nanostructured material. This is as for titania the largest theoretical electron diffusion coefficient is for materials with the greatest degree of ordering between nanocrystals.<sup>122</sup>

### ***1.5.1. Templated Nanostructures of Titania***

Macroscopic templates for titania include nanostructured alumina or polymeric filters, nanoporous tin oxide electrodes and electrospun polymer scaffolds. Dip-coating of such materials into sols of titanium isopropoxide or titanium butoxide or with suspensions of pre-formed titania nanoparticles have produced nanostructured titania.<sup>123-125</sup> Fibrils and porous fibres of titania have also been formed by the electrospinning of titania precursors such as titanium isopropoxide or titanium propoxide with a scaffold polymer. Titania is condensed as both the polymer and precursor are electrospun, after which the scaffold may be removed by calcination. Scaffold polymers for such fibres include cellulose acetate, poly(vinylacetate) and poly(vinylpyrrolidone).<sup>126-128</sup> Macroscopic templates produced by lithography are well documented. For instance, while stamp-lithography of sacrificial polymers on a titania substrate permit the selective condensation of hexafluorotitanate upon bare titania, sulfate groups grafted to polypropylene allow the preferential deposition of titania on exposed regions of the untreated and hydrophobic polymer.<sup>129, 130</sup> Similarly, poly(ethylenephthalate) has been functionalised by an aromatic silane, which after selective exposure to UV light produced patterns of hydrophilic silanol groups. The exposed silanol functionalities were then used for the deposition of titania.<sup>131</sup> In a more complex technique, lithographic patterning of substrates has been used to nanofabricate titania by the stamping of organic masks (Fig. 1.8). Gold patterned with

hexadecanethiol and 4-(2-mercaptoethyl)styrylethylether was exposed to styrene, which polymerised upon areas covered by the mercapto-ether. Titania was then deposited upon the entire surface by the hydrolysis of titanium isopropoxide. By cleavage of the ether functionality, areas stamped with 4-(2-mercaptoethyl)styrylethylether were cleared of both polystyrene and titania.<sup>132</sup>

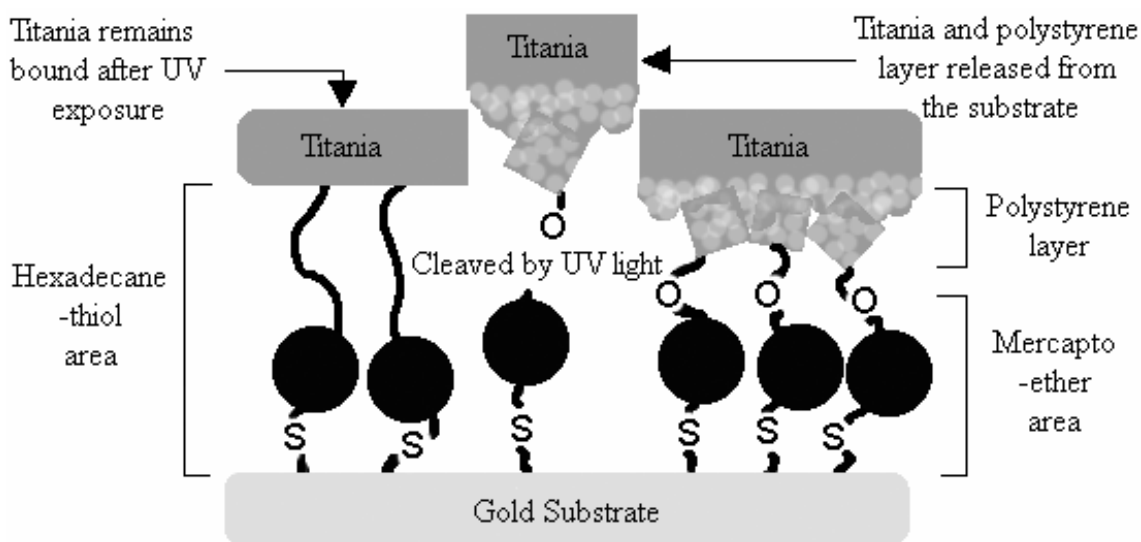


**Figure 1.8.** A representation of the patterning of titania upon gold *via* the sacrificial organic intermediary of polystyrene, as described by M. Bartz *et al*, 2000.<sup>132</sup>

Organic templates have been employed in the nanostructuring of pre-formed crystalline titania by screen-printing or tape-casting. On calcination the organic material is destroyed to leave voids, producing disordered, mesoporous and nanocrystalline titania of the type used within Grätzel cells. Tape-casting of titania with sacrificial organic species has produced films with a bimodal distribution of pore sizes by virtue of both intra- and inter-particle voids.<sup>133-135</sup> Mixtures of preformed titania and polymeric templates for mesoporous and nanocrystalline titania may also be deposited by screen-printing, spin-coating and dip-coating. Examples of polymeric templates include polyethylene glycol and block co-polymers of polyethylene-*co*-butylene and polyethylene oxide.<sup>136-138</sup> Molecular templation has been used to nanostructure titania, following the exposure of wet, spin-coated, titania sol-gel films to the quaternary

ammonium surfactant cetyltrimethylammonium chloride. The introduced porosity is due to the surfactant, which may act by inhibition of film shrinkage during the drying process.<sup>139</sup>

In the formation of mesoporous and nanocrystalline titania, physical templates such as opals and certain surfactants result in bicontinuous three dimensional structures. Alcoholic solutions of titanium alkoxides stabilised by acids, such as hydrochloric acid or trifluoroacetic acid, have been dip- and spin-coated with the template Pluronic P-123 ( $\text{HO}(\text{CH}_2\text{CH}_2\text{O})_{20}(\text{CH}_2\text{CH}(\text{CH}_3)\text{O})_{70}(\text{CH}_2\text{CH}_2\text{O})_{20}\text{H}$ ), which is a non-ionic triblock copolymer of polyethylene oxide and polypropylene oxide. On elimination of the polymer by calcination, ordered, mesoporous and three-dimensional structures of anatase with close-packed cavities were produced, which in some cases resembled inverse opals.<sup>140-143</sup> Analogous to the formation of inverse opals, the templation and subsequent dissolution or calcination of loose polymer beads has garnered discrete spheres of titania.<sup>144, 145</sup>

### ***1.5.2. Inverse Opals of Titania***

Inverse opals are formed upon opaline templates in order to mirror the long-range ordering of cubic close-packed or hexagonally close-packed colloidal particles (Fig. 1.9). The infiltration of opals and the subsequent removal of the template yield material with an ordered and three-dimensional mesoporosity. Inverse opals have been also been described as inverse or reverse contrast colloidal crystals and as air-sphere colloidal crystals. High-quality opals may be completely or partially infiltrated by solutions or sols of titania precursors to give morphologies ranging from the ideal 'honeycomb' lattice to 'skeletal' inverse opals.<sup>146, 147</sup> Inverse opals have been synthesised of both organic and inorganic materials, including polypyrrole, silicon, gallium nitride, silica, germanium and titania.<sup>148-150</sup>

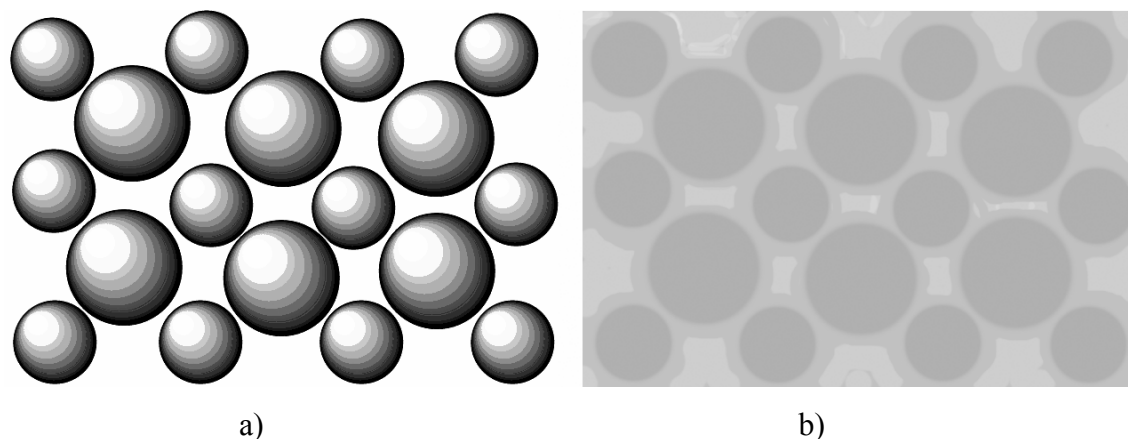


**Figure 1.9.** A cartoon of a binary opal (a) and the resulting inverse opal (b).

Inverse opaline, photonic crystals have been used within both Grätzel cells and solid-state DSSCs to produce a small amplification of incident light. Reported studies include capping of the top surface of an inverse opal with nanocrystalline, mesoporous titania, upon which sensitizer dyes were adsorbed. The enhancement of red light absorption may be due to the inverse colloidal crystal, through a combination of a slower propagation of light and incoherent scattering from disordered areas.<sup>3, 151</sup> A theoretical study has suggested that the enhancement of light absorption is a result of interactions at the interface of the inverse opal and the capping nanocrystalline layer. In order to receive an enhancement in light absorption from the ‘colloidal crystal mirror’, only the nanocrystalline material requires sensitisation.<sup>152</sup> A similar photonic enhancement of Grätzel cell efficiencies has been found for lithographically-defined titania arrays sporting 1  $\mu\text{m}$  cavities.<sup>129</sup>

### 1.5.3. *Template-less Nanostructures of Titania*

Titania has been nanostructured by template-less methods that include the direct deposition of anatase nanoparticles onto a substrate by exposure to a reactive precursor such as titanium tetrachloride, by chemical vapour deposition and by electrophoresis of preformed colloids.<sup>35, 153, 154</sup> The electrophoretic deposition of crystalline titania upon ITO-coated poly(ethyleneterephthalate) has produced titania electrodes with a high surface area (60 to 170  $\text{m}^2 \text{g}^{-1}$ ), which under 100  $\text{mW cm}^2$  illumination give a 3% power

conversion efficiency in Grätzel cells.<sup>53, 155</sup> Spherical and fibrillar nanostructures have been formed without templation by the condensation of titania precursors using supercritical carbon dioxide as the solvent.<sup>156</sup> Titania can also be nanostructured *via* intermediary forms of hydrogen titanate nanometre-sized tubes, wires and ribbons. Titanate nanotubes and ribbons are formed by the treatment of titania by hydrothermal treatment of crystalline titania with sodium hydroxide, while the use of potassium hydroxide forms wires. This is in contrast to the treatment of titania with mineral acids, which facilitates the dissolution and reformation of anatase into rutile. It is possible that under alkaline conditions titania is exfoliated into titanate sheets which may then reform into such fibrillar structures. Dependent on the tube diameter, hydrothermal treatment under neutral conditions or calcination at 400 to 600°C transforms hydrogen titanate nanotubes into nanoparticles, single- or multicrystalline wires.<sup>157-162</sup> Titanate nanotubes have been directly deposited by electrophoresis onto conducting fluoride-doped tin oxide.<sup>163</sup> Aligned titania rods have also been produced by the anodization of titanium foil.<sup>164, 165</sup>

With the aid of polyelectrolytes, lamellar structures of titania have been formed upon an electrospun substrate by alternating dip-coating with solutions of cationic titania and of anionic polyacrylic acid.<sup>125</sup> Similarly, substrates such as quartz, silicon and carbon-coated grids have been treated first with poly(ethylenimine), then with poly(styrene-4-sulfonate) to allow the chemisorption of particulate titania and lead sulfide conjoined by mercaptoacetic acid. Subsequent particle layers use intervening strata of the anionic polymer as a binding medium.<sup>166</sup> Once assembled in such a fashion, the material may be sintered to join titania particles and to eliminate organic material for use within Grätzel cells.<sup>167</sup>

Molecular assistance in the nanostructuring of titania has been given by chelating species such as tris ((HOCH<sub>2</sub>)<sub>3</sub>CCH<sub>3</sub>), trizma ((HOCH<sub>2</sub>)<sub>3</sub>CNH<sub>2</sub>), glycine hydroxamate (H<sub>2</sub>NCH<sub>2</sub>CONHOH), and ethanolamine (H<sub>2</sub>N(CH<sub>2</sub>)<sub>2</sub>OH) which have been used to form chains and nanoparticles of titania from titanium tetrachloride. Biotin-avidin and trizma have also been used to guide the aggregation of titania particles into 'pearl necklace' formations.<sup>168-170</sup> In a similar vein, the aggregation of titania nanoparticles stabilised by tri-*n*-octylphosphine oxide into spherical aggregates on the scale of 50 to 100 nm has been observed with the slow evaporation of toluene.<sup>171</sup> Titania particles can be stabilised by encapsulation within a silica shell, while pre-formed titania colloids have

been redispersed by hydrothermal treatment with mineral acids or bases such as tetramethylammonium hydroxide to 'peptise' the surface.<sup>172-174</sup> Sol-gel techniques to obtain both dispersible and aggregated nanoparticles which may display both micro- and mesoporosity are well documented. Typical preparations use a reactive titania precursor, such as titanium tetrachloride or titanium alkoxides within an acidic, alcoholic media and a chelating agent like 1,2-propanediol to stabilise the sol and form a gel. Dispersed titania is most often stabilised by a strongly acidic surface and is amorphous, while aggregated titania is frequently the product of sol-gel titania which has been hydrolysed and then hydrothermally treated to crystallise and grow the primary particles.<sup>158, 175, 176</sup>

An ideal electrode for use within Grätzel cells is a nanostructured superlattice of crystalline titania. If the electrode could be formed without a template and the need for high temperature treatment to physically and electrically connect particles to each other and to the substrate, the primary benefit would be the ability to construct Grätzel cells upon a plastic electrode. The use of plastics like ITO-coated mylar would reduce the cost of production and yield a flexible, transparent and light-weight device. It is probable that a nanostructured superlattice electrode would have a more intimate association with sensitizer dyes and a greater dye loading due to an increased surface area. There may also be improvement in the amount of collected photogenerated charge due to the reduced average path-length of electrons through the titania electrode.<sup>46</sup> Titania arrays of nanoparticulate anatase linked by small, conjugated molecules into a stable physical and electrical network may conceivably be synthesised by a route of chemically-assisted self-assembly.

#### ***1.5.4. Self-Assembly of Titania using Small Molecules***

Tactics to produce chemically-assisted, self-assembled superlattices of titania upon a substrate for use within Grätzel cells are shown in Figure 1.10. One scenario is that only the nanoparticles are functionalised, which then bind to each other and the substrate. Another is that the first particulate layer relies on treatment of the substrate for binding, while subsequent layers are bound after exposure to other linker materials. A third case is where both the substrate and particles are pre-functionalised and salt-

formation or hydrogen bonding between the functionalised materials is required to allow particle deposition. To form completely self-assembled and sensitised titania for Grätzel cells, dye species would need to be adsorbed, either during or after lattice formation. If the affinity of the sensitizer dye for titania is less than that of the linker material, it may be necessary to expose the nanoparticles to the dye prior to assembling the superlattice and to rely on the displacement of a fraction of the dye by linker species. A more involved approach may be to use highly engineered units which tether together hole-acceptors, sensitizers and electron-acceptors into one complex.<sup>177</sup> While there have been no reports of superlattice formation or the binding of nanoparticulate titania to a substrate using only small molecular linkers, similar studies have been reported nanoparticulate gold and metal clusters including polyoxometalates ('Keggin salts').<sup>178, 179</sup>

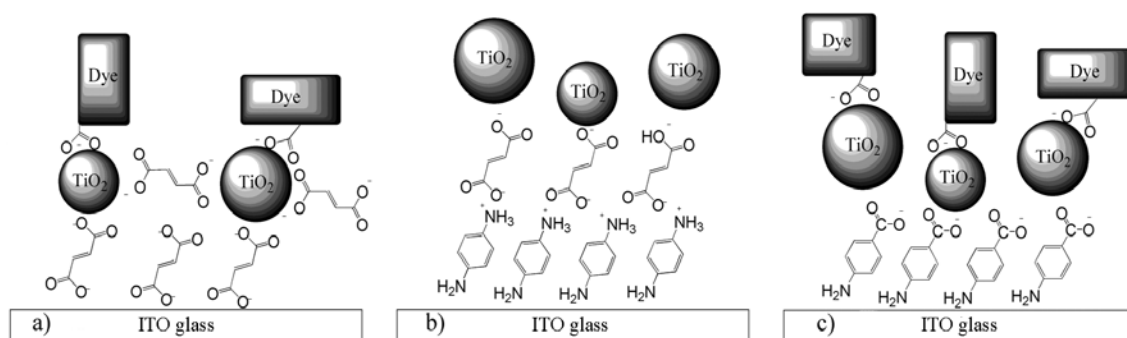


**Figure 1.10.** Potential strategies for forming the first particulate layer of a titania array upon indium-doped tin oxide (ITO). a) A diacid linker binding titania directly to ITO. b) Pre-treatment of ITO with a diamine with binding of acid-functionalised titania *via* salt-formation. c) Pre-treatment of ITO with an amphiprotic linker and binding of pre-sensitized titania without an intervening salt layer.

In the formation of superlattices, restricting the deposition of organic species to a monolayer would minimize the amount of wasted material. Rinsing of the treated substrate may be used to limit deposition to a monolayer, but is reliant upon a reasonably robust attachment of the molecule or particle to the surface. Alternative methods include limiting reagents to quantities that correspond to a theoretical surface coverage and selection of species with substrate-specific termini to minimize cross-

linking and the binding of excess material. The last method has been utilised in the formation of a composite of titania nanoparticles and the polyoxometalate  $K_5[Co(H_2O)PW_{11}O_{39}](PW_{11}Co)$ . The linker triaminopropylsilane condenses with titania at one terminus, while at the other a primary amine functionality binds to the polyoxometalate.<sup>180</sup> Organic monolayers have been formed upon substrates such as glassy carbon, mica and ITO glass for the purpose of binding nanoparticles. An example is the electrodeposition of 4-aminobenzoic acid upon glassy carbon, such that the free carboxylate group may participate in the electrostatic binding of a solvated osmium-poly(4-vinylpyridine) complex. Metal clusters of the polyoxometalate,  $K_{10}H_3[Pr(SiMo_7W_4O_{39})_2]$  may then be electrodeposited to allow detection by voltammetry.<sup>181</sup> Similarly, the dip-coating of ITO glass treated by 1,12-diaminododecane resulted in the electrostatic binding of phosphomolybdic acid clusters.<sup>182</sup> A superlattice of citrate-stabilised gold colloids has been formed upon a monolayer of 3-aminopropyltriethoxysilane on ITO glass. The subsequent dip-coating of the treated substrate into alternating solutions of bipyridine-containing dyes and stabilised gold produced a sensitised, metal-based, nanostructured electrode. The photovoltaic performance of this electrode was found to be poor.<sup>178, 183</sup> Monolayers of aminosilanes upon ITO glass have been used as a reactive surface to which light-harvesting, fullerene-porphyrin dyads have been tethered *via* an osmium cluster. A variation where two adjacent molecules are linked *via* coordination of porphyrin functional groups has been tested within a DSSC (Fig. 1.11) to give a 1.80% incident photon conversion efficiency (IPCE) under illumination at 435 nm and a  $0.96 \text{ mW cm}^{-2}$  intensity.<sup>184</sup> Another self-assembled electrode tested within a solar cell used the electrophoretic deposition of functionalised gold particles onto treated ITO glass to form a nanostructured system with ‘quaternary organisation’ (Fig. 1.12). The ITO glass was coated by particulate tin oxide upon which composite colloidal material was deposited by electrophoresis. The colloids contained a gold core protected by thiolated porphyrin dyes with the further intercalation of buckminsterfullerene between adjacent porphyrin rings. Solar cells fabricated using this system have yielded power conversion efficiencies of 0.61% and 1.50% under conditions of  $3.4 \text{ mW cm}^{-2}$  and  $11.2 \text{ mW cm}^{-2}$ , respectively.<sup>52, 185</sup>

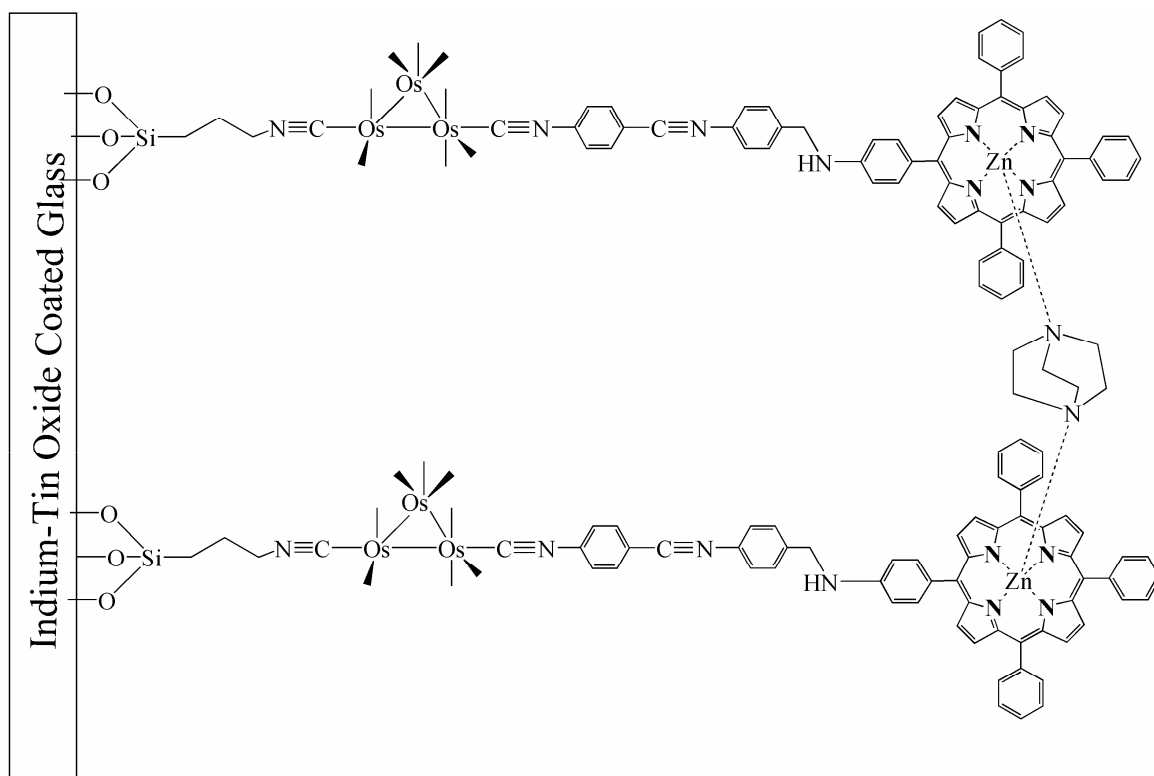


**Figure 1.11.** A schematic of the porphyrin dyad assembly studied by Y.-J Cho *et al*, 2005.<sup>184</sup>

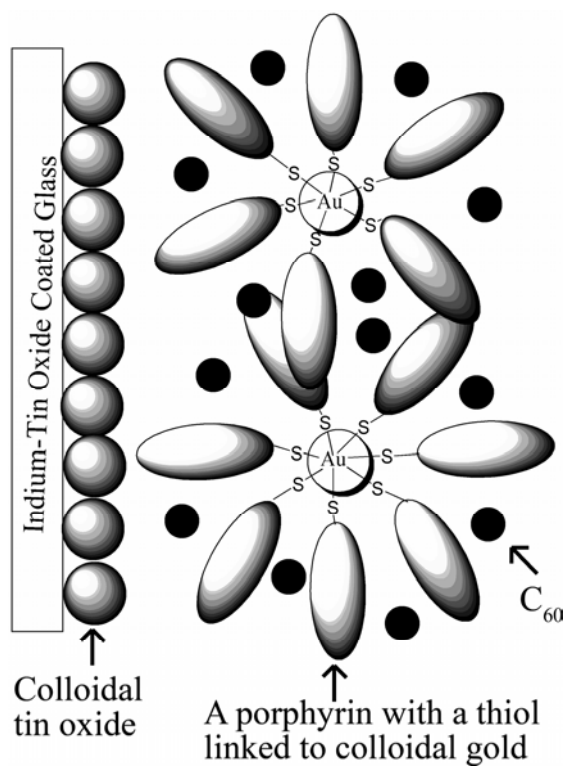


**Figure 1.12.** A schematic of the 'quaternary structure' studied by H. Imahori *et al*, 2004.<sup>52</sup>

To realise the chemically-assisted self-assembly of titania nanoparticles for Grätzel cells, the functionalisation of the conducting substrate is one factor. Another aspect besides the nature of the titania surface is the behaviour of species which may be used as ‘tethers’ and sensitisers.

### **1.6. Sensitiser Binding to Titania for Grätzel Cells**

The light harvesting ability of Grätzel cells may be extended into the visible region of the solar spectrum, either by doping of the titania lattice or by sensitisation of the surface. Lattice doping enables visible light to be absorbed by decreasing the electronic band-gap energy of the material, while surface sensitisation by inorganic or organic species enables the absorption of visible light, which supplements the absorption of UV light by titania.

Surface sensitisers absorb visible light, reach an excited state and inject electrons into the conduction band of titania. Sensitisers include colloidal gold, nanoparticulate inorganic sulfides and ruthenium-based coordination compounds. The species may be either adsorbed or chemically bound to titania after application by methods such as immersion, co-application of precursor materials and dip-coating.<sup>75, 82, 140</sup> For instance, titania electrodes have been coated with particulate cadmium sulfide by repeated and alternating dip-coating with a saturated solution of cadmium nitrate and with a 0.1 M sodium sulfide solution. Inorganic colloids of lead sulfide, cadmium sulfide and silver sulfide have been used to surface sensitise titania electrodes for light harvesting, but are vulnerable to photocorrosion processes.<sup>186-188</sup> For use in Grätzel cells, organic and coordination compounds promise more in the way of flexibility of design in the search for the ideal 'black' surface sensitiser to improve performance by the absorption of visible and near infra-red light. Organic and coordination compound dyes are typically adsorbed onto titania *via* acidic functionalities, such as carboxylic acids. While species that are anchored *via* a phosphonate group are less labile than those tethered by a carboxylate functionality, studies of ruthenium-based and porphyrin-based coordination compounds have shown that higher device efficiencies are gained when dyes use a carboxylate group.<sup>189-192</sup> Coordination compounds provide the highest efficiencies and stability within iodide/triiodide electrolytes, possibly because available, non-bonding d

orbitals may be involved in regenerating the oxidized dye.<sup>42</sup>

Device efficiency is improved by modification of the sensitiser, as exemplified by the use of the “green” zinc porphyrin dye, 2-cyano-3-(2'-(5',10',15',20'-tetraphenylporphyrinato zinc(II)yl)acrylic acid, the ruthenium “N3” dye, di(thiocyanato)-bis(2,2'-bipyridyl-4,4'-dicarboxylate) ruthenium(II) and the “Black” dye, tri(thiocyanato)-2,2',2''-terpyridyl-4,4',4''-tricarboxylate ruthenium(II), which are illustrated in Figure 1.13. Under simulated global solar radiation of  $100 \text{ mW cm}^{-2}$  respective power conversion efficiencies of 5.2%, 11.0% and 10.4% have been reported using Grätzel cells.<sup>193, 194</sup>

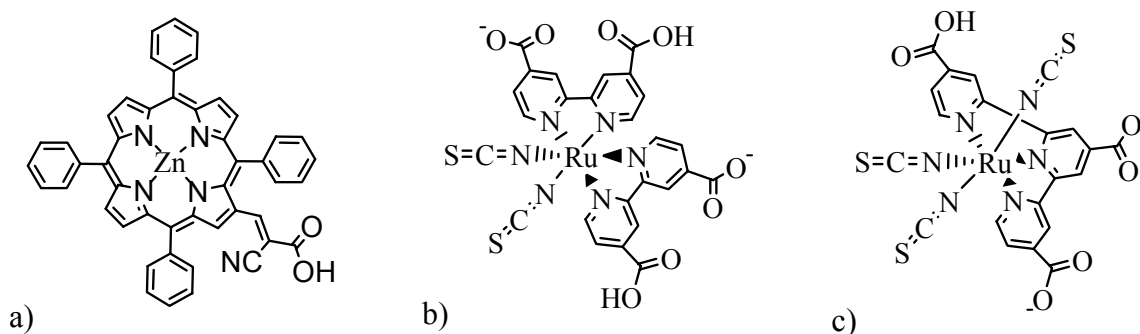


**Figure 1.13.** a) The “green” zinc porphyrin dye, 2-cyano-3-(2'-(5',10',15',20'-tetraphenylporphyrinato zinc(II)yl)acrylic acid. b) The ruthenium “N3” dye, di(thiocyanato)-bis(2,2'-bipyridyl-4,4'-dicarboxylate) ruthenate(II) di-anion. c) The “Black” dye, tri(thiocyanato)-2,2',2''-terpyridyl-4,4',4''-tricarboxylate ruthenate(II) di-anion.

### 1.6.1. The Binding of Dye to Titania

The assembly of dyes upon titania is largely determined by the number and type of binding groups of the dye, together with the steric constraints of the molecule. Studies of dye binding to titania tend to use sintered aggregated material in the form of a powder or a film. As an amphoteric oxide, titania may be sensitised by acidic or basic species though the former is more common. Typical adsorbates are small organic or

coordination compounds using carboxylic, phosphoric or sulfonic acid functionalities as binding groups. Dyes bound to titania by multiple carboxylic acid groups provide higher Grätzel cell efficiencies than dyes with a single acid group, though this may also indicate that the binding geometry has a significant role in cell performance.<sup>195</sup>

The environment experienced by the electrode influences the interaction of adsorbed species upon titania. For instance, in solutions with a pH of 8.5, a polypyridine-based ruthenium dye (Fig. 1.14) has been found to desorb from titania.<sup>134</sup>

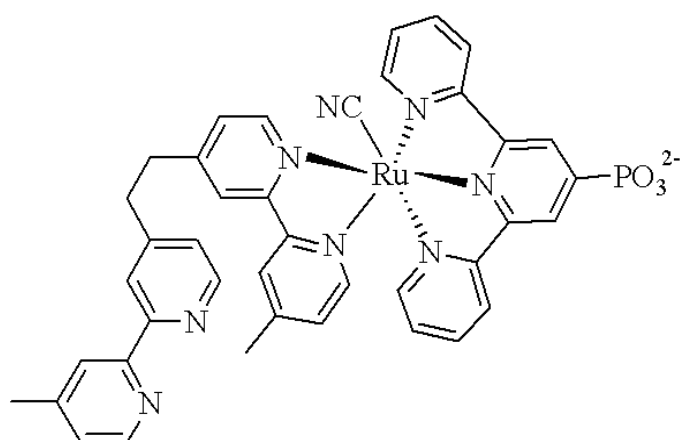


**Figure 1.14.** Ru(II)LL'CN. L is 4'-phosphonic acid-2,2':6'2''-terpyridine and L' is 1,2-bis(4'-methyl-2,2'-bipyridyl-4-yl)ethane.

Dyes have been modified to improve chemical and electronic interactions across dye-titania and dye-electrolyte interfaces. For example, a ruthenium dye with a coordinated triphenylamine species has been synthesised, in order to bring the excited-state energy level of the dye towards that of the spiro-based hole-conducting polymer. Charge transfer across the dye-polymer interface was thereby improved, together with DSSC performance.<sup>66</sup> However, it is difficult to draw generalisations on what characteristics sensitiser dyes should possess in order to yield optimal results within a Grätzel cell. For instance, the benefit of a fully conjugated dye is under question, as the use of both fully-conjugated porphyrin-based sensitiser dyes and incompletely-conjugated indolene dyes

yield reasonable efficiencies.<sup>196, 197</sup> There are also contrasting reports on whether the aggregation of sensitiser dyes has a negative or positive effect upon cell performance. While aggregation *via*  $\pi$ - $\pi$  interactions may cause the quenching of photoexcited dyes by neighbouring molecules, producing a lower performance, aggregation has also been reported to improve efficiency by increasing the region over which light is absorbed.<sup>47, 198, 199</sup> As such, techniques such as tailoring the 'footprint' size of dyes to control the extent of aggregation upon surfaces have been used to study the impact upon cell efficiency.<sup>200</sup>

By investigating the behaviour of both simple 'probe' molecules and sensitiser dyes, the spectral analysis of adsorbates upon titania may be simplified. It may then be reasonable to draw general relationships between structure and efficacy within Grätzel cells.

### 1.7. *Opportunities for Novel Research in Nanostructured and Functionalised Titania*

The opportunities to contribute to knowledge in the field of nanostructured and functionalised titania include that:

- At the time of writing, there were no publications on the performance of Grätzel cells using titania inverse opaline electrodes sensitised with a range of organic and coordination compound dyes.
- As yet, there are no publications on the self-assembly of nanoparticulate titania electrodes *via* small, fully conjugated organic species. As a condition of complete conjugation through the organic linker, the use of alkoxy silane species to bind to ITO must be avoided.
- The use of small and fully conjugated molecules in the formation of electrodes may allow efficient electronic communication between tethered nanoparticles and the substrate.
- The formation of such self-assembled titania nanoparticulate electrodes without sintering would then permit the use of conductive plastic substrates.
- The mode of binding by sensitizer dyes *via* carboxylic acid groups upon titania still requires clarification.
- In terms of spectroscopic studies of the binding of organic species to titania, there have not yet been reported <sup>1</sup>H NMR spectra of small molecules adsorbed onto the surface of dispersed titania particles.

## 1.8. *Objectives and Hypotheses*

First the nanostructuring of titania by established methods is to be investigated. In particular, it was hoped that the use of inverse opaline titania would enable the use of species such as porphyrin dendrimers to sensitise the surface without aggregation. Secondly, adsorption of dyes *via* carboxylic functionality to the surface of titania is to be studied, in order to resolve debate over the mode of dye binding. Understanding the mode of acid binding to titania would also aid work towards the formation of chemically-assisted, self-assembled superlattices of titania nanoparticles. The ideal case would be for stable, multiple layers of dye-sensitised titania nanoparticles to be adsorbed onto a transparent conducting substrate by facilitation with fully conjugated, monomeric, organic species.

Objectives include:

- The formation of nanostructured titania electrodes by methods such as templation of opals, screen-printing, spin- and dip-coating and by sol-gel techniques.
- To produce and test inverse opaline titania for Grätzel cell efficiency and to use nanostructured titania in studies to investigate the binding of dye to titania.
- To functionalise ITO glass with small, fully conjugated molecules which bind *via* an amine or carboxylic acid functionality, rather than a non-conjugated alkoxy silane species.
- To work towards the assembly of a titania nanoparticle superlattice electrode upon ITO glass by the use of small and fully conjugated species.
- To investigate how sensitizer dyes and ‘probe’ species bind onto a titania surface *via* carboxylic acid groups.

## 1.9. References

1. Monro, A D; Gibbs, H S. Vanadium and Titanium in Taranaki Ironsand. *New Zealand Journal of Science and Technology* **1938**, 19, 523-526.
2. Mason, B. Utilization of New Zealand Ironsands as a Source of Fe, Ti, and V. *New Zealand Journal of Science and Technology* **1945**, 26B, 227-238.
3. Nishimura, S; Abrams, N; Lewis, B; Halaoui, L I; Mallouk, T E; Benkstein, K D; van de Lagemaat, J; Frank, A J. Standing Wave Enhancement of Red Absorbance and Photocurrent in Dye-Sensitized Titanium Dioxide Photoelectrodes Coupled to Photonic Crystals. *Journal of the American Chemical Society* **2003**, 125, 6306-6310.
4. Kuo, M-Y; Chen, C-L; Hua, C-Y; Yang, H-C; Shen, P. Density Functional Theory Calculations of Dense TiO<sub>2</sub> Polymorphs: Implication for Visible-Light-Responsive Photocatalysts. *Journal of Physical Chemistry B* **2005**, 109, 8693-8700.
5. Ren, R; Yang, Z; Shaw, L L. Polymorphic Transformation and Powder Characteristics of TiO<sub>2</sub> during High Energy Milling. *Journal of Materials Science* **2000**, 35, 6015-6026.
6. Roberts, W L; Campbell, T J; Rapp, G R J. *Encyclopedia of Materials*. 2<sup>nd</sup> ed, Van Nostrand Reinhold Co.: New York, USA, **1990**.
7. Kim, D J; Hahn, S H; Oh, S H; Kim, E J. Influence of Calcination Temperature on Structural and Optical Properties of TiO<sub>2</sub> Thin Films Prepared by Sol-Gel Dip Coating. *Materials Letters* **2002**, 57, 355-360.
8. Zhang, Y; Ebbinghaus, S G; Weidenkaff, A; Kurz, T; Krug von Nidda, H-A; Klar, P J; Gungerich, M; Reller, A. Controlled Iron-Doping of Macrot textured Nanocrystalline Titania. *Chemistry of Materials* **2003**, 15, 4028-4033.
9. Jung, H S; Shing, H; Kim, J-R; Kim, J Y; Hong, K S; Lee, J-K. *In Situ* Observation of the Stability of Anatase Nanoparticles and their Transformation to Rutile in an Acidic Solution. *Langmuir* **2004**, 20, 11732-11737.
10. Yang, Q; Xie, C; Xu, Z; Gao, Z; Du, Y. Synthesis of Highly Active Sulfate-Promoted Rutile Titania Nanoparticles with a Response to Visible Light. *Journal of Physical Chemistry B* **2005**, 109, 5554-5560.
11. Beltran, A; Gracia, L; Andres, J. Density Functional Theory Study of the Brookite Surfaces and Phase Transitions Between Natural Titania Polymorphs. *Journal of Physical Chemistry B* **2006**, 110, 23417-23423.
12. Li, J-G; Ishigaki, T. Brookite to Rutile Phase Transformation of TiO<sub>2</sub> Studied with Monodispersed Particles. *Acta Materialia* **2004**, 52, 5143-5150.
13. So, W W; Park, S B; Kim, K J; Shin, C H; Moon, S J. The Crystalline Phase Stability of Titania Particles Prepared at Room Temperature by the Sol-Gel Method. *Journal of Materials Science* **2001**, 36, 4299-4305.
14. Olsen, J S; Gerwald, L; Jiang, J Z. On the Rutile/ $\alpha$ -PbO<sub>2</sub>-type Phase Boundary of TiO<sub>2</sub>. *Journal of Physics and Chemistry of Solids* **1999**, 60, 229-233.
15. Withers, A C; Essene, E J; Zhang, Y. Rutile/TiO<sub>2</sub>-II Phase Equilibria. *Contributions to Mineralogy and Petrology* **2003**, 145, 199-204.
16. Hong, X; Wang, Z; Cai, W; Lu, F; Zhang, J; Yang, Y; Ma, N; Liu, Y. Visible-Light-Activated Nanoparticle Photocatalyst of Iodine-Doped Titanium Dioxide. *Chemistry of Materials* **2005**, 17, 1548-1552.

17. Al-Salim, N I; Bagshaw, S A; Bittar, A; Kemmitt, T; McQuillan, A J; Mills, A M; Ryan, M J. Characterisation and Activity of Sol-Gel Prepared TiO<sub>2</sub> Photocatalysts Modified with Ca, Sr, or Ba Ion Additives. *Journal of Materials Chemistry* **2000**, 10, 2358-2363.
18. Livraghi, S; Paganini, M C; Giamello, E; Selloni, A; Di Valentin, C; Pacchioni, G. Origin of Photoactivity of Nitrogen-Doped Titanium Dioxide Under Visible Light. *Journal of the American Chemical Society* **2006**, 128, 15666-15671.
19. Burda, C; Lou, Y; Chen, X; Samia, A C S; Stout, J; Gole, J L. Enhanced Nitrogen Doping in TiO<sub>2</sub> Nanoparticles. *Nano Letters* **2003**, 3, 1049-1051.
20. Bacsa, R; Kiwi, J; Ohno, T; Albers, P; Nadtochenko, V. Preparation, Testing and Characterisation of Doped TiO<sub>2</sub> Active in the Peroxidation of Biomolecules under Visible Light. *Journal of Physical Chemistry B* **2005**, 109, 5994-6003.
21. Chen, X; Burda, C. Photoelectron Spectroscopic Investigation of Nitrogen-Doped Titania Nanoparticles. *Journal of Physical Chemistry B* **2004**, 108, 15446-15449.
22. Ma, T; Akiyama, M; Abe, E; Imai, I. High-Efficiency Dye-Sensitized Solar Cell Based on a Nitrogen-Doped Nanostructured Titania Electrode. *Nano Letters* **2005**, 5, 2543-2547.
23. Diamant, V; Chen, S G; Melamed, O; Zaban, A. Core-Shell Nanoporous Electrode for Dye Sensitized Solar Cells: the Effect of the SrTiO<sub>3</sub> Shell on the Electronic Properties of the TiO<sub>2</sub> Core. *Journal of Physical Chemistry B* **2003**, 107, 1977-1981.
24. Chen, S G; Chappel, S; Diamant, Y; Zaban, A. Preparation of Nb<sub>2</sub>O<sub>5</sub> Coated TiO<sub>2</sub> Nanoporous Electrodes and their Application in Dye-Sensitized Solar Cells. *Chemistry of Materials* **2001**, 13, 4629-4634.
25. Allen, N S; Edge, M; Ortega, A; Sandoval, G; Liauw, C M; Verran, J; Stratton, J; McIntyre, R B. Degradation and Stabilisation of Polymers and Coatings: Nano versus Pigmentary Titania Particles. *Polymer Degradation and Stability* **2004**, 85, 927-946.
26. Davit, P; Martra, G; Coluccia, S; Augugliaro, V; Garcia Lopez, E; Loddo, V; Marci, G; Palmisano, L; Schiavello, M. Adsorption and Photocatalytic Degradation of Acetonitrile: FT-IR Investigation. *Journal of Molecular Catalysis A: Chemical* **2003**, 204-205, 693-701.
27. Kemmitt, T; Al-Salim, N I; Waterland, M; Kennedy, V J; Markwitz, A. Photocatalytic Titania Coatings. *Current Applied Physics* **2004**, 4, 189-192.
28. Zhang, X-T; Sato, O; Taguchi, M; Einaga, Y; Murakami, T; Fujishima, A. Self-Cleaning Particle Coating with Antireflection Properties. *Chemistry of Materials* **2005**, 17, 696-700.
29. San Vicente, G; Morales, A; Gutierrez, M T. Sol-Gel TiO<sub>2</sub> Antireflective Films for Textured Monocrystalline Silicon Solar Cells. *Thin Solid Films* **2002**, 403-404, 335-338.
30. Eranna, G; Joshi, B C; Runthala, D P; Gupta, R P. Oxide Materials for Development of Integrated Gas Sensors - A Comprehensive Review. *Critical Reviews in Solid State and Materials Sciences* **2004**, 29, 111-188.
31. Parker, G J; Charlton, M D B. Photonic Crystals. <http://physicsweb.org/articles/world/13/8/9/1> (5th April),
32. Grätzel, M. Sol-Gel Processed TiO<sub>2</sub> Films for Photovoltaic Applications. *Journal of Sol-Gel Science and Technology* **2001**, 22, 7-13.
33. Premkumar, J. Highly Hydrophilic TiO<sub>2</sub> Surface Induced by Anodic Potentials. *Chemistry of Materials* **2005**, 17, 944-946.
34. Stevens, N; Priest, C I; Sedev, R; Ralston, J. Wettability of Photoresponsive Titanium Dioxide

Surfaces. *Langmuir* **2003**, 19, 3272-3275.

35. Mills, A; Lepre, A; Elliott, N; Bhopal, S; Parkin, I P; O'Neill, S A. Characterisation of the Photocatalyst Pilkington Activ™: a Reference Film Photocatalyst. *Journal of Photochemistry and Photobiology A: Chemistry* **2003**, 160, 213-224.

36. Subramanian, V; Wolf, E E; Kamat, P V. Catalysis with TiO<sub>2</sub>/Gold Nanocomposites. Effect of Metal Particle Size on the Fermi Level Equilibration. *Journal of the American Chemical Society* **2004**, 126, 4943-4950.

37. Hurum, D C; Gray, K A; Rajh, T; Thurnauer, M C. Recombination Pathways in the Degussa P25 Formulation of TiO<sub>2</sub>: Surface versus Lattice Mechanisms. *Journal of Physical Chemistry B* **2005**, 109, 977-980.

38. Jochem, E K. An Efficient Solution. *Scientific American* **2006**, September, 40-43.

39. Heywood, J B. Fueling Our Transportation Future. *Scientific American* **2006**, September, 36-39.

40. Kammen, D M. The Rise of Renewable Energy. *Scientific American* **2006**, September, 60-69.

41. Eisenberg, R; Nocera, D G. Preface: Overview of the Forum on Solar and Renewable Energy. *Inorganic Chemistry* **2005**, 44, 6799-6801.

42. Tributsch, H. Dye Sensitization Solar Cells: a Critical Assessment of the Learning Curve. *Coordination Chemistry Reviews* **2004**, 248, 1511-1530.

43. Deb, S K. Frontiers in Photovoltaic Materials and Devices. *Current Opinion in Solid State and Materials Science* **1998**, 3, 51-59.

44. Krc, J; Cernivec, G; Campa, A; Malmstrom, J; Edoff, M; Smole, F; Topic, M. Optical and Electrical Modelling of Cu(In, Ga)Se<sub>2</sub> Solar Cells. *Optical and Quantum Electronics* **2006**, 38, 1115-1123.

45. Green, M A; Emery, K; King, D L; Hishikawa, Y; Warta, W. Solar Cell Efficiency Tables (Version 29). *Progress in Photovoltaics: Research and Applications* **2007**, 15, 35-40.

46. Kannan, B; Castelino, K; Majumdar, A. Design of Nanostructured Heterojunction Polymer Photovoltaic Devices. *Nano Letters* **2003**, 3, 1729-1733.

47. Moliton, A; Hiorns, R C. Review of Electronic and Optical Properties of Semiconducting  $\pi$ -Conjugated Polymers: Applications in Optoelectronics. *Polymer International* **2004**, 53, 1397-1412.

48. Yang, X; Loos, J; Veenstra, S C; Verhees, W J H; Wienk, M M; Kroon, J M; Michels, M A J; Janssen, R A J. Nanoscale Morphology of High-Performance Polymer Solar Cells. *Nano Letters* **2005**, 5, 579-583.

49. Dyakonov, V. Mechanisms Controlling the Efficiency of Polymer Solar Cells. *Applied Physics A: Materials Science & Processing* **2004**, 79, 21-25.

50. Ma, W; Yang, C; Gong, X; Lee, K; Heeger, A J. Thermally Stable, Efficient Polymer Solar Cells with Nanoscale Control of the Interpenetrating Network Morphology. *Advanced Functional Materials* **2005**, 15, 1617-1622.

51. Sun, S-S; Sacriciftci, N S. *Organic Photovoltaics. Mechanisms, Materials and Devices*. Taylor & Francis Group, Florida, USA: **2005**.

52. Imahori, H. Giant Multiporphyrin Arrays as Artificial Light-Harvesting Antennas. *Journal of Physical Chemistry B* **2004**, 108, 6130-6143.

53. Miyasaka, T; Kijitori, Y. Low-Temperature Fabrication of Dye-Sensitised Plastic Electrodes by

- Electrophoretic Preparation of Mesoporous TiO<sub>2</sub> Layers. *Journal of the Electrochemical Society* **2004**, 151, A1767-A1773.
54. Nissfolk, J; Fredin, K; Hagfeldt, A; Boschloo, G. Recombination and Transport Processes in Dye-Sensitized Solar Cells Investigated Under Working Conditions. *Journal of Physical Chemistry B* **2006**, 110, 17715-17718.
55. Splan, K E; Massari, A M; Hupp, J T. A Porous Multilayer Dye-Based Photoelectrochemical Cell that Unexpectedly Runs in Reverse. *Journal of Physical Chemistry B* **2004**, 108, 4111-4115.
56. Koelsch, M; Cassaignon, S; Ta Thanh Minh, C; Guillemoles, J-F; Jolivet, J-P. Electrochemical Comparative Study of Titania (Anatase, Brookite and Rutile) Nanoparticles Synthesized in Aqueous Medium. *Thin Solid Films* **2004**, 451-452, 86-92.
57. Park, N-G; van de Lagemaat, J; Frank, A J. Comparison of Dye-Sensitized Rutile- and Anatase-Based TiO<sub>2</sub> Solar Cells. *Journal of Physical Chemistry B* **2000**, 104, 8989-8994.
58. Keis, K; Magnusson, E; Lindstrom, H; Lindquist, S-E; Hagfeldt, A. A 5% Efficient Photoelectrochemical Solar Cell Based on Nanostructured ZnO Electrodes. *Solar Energy Materials & Solar Cells* **2002**, 73, 51-58.
59. Tan, B; Toman, E; Li, Y; Wu, Y. Zinc Stannate (Zn<sub>2</sub>SnO<sub>4</sub>) Dye-Sensitized Solar Cells. *Journal of the American Chemical Society* **2007**, 129, 4162-4163.
60. Niinobe, D; Makari, Y; Kitamura, T; Wada, Y; Yanagida, S. Origin of Enhancement in Open-Circuit Voltage by Adding ZnO to Nanocrystalline SnO<sub>2</sub> in Dye-Sensitized Solar Cells. *Journal of Physical Chemistry B* **2005**, 109, 17892-17900.
61. Berger, T; Sterrer, M; Diwald, O; Knozinger, E; Panayotov, D; Thompson, T L; Yates, J T J. Light-Induced Charge Separation in Anatase TiO<sub>2</sub> Particles. *Journal of Physical Chemistry B* **2005**, 109, 6061-6068.
62. Zhang, Z; Zakeeruddin, S M; O'Regan, B C; Humphry-Baker, R; Grätzel, M. Influence of 4-Guanidinobutyric Acid as Coadsorbent in Reducing Recombination in Dye-Sensitized Solar Cells. *Journal of Physical Chemistry B* **2005**, 109, 21818-21824.
63. Yang, H; Yu, C; Song, Q; Xia, Y; Li, F; Chen, Z; Li, X; Yi, T; Huang, C. High-Temperature and Long-Term Stable Solid-State Electrolyte for Dye-Sensitized Solar Cells by Self-Assembly. *Chemistry of Materials* **2006**, 18, 5173-5177.
64. Kubo, W; Kambe, S; Nakade, S; Kitamura, T; Hanabusa, K; Wada, Y; Yanagida, S. Photocurrent-Determining Processes in Quasi-Solid-State Dye-Sensitized Solar Cells Using Ionic Gel Electrolytes. *Journal of Physical Chemistry B* **2003**, 107, 4374-4381.
65. Smestad, G P; Spiekermann, S; Kowalik, J; Grant, C D; Schwartzberg, A M; Zhang, J; Tolbert, L M; Moons, E. A Technique to Compare Polythiophene Solid-State Dye Sensitized TiO<sub>2</sub> Solar Cells to Liquid Junction Devices. *Solar Energy Materials & Solar Cells* **2003**, 76, 85-105.
66. Peter, K; Wietasch, H; Peng, B; Thelakkat, M. Dual-Functional Materials for Interface Modifications in Solid-State Dye-Sensitized TiO<sub>2</sub> Solar Cells. *Applied Physics A: Materials Science & Processing* **2004**, 79, 65-71.
67. Nakade, S; Makimoto, Y; Kubo, W; Kitamura, T; Wada, Y; Yanagida, S. Roles of Electrolytes on Charge Recombination in Dye-Sensitized TiO<sub>2</sub> Solar Cells (1): the Case of Solar Cells Using the I<sup>-</sup>/I<sub>3</sub><sup>-</sup> Redox Couple. *Journal of Physical Chemistry B* **2005**, 109, 3480-3487.
68. Nakade, S; Makimoto, Y; Kubo, W; Kitamura, T; Wada, Y; Yanagida, S. Roles of Electrolytes on Charge Recombination in Dye-Sensitized TiO<sub>2</sub> Solar Cells (2): the Case of Solar Cells Using Cobalt Complex Redox Couples. *Journal of Physical Chemistry B* **2005**, 109, 3488-3493.

69. Olson, C L; Ballard, I. Charge Accumulation and Polarization in Titanium Dioxide Electrodes. *Journal of Physical Chemistry B* **2006**, 110, 18286-18290.
70. Boschloo, G; Hagglman, L; Hagfeldt, A. Quantification of the Effect of 4-*tert*-Butylpyridine Addition to  $I^-/I_3^-$  Redox Electrolytes in Dye-Sensitized Nanostructured  $TiO_2$  Solar Cells. *Journal of Physical Chemistry B* **2006**, 110, 13144-13150.
71. Peter, L M; Wijayantha, K G U. Electron Transport and Back Reaction in Dye Sensitized Nanocrystalline Photovoltaic Cells. *Electrochimica Acta* **2000**, 45, 4543-4551.
72. Cameron, P J; Peter, L M; Hore, S. How Important is the Back Reaction of Electrons via the Substrate in Dye-Sensitized Nanocrystalline Solar Cells? *Journal of Physical Chemistry B* **2005**, 109, 930-936.
73. Bisquert, J; Cahen, D; Hodes, G; Ruhle, S; Zaban, A. Physical Chemical Principles of Photovoltaic Conversion with Nanoparticulate, Mesoporous Dye-Sensitized Solar Cells. *Journal of Physical Chemistry B* **2004**, 108, 8106-8118.
74. Frank, A J; Kopidakis, N; van de Lagemaat, J. Electrons in Nanostructured  $TiO_2$  Solar Cells: Transport, Recombination and Photovoltaic Properties. *Coordination Chemistry Reviews* **2004**, 248, 1165-1179.
75. Chandrasekharan, N; Kamat, P V. Improving the Photoelectrochemical Performance of Nanostructured  $TiO_2$  Films by Adsorption of Gold Nanoparticles. *Journal of Physical Chemistry B* **2000**, 104, 10851-10857.
76. Wang, P; Wang, L; Ma, B; Li, B; Qiu, Y.  $TiO_2$  Surface Modification and Characterization with Nanosized PbS in Dye-Sensitized Solar Cells. *Journal of Physical Chemistry B* **2006**, 110, 14406-14409.
77. Park, H; Choi, W. Effects of  $TiO_2$  Surface Fluorination on Photocatalytic Reactions and Photoelectrochemical Behaviours. *Journal of Physical Chemistry B* **2004**, 108, 4086-4093.
78. Wang, Z-S; Yanagida, M; Sayama, K; Sugihara, H. Electronic-Insulating Coating of  $CaCO_3$  on  $TiO_2$  Electrode in Dye-Sensitized Solar Cells: Improvement of Electron Lifetime and Efficiency. *Chemistry of Materials* **2006**, 18, 2912-2916.
79. Hagfeldt, A; Grätzel, M. Molecular Photovoltaics. *Accounts of Chemical Research* **2000**, 33, 269-277.
80. Grätzel, M. Mesoporous Oxide Junctions and Nanostructured Solar Cells. *Current Opinion in Colloid & Interface Science* **1999**, 4, 314-321.
81. Nakade, S; Saito, Y; Kubo, W; Kitamura, T; Wada, Y; Yanagida, S. Influence of  $TiO_2$  Nanoparticle Size on Electron Diffusion and Recombination in Dye-Sensitized  $TiO_2$  Solar Cells. *Journal of Physical Chemistry B* **2003**, 107, 8607-8611.
82. Grätzel, M. Solar Energy Conversion by Dye-Sensitized Photovoltaic Cells. *Inorganic Chemistry* **2005**, 44, 6841-6851.
83. Sommeling, P M; O'Regan, B C; Haswell, R R; Smit, J J P; Bakker, N J; Smits, J J T; Kroon, J M; van Roosmalen, J A M. Influence of a  $TiCl_4$  Post-Treatment on Nanocrystalline  $TiO_2$  Films in Dye-Sensitized Solar Cells. *Journal of Physical Chemistry B* **2006**, 110, 19191-19197.
84. Halaoui, L I; Abrams, N M; Mallouk, T E. Increasing the Conversion Efficiency of Dye-Sensitized  $TiO_2$  Photoelectrochemical Cells by Coupling to Photonic Crystals. *Journal of Physical Chemistry B* **2005**, 109, 6334-6342.
85. Berg, M C; Choi, J; Hammond, P T; Rubner, M F. Tailored Micropatterns through Weak Polyelectrolyte Stamping. *Langmuir* **2003**, 19, 2231-2237.

86. Bhattarai, N; Cha, D I; Bhattarai, S R; Khil, M S; Kim, H Y. Biodegradable Electrospun Mat: Novel Block Copolymer of Poly(*p*-dioxanone-*co*-lactide)-block-poly(ethylene glycol). *Journal of Polymer Science: Part B: Polymer Physics* **2003**, 41, 1955-1964.
87. Gates, B D; Xu, Q; Stewart, M; Ryan, D; Willson, C G; Whitesides, G M. New Approaches to Nanofabrication: Moulding, Printing, and Other Techniques. *Chemical Reviews* **2005**, 105, 1171-1196.
88. Masuda, Y; Itoh, T; Itoh, M; Koumoto, K. Self-Assembly Patterning of Colloidal Crystals Constructed from Opal Structure or NaCl Structure. *Langmuir* **2004**, 20, 5588-5592.
89. Gu, Z-Z; Fujishima, A; Sato, O. Patterning of a Colloidal Crystal Film on a Modified Hydrophilic and Hydrophobic Surface. *Angewandte Chemie, International Edition* **2002**, 41, 2067-2070.
90. Zhou, Z; Yan, Q; Li, Q; Zhao, X S. Fabrication of Binary Colloidal Crystals and Non-Close-Packed Structures by a Sequential Self-Assembly Method. *Langmuir* **2007**, 23, 1473-1477.
91. Linden, M; Schacht, S; Schuth, F; Steel, A; Unger, K K. Recent Advances in Nano- and Macroscale Control of Hexagonal, Mesoporous Materials. *Journal of Porous Materials* **1998**, 5, 177-193.
92. Qadri, S B; Skelton, E F; Hsu, D; Dinsmore, A D; Yang, J; Gray, H F; Ratna, B R. Size-Induced Transition-Temperature Reduction in Nanoparticles of ZnS. *Physical Review B* **1999**, 60, 9191-9193.
93. Yang, J P; Qadri, S B; Ratna, B R. Structural and Morphological Characterization of PbS Nanocrystallites Synthesized in the Bicontinuous Cubic Phase of a Lipid. *Journal of Physical Chemistry* **1996**, 100, 17255-17259.
94. Stathatos, E; Lianos, P; Del Monte, F; Levy, D; Tsiourvas, D. Formation of TiO<sub>2</sub> Nanoparticles in Reverse Micelles and Their Deposition as Thin Films on Glass Substrates. *Langmuir* **1997**, 13, 4295-4300.
95. Szekeres, M; Kamalin, O; Grobet, P G; Schoonheydt, R A; Wostyn, K; Clays, K; Persoons, A; Dekany, I. Two-Dimensional Ordering of Stober Silica Particles at the Air/Water Interface. *Colloids and Surfaces A: Physicochemical and Engineering Aspects* **2003**, 227, 77-83.
96. Saunders, A E; Shah, P S; Sigman, M B J; Hanrath, T; Hwang, H S; Lim, K T; Johnston, K P; Korgel, B A. Inverse Opal Nanocrystal Superlattice. *Nano Letters* **2004**, 4, 1943-1948.
97. Mafune, F; Kohno, J-y; Takeda, Y; Kondow, T. Formation of Stable Platinum Nanoparticles by Laser Ablation in Water. *Journal of Physical Chemistry B* **2003**, 2003.
98. Heine, J R; Rodriguez-Viejo, J; Bawendi, M G; Jensen, K F. Synthesis of CdSe Quantum Dot-ZnS Matrix Thin Films via Electrospray Organometallic Chemical Vapour Deposition. *Journal of Crystal Growth* **1998**, 195, 564-568.
99. Park, S H; Xia, Y. Assembly of Mesoscale Particles over Large Areas and Its Application in Fabricating Tunable Optical Filters. *Langmuir* **1999**, 15, 266-273.
100. Yusuf, H; Kim, W-G; Lee, D H; Aleshyna, M; Brolo, A G; Moffit, M G. A Hierarchical Self-Assembly Route to Three Dimensional Polymer-Quantum Dot Photonic Arrays. *Langmuir* **2007**, 23, 5251-5254.
101. Sadana, A K; Liang, F; Brinson, B; Arepalli, S; Farhat, S; Hauge, R H; Smalley, R E; Billups, W E. Functionalisation and Extraction of Large Fullerenes and Carbon-Coated Metal Formed During the Synthesis of Single Wall Carbon Nanotubes by Laser Oven, Direct Current Arc and High-Pressure Carbon Monoxide Production Methods. *Journal of Physical Chemistry B* **2005**, 109, 4416-4418.
102. Georgakilas, V; Guldi, D M; Signorini, R; Bozio, R; Prato, M. Organic Functionalization and Optical Properties of Carbon Onions. *Journal of the American Chemical Society* **2003**, 125, 14268-14269.
103. Feldman, Y; Lyakhovitskaya, V; Tenne, R. Kinetics of Nested Inorganic Fullerene-like

- Nanoparticle Formation. *Journal of the American Chemical Society* **1998**, 120, 4176-4183.
104. Kondo, D; Kawabata, A; Horibe, M; Nihei, M; Awano, Y. Vertically Aligned Peapod Formation of Position-Controlled Multi-Walled Carbon Nanotubes (MWNTs). *Superlattices and Microstructures* **2003**, 34, 389-394.
105. Yoon, J D; Park, K Y; Jang, H D. Comparison of Titania Particles Between Oxidation of Titanium Tetrachloride and Thermal Decomposition of Titanium Tetraisopropoxide. *Aerosol Science and Technology* **2003**, 37, 621-627.
106. Hyde, K; Rusa, M; Hinestroza, J. Layer-by-Layer Deposition of Polyelectrolyte Nanolayers on Natural Fibres: Cotton. *Nanotechnology* **2005**, 16, S422-S428.
107. Hao, E; Yang, B; Ren, H; Qian, X; Xie, T; Shen, J; Li, D. Fabrication of Composite Film Comprising TiO<sub>2</sub>/CdS and Polyelectrolytes Based on Ionic Attraction. *Materials Science and Engineering C* **1999**, 10, 119-122.
108. Hao, E; Lian, T. Buildup of Polymer/Au Nanoparticle Multilayer Thin Films Based on Hydrogen Bonding. *Chemistry of Materials* **2000**, 12, 3392-3396.
109. Costa, C A R; Leite, C A P; Galembeck, F. Size Dependence of Stober Silica Nanoparticle Microchemistry. *Journal of Physical Chemistry B* **2003**, 107, 4747-4755.
110. Bogush, G H; Tracey, M A; Zukoski, C F I. Preparation of Monodisperse Silica Particles: Control of Size and Mass Fraction. *Journal of Non-Crystalline Solids* **1988**, 104, 95-106.
111. Brust, M; Fink, J; Bethell, D; Schriffin, D J; Kiely, C. Synthesis and Reactions of Functionalised Gold Nanoparticles. *Journal of the Chemical Society, Chemical Communications* **1995**, 16, 1655-1656.
112. Murray, C B; Norris, D J; Bawendi, M G. Synthesis and Characterisation of Nearly Monodisperse CdE (E=S, Se, Te) Semiconductor Nanocrystallites. *Journal of the American Chemical Society* **1993**, 115, 8706-8715.
113. Maye, M M; Lim, I-I S; Luo, J; Rab, Z; Rabinovich, D; Liu, T; Zhong, C-J. Mediator-Template Assembly of Nanoparticles. *Journal of the American Chemical Society* **2005**, 127, 1519-1529.
114. Chen, C-C; Yet, C-P; Wang, H-N; Chao, C-Y. Self-Assembly of Monolayers of Cadmium Selenide Nanocrystals with Dual Colour Emission. *Langmuir* **1999**, 15, 6845-6850.
115. Mitchell, G P; Mirkin, C A; Letsinger, R L. Programmed Assembly of DNA Functionalized Quantum Dots. *Journal of the American Chemical Society* **1999**, 121, 8122-8123.
116. Supriya, L; Claus, R O. Colloidal Au/Linker Molecule Multilayer Films: Low-Temperature Thermal Coalescence and Resistance Changes. *Chemistry of Materials* **2005**, 17, 4325-4334.
117. McQuillan, A J. Probing Solid-Solution Interfacial Chemistry with ATR-IR Spectroscopy of Particle Films. *Advanced Materials* **2001**, 13, 1034-1038.
118. Adams, L K; Lyon, D Y; Alvarez, P J J. Comparative Eco-Toxicity of Nanoscale TiO<sub>2</sub>, SiO<sub>2</sub> and ZnO Water Suspensions. *Water Research* **2006**, 40, 3527-3532.
119. Huang, W; Tang, X; Wang, Y; Kolytyn, Y; Gedanken, A. Selective Synthesis of Anatase and Rutile via Ultrasound Radiation. *Chemical Communications* **2000**, 1415-1416.
120. Jaroenworoluck, A; Sunsaneeyametha, W; Kosachan, N; Stevens, R. Characteristics of Silica-Coated TiO<sub>2</sub> and Its UV Absorption for Sunscreen Cosmetic Applications. *Surface and Interface Analysis* **2006**, 38, 473-477.
121. Wolfbauer, G; Bond, A M; Ekund, J C; MacFarlane, D R. A Channel Flow Cell System Specifically Designed to Test the Efficiency of Redox Shuttles in Dye Sensitized Solar Cells. *Solar Energy Materials*

& *Solar Cells* **2001**, 70, 85-101.

122. Tirosh, S; Dittrich, T; Ofir, A; Grinis, L; Zaban, A. Influence of Ordering in Porous TiO<sub>2</sub> Layers on Electron Diffusion. *Journal of Physical Chemistry B* **2006**, 110, 16165-16168.

123. Lakshmi, B B; Patrissi, C J; Martin, C R. Sol-Gel Template Synthesis of Semiconductor Oxide Micro- and Nanostructures. *Chemistry of Materials* **1997**, 9, 2544-2550.

124. Chappel, S; Chen, S-G; Zaban, A. TiO<sub>2</sub>-Coated Nanoporous SnO<sub>2</sub> Electrodes for Dye-Sensitized Solar Cells. *Langmuir* **2002**, 18, 3336-3342.

125. Ding, B; Kim, J; Kimura, E; Shiratori, S. Layer-by-Layer Structured Films of TiO<sub>2</sub> Nanoparticles and Poly(acrylic acid) on Electrospun Nanofibres. *Nanotechnology* **2004**, 15, 913-917.

126. Kim, I-D; Rothschild, A L, Byong Hong; Kim, Dong, Young; Jo, Seong Mu; Tuller, Harry L;. Ultrasensitive Chemiresistors Based on Electrospun TiO<sub>2</sub> Nanofibers. *Nano Letters* **2006**, 6, 2009-2013.

127. Ostermann, R; Li, D Y, Yadong; McCann, Jesse T; Xia, Younan;. V<sub>2</sub>O<sub>5</sub> Nanorods of TiO<sub>2</sub> Nanofibres: A New Class of Hierarchical Nanostructures Enabled by Electrospinning and Calcination. *Nano Letters* **2006**, 6, 1297-1302.

128. Kokubo, H; Ding, B; Naka, T; Tsuchihira, H; Shiratori, S. Multi-Core Cable-Like TiO<sub>2</sub> Nanofibrous Membranes for Dye-Sensitized Solar Cells. *Nanotechnology* **2007**, 18, 165604.

129. Tokuhisa, H; Hammond, P T. Solid-State Photovoltaic Thin Films Using TiO<sub>2</sub>, Organic Dyes, and Layer-by-Layer Polyelectrolyte Nanocomposites. *Advanced Functional Materials* **2003**, 13, 831-839.

130. Yang, P; Yang, M; Zou, S; Xie, J; Yang, W. Positive and Negative TiO<sub>2</sub> Micropatterns on Organic Polymer Substrates. *Journal of the American Chemical Society* **2007**, 129, 1541-1552.

131. Xiang, J; Masuda, Y; Koumoto, K. Fabrication of Super-Site-Selective TiO<sub>2</sub> Micropattern on a Flexible Polymer Substrate Using a Barrier-Effect Self-Assembly Process. *Advanced Materials* **2004**, 16, 1461-1464.

132. Bartz, M; Terfort, A; Knoll, W; Tremel, W. Stamping of Monomeric SAMs as a Route to Structured Crystallization Templates: Patterned Titania Films. *Chemistry - a European Journal* **2000**, 6, 4149-4153.

133. Lindstrom, H; Holmber, A; Magnusson, E; Lindquist, S-E; Malmqvist, L; Hagfeldt, A. A New Method for Manufacturing Nanostructured Electrodes on Plastic Substrates. *Nano Letters* **2001**, 1, 91-100.

134. Zaban, A; Ferrere, S; Sprague, J; Gregg, B A. pH-Dependent Redox Potential Induced in a Sensitizing Dye by Adsorption onto TiO<sub>2</sub>. *Journal of Physical Chemistry B* **1997**, 101, 55-57.

135. Kim, J; Song, K C; Pratsinis, S E. The Effect of Hydrolysis Temperature on Synthesis of Bimodally Nanostructured Porous Titania. *Journal of Nanoparticle Research* **2000**, 2, 419-424.

136. Ma, T; Kida, T; Akiyama, M; Inoue, K; Tsunematsu, S; Yao, K; Noma, H; Eiichi, A. Preparation and Properties of Nanostructured TiO<sub>2</sub> Electrode by a Polymer Organic-Medium Screen-Printing Technique. *Electrochemistry Communications* **2003**, 5, 369-372.

137. Choi, S Y; Mamak, M; Coombs, N; Chopra, N; Ozin, G A. Electrochromic Performance of Viologen-Modified Periodic Mesoporous Nanocrystalline Anatase Electrodes. *Nano Letters* **2004**, 4, 1231-1235.

138. Smarsly, B; Grosso, D; Brezesinski, T; Pinna, N; Boissiere, C; Antonietti, M; Sanchez, C. Highly Crystalline Cubic Mesoporous TiO<sub>2</sub> with 10 nm Pore Diameter Made with a New Block Copolymer Template. *Chemistry of Materials* **2004**, 16, 2948-2952.

139. Yusuf, M M; Imai, H; Hirashima, H. Preparation of Mesoporous TiO<sub>2</sub> Thin Films by Surfactant

- Templating. *Journal of Non-Crystalline Solids* **2001**, 285, 90-95.
140. Bartl, M H; Boettcher, S W; Frindell, K L; Stucky, G D. 3D Molecular Assembly of Function in Titania-Based Composite Material Systems. *Accounts of Chemical Research* **2005**, 38, 263-271.
141. Wu, C-W; Ohsuna, T; Kuwabara, M; Kuroda, K. Formation of Highly Ordered Mesoporous Titania Films Consisting of Crystalline Nanopillars with Inverse Mesospace by Structural Transformation. *Journal of the American Chemical Society* **2006**, 128, 4544-4545.
142. Zukalova, M; Zukai, A; Kavan, L; Nazeeruddin, M K; Liska, P; Grätzel, M. Organized Mesoporous TiO<sub>2</sub> Films Exhibiting Greatly Enhanced Performance in Dye-Sensitized Solar Cells. *Nano Letters* **2005**, 5, 1789-1792.
143. Choi, S Y; Mamak, M; Coombs, N; Chopra, N; Ozin, G A. Thermally Stable Two-Dimensional Hexagonal Mesoporous Nanocrystalline Anatase, Meso-nc-TiO<sub>2</sub>: Bulk and Crack-Free Thin Film Morphologies. *Advanced Functional Materials* **2004**, 14, 335-344.
144. Zhang, K; Zhang, Z; Chen, H; Chen, X; Zheng, L; Zhang, J; Yang, B. Hollow Titania Spheres with Movable Silica Spheres Inside. *Langmuir* **2004**, 20, 11312-11314.
145. Cheng, X; Chen, M; Wu, L; Gu, G. Novel and Facile Method for the Preparation of Monodispersed Titania Hollow Spheres. *Langmuir* **2006**, 22, 3858-3863.
146. McComb, D W; Treble, B M; Smith, C J; De La Rue, R M; Johnson, N P. Synthesis and Characterisation of Photonic Crystals. *Journal of Materials Chemistry* **2001**, 11, 142-148.
147. Dong, W; Bongard, H J; Marlow, F. New Type of Inverse Opals: Titania With Skeleton Structure. *Chemistry of Materials* **2003**, 15, 568-574.
148. Cassagneau, T; Caruso, F. Conjugated Polymer Inverse Opals for Potentiometric Biosensing. *Advanced Materials* **2002**, 14, 1837-1841.
149. Kittel, C. *Introduction to Solid State Physics*. 7<sup>th</sup> ed, John Wiley & Sons: Canada, **1996**.
150. Lopez, C. Materials Aspects of Photonic Crystals. *Advanced Materials* **2003**, 15, 1679-1704.
151. Huisman, C L; Schoonman, J; Goossens, A. The Application of Inverse Titania Opals in Nanostructured Solar Cells. *Solar Energy Materials & Solar Cells* **2005**, 85, 115-124.
152. Mihi, A; Miguez, H. Origin of Light-Harvesting Enhancement in Colloidal-Photonic-Crystal-Based Dye-Sensitized Solar Cells. *Journal of Physical Chemistry B* **2005**, 109, 15968-15976.
153. Woo, K; Lee, W I; Lee, J S; Kang, S O. Novel Titanium Compounds for Metal-Organic Chemical Vapor Deposition of Titanium Dioxide Films with an Ultrahigh Deposition Rate. *Inorganic Chemistry* **2003**, 42, 2378-2383.
154. Yang, H G; Zeng, H C. Control of Nucleation in Solution Growth of Anatase TiO<sub>2</sub> on Glass Substrate. *Journal of Physical Chemistry B* **2003**, 107, 12244-12255.
155. Pflieger, J; Pavlik, M; Hebestreit, N; Plieth, W. Photosensitive Layers of TiO<sub>2</sub>/Polythiophene Composites Prepared by Electrodeposition. *Macromolecules Symposium* **2004**, 212, 539-548.
156. Sui, R; Rizkalla, A S; Charpentier, P A. FTIR Study on the Formation of TiO<sub>2</sub> Nanostructures in Supercritical CO<sub>2</sub>. *Journal of Physical Chemistry B* **2006**, 110, 16212-16218.
157. Bavykin, D V; Friedrich, J M; Lapkin, A A; Walsh, F C. Stability of Aqueous Suspensions of Titanate Nanotubes. *Chemistry of Materials* **2006**, 18, 1124-1129.
158. Mao, Y; Wong, S S. Size- and Shape-Dependent Transformation of Nanosized Titanate into Analogous Anatase Titania Nanostructures. *Journal of the American Chemical Society* **2006**, 128, 8217-

8226.

159. Yuan, Z-Y; Su, B-L. Titanium Oxide Nanotubes, Nanofibres and Nanowires. *Colloids and Surfaces A: Physicochemical Engineering Aspects* **2004**, 241, 173-183.
160. Yue, L; Gao, W; Zhang, D; Guo, X; Ding, W; Chen, Y. Colloids Seeded Deposition: Growth of Titania Nanotubes in Solution. *Journal of the American Chemical Society* **2006**, 128, 11042-11043.
161. Kasuga, T; Hiramatsu, M; Hoson, A; Sekino, T; Niihara, K. Titania Nanotubes Prepared by Chemical Processing. *Advanced Materials* **1999**, 11, 1307-1311.
162. Tsai, C-C; Teng, H. Structural Features of Nanotubes Synthesised from NaOH Treatment on TiO<sub>2</sub> with Different Post-Treatments. *Chemistry of Materials* **2006**, 18, 367-373.
163. Kim, G-S; Seo, H-K; Godble, V P; Kim, Y-S; Yang, O-B; Shin, H-S. Electrophoretic Deposition of Titanate Nanotubes from Commercial Titania Nanoparticles: Application to Dye-Sensitized Solar Cells. *Electrochemistry Communications* **2006**, 8, 961-966.
164. Paulose, M; Shankar, K; Yoriya, S; Prakasam, H E; Varghese, O K; Mor, G K; Latempa, T A; Fitzgerald, A; Grimes, C A. Anodic Growth of Highly Ordered TiO<sub>2</sub> Nanotube Arrays to 134 μm in Length. *Journal of Physical Chemistry B* **2006**, 110, 16179-16184.
165. Mor, G K; Varghese, O K; Paulose, M; Grimes, C A. Transparent Highly Ordered TiO<sub>2</sub> Nanotube Arrays via Anodization of Titanium Thin Films. *Advanced Functional Materials* **2005**, 15, 1291-1296.
166. Sun, Y; Hao, E; Zhang, X; Yang, B; Shen, J; Chi, L; Fuchs, H. Buildup of Composite Films Containing TiO<sub>2</sub>/PbS Nanoparticles and Polyelectrolytes Based on Electronic Interaction. *Langmuir* **1997**, 13, 5168-5174.
167. He, J-A; Mosurkal, R; Ssamuelson, L A; Li, L; Kumar, J. Dye-Sensitized Solar Cell Fabricated by Electrostatic Layer-by-Layer Assembly of Amphoteric TiO<sub>2</sub> Nanoparticles. *Langmuir* **2003**, 19, 2169-2174.
168. Polleux, J; Pinna, N; Antonietti, M; Hess, C; Wild, U; Scholgl, R; Niederberger, M. Ligand Functionality as a Versatile Tool to Control the Assembly Behaviour of Preformed Titania Nanocrystals. *Chemistry - a European Journal* **2005**, 11, 3541-3551.
169. Dimitrijevic, N M; Saponjic, Z A; Rabatic, B M; Rajh, T. Assembly and Charge Transfer in Hybrid TiO<sub>2</sub> Architectures Using Biotin-Avidin as a Connector. *Journal of the American Chemical Society* **2005**, 127, 1344-1345.
170. Polleux, J; Pinna, N; Antonietti, M; Niederberger, M. Ligand-Directed Assembly of Preformed Titania Nanocrystals into Highly Anisotropic Nanostructures. *Advanced Materials* **2004**, 16, 436-439.
171. Parala, H; Devi, A; Bhakta, R; Fischer, R A. Synthesis of Nano-Scale TiO<sub>2</sub> Particles by a Nonhydrolytic Approach. *Journal of Materials Chemistry* **2002**, 12, 1625-1627.
172. Marcinko, S; Fadeev, A Y. Hydrolytic Stability of Organic Monolayers Supported on TiO<sub>2</sub> and ZrO<sub>2</sub>. *Langmuir* **2004**, 20, 2270-2273.
173. Shin, H; Jung, H S; Hong, K S; Lee, J-K. Crystallization Process of TiO<sub>2</sub> Nanoparticles in an Acidic Solution. *Chemistry Letters* **2004**, 33, 1382-1383.
174. Burnside, S D; Shklover, V; Barbe, C; Comte, P; Arendse, F; Brooks, K; Grätzel, M. Self-Organization of TiO<sub>2</sub> Nanoparticles in Thin Films. *Chemistry of Materials* **1998**, 10, 2419-2425.
175. Elser, M J; Berger, T; Brandhuber, D; Bernardi, J; Diwald, O; Knozinger, E. Particles Coming Together: Electron Centres in Adjoined TiO<sub>2</sub> Nanocrystals. *Journal of Physical Chemistry B* **2006**, 110, 7605-7608.

176. O'Regan, B; Moser, J; Anderson, M; Grätzel, M. Vectorial Electron Injection into Transparent Semiconductor Membranes and Electric Field Effects on the Dynamics of Light-Induced Charge Separation. *Journal of Physical Chemistry* **1990**, 94, 8720-8726.
177. Linke-Schaetzel, M; Bhise, A D; Gliemann, H; Koch, T; Schimmel, T; Balaban, T S. Self-Assembled Chromopores for Hybrid Solar Cells. *Thin Solid Films* **2004**, 451-452, 16-21.
178. Shipway, A N; Lahav, M; Willner, I. Nanostructured Gold Colloid Electrodes. *Advanced Materials* **2000**, 12, 993-998.
179. Oh, S-Y; Yun, Y-J; Hyung, K-H; Han, S-H. Self-Assembled Monolayers of Diamine Molecules and Phosphomolybdic Acid on an ITO Surface. *New Journal of Chemistry* **2004**, 28, 495-501.
180. Yang, Y; Guo, Y; Hu, C; Wang, Y; Wang, E. Preparation of Surface Modifications of Mesoporous Titania With Monosubstituted Keggin Units and Their Catalytic Performance for Organochlorine Pesticide and Dyes Under UV Irradiation. *Applied Catalysis A: General* **2004**, 273, 201-210.
181. Liu, J; Cheng, L; Liu, B; Dong, S. Covalent Modification of a Glassy Carbon Surface by 4-Aminobenzoic Acid and Its Application in Fabrication of a Polyoxometalates-Consisting Monolayer and Multilayer Films. *Langmuir* **2000**, 16, 7471-7476.
182. Oh, S-Y; Yun, Y-J; Kim, D-Y; Han, S-H. Formation of a Self-Assembled Monolayer of Diaminododecane and a Heteropolyacid Monolayer on the ITO Surface. *Langmuir* **1999**, 15, 4690-4692.
183. Lahav, M; Heleg-Shabtai, V; Wasserman, J; Katz, E; Willner, I; Durr, H; Hu, Y-Z; Bossmann, S H. Photoelectrochemistry with Integrated Photosensitizer-Electron Acceptor and Au-Nanoparticle Arrays. *Journal of the American Chemical Society* **2000**, 112, 11480-11487.
184. Cho, Y-J; Ahn, T K; Song, H; Kim, K S; Lee, C Y; Seo, W S; Lee, K; Kim, S K; Kim, D; T; P J. Unusually High Performance Photovoltaic Cell Based on a [60]Fullerene Metal Cluster-Porphyrin Dyad SAM on an ITO Electrode. *Journal of the American Chemical Society* **2005**, 127, 2380-2381.
185. Hasobe, T; Imahori, H; Kamat, P V; Ahn, T K; Kim, S K; Kim, D; Fujimoto, A; Hirakawa, T; Fukuzumi, S. Photocatalytic Cells Using Composite Nanoclusters of Porphyrins and Fullerenes with Gold Nanoparticles. *Journal of the American Chemical Society* **2005**, 127, 1216-1228.
186. Qian, X; Qin, D; Bai, Y; Li, T; Tang, X; Wang, E; Dong, S. Photosensitization of TiO<sub>2</sub> Nanoparticulate Thin Film Electrodes by CdS Nanoparticles. *Journal of Solid State Electrochemistry* **2001**, 5, 562-567.
187. Vogel, R; Hoyer, P; Weller, H. Quantum-Sized PbS, CdS, Ag<sub>2</sub>S, Sb<sub>2</sub>S<sub>3</sub>, and Bi<sub>2</sub>S<sub>3</sub> Particles as Sensitisers for Various Nanoporous Wide-Bandgap Semiconductors. *Journal of Physical Chemistry* **1994**, 98, 3183-3188.
188. Yang, S-M; Huang, C-H; Zhai, J; Wang, Z-S; Jiang, L. High Photostability and Quantum Yield of Nanoporous TiO<sub>2</sub> Thin Film Electrodes Sensitized with Capped Sulfides. *Journal of Materials Chemistry* **2002**, 12, 1459-1464.
189. Angelome, P C; Aldabe-Bilmes, S; Calvo, M E; Crepaldi, E; Grosso, D; Sanchez, C; Soler-Illia, G J A A. Hybrid Non-Silica Mesoporous Thin Films. *New Journal of Chemistry* **2005**, 29, 59-63.
190. Pawsey, S; Yach, K; Reven, L. Self-Assembly of Carboxyalkylphosphonic Acids on Metal Oxide Powders. *Langmuir* **2002**, 18, 5205-5212.
191. Bae, E; Choi, W; Park, J; Shin, H S; Kim, S B; Lee, J S. Effects of Surface Anchoring Groups (Carboxylate vs Phosphonate) in Ruthenium-Complex-Sensitized TiO<sub>2</sub> on Visible Light Reactivity in Aqueous Suspensions. *Journal of Physical Chemistry B* **2004**, 108, 14093-14101.
192. Nazeeruddin, M K; Humphry-Baker, R; Officer, D L; Campbell, W M; Burrell, A K; Grätzel, M. Application of Metalloporphyrins in Nanocrystalline Dye-Sensitized Solar Cells for Conversion of

Sunlight into Electricity. *Langmuir* **2004**, 20, 6514-6517.

193. Wang, Q; Campbell, W M; Bonfantani, E E; Jolley, K W; Officer, D L; Walsh, P J; Gordon, K; Humphry-Baker, R; Nazeeruddin, M K; Grätzel, M. Efficient Light Harvesting by Using Green Zn-Porphyrin-Sensitized Nanocrystalline TiO<sub>2</sub> Films. *Journal of Physical Chemistry B* **2005**, 109, 15397-15409.

194. Grätzel, M. Conversion of Sunlight to Electric Power by Nanocrystalline Dye-Sensitised Solar Cells. *Journal of Photochemistry and Photobiology A: Chemistry* **2004**, 164, 3-14.

195. Hara, K; Sugihara, H; Tachibana, Y; Islam, A; Yanagida, M; Sayama, K; Arakawa, H. Dye-Sensitised Nanocrystalline TiO<sub>2</sub> Solar Cells Based on Ruthenium(II) Phenanthroline Complex Photosensitisers. *Langmuir* **2001**, 17, 5992-5999.

196. Campbell, W M; Burrell, A K; Officer, D L; Jolley, K W. Porphyrins as Light Harvesters in the Dye-Sensitised TiO<sub>2</sub> Solar Cell. *Coordination Chemistry Reviews* **2004**, 248, 1363-1379.

197. Horiuchi, T; Miura, H; Uchida, S. Highly Efficient Metal-Free Organic Dyes for Dye-Sensitized Solar Cells. *Journal of Photochemistry and Photobiology A: Chemistry* **2004**, 164, 29-32.

198. Onozawa-Komatsuzaki, N; Kitao, O; Yanagida, M; Himeda, Y; Sugihara, H; Kasuga, K. Molecular and Electronic Ground and Excited Structures of Heteroleptic Ruthenium Polypyridyl Dyes for Nanocrystalline TiO<sub>2</sub> Solar Cells. *New Journal of Chemistry* **2006**, 30, 689-697.

199. Sayama, K; Tsukagoshi, S; Hara, K; Ogha, Y; Shinpou, A; Abe, Y; Suga, S; Arakawa, H. Photoelectrochemical Properties of J Aggregates of Benzothiazole Merocyanine Dyes on a Nanostructured TiO<sub>2</sub> Film. *Journal of Physical Chemistry B* **2002**, 106, 1363-1371.

200. Galoppini, E. Linkers for Anchoring Sensitizers to Semiconductor Nanoparticles. *Coordination Chemistry Reviews* **2004**, 248, 1283-1297.

## 2. ***SYNTHESES OF TITANIA, MOLECULES FOR ITS SELF-ASSEMBLY, DYEING AND EXPERIMENTAL TECHNIQUES***

### 2.1. ***Materials***

Materials were obtained from a range of sources. All of the materials used were at least Analytical Reagent (AR) grade or were purified to reach AR grade. The ethylcellulose used for screen-printing experiments had a 2.42 to 2.53 degree of substitution, a 4.75 to 4.90% ethoxy content and a 5% wt/wt solution would have a viscosity of 14 cP at 25°C in a solvent of 80 : 20 wt/wt mixture of toluene to ethanol. Triton X-100 is a trade name for polyoxyethylene(10)-isooctylphenylether. Corning 1737 aluminosilicate glass coated with indium-doped tin oxide (ITO) had a sheet resistance of 5 to 15  $\Omega$  and was sourced from Delta Technologies Ltd. Degussa P25 hydrophilic fumed titania had a purity of greater than 99.5%, a mean diameter 21 nm, a surface area of  $50 \pm 15 \text{ m}^2 \text{ g}^{-1}$  and a tapped density of  $0.130 \text{ g mL}^{-1}$ . If Degussa P25 was composed of only 21 nm diameter spheres, then the molar mass would be  $100446960 \text{ g mol}^{-1}$ . Dyesol preformed screen-printed titania plates were of the batch PI. Dyesol transparent screen-printing paste was STA18-NRT, lot 115/GDI. The composition of the Dyesol screen-printing titania paste for opaque plates (142op) is that of the transparent paste (148), but with a 20% content of 400 nm diameter particles.<sup>1</sup>

### 2.2. ***Techniques***

#### *Ball-Milling*

Massey University, Institute of Fundamental Sciences: Pascal Engineering Rotary Regavolt motor. A ceramic container with a 14 cm diameter was used with 201 ceramic balls of 1 cm in diameter.

#### *Centrifugation*

Massey University, Nanomaterials Research Centre: Clandron swinging-bucket centrifuge with a 12 cm radius.

Massey University, Institute of Molecular and Biological Sciences: Sorvall Evolution RC Superspeed Centrifuge, SS-34 rotor.

### *Computer Modelling*

*Ab initio* modelling of cinnamylidenemalonic acid (**6.1**) was executed with Gaussian 03, revision C.02 by Dr. Mark Waterland.<sup>2</sup> The hybrid functional B3LYP was used with the basis set 6-31G.

### *Dip-Coating*

Massey University, Nanomaterials Research Centre: a battery-operated mechanical dipper was used. The dipper arm-length, gears and a variable resistor were used to control the dip-speed.

### *Dynamic Light Scattering (DLS)*

Massey University, Institute of Food Nutrition and Human Health: Malvern Zetasizer NanoZS, Red Badge model, ZEN-3600. Light scattering used a 633 nm laser light, with a detection range from 1 nm to 1  $\mu\text{m}$ .

### *Electron Microscopy*

Massey University, Institute of Veterinary and Biomedical Sciences: Reichert-Jung Ultracut E Ultramicrotome. Spurr's Low Viscosity Resin was used for embedding samples, sourced from ProSci Tech, Australia. Spurr's Resin: 10 g vinylcyclohexenedioxide, 6 g of the diglycidyl ether of polypropylene etheneglycol (DER 738), 26 g of nonenylsuccinic anhydride and 0.4 g of dimethylaminoethanol. The resin was cured at 70°C, for 8 hours in air.<sup>3,4</sup>

### *Transmission Electron Microscopy (TEM)*

HortResearch: Phillips 201c TEM, and Phillips CM-10 TEM. Formvar-coated 200 mesh copper grids were used. Formvar is a polyvinyl acetal, produced from polyvinyl acetate and formaldehyde. Approximately half a drop of 0.5% wt/wt bovine serum albumin in water was added to 0.1 to 0.5 mL of dispersion, to aid particle deposition on the grid.

Victoria University of Wellington, School of Physical and Chemical Sciences: JEOL-2010 TEM. Samples were supported by ProSciTech strong carbon film on 200 mesh copper grids.

### *Scanning Electron Microscopy (SEM)*

HortResearch: Cambridge 250 Mark III SEM. Samples were sputter-coated by gold and occasionally were earthed to the puck with a strap of conductive carbon-tape.

Victoria University of Wellington, School of Physical and Chemical Sciences: JEOL 6500F Field Emission SEM. Samples were coated with 8 nm of platinum and electrically connected to the puck with silver paint.

### *Fluorescence*

Massey University, Nanomaterials Research Centre: Perkin Elmer Luminescence Spectrometer, LS-50B. FL WinLab v.4.00.02 software was used.

Massey University, Nanomaterials Research Centre: Ocean Optics HR-4000 spectrometer, using either a PX-2 white light source with a Breakout Box or diode light sources of 518 and 470 nm. Spectra Suite software was used.

### *Fourier Transform Infra-red (FTIR) Spectroscopy*

Massey University, Institute of Fundamental Sciences: ThermoElectron Corporation Nicolet 5700. The attenuated total internal reflectance (ATR) attachment samples using single-reflection with a polished germanium crystal.

### *Karl-Fischer Titrations*

Massey University, Nanomaterials Research Centre: Mettler Karl-Fischer DL-18. The standard titrant was Aquagent<sup>®</sup> Complet5, single-component reagent, pyridine free. 1 mL of titrant contained 5 mg of water, had a density of 1.17 g mL<sup>-1</sup>. Lot = AQ0003.

### *Nuclear Magnetic Resonance (NMR)*

Massey University, Institute of Fundamental Sciences: 400 MHz and 500 MHz Bruker NMR and analysed using Bruker TopSpin 1.3 software.

### *Optical Micrography*

Massey University, Institute of Molecular and Biological Sciences, Institute of Veterinary and Biomedical Sciences: Olympus 100x.

### *Profilometry*

Industrial Research Limited, Materials Physics Group: Sloan Dektak Profilometer,

serial code: E-1762. For measurements of screen-printed STA 18-NRT titania the instrument was set for an output range of 50  $\mu\text{m}$  and a stylus speed of 1  $\text{mm min}^{-1}$ .

#### *Raman - Backscattering*

University of Auckland: Renishaw Raman RM-2, with Olympus 20x objective lens, 785 nm excitation from a diode laser, with power varied from 0.26 to 26 mW to study photosensitivity. Scattered light collected at 180° geometry, with 2  $\text{cm}^{-1}$  resolution and 10 to 20 scans per spectrum.

#### *Raman - Resonance*

Massey University, Institute of Fundamental Sciences: The detector was an Acton Spectra Pro<sup>®</sup>, 2550i, 0.500 m, with imaging by a single-stage monochromator/spectrograph, which was nitrogen-cooled to reduce electronic noise. Samples were excited at 532 nm and 514 nm, with a 135° backscattered configuration. The 532 nm light source was a Quantel Brilliant b, vertically polarised, Q-switched Nd:YAG pulse laser. The 514 nm light source was a Multiline Stellar-PRO continuous wave, 150 mW Argon laser. The laser power was adjusted so that the sample received approximately 20 mW of energy.

#### *Scanning Probe Microscopy (SPM)*

Massey University, Institute of Engineering and Technology: Digital Instruments LFM-2, using an E-head and a J-head scanner.

#### *Screen-Printing*

Massey University, Nanomaterials Research Centre: The screen was polyester fabric with a mesh of 156 threads per square inch. The screen-substrate gap was 3 mm and the blade was plastic.

#### *Spin-Coater*

Massey University, Nanomaterials Research Centre: Laurell Technologies Corporation, model WS-400A-6Npp/LITE.

#### *Surface Area Measurements*

Victoria University of Wellington, School of Physical and Chemical Sciences: Nitrogen

sorption BET measurements were done on a Micrometrics FlowsorbII-2300.

Quantachrome Instruments Ltd: Multipoint nitrogen sorption BET measurements were collected. Krypton was used for samples with a very low surface area.

#### *Solar-Cell Testing*

Massey University, Nanomaterials Research Centre: The solar cell testing protocols were established by Dr. Wayne Campbell. Lamps were calibrated to one sun (AM 1.5, 100 mW cm<sup>-2</sup>) for 0.907 mA with Photodiode 1 and 0.131 V with the Darlington phototransistor 3 (which is 2 transistors paired together for amplification). The Olympus microscope translational stages are set for (x, y) = (68 mm, 15 mm) and the lamp power settings are 11.00 V and 3.90 A. A recent calibration was for 0.8 sun (AM 1.2).

#### *Ultrasound bath*

Massey University, Nanomaterials Research Centre: Dandelin Sonorex Super 10P digital.

#### *Ultraviolet-Visible (UV-Vis) Spectroscopy*

Massey University, Nanomaterials Research Centre: Shimadzu UV-3101PC, UV-Vis. UV Probe software was used.

Massey University, Nanomaterials Research Centre: Ocean Optics HR-4000 spectrometer, DT-Mini-2-GS tungsten and deuterium light source. Spectra Suite software was used.

#### *Voltammetry*

Massey University, Nanomaterials Research Centre: Eco Chemie Autolab with PGSTAT30 Differential Electrometer Amplifier, and General Purpose Electrochemical System (GPES) software was used.

#### *X-ray Diffraction*

Victoria University, School of Physical and Chemical Sciences: Phillips PW-1730 diffractometer with a PW-3710mpd controller, PW-3719 counter and a copper source.

Industrial Research Ltd: Bruker D8 Advance with grazing incidence geometry and a copper source.

Massey University, Institute of Natural Resources, Soil & Earth Sciences Group: Phillips PW-1840 diffractometer with a PW-1729 X-ray generator and a cobalt source (1.7902 Å).

### **2.3. Nanostructured Titania: Inverse Opals**

#### **2.3.1. Colloid Synthesis**

Silica colloids were synthesised by a variant of the Stober-Fink-Bohn process, which is the base-catalysed hydrolysis of tetraethylorthosilicate (TEOS).<sup>5, 6</sup> A typical synthesis involved 7.5 mL (0.42 mol, 0.34 M) of TEOS added rapidly to a vigorously stirred solution of 28.6 mL (0.03 mol, 4 M) of 28% ammonia in 64 mL of methanol, at 60°C. The solution instantly became white, homogenous and opaque and for two hours was stirred at 60°C. The solids were washed with 95% ethanol by eight cycles of 15 minutes centrifugation at 3000g of relative centrifugal force (rcf) and redispersion using an ultrasonic bath. From TEM images the sample displayed an average diameter of 244 nm, a mode of 247 nm, an interquartile range of 237 to 247 nm and a standard deviation of 12 nm for a sample of 345 particles. Dynamic light scattering (DLS) measurements gave a number-average hydrodynamic radius of 320 nm.

#### **2.3.2. Opal Formation**

Silica opaline templates were formed upon glass coated with indium-doped tin oxide (ITO) using the method of vertical deposition by a falling meniscus of an alcoholic dispersion of silica colloids.<sup>7, 8</sup> ITO glass was suspended vertically in a 0.5% wt/wt dispersion of silica colloids in 95% v/v ethanol. The opal was deposited by the removal of solvent, after placing the sample in a 60°C oven, overnight. The silica opals were sintered in air, by a stepwise ramping from 100°C in 50°C steps every half hour, until reaching 500°C. After annealing for an hour, the oven was turned off and the material allowed to cool with the oven door closed. As an indication of the rate of cooling, after 15 minutes the oven temperature was 400°C, was 250°C after 1.5 hours and after 4.5 hours was 80°C.

### 2.3.3. *Inverse Opals of Titania*

The formation of titania inverse opals were formed using a modified method found in the literature.<sup>9</sup> A solution with a 1 : 40 : 0.6 molar ratio of titanium isopropoxide to dry ethanol to ethylenediamine was used to infiltrate the opaline template. Opals were soaked for 20 to 30 minutes under 3000g of rcf.<sup>10</sup> The substrates were lifted from the infiltration solution by a dip-coating method, to ensure a uniform film of the titania precursor over the surface. Samples were then placed into a rinsing solution of a 1 : 120 : 0.6 molar ratio of reactants and immediately withdrawn. Substrates were withdrawn vertically and were mechanically lifted at approximately 40 mm min<sup>-1</sup> from the solution vials, which were topped with dry argon to prevent the premature hydrolysis of the titanium alkoxide. The samples were then immersed for an hour in water at 60°C. The composite was then dried for an hour at 60°C, before further cycles of infiltration. The dulled, opaque, white titania-silica composites were sintered at 500°C, using the same protocol as for the heat-treatment of the opaline template. The opaline templates were sacrificed by soaking overnight in an aqueous 30% wt/wt solution of sodium hydroxide,<sup>11</sup> then were rinsed with ethanol. The resulting material exhibited an opalescence that was slightly weaker than that of the template. Typical samples produced by this method are s01/02/05 and s02/02/05.

The opaline template of s01/02/05 was twice treated with three rounds of infiltration. After each set of three rounds, the sample was immersed in water at 60°C overnight then oven-dried. The opaline template was infiltrated by a solution with a 1 : 20 : 0.6 molar ratio of titanium isopropoxide to dry ethanol to ethylenediamine for 20 minutes under 3000g of rcf. The samples were withdrawn vertically at 40 mm min<sup>-1</sup> from the infiltration solution, then rinsed with a 1 : 120 : 0.6 molar ratio of titanium isopropoxide to dry ethanol to ethylenediamine by a vertical dip at 40 mm min<sup>-1</sup>. The opal of s02/02/05 underwent a single treatment of five rounds of infiltration. Both samples were sintered using a temperature ramp of approximately 50°C every 30 min to reach 500°C, at which the samples sat for an hour. The samples were cooled overnight to room temperature, before immersion in a 30% wt/wt aqueous solution of sodium hydroxide for 6 hours at 60°C. The sample was rinsed by immersion in a 20% wt/wt, then 10% wt/wt, then 5% wt/wt aqueous solution of sodium hydroxide. The aqueous solution was then replaced first by 25% v/v, then 50% v/v, then 75% v/v, then a 95%

v/v solution of ethanol before drying at room temperature.

Alternative titania precursor formulations include solutions with molar ratios 1 : 5.5 : 6.7 : 1.2 of tetraisopropyl orthotitanate to millipore water to dry ethanol to 69% nitric acid<sup>12</sup> and 1 : 9 : 0.1 of tetraisopropyl orthotitanate to dry ethanol to glacial acetic acid. However, these solutions proved to be too viscous and resulted in the deposition of excess titania on the templates.

## **2.4. Nanostructured Titania for Binding Studies**

Flat and non-porous titania was produced by the dip-coating of ITO glass, following a similar protocol to that used in the formation of inverse opaline titania. Substrates were dip-coated with a solution containing a 1 : 40 : 0.6 molar ratio of tetraisopropyl orthotitanate to dry ethanol to ethylene diamine and withdrawn vertically at 40 mm min<sup>-1</sup>. Multiple coats were formed without an intervening treatment with water, as titanium alkoxide immediately hydrolysed with atmospheric moisture. Transparent and colourless titania films resulted. Characterisation of both flat, non-porous titania and of titania inverse opals was done by low angle X-ray diffraction (XRD). This was confirmed by backscattering Raman, using an excitation wavelength of 785 nm. Raman shift signals at 637, 514 and 394 nm showed that anatase was the only form of titania detected.

### **2.4.1. Thin and Non-porous Titania**

A variant of the solution used in the formation of inverse opals (Section 3.5) was simplified to produce thin and non-porous titania by the dip-coating of ITO glass. The samples required neither rinsing, nor treatment with water as atmospheric moisture was sufficient to completely hydrolyse the titania precursor. Mechanical vertical withdraw speeds ranged from 20 to 40 mm min<sup>-1</sup>, a higher dip speed produced smoother films. Typically, thin and non-porous titania was formed by two sequential dip-coats into a solution with a 1 : 40 : 0.6 molar ratio of titanium isopropoxide : dry ethanol : diethanolamine. When a 40 mm min<sup>-1</sup> dip speed was used, films with a RMS roughness

of 10 nm resulted.

#### 2.4.2. *Aggregated and Sintered Titania*

##### *Screen-printing of titania*

Degussa P25 and sol-gel titania were screen-printed using a variation of published protocols.<sup>13, 14</sup> In preparation for screen-printing, 12 g (150 mmol TiO<sub>2</sub> or  $1.14 \times 10^{-7}$  mol of 21 nm diameter titania particles) of Degussa P25 titania was ball milled with 4 mL of water and 0.40 mL of distilled 2,4-propanediol for 5 hours to aid the redispersion of material. The samples were printed by a single pass of the blade through a polyester mesh fixed at 3.2 mm above a glass substrate. Samples were sintered using the same regime as for inverse opals of titania.

A screen-printing paste of Degussa P25 was composed of 4 g of ball-milled Degussa P25 (50 mmol TiO<sub>2</sub> or  $3.98 \times 10^{-8}$  mol of 21 nm diameter titania particles) with 0.18 g of ethylcellulose and 6.8 mL of mixed isomers of terpineol (40 mmol). This gave a mass ratio of 22 : 1 of titania to ethylcellulose and a molar ratio of 1.2 : 1 for TiO<sub>2</sub> to terpineol (or a molar ratio of 1030000 : 1 for 21 nm diameter titania to terpineol). The opaque paste was off-white in colour. Screen-printing pastes of sol-gel titania used the same, dispersed material as described in section 2.4.3: 0.2 g of sol-gel titania (0.09 g of TiO<sub>2</sub>, 1 mmol, or  $8.6 \times 10^{-6}$  mol of 2 nm diameter titania particles) with 0.045 g of ethylcellulose and 0.17 mL of mixed isomers of terpineol (1 mmol). This gave a mass ratio of 2 : 1 of titania to ethylcellulose and a molar ratio of 1 : 1 for TiO<sub>2</sub> to terpineol (or a molar ratio of 120 : 1 for 2 nm diameter titania to terpineol). The opaque paste was cream-tan in colour.

##### *Spin-thinning of titania*

Prior to calcination of the films, samples were spin-thinned by rotation of individual screen-printed squares using a spin-coater. A typical program for spin-thinning titania pastes involved 60 seconds each at 500, 1500, 3000, 4500, then 6000rpm, with a nominal acceleration of 20. Square forms with an area of 1 cm<sup>2</sup> were produced after sintering the prints in air at 490°C for an hour. The clear and colourless films were sintered, which resulted in cracked and slightly opaque films approximately 1 µm thick.

### 2.4.3. *Dispersible Titania*

The synthesis of the sol-gel titania follows a reported method.<sup>15</sup> The solution was stirred vigorously throughout this procedure, where into 80 mL of methanol chilled on an ice bath, 2.4 mL (22 mmol) of titanium tetrachloride was added. Then a solution of 0.25 mL (3 mmol) of 1.18 g mL<sup>-1</sup> concentrated hydrochloric acid in 2.0 mL of charcoal-distilled water was added. The stirred solution was given two hours to warm to room temperature, after which the clear, colourless solution was refluxed for two hours. The sample was dried by rotary evaporation on a 50°C water bath to yield an hygroscopic yellow foam. Residual water was removed by six rounds of resolution in dry acetonitrile and rotary evaporation over a 40°C water bath. However, according to Olsen *et al*, some water will remain adsorbed on the surface of the titania.

### 2.5. *Towards the Self-Assembly of Titania using Small Molecules*

#### *Synthesis of N-(ferrocenylmethylidene)-4-phenylenediamine (5.3)*

A known compound.<sup>16, 17</sup> Synthesised by Ms. Yvonne Ting.

0.10g (0.05 mmol) of ferrocenemonocarboxaldehyde in 4 mL of 2,2'-dimethoxypropane was dropped into a stirred solution of 0.22 g (2 mmol) of 4-phenylenediamine in methanol. The solution was stirred for one and a half hours at 45°C, after which black-brown solids of poly(4-phenylenediamine) were filtered off and the filtrate was concentrated by rotary evaporation. Solids that crystallised from the concentrated filtrate were separated and rinsed with a few millilitres of methanol, while the supernatant solution was reserved. Recrystallisation from the supernatant was repeated to collect six fractions, which despite varying in colour from light orange to brown was the same product. The product was then characterised by <sup>1</sup>H-NMR, electrospray mass spectroscopy, UV-Vis and FTIR. The yield was 33%. <sup>1</sup>H-NMR : (CD<sub>3</sub>OD) δ<sub>H</sub>: 4.25 (s, 5H, C<sub>5</sub>H<sub>5</sub>), 4.52 (t, 2H, C<sub>5</sub>H<sub>5</sub>), 4.82 (t-possibly, 2H, C<sub>5</sub>H<sub>5</sub>), 6.73-6.76 (d, 2H, C<sub>5</sub>H<sub>6</sub>), 7.04-7.06 (d, 2H, C<sub>5</sub>H<sub>6</sub>), 8.40 (s, 1H, CH=N). The amine NH<sub>2</sub> is possibly lost to oxidation. Electrospray mass spectroscopy was done in positive mode, giving a result of 305 m/z, which was expected, as the calculated molar mass was 304 g mol<sup>-1</sup>. UV-Vis

spectroscopy absorbance maxima in methanol were at 320 and 350 nm. FTIR:  $\nu(\text{N-H})$ ,  $3370\text{ cm}^{-1}$ ;  $\nu(\text{C=N})$ ,  $1617\text{ cm}^{-1}$ ;  $\delta(\text{C-H})$ ,  $823\text{ cm}^{-1}$ . The  $\delta(\text{C-H})$  signal may be due to a partially oxidized Schiff base.

#### *Synthesis of N, N'-di(ferrocenylmethylidene)-4-phenylenediamine*

A known compound.<sup>16, 17</sup> Synthesised by Ms. Yvonne Ting.

An excess of ferrocenemonocarboxaldehyde was used to ensure that the di-imine was formed. 0.214 g (1 mmol) of ferrocenemonocarboxaldehyde, 0.05 g (0.5 mmol) of 4-phenylenediamine and 0.06 mL (5  $\mu\text{mol}$ ) of 0.175 M acetic acid was stirred overnight in 0.5 mL of methanol. The red-brown product was washed with methanol. The yield was 43%.

#### *Synthesis of 2-(4-aminophenyl)ethenylferrocene (5.4)*

A known compound.<sup>18</sup> Synthesised by Mr. Ross Davidson.

Produced by the method used by Ms. Amy Watson (Lab book 1, 27<sup>th</sup> February 2003 and 6<sup>th</sup> March 2003). The sample was produced by refluxing a 1.2 : 1 : 1.2 molar ratio of 1,8-diazobicyclo[5.4.0]undec-7-ene to ferrocenemonocarboxaldehyde to the bromide salt of (4-nitrophenyl)methyltriphenylphosphonium bromide in 100 mL of toluene for 12 hours. The product was then washed twice by 50 mL of 1 M hydrochloric acid, then once by 50 mL of 0.1 M sodium carbonate and brine.

#### *Synthesis of carbonyl(5',10',15',20'-tetraphenylporphyrinato)ruthenium(II)*

A known compound.<sup>19</sup> Synthesised by Dr. Sanjeev Ghambir.

<sup>1</sup>H-NMR : ( $\delta_{\text{H}}$  (ppm) D<sub>6</sub>-DMF): 7.83 (m, 12 H, *m*-, *p*- overlap of C<sub>6</sub>H<sub>5</sub>), 8.19 (d,  $J = 6.7$  Hz, 4H, *o*-protons of C<sub>6</sub>H<sub>5</sub>), 8.27 (t,  $J = 2.9, 3.0$  Hz, 4H, *o*-protons of C<sub>6</sub>H<sub>5</sub>), 8.67 (s, 8H,  $\beta$ -pyrrolic protons).

#### *Synthesis of 4-(trans-2-(4-pyridinyl)ethenyl)benzoic acid*

A known compound.<sup>20, 21</sup> Synthesised using a procedure modified by Dr. Pawel Wagner.

0.66 mL (7 mmol) of 4-picoline and 1.0 g (7 mmol) of 4-carboxybenzaldehyde was heated in 1.0 mL (11 mmol) of acetic anhydride at 100°C for a day. The initial opaque, tan-coloured mixture became a cream-orange solid in an orange solution. The solid

product was washed by reverse osmosis water to remove acetic anhydride, then with approximately 50 mL of 95% ethanol to receive cream-yellow powder. The yield was 7%.  $^1\text{H-NMR}$  : ( $\delta_{\text{H}}$  (ppm)  $\text{D}_6$ -DMF): 7.48 (d,  $J = 16.3$  Hz, 2H, vinyl proton next to the pyridine ring), 7.84 (d,  $J = 8.5$  Hz, 2H,  $\text{C}_6\text{H}_4$ ), 7.87 (d,  $J = 16.4$  Hz, 2H, vinyl proton next to the benzoic acid ring), 8.17 (d,  $J = 6.3$  Hz, 2H,  $\text{C}_4\text{H}_4\text{N}$ ), 8.23 (d,  $J = 8.5$  Hz, 2H,  $\text{C}_6\text{H}_4$ ), 8.6756 ppm (t,  $J = 3.5, 6.6$  Hz, 2H,  $\text{C}_4\text{H}_4\text{N}$ ). Matrix-assisted laser desorption ionisation (Maldi) mass spectroscopy gave a result of 225 m/z, which corresponds to the calculated molar mass.

*Coordination of carbonyl(5',10',15',20'-tetraphenylporphyrinato)ruthenium(II) with 4-(trans-2-(4-pyridinyl)ethenyl)benzoic acid*

A known compound.<sup>22</sup>

060327: 20.6 mg (27  $\mu\text{mol}$ ) of RuTPPCO and 6.3 mg (28  $\mu\text{mol}$ ) of 4-(trans-2-(4-pyridinyl)ethenyl)benzoic acid was dissolved in 10 mL of *N,N*-dimethylformamide. The blood-red-orange solution was stirred for an hour at room temperature and then was filtered through cotton to remove the black solids of decomposed coordination compound. The filtrate was dried by rotary evaporation for orange-purple solids. The yield was 77%.  $^1\text{H-NMR}$  : ( $\delta_{\text{H}}$  (ppm)  $\text{D}_6$ -DMF): 1.56 (d,  $J = 10.9$  Hz, 2H,  $\text{C}_4\text{H}_4\text{N}$ ), 5.76 (d,  $J = 5.6$  Hz, 2H,  $\text{C}_4\text{H}_4\text{N}$ ), 6.33 (d,  $J = 16.6$  Hz, 1H, vinyl proton next to the pyridine ring), 6.74 (d,  $J = 16.2$  Hz, 1H, vinyl proton next to the benzoic acid ring), 7.33 (d,  $J = 8.0$  Hz, 2H,  $\text{C}_6\text{H}_4$ ), 7.86 to 7.77 (m, 12 H, *m*-, *p*- overlap of  $\text{C}_6\text{H}_4$ ), 8.15 (d,  $J = 6.5$  Hz, 4H, *o*-protons  $\text{C}_6\text{H}_5$ ), 8.27 (d,  $J = 3.5$  Hz, 4 H, *o*-protons  $\text{C}_6\text{H}_5$ ), 8.67 (s, 8 H,  $\beta$ -pyrrolic protons). Maldi mass spectroscopy gave a result of 939 m/z, which corresponds to a loss of carbon monoxide; the calculated molar mass was 967  $\text{g mol}^{-1}$ .

### 2.5.1 The Functionalisation of ITO Electrodes

Prior to functionalisation, ITO glass was cleaned by washing with detergent, then ultrasonication for 15 minutes within each of acetone, water, ethanol, then dried in air. The substrate was then ultrasonicated within a 1 : 1 : 5 v/v solution of 30% hydrogen peroxide to 28% ammonia to reverse-osmosis water, then rinsed thoroughly with water, then AR grade ethanol. This base treatment was an effort to remove organic

contaminants and ensure the presence of hydroxyl groups on the surface of the ITO.<sup>23</sup>

The deposition of what may be a monolayer, or thin film of organic species, such as 4-phenylenediamine and 4-aminobenzoic acid upon ITO glass was performed in dry and dark conditions to prevent oxidation, or polymerisation. A typical solution contained 5 mM of the adsorbate in dry ethanol or 1,4-dioxane, under an inert atmosphere. The period of treatment of ITO glass varied from two days to a month at 30 to 80°C. The slow oxidation of the aniline derivative was inferred by the gradual colour change of the soaking solution from clear and colourless, to a light apricot after two days, or a clear, blood-red after a month. The ITO slides were then rinsed with AR methanol and air-dried.

For the overgrafting of ferrocenemonocarboxaldehyde to 4-phenylenevinylene, ITO glass was first immersed for two and a half days in a 120 mM solution of 4-phenylenediamine in 1,4-dioxane, at 30°C. The ITO samples were then soaked within a 1.3 mM solution of ferrocenemonocarboxaldehyde in 2,2'-dimethoxypropane, for a day at 20 to 25°C. The treatment of ITO glass with ferrocenemonocarboxaldehyde or with *N*-(ferrocenylmethylidene)-4-phenylenediamine was done by using 2,2'-dimethoxypropane as a solvent and concentrations in the order of 50 mM. Samples were soaked at 20 to 40°C for a few days, before rinsing with AR methanol and then air-dried and stored in the dark. Alternatively, species such as 2-(4-aminophenyl)ethenylferrocene were adsorbed onto ITO by immersion for 2 hours at room temperature in a 2 mM solution, using a mixed solvent of 6% v/v of 1,4-dioxane in hexane. The ITO samples were then rinsed with a 5% v/v solution of 1,4-dioxane in hexane.

UV-Vis spectra were collected using a step-size of 0.5 nm and a very slow scan speed to collect data from 250 nm to 700 nm over ten minutes. A 2 nm slit width gave a maximum illuminated area of 0.44 cm<sup>2</sup>. Before use, efforts were made to minimise the effects of the low signal-to-noise ratio by allowing a minimum of 90 minutes for the tungsten and deuterium lamps to stabilise prior to use. In general, a single baseline of air alone was collected prior to each day's experiments and had a range of  $\pm 0.0004$  absorbance units. Typically, three such scans were collected and averaged for samples of ITO glass before and after the deposition and further treatment of species, such as 4-

phenylenediamine. Mathematical subtraction was used to extract peak position and intensities for treated samples. The positioning of the sample holder with respect to the beam has an uncertainty of  $\pm 1^\circ$  at most. This was not a concern, as there was no detectable change in absorbance position or intensity on tilting samples by up to  $5^\circ$  from the perpendicular, with respect to the light beam.

Voltammetry was done using 0.1 M tetrabutylammonium perchlorate (TBAP) in dry tetrahydrofuran or dry dichloromethane as the electrolyte. A minimum of three sequential scans was collected for each dye. Dry air hoods for voltammetry were not available, and despite bubbling with dry nitrogen, atmospheric moisture was absorbed into the voltammetry samples. As a consequence, the data was only collected for the dye/dye<sup>+</sup> couple. Typical data collection parameters used a scan rate of 100 mV s<sup>-1</sup> and a data interval of 2.5 mV was used for collection. The counter electrode was platinum mesh and the working electrode was either a platinum disc 2 mm in diameter (0.03 cm<sup>2</sup>) or ITO glass. A pseudo-reference electrode of Ag/AgNO<sub>3</sub> within 0.1 M TBAP in acetonitrile was used for non-aqueous experiments. The inner electrode contained silver wire immersed in a 1 mM solution of AgNO<sub>3</sub> in electrolyte, while the outer electrode had a plain electrolyte of 0.1 M TBAP in acetonitrile. A pseudo-reference electrode of Ag/AgCl in saturated potassium chloride was used for aqueous experiments. Potentials were adjusted to standard calomel electrode (SCE) values by adjusting for the difference between experimental and literature values for the ferrocene/ferrocenium redox couple. For data shown in Chapter 5, depending on the data set, a half-wave potential of either 0.115 or 0.110 V<sub>Ag/Ag+</sub> was obtained for the ferrocene/ferrocenium redox couple. The adjustment to convert values to the SCE scale was to add either 0.043 or 0.048 V, respectively.

A calculated bracket for monolayer coverage of 2-(4-aminophenyl)ethenylferrocene (**5.4**) on a flat surface was done using maximum and minimum footprint areas (Fig. 2.1). The depth of **5.4** was taken as 6.6 Å, which is that of a freely-rotating ferrocenyl group.<sup>24</sup> The width of **5.4** was estimated using Chem3D<sup>®</sup>: bound by the amine group, the minimum and maximum footprint areas, as shown in Figure 2.1, are 4.3 and 5.3 x 10<sup>-19</sup> m<sup>2</sup>, respectively. The bracket for monolayer coverage for **5.4** is then 3.2 - 3.9 x 10<sup>-10</sup> mol cm<sup>-2</sup>.

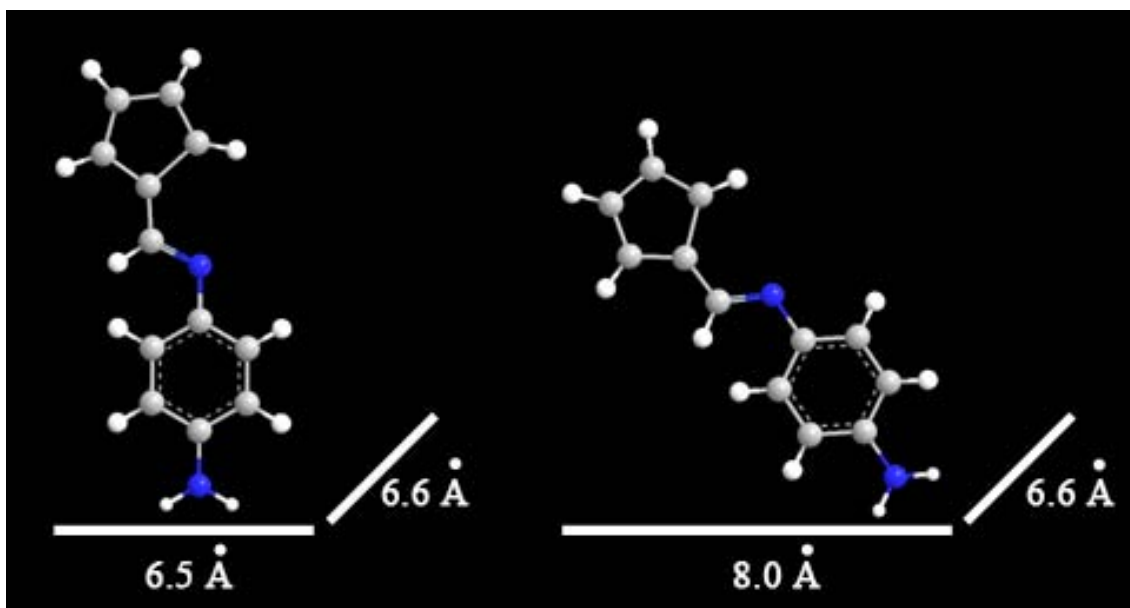


**Figure 2.1.** Chem3D<sup>®</sup> representations of **5.4** with estimates of the maximum and minimum rectangular footprint area. For clarity, only one cyclopentadiene ring of the ferrocenyl group is shown.

Experimental surface coverage estimates of **5.4** upon ITO glass were done using both voltammetry and UV-Vis spectroscopy. In order to calculate the number of moles adsorbed onto ITO by voltammetry, the current under the oxidation peak was integrated for the single-electron process, using a Gaussian peak fit of the oxidation peak. Data was taken from the second scan and the assumption was made that the current measured was due to adsorbed molecules only. The calculation of surface coverage by **5.4** from UV-Vis absorbance involved a concentration calibration plot using standard solutions. To plot the absorbance of **5.4** on ITO glass directly against the calibration data to find the number of moles in the illuminated area, in terms of mol cm<sup>-2</sup>, the concentration of the standard solutions was converted from mol L<sup>-1</sup> to mol. A 2 nm slit width gave an illuminated area of 0.44 cm<sup>2</sup>, which combined with a 1 cm path length solution cell, gave an illuminated volume of 0.44 cm<sup>3</sup>. The number of moles of **5.4** in the light path was then the concentration of the standard multiplied by 0.44 cm<sup>3</sup>. However, the calibration is not an ideal one as there will be light losses due to scattering within the solution cell. The uncertainty in the surface coverage calculation using UV-Vis spectroscopy is  $\pm 5\%$ , which was derived from error in the concentration of the standard solutions, UV-Vis absorbance values and the uncertainty in the calibration plot.

### 2.5.2. *Towards Chemically-Assisted Self-Assembled Titania Arrays*

ITO glass was first immersed within a 1 mM solution of 4-aminobenzoic acid in 1,4-dioxane at room temperature for 11 days. The sample was then soaked within a suspension of Degussa P25 titania acidified by hydrochloric acid for a pH value of 2.

### 2.6. *The Binding of Dye to Titania*

#### *Synthesis of 4-methoxybenzylidenemalonic acid (6.1)*

A known compound.<sup>25</sup> Synthesised by Ms. Yvonne Ting.

The acid was produced by stirring 0.45 mL (4 mmol) of 4-methoxybenzaldehyde in 1 mL (17 mmol) of glacial acetic acid with 1.18 g (11 mmol) of malonic acid. Approximately 0.3 g (4 mmol) of ammonium acetate was added to aid the dissolution of malonic acid. The clear and colourless mixture became a clear, homogenous green solution, which after 3 hours was an opaque, lime-green slurry. The solids were filtered on a number 4 sinter filter, rinsed with first water, then with diethylether. The lemon-yellow solids were dried in a dessicator under active vacuum overnight. The product was judged to be pure by HPLC and <sup>1</sup>H-NMR spectroscopy. The yield was 22%. <sup>1</sup>H-NMR ( $\delta_{\text{H}}$  (ppm) in CD<sub>3</sub>OD): 7.61 (s, 1H), 7.55 (d,  $J = 10$  Hz, 2H), 6.96 (d,  $J = 10$  Hz, 2H), 3.83 (s, 3H). Acidic protons are not observed in the protic solvent. <sup>1</sup>H-NMR ( $\delta_{\text{H}}$  (ppm) in (CD<sub>3</sub>)<sub>2</sub>SO): 13.15 (s, 2H), 7.56 (d,  $J = 10$  Hz, 2H), 7.48 (s, 1H), 7.01 (d,  $J = 10$  Hz, 2H), 3.80 (s, 3H).

#### *Synthesis of cinnamylidenemalonic acid (6.2)*

A known compound.<sup>26</sup> Synthesised by Mr. Adam Stephenson.

<sup>1</sup>H-NMR ( $\delta_{\text{H}}$  (ppm) in CD<sub>3</sub>OD): 7.85 (d,  $J = 10$  Hz, 1H), 7.77 (dd,  $J = 25$  Hz, 11.5 Hz, 1H), 7.60 (d,  $J = 8$  Hz, 2H), 7.42-7.33 (m, 3H), 7.28 (d,  $J = 15$  Hz, 1H). Acidic protons are not observed in the protic solvent. <sup>1</sup>H-NMR ( $\delta_{\text{H}}$  (ppm) in (CD<sub>3</sub>)<sub>2</sub>SO): 12.78 (s, 2H), 7.54 (d,  $J = 7$  Hz, 2H), 7.43 (d,  $J = 12$  Hz, 1H), 7.41-7.35 (m, 3H), 7.27 (d,  $J = 15.6$  Hz, 1H), 7.18 (dd,  $J = 30$  Hz, 11 Hz, 1H).

### *Synthesis of trans-stilbene*

A known compound.<sup>27</sup> Synthesised by Dr. Wayne Campbell.

<sup>1</sup>H-NMR ( $\delta_{\text{H}}$  (ppm) in CD<sub>3</sub>OD): 7.45 (d,  $J = 5$  Hz, 4H), 7.34 (t,  $J = 5$  Hz, 4H), 7.24 (t,  $J = 5$  Hz, 2H), 7.16 (s, 2H).

### *Synthesis of ter(thienylenevinylene)malonic acid (6.3), ter(thienylenevinylene)-cyanoacetic acid (6.4), 8,15-dicyanoter(thienylenevinylene)malonic acid (6.5) and ter(thienylenevinylene)rhodanine acetic acid (6.6)*

Novel compounds.<sup>28</sup> Synthesised by Dr. Pawel Wagner.

E-491: <sup>1</sup>H-NMR ( $\delta_{\text{H}}$  (ppm) in CD<sub>3</sub>OD): 8.34 (s, 1H), 7.52 (d,  $J = 5$  Hz, 1H), 7.30 (d,  $J = 5$  Hz, 1H), 7.30 (d,  $J = 16.5$  Hz, 1H), 7.17 (d,  $J = 4$  Hz, 1H), 7.13 (dd,  $J = 3.5$  Hz, 1H), 7.13 (d,  $J = 16.5$  Hz, 1H), 7.08 (dd,  $J = 3.5$  Hz, 1H), 7.07 (d,  $J = 16.5$  Hz, 1H), 7.05 (d,  $J = 16.5$  Hz, 1H), 7.02 (d,  $J = 3.5$  Hz, 1H), 7.01 (dd,  $J = 3.5$  Hz, 1H).

### *Synthesis of terthienylvinylene malonic acid and terthienylcyanoacrylic acid*

Synthesised by Dr. Sanjeev Ghambir. Novel compounds.<sup>29</sup>

Sample codes: SG-72/5 and SG-74/5 for the respective compounds

#### **2.6.1. UV-Vis Spectroscopy**

It was first confirmed that on deviation of the titania plate up to 5° from the normal with respect to the light path, there is no effect on either the position or intensity of UV-Vis absorption peaks. Spectra were collected using a 2 nm slit width, step-size of 0.5 nm and a variable scan speed, to collect data from 250 nm to 700 nm over ten minutes. The illuminated area was 0.44 cm<sup>2</sup> for the majority of samples, though a masked area of 0.32 cm<sup>2</sup> was used for smaller samples.

#### **2.6.2. FTIR Spectroscopy**

Transmission FTIR spectra were recorded using pressed potassium bromide discs. Typically 16 scans were collected with a resolution of 4 cm<sup>-1</sup>. ATR-FTIR spectra were

collected by placing the sample upon the germanium crystal, then applying the pressure tower for solid samples. In general, 32 scans with a resolution of  $4\text{ cm}^{-1}$  were collected.

### **2.6.3. Raman and Fluorescence Spectroscopy**

Resonance Raman spectra were collected using green light of 532 and 514 nm. A McCreery solvent of a 1 : 1 v/v mixture of toluene to acetonitrile was used for the calibration of Raman shifts.<sup>30</sup>

Fluorescence spectra were collected using a quartz cuvette for solution samples, or with a reflection probe for solid-state samples. Typical data collection parameters for the Perkin Elmer machine included an excitation slit width of 10 nm, an emission slit width of 20 nm and a scan rate of 100 to 500 nm min<sup>-1</sup>. It must be noted that when different machines or sample concentrations are used that the self-absorbance of fluorescent light alters the energy distribution of light that reaches the detector, resulting in an apparent shift in the value of maximum fluorescence. Samples were not corrected for self-absorbance.

### **2.6.4. NMR Spectroscopy**

<sup>1</sup>H-NMR experiments were run at 298K, with 1D proton spectra collected using 16 scans. <sup>1</sup>H-NMR T<sub>2</sub> and diffusion experiments were performed by Dr. Patrick Edwards. Spectra collected in organic solvents, such as deuteromethanol (CD<sub>3</sub>OD) were referenced to tetramethylsilane (TMS). Spectra collected in deuterium oxide (D<sub>2</sub>O) were referenced to either the sodium salt of 3-(trimethylsilyl)-1-propanesulfonic acid (DSS) or to the chemical shift of water.

Direct titration experiments involved the dissolution of dye and titania into CD<sub>3</sub>OD. <sup>1</sup>H-NMR spectra of either the pure dye or titania solution were collected prior to addition of aliquots of the other titrant directly into the NMR sample tube. The samples were well shaken prior to recording spectra. A 1 mL automatic pipette was used to

deliver volumes of 0.05 mL, with an uncertainty of  $\pm 3\%$ . When weighing the mass of dry samples on a 5 decimal place balance, an uncertainty of 0.02 mg for a sample of 2 mg corresponds to an error of  $\pm 2\%$ . The error in the mass of water in sol-gel titania is  $\pm 1\%$ , while a conservative estimate of uncertainty in the calculated number of moles of dye is  $\pm 6\%$ . The uncertainty in the mole ratio of dye to 2 nm diameter titania is then approximately  $\pm 7\%$ .

Resuspension experiments first titrated dye with titania. The titrated mixture was drop-dried onto glass, rinsed with tetrahydrofuran to remove excess dye, then resuspended in methanol. The uncertainty in the mole ratio of dye to titania for these experiments will be higher than that of direct titration, as only a portion of the drop-dried material was able to be resuspended.

Solvent partition experiments used  $D_2O$  to solvate native sol-gel titania and deuteriochloroform ( $CDCl_3$ ) to produce a saturated solution of dye. In a typical trial 7.3 mg (0.3  $\mu\text{mol}$ ) of amorphous, acidic sol-gel titania was dissolved in 0.7 mL of deuterium oxide, which was then added to a saturated solution of 1.2 mg (6  $\mu\text{mol}$ ) of 4-methoxybenzylidenemalononic acid (**6.1**) in 0.7 mL of deuteriochloroform. This produced a 19 : 1 mole ratio of **6.1** to 2 nm titania particles. After standing for 15 minutes, the organic layer had become a clear, homogenous pale-yellow solution, while the aqueous layer became a clear, bright yellow colour. The  $D_2O$  layer was removed and  $^1\text{H-NMR}$  spectra collected.

Spin-spin  $T_2$  relaxation times for free and bound **6.1** were collected by direct measurement from a  $^1\text{H-NMR}$  Carr-Purcell-Meiboom-Gill (CPMG) spin echo experiment, while diffusion coefficients were measured by  $^1\text{H-NMR}$  spectroscopy using a pulsed field gradient and a simulated echo.

## 2.7. *Solar Cell Testing*

Flat, non-porous titania, Dyesol nanocrystalline titania, and titania inverse opals were tested for Grätzel cell efficiency using sample cell holders (Fig. 2.1) and solar-cell

testing apparatus designed by Dr. Wayne Campbell. Titania electrodes were heated at 400°C for an hour to remove organic contaminants and moisture, then allowed to cool to approximately 100°C. The titania plates were then soaked for a minimum of two hours in  $2.0 \times 10^{-4}$  M solution of dye in dry tetrahydrofuran. The samples were then either patted by lint-free tissue or gently rinsed in dry tetrahydrofuran, before being dried under vacuum in the dark for 3 minutes. Non-sealed Grätzel cells were then formed using a platinum metal counter electrode and an iodine/triiodide electrolyte.

Two electrolytes used were E-Zn-2 and E-Zn-3. E-Zn-2 was a solution of 0.1 M lithium iodide, 0.05 M iodine, 0.5 M 4-*tert*-butylpyridine and 0.6 M butylmethylimidazolium iodide in a 1:1 v/v solution of valeronitrile to glutaronitrile. The electrolyte E-Zn-3 was composed of 0.1 M lithium iodide, 0.05 M iodine, 0.5 M 4-*tert*-butylpyridine, 0.6 M butylmethylimidazolium iodide and 0.5 M 3,5-*tert*-butyl-4-hydroxytoluene in a 1:1 v/v solution of valeronitrile to glutaronitrile. The electrolyte E-Zn-3 has a light absorption of light of wavelengths of 450 nm and shorter.



**Figure 2.2.** A sample holder containing a Grätzel cell with a green porphyrin dye on a Dyesol nanocrystalline, mesoporous titania electrode.

Flat and non-porous titania, along with ‘standard’ nanocrystalline and mesoporous, pre-formed screen-printed Dyesol titania were the standards of comparison for the evaluation titania inverse opaline electrodes within Grätzel cells. The testing of the inverse opaline titania within solar cells was to be done with comparison between porphyrin-based dyes such as **6.9** and a ruthenium-based dye, *cis*-bis(isothiocyanato)bis(2,2'-bipyridyl-4,4'-dicarboxylato)-ruthenium(II) bis-tetrabutylammonium (‘Ru-535 bis-TBA’, ‘N3’ dye, Dyesol B2/N719). Also to be tested were a range of porphyrin-based sensitizers, synthesised in-house by the Nanomaterials Research Centre. However, due to the fragility of the inverse opals, such testing

remains to be done in the future.

Inverse opaline titania used in testing were samples that were infiltrated by titania precursor solution up to six times. Thin and dense titania films used for Grätzel cell testing were samples with up to two coats. Titania tested for Grätzel cell efficiency was dyed by immersion in a 0.2 mM solution of **6.9** in SDS brand tetrahydrofuran. The titania plates became a light green colour and were tested with electrolyte E-Zn-2.

## 2.8. References

1. Bertoz, M. The opaque paste 142op is the same as the transparent screen-printing paste 148, but that 20% of the titania is of 400 nm particles. *Dyesol Ltd.* **2006**, (October)
2. Frisch, M J; Trucks, G W; Schlegel, H B; Scuseria, G E; Robb, M A; Cheeseman, J R; Montgomery, J, J. A.; ; Vreven, T; Kudin, K N; Burant, J C; Millam, J M; Iyengar, S S; Tomasi, J; Barone, V; Mennucci, B; Cossi, M; Scalmani, G; Rega, N; Petersson, G A; Nakatsuji, H; Hada, M; Ehara, M; Toyota, K; Fukuda, R; Hasegawa, J; Ishida, M N, T.; Honda, Y.; Kitao, O.; Nakai, H.; Klene, M.; Li, X.; Knox, J. E.; Hratchian, H. P.; Cross, J. B.; Bakken, V.; Adamo, C.; Jaramillo, J.; Gomperts, R.; Stratmann, R. E.; Yazyev, O.; Austin, A. J.; Cammi, R.; Pomelli, C.; Ochterski, J. W.; Ayala, P. Y.; Morokuma, K.; Voth, G. A.; Salvador, P.; Dannenberg, J. J.; Zakrzewski, V. G.; Dapprich, S.; Daniels, A. D.; Strain, M. C.; Farkas, O.; Malick, D. K.; Rabuck, A. D.; Raghavachari, K.; Foresman, J. B.; Ortiz, J. V.; Cui, Q.; Baboul, A. G.; Clifford, S.; Cioslowski, J.; Stefanov, B. B.; Liu, G.; Liashenko, A.; Piskorz, P.; Komaromi, I.; Martin, R. L.; Fox, D. J.; Keith, T.; Al-Laham, M. A.; Peng, C. Y.; Nanayakkara, A.; Challacombe, M.; Gill, P. M. W.; Johnson, B.; Chen, W.; Wong, M. W.; Gonzalez, C.; and Pople, J. A.; Gaussian 03, Revision C.02; Gaussian, Inc: Wallingford CT, **2004**.
3. Spurr, A R; Harris, W M. *American Journal of Botany* **1968**, 55.
4. Spurr, A R. *Journal of Ultrastructure Research* **1969**, 26, 31.
5. Szekeres, M; Kamalin, O; Schoonheydt, R A; Wostyn, K; Clays, K; Persoons, A; Dekany, I. Ordering and Optical Properties of Monolayers and Multilayers of Silica Spheres Deposited by the Langmuir-Blodgett Method. *Journal of Materials Chemistry* **2002**, 12, 3268-3274.
6. Szekeres, M; Kamalin, O; Grobet, P G; Schoonheydt, R A; Wostyn, K; Clays, K; Persoons, A; Dekany, I. Two-Dimensional Ordering of Stober Silica Particles at the Air/Water Interface. *Colloids and Surfaces A: Physicochemical and Engineering Aspects* **2003**, 227, 77-83.
7. Wong, S; Kitaev, V; Ozin, G A. Colloidal Crystal Films: Advances in Universality and Perfection. *Journal of the American Chemical Society* **2003**, 125, 15589-15598.
8. Jiang, P; Bertone, J F; Hwang, K S; Colvin, V L. Single-Crystal Colloidal Multilayers of Controlled Thickness. *Chemistry of Materials* **1999**, 11, 2132-2140.
9. Kuai, S L; Hu, X F; Truong, V-V. Synthesis of Thin Film Titania Photonic Crystals Through a Dip-Infiltrating Sol-Gel Process. *Journal of Crystal Growth* **2003**, 259, 404-410.
10. Sakamoto, J S; Dunn, B. Hierarchical Battery Electrodes Based on Inverted Opal Structures. *Journal of Materials Chemistry* **2002**, 12, 2859-2861.
11. Huisman, C L; Schoonman, J; Goossens, A. The Application of Inverse Titania Opals in Nanostructured Solar Cells. *Solar Energy Materials & Solar Cells* **2005**, 85, 115-124.
12. Grant, C D; Schwartzberg, A M; Smestad, G P; Kowalik, J; Tolbert, L M; Zhang, J Z. Optical and Electrochemical Characterization of Poly(3-undecyl-2'-bithiophene) in Thin Film Solid State TiO<sub>2</sub> Photovoltaic Solar Cells. *Synthetic Metals* **2003**, 132, 197-204.
13. Burnside, S; Winkel, S; Brooks, K; Shklover, V; Grätzel, M; Hinsch, A; Kinderman, R; Bradbury, C; Hagfeldt, A; Pettersson, H. Deposition and Characterization of Screen-Printed Porous Multi-Layer Thick Film Structures From Semiconducting and Conducting Nanomaterials for Use in Photovoltaic Devices. *Journal of Materials Science: Materials in Electronics* **2000**, 11, 355-362.
14. Nazeeruddin, M K; Pechy, P; Renouard, T; Zakeeruddin, S M; Humphry-Baker, R; Comte, P; Liska, P; Cevey, L; Costa, E; Shklover, V; Spicca, L; Deacon, G B; Bignozzi, C S; Grätzel, M. Engineering of Efficient Panchromatic Sensitizers for Nanocrystalline TiO<sub>2</sub>-Based Solar Cells. *Journal of the American Chemical Society* **2001**, 123, 1613-1624.

15. Olsen, C M; Waterland, M R; Kelley, D F. Electron Injection Dynamics of Ru<sup>II</sup>(dcbpy)<sub>2</sub>(SCN)<sub>2</sub> on Zirconia. *Journal of Physical Chemistry B* **2002**, 106, 6211-6219.
16. Base, T; Cisarova, I; Stepnicka, P. Acid-Catalyzed Self-Alkylation of FcCH<sub>2</sub>NHPh. Solid-State Structures of FcCH<sub>2</sub>NHPh and (FcCH<sub>2</sub>)NPh. *Inorganic Chemistry Communications* **2002**, 5, 46-50.
17. Pal, S K; Alagesan, K; Samuelson, A G; Pebler, J. Synthesis and Characterization of Novel Charge Transfer Complexes formed by *N, N'*-bis(ferrocenylmethylidene)-*p*-phenylenediamine and *N*-(ferrocenylmethylidene)aniline. *Journal of Organometallic Chemistry* **1999**, 575, 108-118.
18. Toma, S; Gaplovsky, A; Elecko, P. Synthesis and Electronic Spectra of 1-aryl-2-ferrocenylethylenes. *Chemical Papers* **1985**, 39, 115-124.
19. McKeown, N B; Chambrier, I; Cook, M J. *Journal of the Chemical Society. Perkin Transactions 1* **1990**, 1169.
20. *Journal of the Chemical Society* **1947**, 560-561.
21. Chiang, M C; Hartung, W H. Synthesis of Some Stilbazole Derivatives. *Journal of Organic Chemistry* **1945**, 10, 21-25.
22. Cammidge, A N; Berber, G; Chambrier, I; Hough, P W; Cook, M J. Octaalkylphthalocyanato Ruthenium(II) Complexes with Mixed Axial Ligands and Supramolecular Porphyrin:Phthalocyanine Structures Derived From Them. *Tetrahedron* **2005**, 61, 4067-4074.
23. Hillebrandt, H; Tanaka, M. Electrochemical Characterisation of Self-Assembled Alkylsiloxane Monolayers on Indium-Tin-Oxide (ITO) Semiconductor Electrodes. *Journal of Physical Chemistry B* **2001**, 105, 4270-4276.
24. Chidsey, C E D; Bertozzi, C R; Putvinski, T M; Mujsee, A M. Coadsorption of Ferrocene-Terminated and Unsubstituted Alkanethiols on Gold: Electroactive Self-Assembled Monolayers. *Journal of the American Chemical Society* **1990**, 112, 4301-4306.
25. Tan, C Y K; Weaver, D F. A One-Pot Synthesis of 3-Amino-3-Arylpropionic Acids. *Tetrahedron* **2002**, 58, 7449-7461.
26. Hoogen, N; Nuyken, O. Synthesis and Photoreactions of Polyesters Containing Triazine and Cinnamylidene Malonyl Units. *Journal of Polymer Science: Part A: Polymer Chemistry* **2000**, 38, 1903-1910.
27. Baumgart, R J. A Novel Deamination. 2. Synthesis of Styrene and *Trans*-stilbene from 2-phenylethylamine and *N*-1,2-diphenylethylamine via Utilisation of Amide and Imide Anions as Leaving Groups. *Journal of Organic Chemistry* **1968**, 33, 234-238.
28. Wagner, P; Officer, D L. Unpublished results from our laboratories. **2007**.
29. Ghambir, S; Officer, D L. Unpublished results from our laboratories. **2007**.
30. McCreery, R L. *Raman Spectroscopy for Chemical Analysis*. Wiley Intersciences, John Wiley and Sons Inc.: Ohio, **2000**; Vol. 157.



### 3. *NANOSTRUCTURED TITANIA: INVERSE OPALS*

#### 3.1. *Introduction*

Inverse opals display a three-dimensional, periodic and regular array of material and are formed by deposition upon an opaline template. Particular interest in ideal inverse opaline structures stems from potential applications as photonic crystals. To display photonic band-gap properties there must be sufficient dielectric or refractive contrast in the crystal. Bragg scattering may be observed when the wavelength of incident light is comparable to the periodicity of the crystal, dependent on whether the material has a partial or complete photonic band-gap (Figure 3.1). A material with a full photonic band-gap will transmit or exclude light of every wavelength covered by the band-gap, regardless of polarisation, at every angle of incidence. A partial photonic band-gap will only allow the trapping and amplification of light of a certain wavelength at all angles of incidence.<sup>1</sup> Opals and inverse opals with tunable photonic band-gaps have been produced by infiltration by an optically birefringent nematic liquid crystal. The application of an electric field or thermal energy induces a change in phase and refractive index of the liquid crystal, which alters the photonic band-gap of the composite material.<sup>2, 3</sup> An opal will trap or reflect light at a particular angle of incidence, provided that the periodicity of the crystal approximates the wavelength of the incident light.

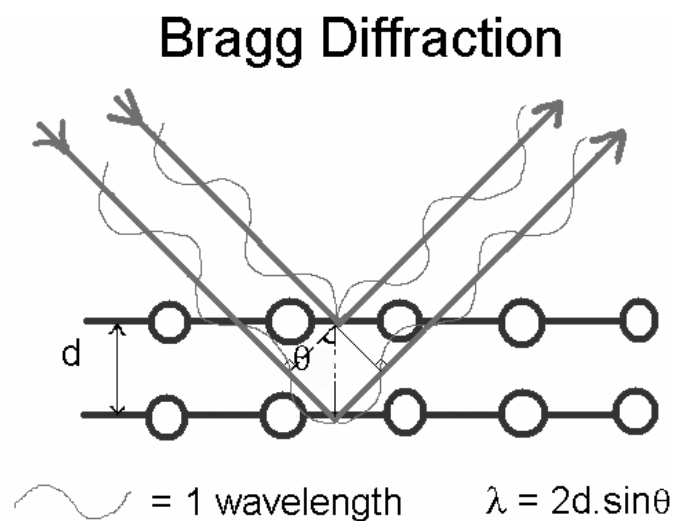


**Figure 3.1.** A schematic of the concept of Bragg diffraction of light from a regular, periodic array.

Inverse opals may display the same photonic properties and have been produced with a diverse range of materials, including polypyrrole and lithium niobate.<sup>4, 5</sup> An ideal titania inverse opaline electrode would be opaque, so that light lost by transmission through the Grätzel cell is minimised. The electrode should also display a ‘honeycomb’ structure, be mechanically robust, free of crystal boundary defects and have excellent physical and electrical contact to the substrate. For application within a Grätzel cell, the inverse opal must have open pores and a uniform coverage to ensure the total penetration of sensitizer dye and electrolyte to give consistent performance across the electrode. It was envisaged that a number of identical titania electrodes with a minimum usable area of 1 cm<sup>2</sup> would be required for testing with various sensitizer dyes.

### 3.2. *Opals*

In order to form opaline templates, the colloids involved must show narrow size-distributions. For cost-efficiency opals tend to be made of silica or polymers such as polystyrene and polyacrylates, though opals of materials such as colloidal gold have also been produced. The colloids themselves may be layered materials, such as double-shelled cadmium selenide, encapsulated first by polystyrene and then by silica.<sup>6-9</sup> Opaline templates have been formed by electrophoresis,<sup>10-12</sup> centrifugation,<sup>13</sup> sedimentation or spin-coating with and without lithographically-defined beds,<sup>14, 15</sup> the use of flow-cells<sup>16</sup> and Langmuir-Blodgett troughs.<sup>2</sup> Techniques that utilise a falling meniscus include the dip-coating of a functionalised surface, tape-casting and solvent loss from particle suspensions. A few examples of the last method include deposition onto a vertically-held substrate by solvent evaporation, the use of a peristaltic pump, slow crystallisation of an opal between quartz plates and deposition onto a horizontal substrate bounded by silicone liquid.<sup>17-21</sup> The use of silicone to overlay the boundary of an aqueous suspension forces the evaporation of water to occur evenly over the sample, reducing crack formation.<sup>22</sup> Binary opals have been formed by the shrinking liquid volume of electrosprayed droplets.<sup>23</sup>

### 3.3. *Inverse Opals*

Inverse opals may be made either by the co-deposition of the target material during opal formation or by infiltration of the opal. Infiltration may be done either with preformed nanoparticles or by a precursor solution of the target species. Co-deposition of different sized colloids may form binary or tertiary colloidal crystals, of which the larger colloid is often the template material. In a number of cases, the pH of the colloidal suspension is kept above the isoelectric point of the different species in order to reduce flocculation and aggregation. In this manner, inverse opals of titania, silica, gold and combinations of the three have been formed around disposable polystyrene opals.<sup>23-29</sup> Silica inverse opals have been made with gold embedded within the walls of the structure first by co-deposition of silica-encased gold colloids and polystyrene beads, followed by calcination.<sup>30</sup> Infiltration of pre-formed opals uses capillary force to pull nanoparticle suspensions or precursor solutions into the template voids. Centrifugation or vacuum filtration may be used to assist the complete filling of the template interstices, though repetitive dip-coating has been found to be sufficient.<sup>31-33</sup> Organic inverse opals of polyaniline can be formed by infiltration of a polystyrene opal with aniline, followed by chemical oxidative polymerisation and dissolution of the template with tetrahydrofuran.<sup>34</sup> Electrochemical methods have been used to oxidise titanium trichloride and polymerise pyrrole around an opaline template, for inverse opals of titania and polypyrrole, respectively.<sup>4,35</sup>

Sintering of the composite material is frequently a necessary step in the formation of inorganic inverse opals, as heat may be required to complete hydrolysis from a precursor material, to convert amorphous material to a crystalline phase and to fuse adjacent grains for improved mechanical strength. During sintering, an increase in grain size, a decrease in the number of crystal grain boundaries and a reduction in the surface area of the material may also be observed.<sup>36, 37</sup> Calcination or dissolution is often employed to eliminate polymeric templates, while silica templates may be removed by etching with sodium hydroxide or hydrofluoric acid.<sup>2</sup> In the case of a silica opaline template, sintering prior to infiltration with the target material is necessary to fuse colloids together and to the substrate. The mechanical strength of the template is improved as is the ease with which the template may be removed.<sup>38</sup> A distinct advantage of using polymer opaline templates over inorganic materials is that contact

between colloids and the substrate may be improved by relatively gentle thermal treatment, applied pressure or simply letting the material meld with each other.<sup>17, 39</sup>

### 3.4. *Opaline Templates of Silica*

Sacrificial opaline templates were made of silica, as the material is simple, inexpensive and colloids with a narrow size distribution may be synthesised.<sup>40</sup> For the production of silica colloids a derivation of the Stober-Fink-Bohn ammonia-catalysed hydrolysis of tetraethylorthosilicate was used in this work.<sup>41</sup> In brief, tetraethylorthosilicate was added into a 4 M methanolic solution of ammonia that was stabilised at 60°C and vigorously stirred. The concentration of silica precursor in the total volume was 0.34 M, resulting in colloids with an average diameter of 250 nm. The silica colloids were separated and washed by centrifugation with 95 v/v% ethanol and allowed to air-dry. Scanning electron microscopy (SEM) images show the rough surface of the silica colloids which are formed by the aggregation of primary particles during colloid formation (Fig. 3.2).<sup>42</sup>

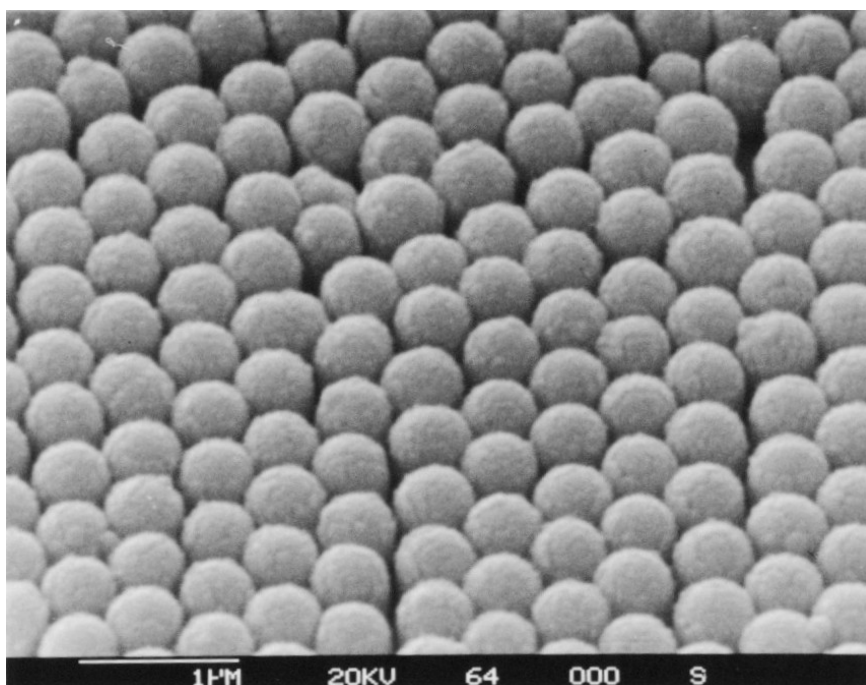


**Figure 3.2.** SEM image of a silica opal deposited upon glass. The scale bar is for 1 μm.

Opals were formed by a technique adapted from the literature, which was a vertical deposition of colloids by the falling meniscus of an evaporating solvent.<sup>19, 40</sup> This method was chosen in order to quickly produce a large number of opals upon a substrate. Drop-drying upon a horizontal substrate was found to be lacking, as a clearly non-uniform opal resulted. Indium-doped tin oxide glass (ITO) was coated with silica opal by suspension of the substrate within a vial of an ethanolic dispersion of silica colloids. By placing the vial in a 60°C oven overnight, thin films of close-packed silica spheres were deposited by the dropping meniscus. The substrate must not contact the vial walls, so that a meniscus of a uniform shape and height may deposit a more uniform opal. All opals formed with 250 nm silica spheres, by this method displayed a green opalescence when viewed from directly above, while 350 nm silica spheres displayed an orange opalescence due to the Bragg diffraction of light off the colloidal crystal. Regions of both hexagonal and cubic close-packing are produced by this method (Fig. 3.3).

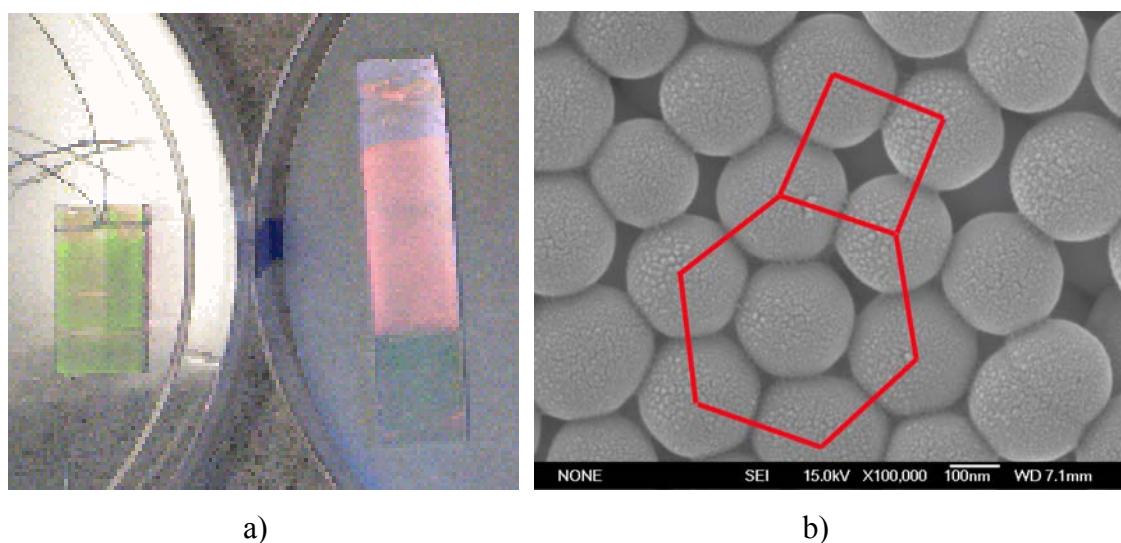


**Figure 3.3.** a) The opal composed of 250 nm silica spheres displays the Bragg diffraction of green light, while the opal made of 350 nm spheres diffracts orange light. b) Detail of silica colloids, with titania nanocrystals. Square and hexagonal close-packing is highlighted. The scale bar is for 100 nm.

Typically, a 0.5% wt/wt dispersion of silica to ethanol was used; at concentrations greater than about 5% wt/wt, the opaline material exhibited heavy ‘banding’. This ‘banding’ has been described as ‘buckled’ domains and are a result of the uneven deposition of material by the falling solvent front.<sup>43</sup> Analogous behaviour has been seen in the formation of thickened edges for drop-dried colloidal crystals, which may be attributed to the higher rate of solvent evaporation at the exposed rim of the suspension.<sup>22</sup> The buckled domains are likely to be a contributing cause to the variable morphology of inverse opals. When silica dispersions are more concentrated than approximately 15 wt/wt% dramatic cracking and delamination occurs (Fig. 3.4). The omnipresent cracking of the template is likely to be due to capillary forces on removal of the solvent during the deposition and drying of the colloidal crystals.<sup>44, 45</sup> Faults that parallel the plane of the substrate may also have been formed by capillary forces and may have reduced the effective thickness of the template. Such planar faults may explain why the formed inverse opals all appeared to display a thickness of less than twenty colloidal layers.

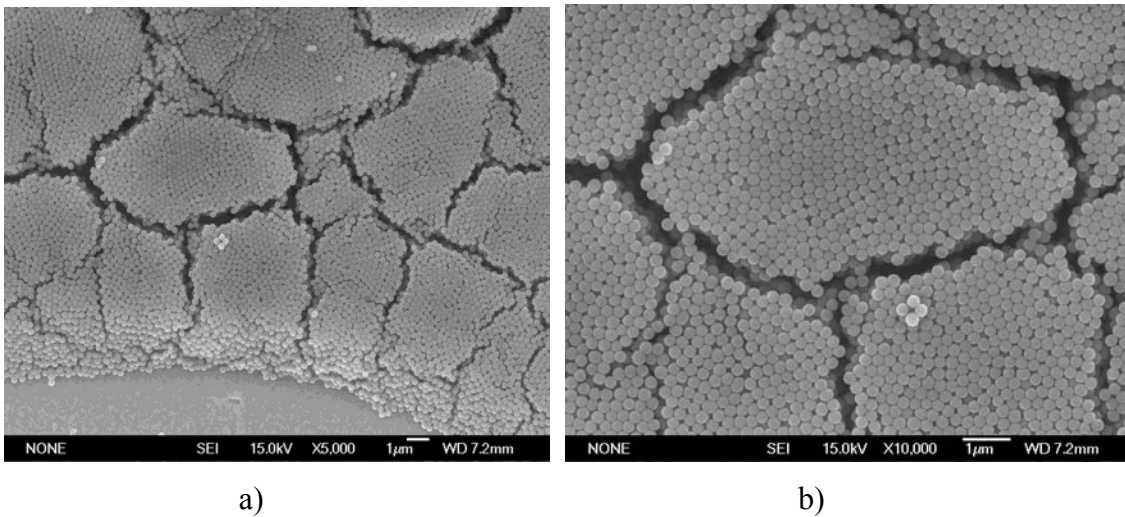


**Figure 3.4.** a) A typical, fractured silica opal. b) The same opal at a higher magnification. The scale bars are for 1 μm.

### 3.5. *Titania Inverse Opals*

The ‘honeycomb’ structure is more physically robust than shell-type structures. An open pore morphology is also necessary for the admission of sensitiser dyes into the bulk of the electrode. The transparency of titania inverse opals upon glass is reduced from that of Dyesol nanocrystalline and mesoporous titania electrodes which are used for Grätzel cell testing in our laboratory. This is as less titania is used to form the inverse opaline electrodes and so less material is available to absorb and scatter incident light. The loss of opacity may be compensated for if the inverse opal was a photonic crystal, with a partial or complete photonic band-gap. The liquid-phase infiltration of a titanium alkoxide solution is a versatile method that was adapted from published techniques. A solution of titanium isopropoxide, dry ethanol and ethylene diamine was used to infiltrate the silica templates and form inverse opals of titania.<sup>31, 38, 46, 47</sup>

Titania inverse opals were formed with a range of morphologies, ranging from partially templated material to close-packed air-spheres in a ‘honeycomb’ form and titania resembling ‘grapes’ (Figs. 3.5, 3.6). The ideal ‘honeycomb’ material implies that the opaline interstices have been completely filled with the titania precursor species. In contrast, the incomplete filling of interstices resulted in highly porous titania shells which resembled ‘grapes’.

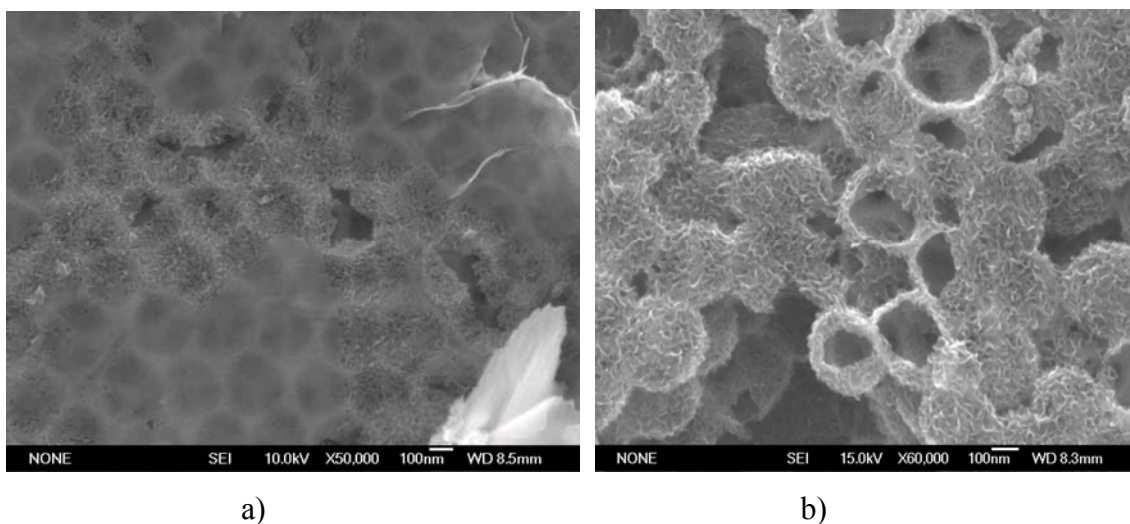


**Figure 3.5.** a) An inverse opal that resembles sealed ‘honeycomb’. b) An inverse opal exhibiting a ‘grape’-like morphology. The scale bars are for 100 nm.

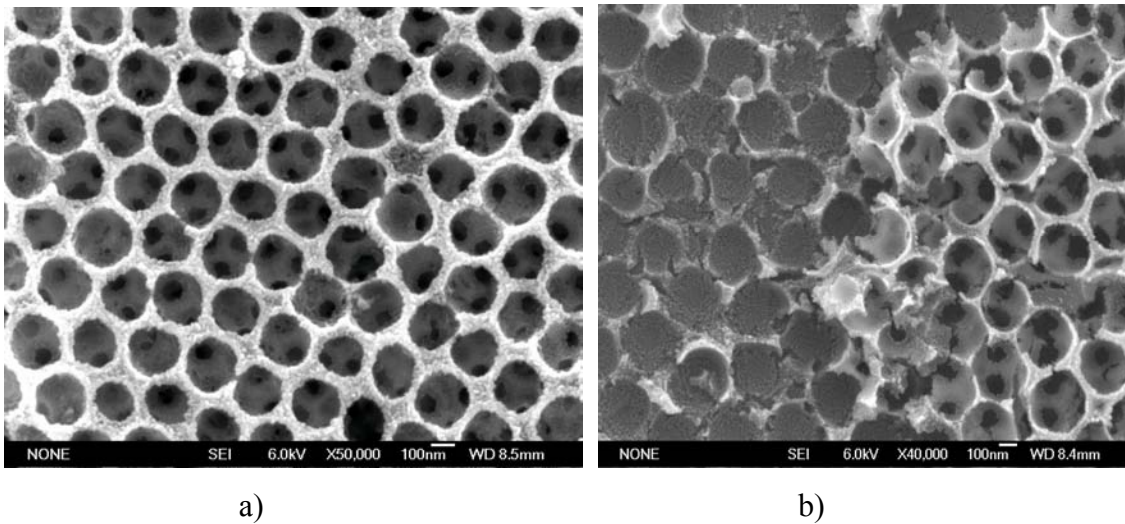
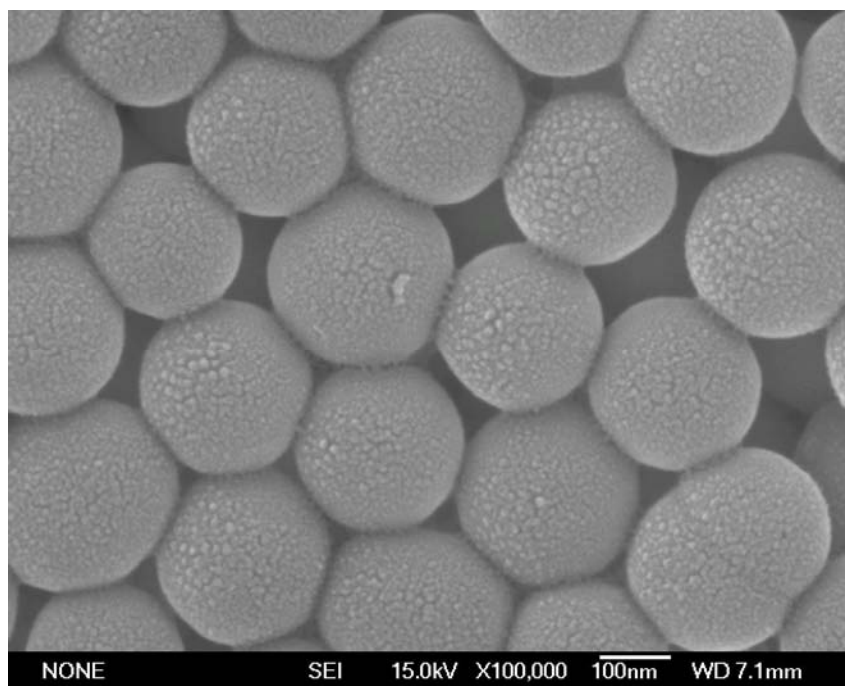
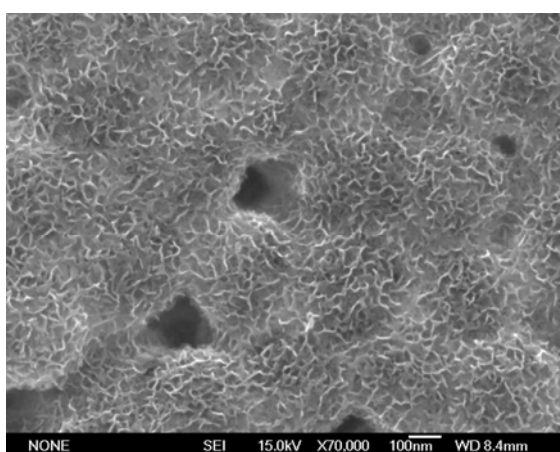


**Figure 3.6.** a) The desired ‘honeycomb’ morphology. Note that windows connect adjacent air-spheres and that the interstices appear to be completely filled. b) Partial, almost ‘skeletal’ inverse opals. The scale bars are for 100 nm.

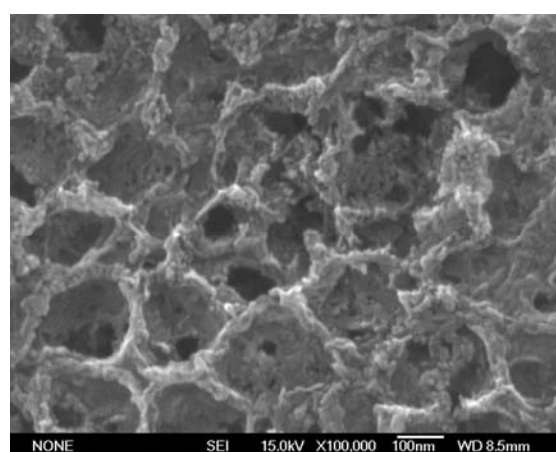
The inverse opals are completely composed of anatase nanocrystals, as shown by grazing incidence X-ray diffraction (XRD) and backscattered resonance Raman spectroscopy. The primary particles may be seen as grains or fibrils upon silica beads which are only lightly templated with titania. Both sintering of the composite material between titania infiltration steps and sintering of titania inverse opals after removal of the opaline template resulted in a loss of definition in structure. The growth of what appear to be the primary particles of the material results in a morphology that resembles ‘coral’ (Fig. 3.7).



a)



b)



c)

**Figure 3.7.** a) Granular and fibrillar titania nanoparticles may be observed on lightly-templated silica colloids, particularly where colloids meet. b) Titania inverse opal formed by six cycles of infiltration and rinsing, with two treatments with water, then sintering at 500°C. c) An inverse opal displaying a ‘coral’-like morphology was displayed, perhaps due to sintering. The sample was treated twice with: three cycles of infiltration and rinsing, a treatment with water and sintering at 500°C. Both samples used 1 : 40 : 0.6 infiltrate and 1 : 120 : 0.6 rinsing solutions. The scale bars are for 100 nm.

A typical treatment protocol that resulted in the formation of macroporous, inverse opals which displayed large regions of either open-faced ‘honeycomb’ or of opened ‘grapes’ is illustrated in Table 3.1. Solutions with either a 1 : 20 : 0.6 or a 1 : 40 : 0.6 molar ratio of titanium isopropoxide : dry ethanol : ethylene diamine were used for infiltration and a solution with a 1 : 120 : 0.6 molar ratio of reactants was used for rinsing after each infiltration. Opals formed upon ITO glass were placed within screw-cap vials with the infiltration solution and topped with argon to keep the precursor solution dry. Samples were then centrifuged for twenty minutes at 3000g of relative centrifugal force (rcf) to aid the capillary force in drawing solution into the template. The infiltrated opals were vertically and mechanically withdrawn from both infiltrate and rinsing solutions at approximately 40 mm min<sup>-1</sup>. To retard the premature formation of titania on the exterior of the template and within solution, vials containing the infiltration and rinsing solutions were refreshed with argon gas after every use. The composition of the precursor solution was modified from the literature as it was found that the addition of a 0.33 molar equivalent of water caused the immediate formation of titania. Repeated infiltration of the opaline template was necessary to ensure that a sufficient amount of titania was deposited.<sup>31, 38</sup> The more promising samples were formed with greater than three infiltration cycles and were treated at least once with water to ensure the complete formation of the titania alkoxide and so prevent shrinkage and warpage of the inverse opals. The composite material was sintered at 500°C for an hour, with a stepped temperature ramp, before the template was dissolved with 30 wt% aqueous sodium hydroxide. Despite the various degrees of fill of the opal interstices and the range of resultant morphologies, all inverse opal samples were transparent and exhibited Bragg diffraction of visible light, though the observed opalescence was notably weaker than that of the templates.

**Table 3.1.** The typical treatment protocol to form inverse opals of titania.

**Opal Formation**

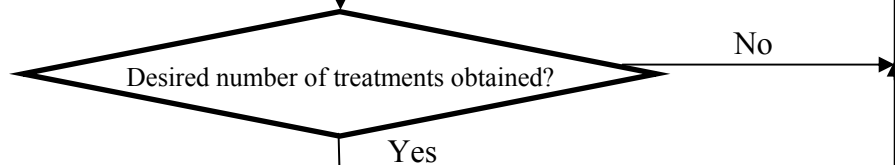
1. ITO glass is cleaned with several times with hexane and ethanol.
2. The ITO is suspended vertically in a vial containing a 0.5 wt/wt% methanolic silica dispersion.
3. The solvent is removed by placing the vial in a 60°C oven, overnight.
4. The resulting opal is sintered for an hour at 500°C. The temperature is ramped.

**Infiltration of the Opal**

1. Opal-covered ITO is placed in a 20 mL screw-cap vial, with 15 mL of infiltrate and argon gas.
2. The infiltrate is a titania precursor solution with 1: 40 : 0.6 molar ratios of tetraisopropylorthotitanate : dry ethanol : diethanolamine, which is kept dry under argon.
3. The vial, containing the opal is centrifuged for 15 min at 3000g of rcf.

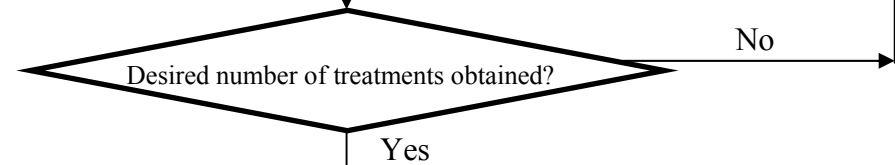
**Withdrawal and Rinsing of the Infiltrated Opal**

2. The opal is withdrawn vertically at 40 mm min<sup>-1</sup>.
3. The opal is immediately placed into a rinser solution.
4. The rinser is a solution with 1 : 120 : 0.6 molar ratios of tetraisopropylorthotitanate : dry ethanol : diethanolamine, kept under argon.
5. The opal is at once withdrawn vertically at 40 mm min<sup>-1</sup>.



**Treatment with Water**

2. To ensure the complete conversion of tetraisopropylorthotitanate to titania, samples are soaked in water for a minimum of one hour, at 60°C.



**Template Disposal**

1. The titania-silica composites are sintered for an hour at 500°C. The temperature is ramped.
2. The template is removed by soaking overnight in 30 wt/wt% aqueous sodium hydroxide, at 60°C.
3. The titania inverse opals are sequentially rinsed in 20, 15, 10 and 5 wt/wt% sodium hydroxide.
4. Samples are sequentially rinsed in 0, 25, 50, 75 and 100 v/v% solutions of 95% ethanol in water.
5. The titania inverse opals are allowed to air-dry.

**END**

Early experiments also involved solutions of a 1 : 40 : 0.6 molar ratio of titanium isopropoxide : dry ethanol : ethylene diamine and were centrifuged for twenty minutes at 1700g or 3000g of rcf. However, these samples were withdrawn manually or with a mechanical withdraw of 20 mm min<sup>-1</sup>. Samples that were not treated with a rinse cycle no longer were opalescent, due to the formation of a white, opaque film of excess titania. The weight of the excess material generally caused the bulk of the sample to delaminate, leaving disordered, semi-detached or fragmented material on the substrate (Fig. 3.8.a). Samples which did not delaminate appeared to have only the top few colloidal layers templated by titania. This may be as these samples were not treated with water, only the precursor solution which lay close to exposed faces was hydrolysed to produce titania. In addition, for such samples which were only top-face templated, it is possible that on sintering, unreacted infiltrate trapped within the composite material forced an exit under pressure. Titania would then be deposited at the surface, leaving voids within the template and material bearing little resemblance to an inverse opal (Fig. 3.8.b). Trapped titanium isopropoxide may also have been hydrolysed at the later stage of template removal. Following the dissolution of silica by sodium hydroxide, it is plausible that condensation of titania without the template would result in an ill-defined macrostructure. Competition between the complete infiltration of the template and sealing of the top face seemed to be controlled by the concentration of the precursor solution, the infiltration protocol and the number of infiltration cycles.

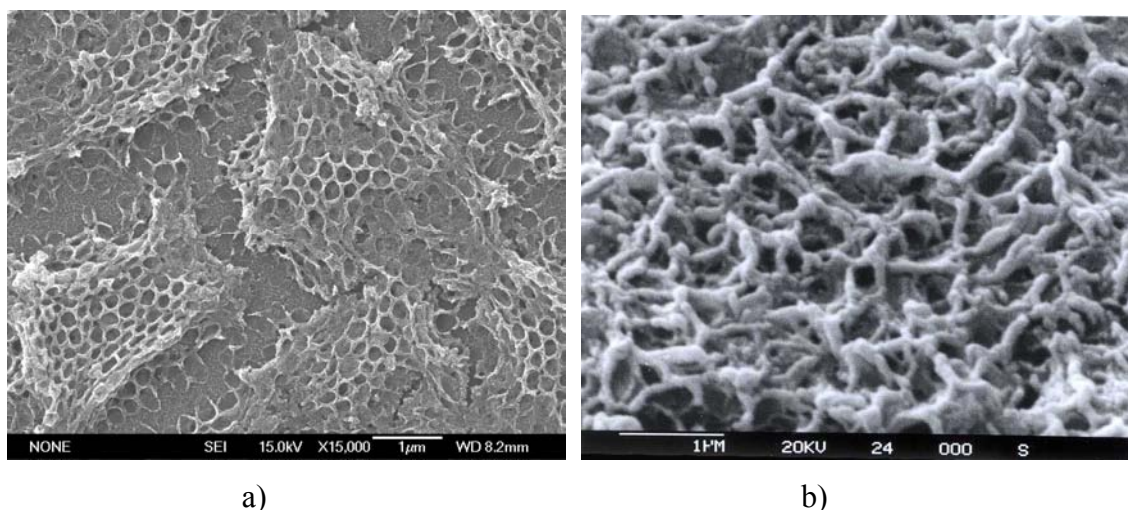


**Figure 3.8.** a) Disordered, fragmented material from a sample that was not treated with water. b) Condensed matter that resulted from two cycles of infiltration and rinsing, without treatment with water. The scale bars are for 1 μm.

The main obstacle in the determination of what treatment parameters influenced nanostructure was that any given inverse opal displayed a number of different morphologies. Optical and transmission electron micrographs showing cross-sections of inverse opals demonstrate the extent of the fractures and faults. It appears that the cracks have not been filled up with titania, indicating that the rinsing step of infiltration is successful in removing excess material from cracks and in reducing the excess material on the top-face of the template (Fig. 3.9). The various faults observed with inverse opaline titania include cracks, packing disorder and sealed faces that may be the result of planar faults in the template. The use of a temperature ramp to sinter the composite material and the removal of sodium hydroxide from inverse opals by rinsing in decreasing sodium hydroxide concentrations, followed by the displacement of water by ethanol were intended to minimise further fracturing or delamination of material.

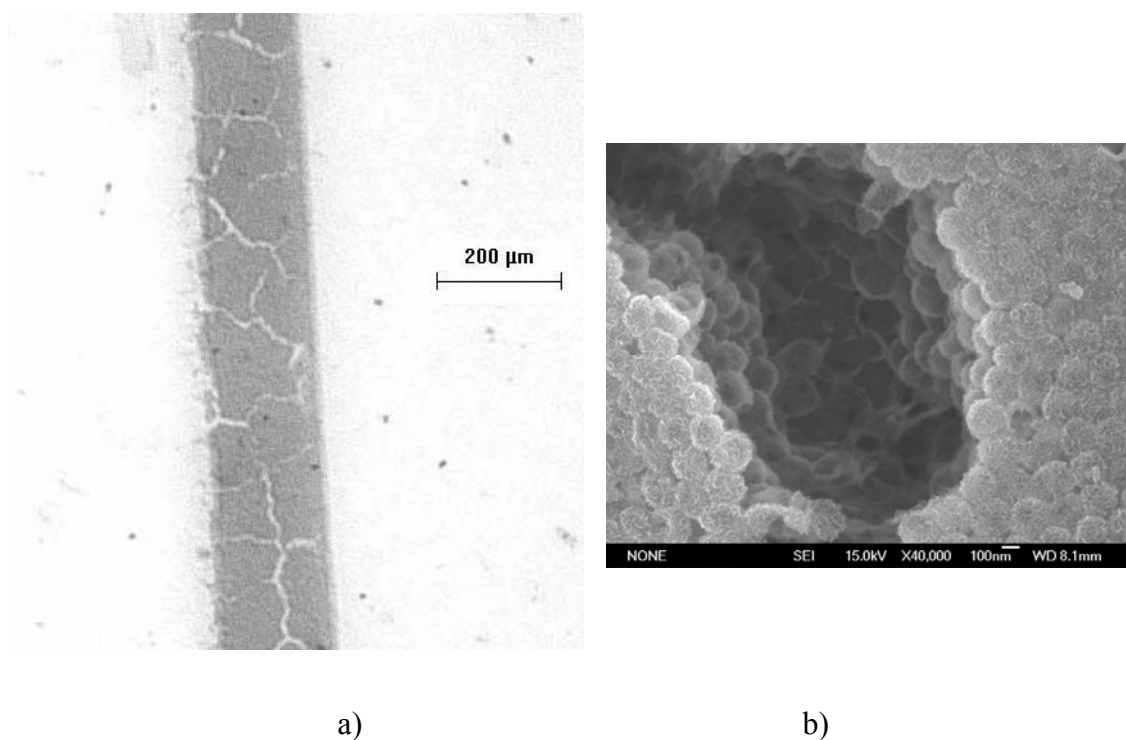


**Figure 3.9.** a) TEM image of a cross-section of a titania inverse opal, illustrating open fractures and a sealed top-face. The scale bar is for 200  $\mu\text{m}$ . b) SEM image of sample which was treated with rinsing steps. Colloids at the crack faces were cleanly templated, without excess titania occupying the crevice. The scale bar is for 100 nm.

To reduce the excess titania that templated the exposed opaline surface, samples were rinsed immediately after infiltration. A dilution of the precursor solution, rather than a pure solvent, was chosen as the rinsing solution. This was under the proposal that the 'osmotic' pressure or concentration gradient between the interior of the opal and solution bulk would then not be so great. The intention was to purge the titania precursor from only the top few colloidal layers. However, it appears as though the bulk of the infiltrated solution was removed. This is as shown by SEM the thickness of the inverse opal is less than twenty colloidal layers while the thickness of the template is a few hundred layers. Variable filling fractions of interstitial voids within the opals have been inferred from samples that display morphologies ranging from the ideal open 'honeycomb' structure to 'grape' formations consisting of close-packed shells. Such materials are reminiscent of examples from the literature of both 'ring and shell' and skeletal structures.<sup>20, 48</sup> The formation of shell structures supports that suggestion that when a rinsing step is employed deposition of titania upon silica colloids occurs first, followed by filling of the interstices. The bulk of the infiltrate may have been displaced during rinsing, leaving only a thin film of infiltrate to coat the silica colloids. In addition, the presence of adsorbed moisture within the template may have resulted in the formation of shells. The infiltrate may have reacted with water on the colloidal surfaces, producing titania nanoparticles prior to rinsing of the template. The presence of pre-formed particles within the infiltrating solution may also have favoured the formation of thicker shells about the template by entrapment of precursor solution during rinsing stages. The sealing of the top-face or of planar faults in the template was prominent near 'buckled' domains, where thinner regions of the template were sealed below a titania film. Such 'sealed honeycomb' often displayed titania film that had fractured and contracted, revealing the underlying inverse opal or ITO glass (Fig. 3.10).

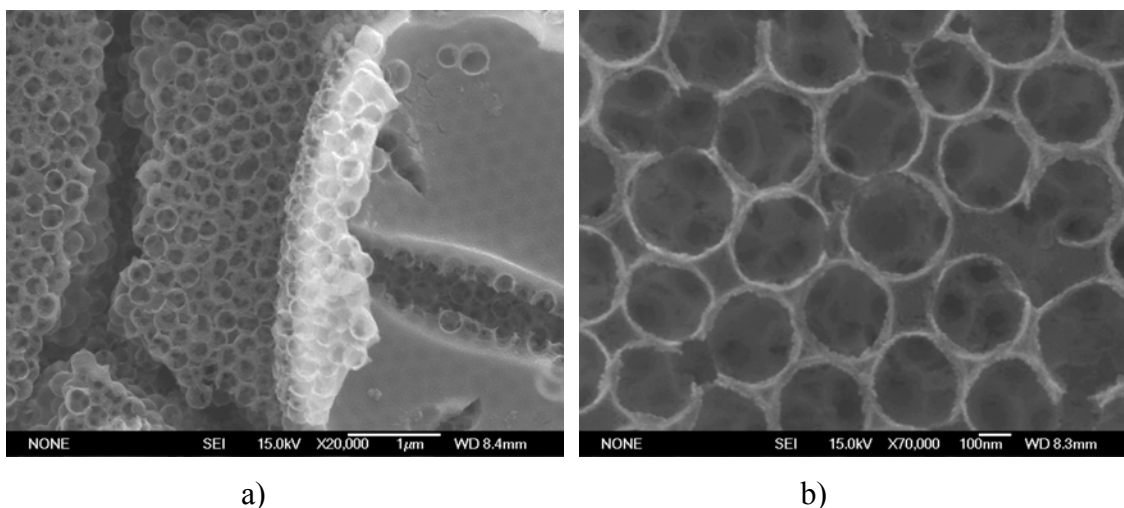


**Figure 3.10.** a) Titania film contracted away from the inverse opal below. This sample had six infiltrations and a treatment with water. The scale bar is for 1  $\mu\text{m}$ . b) The 'honeycomb' morphology, which is composed of thin titania shells. This sample was infiltrated five times and treated once with water. The scale bar is for 100 nm.

Samples treated with twelve cycles of infiltration and rinsing were transparent and adhered to ITO glass as well as samples which were only treated twice, provided that the solutions used were kept dry. A comparison was done of opaline templates treated with a single infiltration and with six infiltrations (Fig. 3.11). The singly-infiltrated sample was treated with water, while a sample infiltrated six times was only allowed to air-dry. The sample of a single infiltration displays only a 'basement' layer of titania, while multiple infiltrations resulted in the deposition of more material and structures that displayed a 'honeycomb' morphology. The formation of such 'basement' structures of titania is likely to be due to the insufficient filling of the template voids such that only the space between the first layer of the template and the substrate was templated. Similarly, titania rings have been formed by the templation of a monolayer of polystyrene spheres by an acidic sol-gel of titania.<sup>49</sup> A large shrinkage in pore size, accompanied by deformation and collapse was evident for samples not treated with water before sintering. The best structures resulted when samples were infiltrated multiple times and treated at least once during the process by soaking in water to ensure the complete conversion of the precursor to titania.

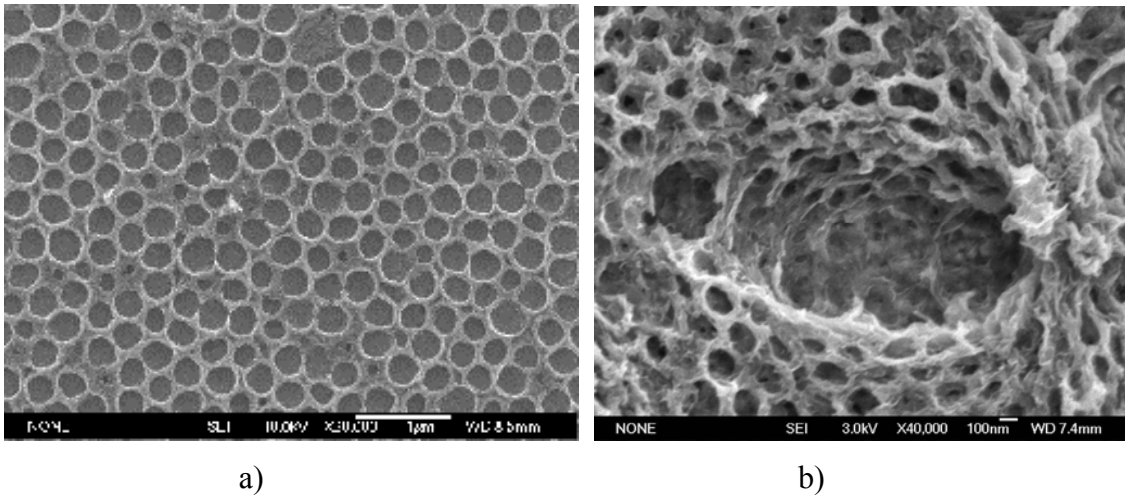
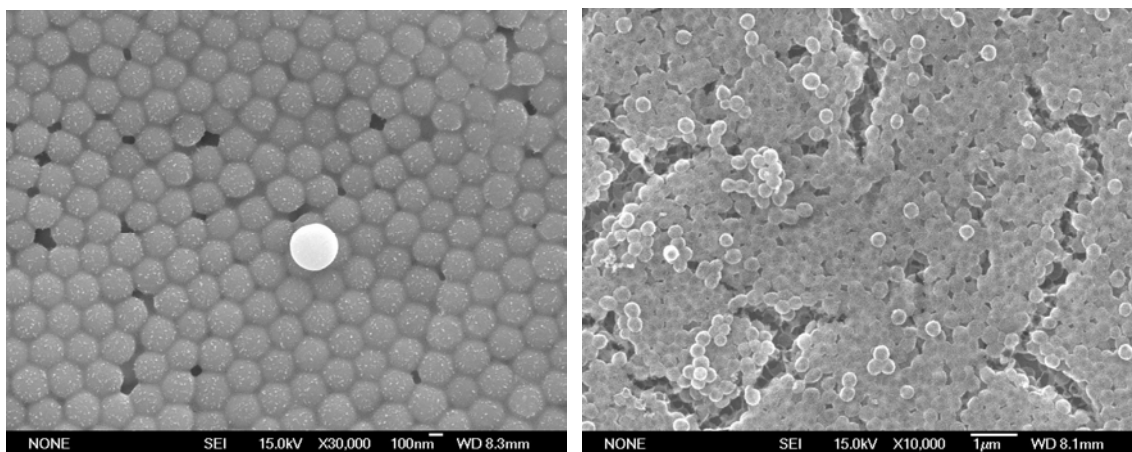


**Figure 3.11.** These samples used an infiltrate with a molar ratio of 1 : 20 : 0.6 and a rinsing solution with 1 : 80 : 0.6 of titanium isopropoxide to dry ethanol to diethanol amine. The scale bar is for 1  $\mu\text{m}$ . a) A ‘basement’ layer of inverse opal that exhibited practically no shrinkage. The opal had two cycles of infiltration, rinsing and treatment with water. b) Significant warpage and shrinkage was observed for this sample that was infiltrated six times and air-dried, before sintering. The scale bar is for 100 nm.

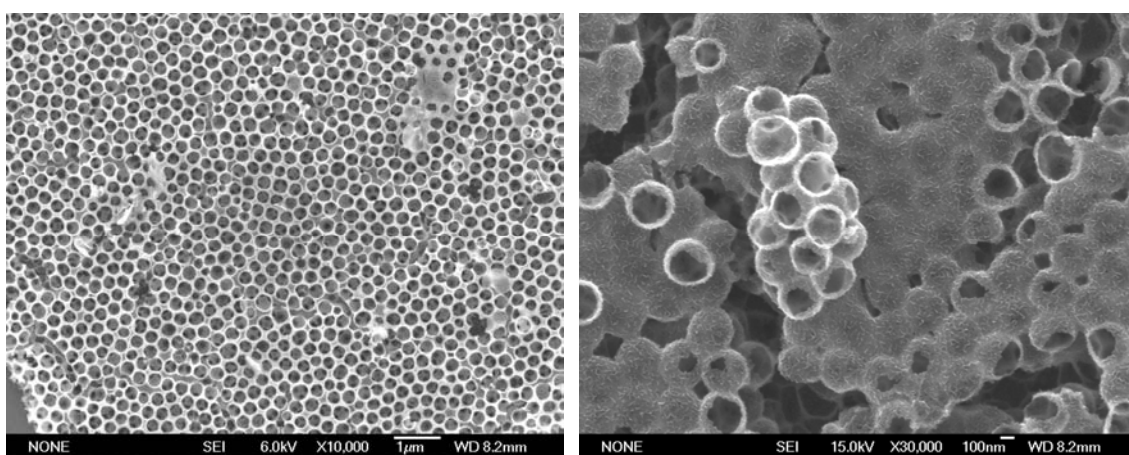
The difficulty of reproducible production of titania inverse opals by this method is illustrated by the variation in sample morphology (Figs. 3.12, 3.13). Six cycles of infiltration, rinsing and two treatments by soaking in water to ensure the complete hydrolysis of titania were used for the samples imaged in Figure 3.12 and Figure 3.13.b. While the concentration of the infiltration and rinsing solutions differed, the resulting inverse opal still displayed a ‘grape-like’ form. This is in contrast to the desired ‘open-face honeycomb’ morphology that was observed when the higher concentration infiltration and rinsing solutions were used to treat the template for a total of twelve cycles (Fig. 3.13.a). This indicated that perhaps simply increasing the number of infiltration cycles to twelve would reproducibly give titania electrodes with a ‘honeycomb’ structure.



a)

b)

**Figure 3.12.** a) Titania-silica composite formed by six cycles of infiltration and rinsing, with two treatments with water, then sintered at 500°C. Molar ratios of 1 : 40 : 0.6 and 1 : 120 : 0.6 for reactants were used for infiltration and rinsing, respectively. The scale bar is for 100 nm. b) The resulting inverse opal displays a ‘grape-like’ morphology. The scale bar is for 1 μm.



a)

b)

**Figure 3.13.** a) Inverse opaline titania, with long-range structure. Twelve cycles of infiltration with centrifugation, then rinsing was followed by one treatment with water before sintering at 500°C. Molar ratios of 1 : 40 : 0.6 and 1 : 120 : 0.6 for reactants were used for the infiltration and rinsing solutions, respectively. The scale bar is for 1 μm. b) A structure that resembles 'grapes'. Six cycles of infiltration were followed with two treatments with water. Solutions with molar ratios of 1 : 20 : 0.6 for both the infiltrate and rinsing solutions were used. The scale bar is for 100 nm.

However, while open- and closed-face ‘honeycomb’ material was produced, the coverage of the substrate appeared to be less than samples treated with only six cycles of infiltration. The increased number of treatments resulted in the samples becoming more prone to delamination off the substrate and there was also a greater variation in the thickness of the adhered titania film (Fig. 3.14).

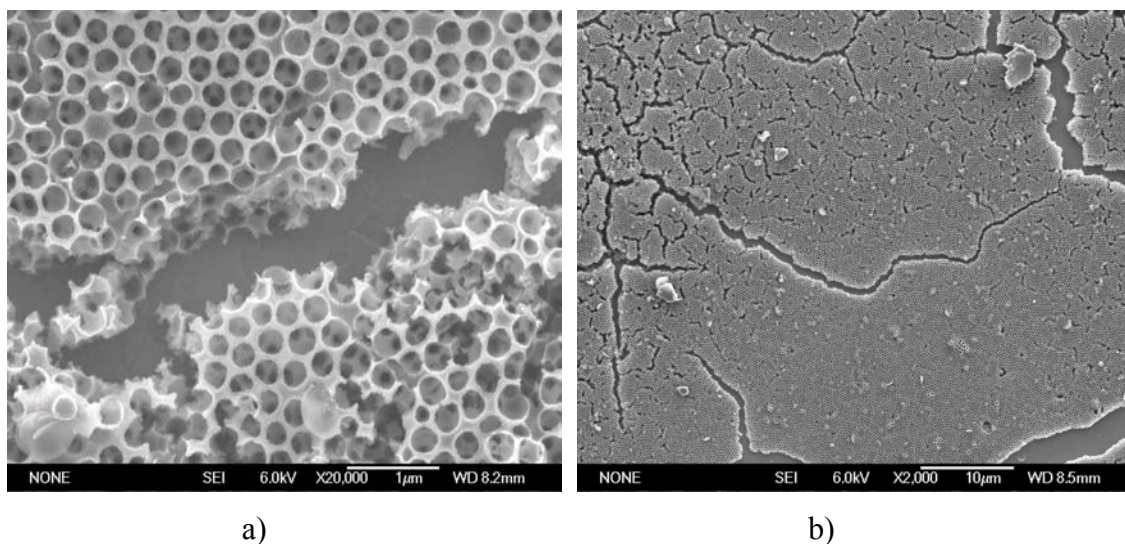


**Figure 3.14.** The difficulty of obtaining reproducible inverse opals is illustrated. Both of these samples were treated by twelve cycles of infiltration with centrifugation and rinsing. This was followed by one treatment with water before sintering at 500°C. Molar ratios of 1 : 40 : 0.6 and 1 : 120 : 0.6 for reactants were used for the infiltration and rinsing solutions, respectively. a) The desired ‘honeycomb’ structure is displayed with filled interstices and windows to adjacent air-spheres. Fractures such as these were common. The scale bar is for 1 μm. b) Open-face ‘honeycomb’ material was received, but with extensive cracking and large variation in film thickness. The scale bar is for 10 μm.

Regarding Grätzel cell testing of the titania inverse opals, a zinc porphyrin dye was chosen for use as a sensitizer, as the extinction coefficient is higher than that of the available ruthenium dye. However, given the profusion of fissures and defects in the titania inverse opals that were produced, the thin, transparent and relatively fragile

nature of the material, it was predictable that the produced photocurrent and photovoltages were comparable to that of flat and non-porous titania. The measured current and voltages were barely detectable, though the dyed electrodes did exhibit colouration to the naked eye.

### **3.6. Conclusions**

Inverse opals of titania were obtained with morphologies that include the ideal 'honeycomb' form, a 'basement' layer of rings and 'grape-like' materials. While titania inverse opals and related structures such as rings, discrete spheres and 'skeletal' structures have been reported in the literature,<sup>49-51</sup> this work showed that a range of morphologies may be observed together. The varied inverse opaline morphologies are likely to be due to incomplete and irreproducible filling of the opaline interstices and faults in the opaline template.

The inverse opaline material formed in this study was fractured, fragile and difficult to reproduce. A rinsing step was necessary during the infiltration process to remove excess material and so prevent sealing of the top face of the opaline template. Treatment with water prior to sintering of the silica-titania composite material ensured the complete hydrolysis of the titania precursor. Shrinkage and warpage of the titania inverse opal following template removal was then reduced. Templatation appears to occur first by deposition onto the silica spheres, followed by filling of the interstices. Delamination appears to be a result of excess material on the top-face of the template. Cracking of the silica templates and the resulting inverse opals probably result during the sintering process, due to a difference in the thermal expansion coefficients of silica, titania and ITO glass. The published data show that the domain size for titania inverse opals is on the order of 10 - 50  $\mu\text{m}$ ,<sup>29</sup> which is comparable to samples of this work (Fig. 3.4), though the domains are much larger for the original opaline templates.<sup>20, 24</sup>

Inverse opaline titania was produced and tested for power conversion efficiency within Grätzel cells. The relatively poor performance of the inverse opals is likely to be due to the fragility and non-uniformity of the material. In addition, as the majority of the volume of an inverse opaline electrode is void, there is less titania available for dye

adsorption and light-harvesting than in the nanocrystalline, screen-printed material that is normally used for Grätzel cell testing. The low Grätzel cell performance may also be due to poor contact between nanoparticles, as studies of lithium cation insertion into anatase inverse opals found that the electrical conductivity between particles was poor.<sup>35</sup> In addition, any regions of disordered inverse opals would have produced up to ten times less photocurrent than perfectly ordered material.<sup>52</sup>

### 3.7. References

1. Kittel, C. *Introduction to Solid State Physics*. 7<sup>th</sup> ed, John Wiley & Sons: Canada, **1996**.
2. Xia, Y; Gates, B; Yin, Y; Lu, Y. Monodispersed Colloidal Spheres: Old Materials With New Applications. *Advanced Materials* **2000**, 12, 693-1041.
3. Kubo, S; Gu, Z-Z; Takahashi, K; Fujishima, A; Segawa, H; Sato, O. Tunable Photonic Band Gap Crystals Based on Liquid Crystal-Infiltrated Inverse Opal Structure. *Journal of the American Chemical Society* **2004**, 126, 8314-8319.
4. Cassagneau, T; Caruso, F. Conjugated Polymer Inverse Opals for Potentiometric Biosensing. *Advanced Materials* **2002**, 14, 1837-1841.
5. Wang, D; Caruso, F. Lithium Niobate Inverse Opals Prepared by Templating Colloidal Crystals of Polyelectrolyte-Coated Spheres. *Advanced Materials* **2003**, 15, 205-210.
6. Halaoui, L I; Abrams, N M; Mallouk, T E. Increasing the Conversion Efficiency of Dye-Sensitized TiO<sub>2</sub> Photoelectrochemical Cells by Coupling to Photonic Crystals. *Journal of Physical Chemistry B* **2005**, 109, 6334-6342.
7. Ji, L; Rong, J; Yang, Z. Opal Gel Templated Synthesis of Oblate Titania Opal Materials. *Chemical Communications* **2003**, 1080-1081.
8. Fink, J; Kiely, C J; Bethell, D; Schiffrin, D J. Self-Organisation of Nanosized Gold Particles. *Chemistry of Materials* **1998**, 10, 922-926.
9. Yang, X; Zhang, Y. Encapsulation of Quantum Nanodots in Polystyrene and Silica Micro-Nanoparticles. *Langmuir* **2004**, 20, 6071-6073.
10. Shiu, J-Y; Kuo, C-W; Chen, P. Actively Controlled Self-Assembly of Colloidal Crystals in Microfluidic Networks by Electrocapillary Forces. *Journal of the American Chemical Society* **2004**, 126, 8096-8097.
11. Gong, T; Wu, D T; Marr, D W M. Electric Field-Reversible Three-Dimensional Colloidal Crystals. *Langmuir* **2003**, 19, 5967-5970.
12. Golding, R K; Lewis, P C; Kumacheva, E. *In Situ* Study of Colloid Crystallization in Constrained Geometry. *Langmuir* **2004**, 20, 1414-1419.
13. Miguez, H; Tetreault, N; Yang, S M; Kitaev, V; Ozin, G A. A New Synthetic Approach to Silicon Colloidal Photonic Crystals with a Novel Topology and an Omni-Directional Photonic Bandgap: Micromoulding in Inverse Silica Opal (MISO). *Advanced Materials* **2003**, 15, 597-600.
14. Chen, S-L. Preparation of Monosize Silica Spheres and their Crystalline Stack. *Colloids and Surfaces A: Physicochemical and Engineering Aspects* **1998**, 142, 59-63.
15. Xia, D; Brueck, S J R. A Facile Approach to Directed Assembly of Patterns of Nanoparticles Using Interference Lithography and Spin Coating. *Nano Letters* **2004**, 4, 1295-1299.
16. Park, S H; Xia, Y. Assembly of Mesoscale Particles over Large Areas and Its Application in Fabricating Tunable Optical Filters. *Langmuir* **1999**, 15, 266-273.
17. Sato, T; Brown, D; Johnson, B F G. Nucleation and Growth of Nano-Gold Colloidal Lattices. *Chemical Communications* **1997**, 1007-1008.
18. Prevo, B G; Velev, O D. Controlled, Rapid Deposition of Structured Coatings from Micro- and Nanoparticle Suspensions. *Langmuir* **2004**, 20, 2099-2107.

19. Wong, S; Kitaev, V; Ozin, G A. Colloidal Crystal Films: Advances in Universality and Perfection. *Journal of the American Chemical Society* **2003**, 125, 15589-15598.
20. Zhou, Z; Zhao, X S. Opal and Inverse Opal Fabricated with a Flow-Controlled Vertical Deposition Method. *Langmuir* **2005**, 21, 4717-4723.
21. Wang, W; Gu, B; Liang, L; Hamilton, W. Fabrication of Two- and Three-Dimensional Silica Nanocolloidal Particle Arrays. *Journal of Physical Chemistry B* **2003**, 107, 3400-3404.
22. Fudouzi, H. Fabricating High-Quality Opal Films with Uniform Structure Over a Large Area. *Journal of Colloid and Interface Science* **2004**, 275, 277-283.
23. Moon, J H; Yi, G-R; Yang, S-M; Pine, D J; Park, S B. Electrospray-Assisted Fabrication of Uniform Photonic Balls. *Advanced Materials* **2004**, 16, 605-609.
24. Meng, Q-B; Fu, C-H; Einaga, Y; Gu, Z-Z; Fujishima, A; Sato, O. Assembly of Highly Ordered Three-Dimensional Porous Structure with Nanocrystalline TiO<sub>2</sub> Semiconductors. *Chemistry of Materials* **2002**, 14, 83-88.
25. Gu, Z-Z; Uetsuka, H; Takahashi, K; Nakajima, R; Onishi, H; Fujishima, A; Sato, O. Structural Color and the Lotus Effect. *Angewandte Chemie, International Edition* **2003**, 42, 894-897.
26. Subrimania, G; Constant, K; Biswas, R; Sigalas, M M; Ho, K-M. Synthesis of Thin Film Photonic Crystals. *Synthetic Metals* **2001**, 116, 445-448.
27. Kitaev, V; Ozin, G A. Self-Assembled Surface Patterns of Binary Colloidal Crystals. *Advanced Materials* **2003**, 15, 75-78.
28. Ruge, A; Tolbert, S H. Effect of Electrostatic Interactions on Crystallization in Binary Colloidal Films. *Langmuir* **2002**, 18, 7057-7065.
29. Gu, Z-Z; Kubo, S; Fujishima, A; Sato, O. Infiltration of Colloidal Crystal with Nanoparticles Using Capillary Forces: A Simple Technique for the Fabrication of Films with an Ordered Porous Structure. *Applied Physics A: Materials Science & Processing* **2002**, 74, 127-129.
30. Wang, D; Salgueirino-Maceira, V; Liz-Marzan, L M; Caruso, F. Gold-Silica Inverse Opals by Colloidal Crystal Templating. *Advanced Materials* **2002**, 14, 908-912.
31. Kuai, S L; Hu, X F; Truong, V-V. Synthesis of Thin Film Titania Photonic Crystals Through a Dip-Infiltrating Sol-Gel Process. *Journal of Crystal Growth* **2003**, 259, 404-410.
32. Sakamoto, J S; Dunn, B. Hierarchical Battery Electrodes Based on Inverted Opal Structures. *Journal of Materials Chemistry* **2002**, 12, 2859-2861.
33. Schroden, R C; Al-Daous, M; Stein, A. Self-Modification of Spontaneous Emission by Inverse Opal Silica Photonic Crystals. *Chemistry of Materials* **2001**, 13, 2945-2950.
34. Wang, D; Caruso, F. Fabrication of Polyaniline Inverse Opals via Templating Ordered Colloidal Assemblies. *Advanced Materials* **2001**, 13, 350-353.
35. Kavan, L; Zukalova, M; Kalbac, M; Grätzel, M. Lithium Insertion into Anatase Inverse Opal. *Journal of the Electrochemical Society* **2004**, 151, A1301-A1307.
36. Blanford, C F; Yan, H; Schroden, R C; Al-Daous, M; Stein, A. Gems of Chemistry and Physics: Macroporous Metal Oxides with 3D Order. *Advanced Materials* **2001**, 13, 401-407.
37. Kambe, S; Murakoshi, K; Kitamura, T; Wada, Y; Yanagida, S; Kominami, H; Kera, Y. Mesoporous Electrodes Having Tight Agglomeration of Single-Phase Anatase TiO<sub>2</sub> Nanocrystallites: Application to Dye-Sensitized Solar Cells. *Solar Energy Materials & Solar Cells* **2000**, 61, 427-441.

38. Kuai, S; Badilescu, S; Bader, G; Bruning, R; Hu, X; Truong, V-V. Preparation of Large-Area 3D Ordered Macroporous Titania Films by Silica Colloidal Crystal Templating. *Advanced Materials* **2003**, 15, 73-75.
39. Schaak, R E; Cable, R E; Leonard, B M; Norris, B C. Colloidal Crystal Microarrays and Two-Dimensional Superstructures: a Versatile Approach for Patterned Surface Assembly. *Langmuir* **2004**, 20, 7293-7297.
40. Jiang, P; Bertone, J F; Hwang, K S; Colvin, V L. Single-Crystal Colloidal Multilayers of Controlled Thickness. *Chemistry of Materials* **1999**, 11, 2132-2140.
41. Szekeres, M; Kamalin, O; Grobet, P G; Schoonheydt, R A; Wostyn, K; Clays, K; Persoons, A; Dekany, I. Two-Dimensional Ordering of Stober Silica Particles at the Air/Water Interface. *Colloids and Surfaces A: Physicochemical and Engineering Aspects* **2003**, 227, 77-83.
42. Park, J; Privman, V; Matijevic, E. Model of Formation of Monodispersed Colloids. *Journal of Physical Chemistry B* **2001**, 105, 11630-11635.
43. Abkarian, M; Nunes, J; Stone, H A. Colloidal Crystallization and Banding in a Cylindrical Geometry. *Journal of the American Chemical Society* **2004**, 126, 5978-5979.
44. Dufresne, E R; Corwin, E I; Greenblatt, N A; Ashmore, J; Wang, D Y; Dinsmore, A D; Cheng, J X; Xie, X S; Hutchinson, J W; Weitz, D A. Flow and Fracture in Drying Nanoparticle Suspensions. *Physical Review Letters* **2003**, 91, 224501-224504.
45. Lee, W P; Routh, A F. Why Do Drying Films Crack? *Langmuir* **2004**, 20, 9885-9888.
46. Fan, Q; McQuillin, B; Ray, A K; Turner, M L; Seddon, A B. High Density, Non-Porous Anatase Titania Thin Films for Device Applications. *Journal of Physics D: Applied Physics* **2000**, 33, 2683-2686.
47. Grant, C D; Schwartzberg, A M; Smestad, G P; Kowalik, J; Tolbert, L M; Zhang, J Z. Optical and Electrochemical Characterization of Poly(3-undecyl-2'-bithiophene) in Thin Film Solid State TiO<sub>2</sub> Photovoltaic Solar Cells. *Synthetic Metals* **2003**, 132, 197-204.
48. Dong, W; Bongard, H J; Tesche, B; Marlow, F. Inverse Opals with a Skeleton Structure: Photonic Crystals with Two Complete Bandgaps. *Advanced Materials* **2002**, 14, 1457-1460.
49. Sun, F; Yu, J C; Wang, X. Construction of Size-Controllable Hierarchical Nanoporous TiO<sub>2</sub> Ring Arrays and Their Modifications. *Chemistry of Materials* **2006**, 18, 3774-3779.
50. Cheng, X; Chen, M; Wu, L; Gu, G. Novel and Facile Method for the Preparation of Monodispersed Titania Hollow Spheres. *Langmuir* **2006**, 22, 3858-3863.
51. Dong, W; Bongard, H J; Marlow, F. New Type of Inverse Opals: Titania With Skeleton Structure. *Chemistry of Materials* **2003**, 15, 568-574.
52. Huisman, C L; Schoonman, J; Goossens, A. The Application of Inverse Titania Opals in Nanostructured Solar Cells. *Solar Energy Materials & Solar Cells* **2005**, 85, 115-124.



## 4. *NANOSTRUCTURED TITANIA FOR BINDING STUDIES*

### 4.1. *Introduction*

To study the behaviour of adsorbed dyes upon titania it was necessary to produce titania in a number of different forms and to apply a range of spectroscopic techniques. Thin film non-porous sintered, porous aggregated sintered and dispersible non-sintered titania was produced for this investigation. Sintered titania was deposited upon a transparent substrate to allow both transmittance and reflectance spectroscopy of adsorbed species. The dispersible form of titania was produced in order to allow the investigation of bound species in homogenous, optically transparent solutions using nuclear magnetic resonance (NMR) spectroscopy, in addition to optical spectroscopic techniques. In addition, the use of dispersed sol-gel titania in dye binding studies may also give an indication regarding the behaviour of adsorbed sensitiser dyes on the surface of a working Grätzel cell, where solvent is endemic. The difference in surface chemistry between the sintered and non-sintered materials was unavoidable. Sintering of titania in air results in an oxidised surface, while any stable dispersion of nanoparticulate titania requires stabilisation from either steric hindrance or electrostatic repulsion.

Sintering is done to ensure a crystalline phase, to meld particles to each other and the substrate and to clear the surface of any organic residue. For Grätzel cells, sintering also dehydrates the titania surface prior to exposure to dyes in order to maximise sensitiser adsorption. A typical regime is to hold the sample at 450°C for 30 minutes in order to ensure the removal of physisorbed and chemisorbed water.<sup>1</sup> Sintering of screen-printed materials is vital in the elimination of the organic component of the film. In the absence of organic species the relatively low temperature of 150°C may be used to sinter 2 to 16 µm thick tape-cast films of pre-formed, crystalline titania.<sup>2</sup> In contrast, to produce stable nanoparticle dispersions of either preformed titania aggregates or colloids, highly acidic solutions or the use of ligating species, such as hydrochloric acid and tri-*n*-octylphosphine oxide, are generally involved.<sup>3,4</sup>

## 4.2. *Thin and Non-porous Titania*

In anticipation that information on the surface coverage, aggregation, binding mode and orientation of adsorbed species may be collected by both transmission and reflectance spectroscopies, sintered thin non-porous titania that was optically transparent was produced. This material was also used as a ‘benchmark’ against which the power conversion efficiency of inverse opaline titania within Grätzel cells was compared (Section 3.5).

Techniques for the formation of dense thin-films of titania include dip-coating, spin-coating and chemical vapour deposition.<sup>5-7</sup> Dip- and spin-coating methods generally rely on the hydrolysis of the stabilised titanium alkoxide by atmospheric moisture. Titania precursor solutions used for dip- and spin-coating are generally alcoholic and contain acid-stabilised titanium alkoxides, though basic chelating species such as diethanolamine have also been used.<sup>8, 9</sup> For vertical dip-coating, reported withdraw rates range from 1.5 to 40 mm min<sup>-1</sup>, depending on the viscosity and relative reactivity of the titania sol. Sols using titanium alkoxides have been used to produce titania of different primary grain sizes upon different substrates. Titania with a primary grain size of 20 nm has been formed on indium-doped tin oxide (ITO), while particles 50 to 150 nm result on monocrystalline silicon. As stable sol-gels of titania are typically amorphous, sintering of films is required to obtain crystalline material.<sup>10-12</sup>

A variant of the solution used in the formation of inverse opals (Section 3.5) was simplified to produce thin and non-porous titania by the dip-coating of ITO glass. The samples required neither rinsing, nor treatment with water as the atmospheric moisture was sufficient to completely hydrolyse the titania precursor. Mechanical vertical withdrawal speeds of approximately 40 mm min<sup>-1</sup>, rather than 20 mm min<sup>-1</sup>, produced smoother films. Thin and non-porous titania appeared to be formed by the deposition of nanosized particles with ‘in-filling’ by the precursor solution. It is debatable whether particles within the film that are visible by scanning electron microscopy (SEM) were pre-formed in solution or nucleated upon defects of the ITO surface (Fig. 4.1.a). Occasional pores are apparent, which may indicate the formation of a bubble in the film or the loss of a partially-embedded particle. Raised, partially-embedded particles were not observed, which provides circumstantial evidence that pores may be formed as a

result of air bubbles displacing the precursor solution from between titania particles. Possible models for the formation of a smooth titania film containing particulate matter include those of La Mer and Dinegar or of Ostwald. The former model describes the initial nucleation of primary particles, followed by the addition of monomers, or oligomers of the reactive species.<sup>13</sup> The latter model states that agglomeration and particle growth occur by the dissolution and reprecipitation of material between contacting particles.<sup>14</sup> An alternative argument was that the contrasting spots observed with SEM may be underlying contours of ITO glass. However, investigation of defective films show that embedded layers of particles may be seen and cross-sections indicate that films are approximately 300 nm thick. Also, pores appear to have a sharp outline, which contradicts the intuitive thought that a smoothing of substrate features would be expected from a dip-coated film. Atomic force microscopy (AFM) has been used to profile the surface and gave a root mean squared (RMS) roughness of 5 to 15 nm, which is larger than the RMS roughness of 2 to 5 nm for bare ITO glass. The increased RMS roughness of titania films may be expected if particulate matter has been embedded within the film (Fig. 4.1.b).

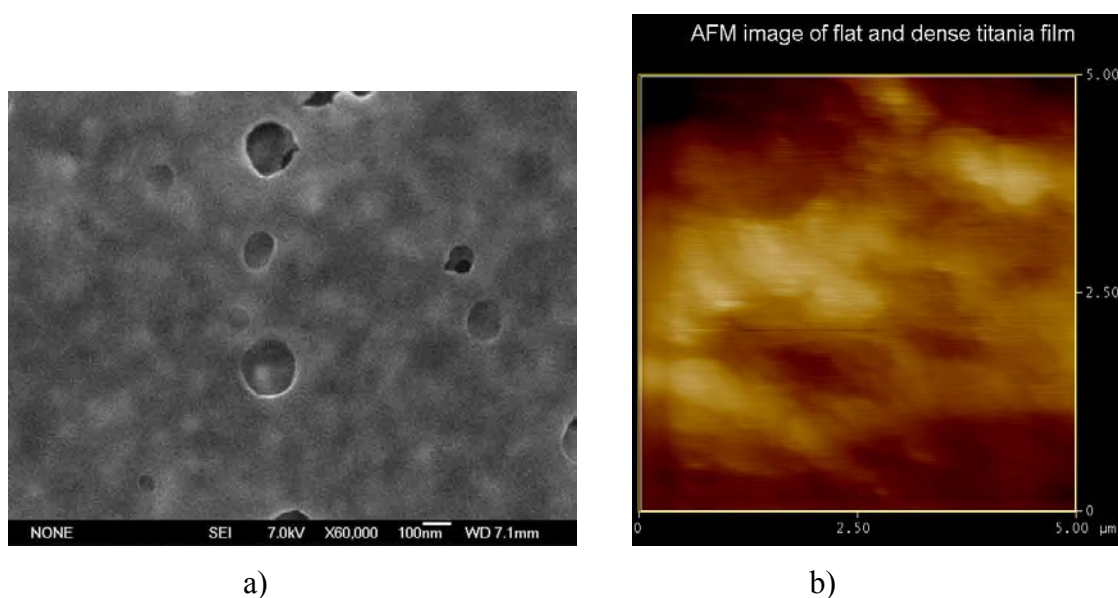


**Figure 4.1.** a) A SEM image of flat and dense titania with two coats. b) A contact mode AFM image of thin and non-porous titania formed by two sequential dip-coats into a solution with a 1 : 40 : 0.6 molar ratio of titanium isopropoxide : dry ethanol : diethanolamine. A 40 mm min<sup>-1</sup> dip speed was used to produce a film with a RMS roughness of 10 nm.

Cyclic voltammetry with hexacyanoferrate was used to confirm that the thin and non-porous titania acted as a blocking layer (Fig. 4.2).<sup>15, 16</sup> Samples with multiple coats of titania displayed a greater suppression of peak charge than singly-coated samples, which indicated that later layers effectively filled in defects of the first coat of titania. Probable defects in the film include cracks, pores and damaged sample edges. The thin and dense titania was highly resistive, so the use of scanning tunnelling microscopy (STM) to investigate dyes adsorbed to the surface was not an option. By grazing incidence X-ray diffraction (XRD) and Raman scattering at 785 nm, thin and non-porous titania films and titania inverse opals formed in this work were verified to be purely anatase. The photocurrents obtained from Grätzel cells tested with thin and dense titania electrodes was on the lower limit of detection at 1  $\mu\text{A}$  for an active area of 1  $\text{cm}^2$  and was on par with the efficiencies recorded for cells using inverse opaline titania electrodes.

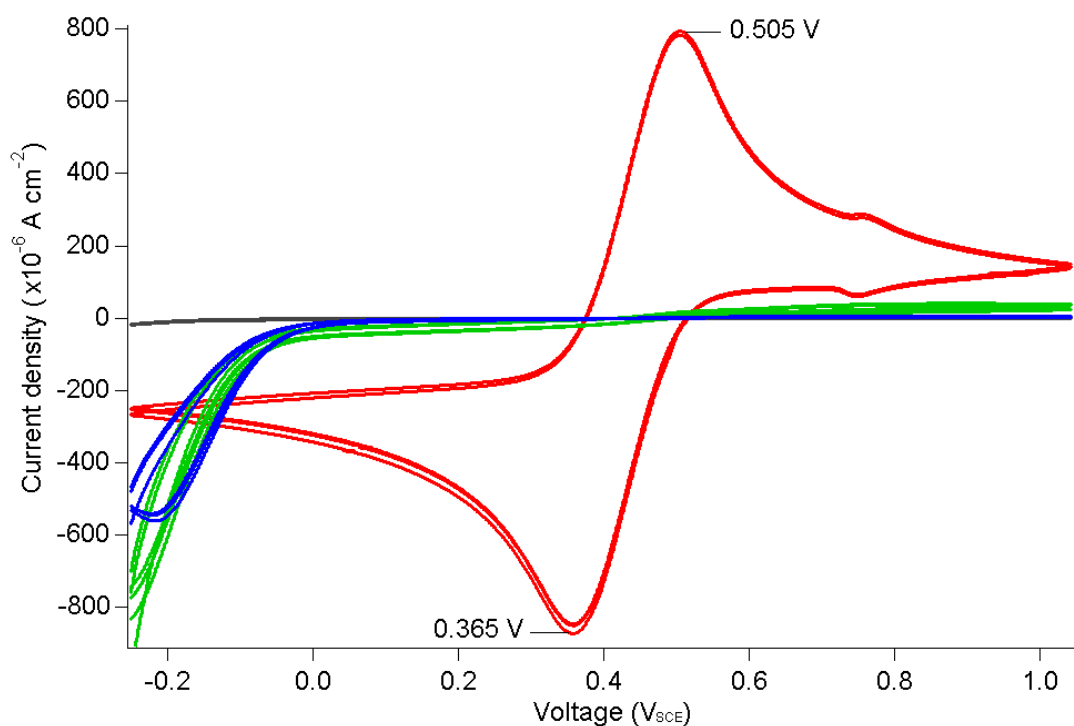


**Figure 4.2.** Cyclic voltammetry of blank ITO and ITO dip-coated with thin and non-porous titania in a 1 mM hexacyanoferrate solution: blank ITO glass (—), a single coat (—), a double coat (—) and a triple coat (—). Redox activity is suppressed with increasing coats of thin and non-porous titania. The electrolyte was 0.1 M tetrabutylammonium perchlorate in acetonitrile, voltage is given with respect to the standard calomel electrode. The scan rate was 100  $\text{mV s}^{-1}$ .

### 4.3. *Aggregated and Sintered Titania*

Sintered and aggregated titania used for dye adsorption include Dyesol opaque pre-formed titania plates, Dyesol screen-printing paste, Degussa Aeroxide<sup>®</sup> P25 hydrophilic fumed titania and acidic sol-gel titania. Application of Degussa P25 and sol-gel titania powders onto glass substrates was by screen-printing and ‘spin-thinning’ methods, respectively.

Pre-formed and pre-sintered Dyesol titania electrodes are opaque screen-printed, nanocrystalline, mesoporous titania. These electrodes are currently used for efficiency tests of Grätzel cells in our laboratory. Dynamic light scattering (DLS) measurements of the sintered material give an average diameter of 1.5  $\mu\text{m}$ . SEM images show that the screen-printed films are approximately 12  $\mu\text{m}$  thick films, which is in agreement with micrometer measurements (Fig. 4.3.a). By powder XRD the material is approximately 3 : 1 anatase to rutile in composition, while Brunauer-Emmett-Teller (BET) nitrogen adsorption isotherm experiments gave an available surface area of 60.0  $\text{m}^2 \text{g}^{-1}$ .

Screen-printed films vary in thickness from 5 to 20  $\mu\text{m}$ , depending on the composition and viscosity of the screen-printing paste. Screen-printing pastes typically use polymers such as polyethyleneglycol (Carbowax, MW of 600 or 20,000), Triton X-100 (polyoxyethylene(10)-isooctylphenylether), poly(vinylbutaryl) and ethylcellulose to increase viscosity and to bind or disperse particulate content. Ultrasonication or ball-milling of the binder or dispersant with titania powder to form pastes is often done within alcohols or solvents with high boiling points such as methylethylketone and terpinol. Monomeric species like butylcarbitol and butylbenzylphthalate, dodecanoic and 4-hydroxybenzoic acid have also been used to further modify the paste for screen-printing.<sup>17-21</sup> The screen-printing of mesoporous films using particles as small as 16 nm requires a large proportion of organic vehicle. Literature methods to form crack-free screen-printed films composed of titania nanoparticles include the cross-linking of polymeric species by ultraviolet light prior to calcination of the organic material.<sup>22, 23</sup> ‘Spin-thinning’ involves the screen-printing of a film, followed by thinning using a spin-coating apparatus. Recommended viscosities of spin-coating mixtures are from 4 to 10 cP, but vary depending on the spin-speed and duration, which may be in the order

of 3000rpm for 60 seconds.<sup>24, 25</sup>

Methods were adapted from the literature to screen-print and 'spin-thin' viscous pastes of Degussa P25 and sol-gel titania. The pastes contained ethylcellulose with mixed isomers of terpineol and by a single pass of the blade were printed through a polyester mesh fixed at 3.2 mm above a glass substrate. Square forms with an area of 1 cm<sup>2</sup> were produced after sintering the prints in air at 490°C for an hour.<sup>21, 23, 26</sup>

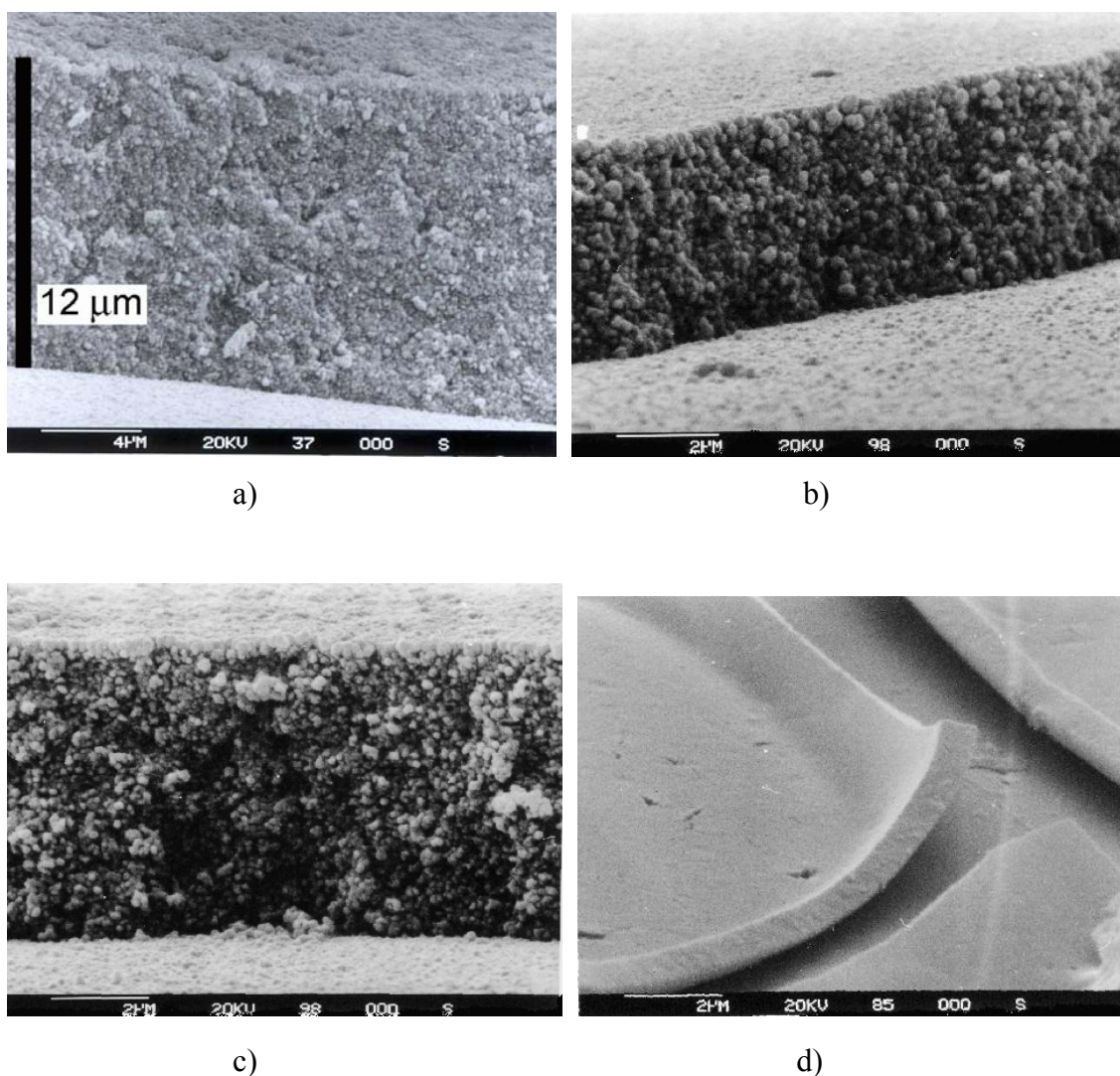
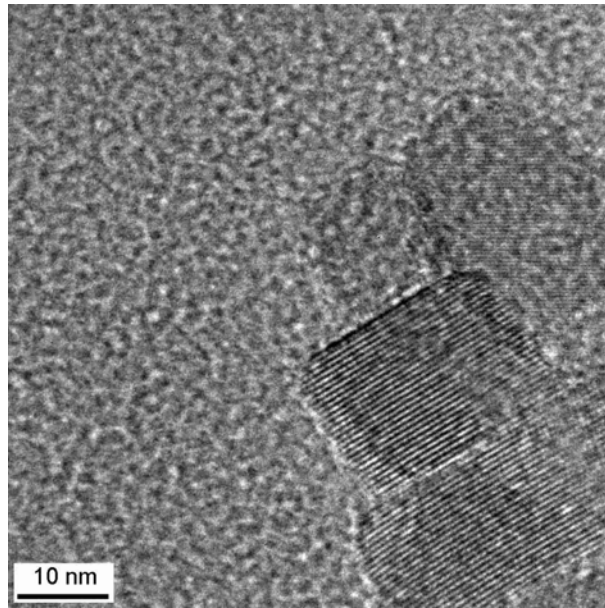


**Figure 4.3.** a) Dyesol opaque titania plate, 12 μm thick. b) Screen-printed Dyesol transparent paste, 4 μm thick. c) Screen-printed Degussa P25, 4 μm thick. d) Spin-thinned sol-gel titania, 1 μm thick.

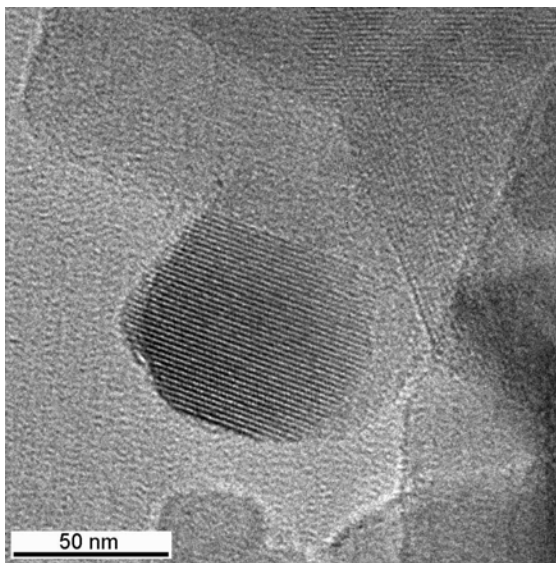
Dyesol paste for the screen-printing of transparent titania electrodes differs in composition from that used for opaque titania electrodes only in that 20% of the titania used in the latter is approximately 400 nm in size. The Dyesol paste contains terpineol and ethylcellulose, both of which are common components of screen-printing media.<sup>27</sup> Modelling has shown that particles 125 to 150 nm in diameter may increase the scattering of light within Grätzel cells, though the back-scattering of light out of the cell also increased.<sup>28</sup> Prior to sintering, the Dyesol screen-printing titania was dispersible in alcohols, allowing measurements by DLS in 95% ethanol, giving an average diameter of 100 nm. High resolution transmission electron microscopy (HR-TEM) images show that the titania is composed of dispersed, polyhedral crystals which appear to be free of amorphous material (Fig. 4.4.a). The Moire interference patterns of the crystal lattices appear to extend to the particle surface, without the ‘fringe’ that would indicate an amorphous coating. The tan-coloured paste was screen-printed, then sintered to yield transparent films with a slight white opacity (Fig. 4.3.b). The average particle diameter as measured by DLS showed an increase to 200 nm, while the surface area given by BET nitrogen adsorption was  $82.6 \text{ m}^2 \text{ g}^{-1}$ . Both measurements reflect the extent of particle aggregation after sintering. Powder XRD using a copper X-ray source was used to confirm that the material was anatase.

Degussa Aeroxide<sup>®</sup> P25 titania formed by the flame hydrolysis of titanium tetrachloride has a nominal average diameter of 25 nm and a surface area of  $50 \text{ m}^2 \text{ g}^{-1}$ . FTIR studies of pyridine adsorption have reported that the surface of Degussa P25 titania is acidic.<sup>29, 30</sup> As measured by DLS there is a wide distribution in size with an average particle diameter of 200 nm to 2  $\mu\text{m}$ . This observation is supported by HR-TEM images which show that small, crystalline particles are fused into much larger aggregates (Fig. 4.4.b). Similar and significant aggregation has also been observed with ‘nanoparticulate’ silica and zinc oxide.<sup>31</sup> Powder XRD was used to verify the approximate 7 : 3 ratio of anatase to rutile that has been reported for Degussa P25 titania.<sup>7, 32</sup> Sintering of Degussa P25 for an hour in air at 500°C had no effect on the ratio of anatase to rutile. An opaque, white paste of Degussa P25 was screen-printed, then sintered in air to yield opaque, white and cracked films (Fig. 4.3.c).

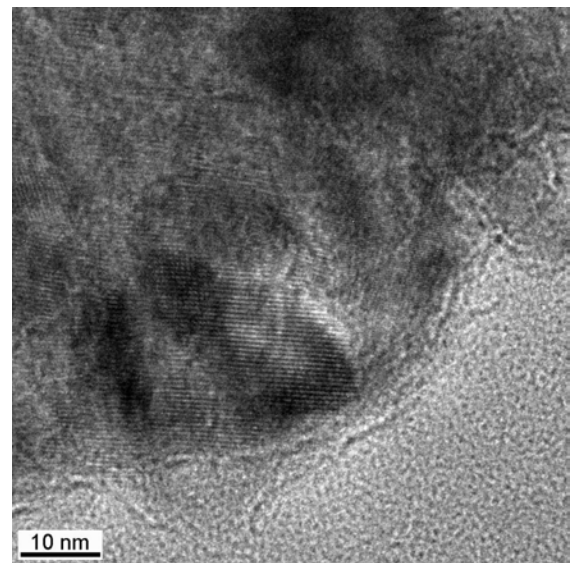
Acidic and amorphous sol-gel titania was prepared as described in Section 4.4 to give a pale-yellow, hygroscopic powder. The sol-gel titania was screen-printed onto glass as a viscous and tan-coloured paste, using the same composition ratios as for Degussa P25. Spin-thinned samples were produced by rotating individual screen-printed squares using a spin-coater at 600rpm for 60 seconds, prior to calcination. The clear and colourless films were then sintered, resulting in cracked and slightly opaque films approximately 1  $\mu\text{m}$  thick (Fig. 4.3.d). For XRD and surface area measurements the same screen-printing mixture was tape-cast using spacers 20 to 50  $\mu\text{m}$  thick, sintered, then scraped from the substrate. Powder XRD show that the amorphous titania was converted to anatase. The 2 nm primary particles of raw sol-gel titania were annealed into larger aggregates after spin-thinning and sintering. DLS measurements show a broader size distribution and an average diameter of 100 to 300 nm. HR-TEM images show that in comparison to Degussa P25 and the Dyesol materials, ‘globular’ aggregates were produced (Fig. 4.4.c). However, the images were unable to show whether a coating of amorphous titania was present. BET krypton adsorption of the native sol-gel material produced a gross underestimate, due to adsorbed solvent, water and acid. The surface areas of the sintered material of both tape-cast and unadulterated sol-gel titania were able to be measured by BET nitrogen adsorption to give respective values of  $37.6 \text{ m}^2 \text{ g}^{-1}$  and  $187.2 \text{ m}^2 \text{ g}^{-1}$ . This may be compared to the reported surface area of  $433 \text{ m}^2 \text{ g}^{-1}$  for amorphous, non-sintered and aggregated 3 nm anatase particles formed by the hydrolysis of titanium ethoxide.<sup>33</sup> The large difference in surface area may be caused by the organic content of the screen-printing mixture, which may bind nanoparticles closer together than in the unadulterated sol-gel titania. That may have resulted in a decreased porosity and smaller surface area for the screen-printed material.



a)



b)



c)

**Figure 4.4.** a) Titania of the Dyesol screen-printing paste for transparent films. b) Degussa P25 hydrophilic fumed titania. c) Sintered sol-gel titania.

#### 4.4. *Dispersible Titania*

An advantage of using dispersed particles is that in comparison to sintered titania, the much larger surface area may allow a higher dye loading and thus reproducible detection of adsorbed species. Dispersed titania nanoparticles may be obtained either directly through sol-gel methods or by the redispersion of aggregated material.

Redispersion has the advantage that many published methods produce crystalline, but precipitated titania. However, the bulk of the material remains aggregated in many redispersion techniques, as evidenced by reports of centrifugation to wash and extract the peptised titania as a cake. Techniques to redisperse titania include neutral, basic and acidic conditions, often with hydrothermal treatment to increase the primary particle size and to obtain crystalline material. A neutral redispersion method is ball-milling of bulk titania with chelating agents like 2,4-pentadione and Triton X-100.<sup>32, 34</sup> Heat treatment of precipitated titania under basic conditions also result in a partial redispersion of material. For instance, refluxing of titania at temperatures of 70 to 135°C for periods of 1 to 6 hours with tetraalkylammonium salts resulted in translucent or slightly opaque blue-tinted dispersions. Of the salts, redispersion with tetrabutylammonium hydroxide gave a smaller proportion of aggregated material.<sup>35, 36</sup> Acidic environments have been used to both crystallise and redisperse titania *via* dissolution then reformation and may produce particles as small as 8 nm in diameter.<sup>37</sup> Hydrochloric, acetic and nitric acid have been used to redisperse titania and to interconvert between anatase and rutile. For instance, a 1 : 2 molar ratio of nitric acid to titanium isopropoxide first produced anatase, which at room temperature reformed into rutile. Without an acidic environment crystallisation from amorphous titania took weeks rather than hours.<sup>38</sup> The concentration and type of acid used during hydrothermal synthesis has been shown to determine whether a phase transition occurred from anatase to rutile or vice versa. For instance, the dissolution of titania in solutions with a high concentration of hydrochloric or nitric acid formed rutile, while a low concentration gave anatase. The opposite applied for resuspension with sulfuric and hydrofluoric acid.<sup>39, 40</sup>

The direct formation of dispersed titania through sol-gel methods requires the hydrolysis of titanium alkoxides in the presence of acids, chelating agents or polymeric

stabilisers. The advantage of sol-gel methods over redispersion techniques in the production of dispersed titania, as the aggregation of nanoparticles is prevented by surface modification during the synthesis. In the formation of titania sol-gels, alcoholic solutions of titanium alkoxides are more frequently used than the more reactive titanium halide species. Modification of titanium alkoxides by ligands with a weaker electron-withdrawing ability, like dimethylaminoethoxide, further reduces the reactivity of the titania precursor with moisture and oxygen. An advantage is the production of smaller particles and a more stable sol-gel. A high molar ratio of water to titanium alkoxide has also been shown to produce a greater proportion of small particles, due to the increased number of nucleation sites, which then stunts particle growth.<sup>39</sup> Chelating agents and acids such as oxalic or hydrochloric acid and tri-*n*-octylphosphine oxide retard the rate of hydrolysis and also provide electrostatic or steric stabilisation, resulting in particles as small as 4 nm in diameter.<sup>4, 24, 25</sup> The sol-gel synthesis of titania using 2,4-pentadione has been used to form particles 2 nm in diameter, provided that an acid such as 4-toluenesulfonic, nitric or perchloric acid is present. Without acid, the distribution of sizes increased to give an average diameter of 7 to 50 nm.<sup>41</sup> Nanoparticulate titania has been reported to aggregate into spherical colloids on the order of 50 nm to 2.5  $\mu\text{m}$ . The primary particles were 10 nm in size and colloids proved to be porous, more so when polymers were employed in particle stabilisation. While the colloidal bulk was amorphous, in some cases there was a fine casing of crystalline titania.<sup>42, 43</sup> Sol-gel titania generally requires either peptisation by a mineral acid in the presence of elevated temperature and water, or hydrothermal treatment before fully crystalline material is garnered, which may also be without an amorphous coating. An acid or chelating agent is necessary for the stabilisation of the particle dispersion during crystallisation. A typical procedure is to reflux an alcoholic sol-gel of titania in the presence of water and acetic or nitric acid at 70 to 80°C for 8 to 24 hours to produce anatase.<sup>33, 35, 37, 44</sup> However, further hydrothermal treatment often results in an increased primary particle size and the aggregation and precipitation of titania.<sup>45</sup>

The acidic, amorphous sol-gel titania used in this study was also used in the formation of spin-thinned titania in Section 4.3. Sol-gel titania was produced by a published protocol for the hydrolysis of titanium tetrachloride within methanol acidified with hydrochloric acid.<sup>3</sup> The acid-stabilised titania sol-gel was refluxed for 2 hours before solvent was removed by rotary evaporation. The resulting yellow foam was dried

overnight under high-vacuum at room temperature to produce a pale-yellow, hygroscopic powder. Use of water as the solvent produced rutile, rather than amorphous titania. However, the particle size increased significantly and rutile aggregated and precipitated from solution. The average hydrodynamic diameter of the sol-gel titania, as measured in water by DLS, was 2.6 nm with a standard deviation of 20%. This particle size is above the theoretical limit of a 1.2 nm diameter for  $\text{Ti}_{16}\text{O}_{32}$  which is the smallest nanoparticle of anatase that is possible. Surface energy calculations for a 10 nm particle have shown that anatase is the favoured crystalline form, while in order to observe bulk properties, titania must have a diameter or thickness greater than the quantum-confined Bohr radius of 6 nm.<sup>46-49</sup> HR-TEM and powder XRD provide evidence that the native sol-gel titania is amorphous and is composed primarily of nanoparticulate titania. The acidic surface of sol-gel titania ensures the dispersion of particles, though a degree of aging of the sol-gel titania occurs whether the solvent is removed or not. This is tentatively attributed to a reduction in electrostatic stabilisation, following the loss of protons from the acidic titania surface as hydrogen chloride gas. Aged sol-gel titania displays a lessened solubility in organic solvents such as methanol and acetonitrile, but when resolvated in water has a diameter similar to that of freshly prepared material. The UV-Vis spectra of solutions of acidic sol-gel titania show a large absorption for wavelengths less than 350 nm. This is characteristic of titania nanoparticles and may not be due to quantum confinement effects. The blue-shift in absorption, relative to bulk anatase has been ascribed to the larger band-gap energy of nanometre-sized titania.<sup>50</sup> The sintering of acidic, amorphous sol-gel titania at 400°C resulted in a 53% mass loss. Karl-Fischer titration of the dried and unadulterated sol-gel titania gave a moisture content of 13% wt/wt, which indicates that the remaining reduction in mass of 40% after sintering may be due to chemisorbed water and hydrochloric acid (Section 8.1).

#### 4.5. *Conclusions*

Powder XRD and HR-TEM imagery confirmed that all of the sintered forms of titania are crystalline and are mostly or fully anatase. The surface area values for Dyesol sintered titania are higher than that of both Degussa P25 and tape-cast sol-gel titania, but are less than that of unadulterated sintered sol-gel titania. The cracking observed in

screen-printed Degussa P25 and sol-gel titania has also been reported for titania films deposited from solution and may be due to capillary stress during drying.<sup>51</sup> Studies of dye adsorption upon these substrates should provide information which is applicable to the titania-dye interface found in Grätzel cells.

The ideal form of dispersible titania would be neutral bare anatase nanocrystals, which is most closely approximated by acidic dispersed amorphous sol-gel titania. Though the arrangement of atoms presented to the environment is random rather than crystalline, the use of hydrochloric acid as a stabiliser maintains the dispersion and minimises any steric hindrance to the approach of adsorbates to the surface. While the use of both acidic titania and acidic adsorbates introduces significant electrostatic repulsion between the two species, which may reduce dye adsorption, at least the salt formation between acidic titania and a basic dye or basic titania and an acidic dye is avoided. Such salt formation may not be distinguishable from dye adsorption on the titania surface. However, as it is the nature of interactions between adsorbed dye and the titania particle itself that is of interest, it is hoped that the use of both acidic titania and acidic dyes will not be a great disadvantage for investigations using solution-phase spectroscopy of titania-dye dispersions.

## 4.6. References

1. Smestad, G P; Spiekermann, S; Kowalik, J; Grant, C D; Schwartzberg, A M; Zhang, J; Tolbert, L M; Moons, E. A Technique to Compare Polythiophene Solid-State Dye Sensitized TiO<sub>2</sub> Solar Cells to Liquid Junction Devices. *Solar Energy Materials & Solar Cells* **2003**, 76, 85-105.
2. Ito, S; Takeuchi, T; Katayama, T; Sugiyama, M; Matsuda, M; Kitamura, T; Wada, Y; Yanagida, S. Conductive and Transparent Multilayer Films for Low-Temperature-Sintered Mesoporous TiO<sub>2</sub> Electrodes of Dye-Sensitized Solar Cells. *Chemistry of Materials* **2003**, 15, 2824-2828.
3. Olsen, C M; Waterland, M R; Kelley, D F. Electron Injection Dynamics of Ru<sup>II</sup>(dcbpy)<sub>2</sub>(SCN)<sub>2</sub> on Zirconia. *Journal of Physical Chemistry B* **2002**, 106, 6211-6219.
4. Parala, H; Devi, A; Bhakta, R; Fischer, R A. Synthesis of Nano-Scale TiO<sub>2</sub> Particles by a Nonhydrolytic Approach. *Journal of Materials Chemistry* **2002**, 12, 1625-1627.
5. Kim, D J; Hahn, S H; Oh, S H; Kim, E J. Influence of Calcination Temperature on Structural and Optical Properties of TiO<sub>2</sub> Thin Films Prepared by Sol-Gel Dip Coating. *Materials Letters* **2002**, 57, 355-360.
6. Chen, W; Zhang, J; Fang, Q; Li, S; Wu, J; Li, F; Jiang, K. Sol-Gel Preparation of Thick Titania Coatings Aided by Organic Binder Materials. *Sensors and Actuators B: Chemical* **2004**, 100, 195-199.
7. Mills, A; Lepre, A; Elliott, N; Bhopal, S; Parkin, I P; O'Neill, S A. Characterisation of the Photocatalyst Pilkington ActivTM: a Reference Film Photocatalyst. *Journal of Photochemistry and Photobiology A: Chemistry* **2003**, 160, 213-224.
8. Fuertes, M C; Soler-Illia, G J A A. Processing of Macroporous Titania Thin Films: From Multiscale Functional Porosity to Nanocrystalline Macroporous TiO<sub>2</sub>. *Chemistry of Materials* **2006**, 18, 2109-2117.
9. Kuai, S; Badilescu, S; Bader, G; Bruning, R; Hu, X; Truong, V-V. Preparation of Large-Area 3D Ordered Macroporous Titania Films by Silica Colloidal Crystal Templating. *Advanced Materials* **2003**, 15, 73-75.
10. Kuai, S L; Hu, X F; Truong, V-V. Synthesis of Thin Film Titania Photonic Crystals Through a Dip-Infiltrating Sol-Gel Process. *Journal of Crystal Growth* **2003**, 259, 404-410.
11. Fan, Q; McQuillin, B; Ray, A K; Turner, M L; Seddon, A B. High Density, Non-Porous Anatase Titania Thin Films for Device Applications. *Journal of Physics D: Applied Physics* **2000**, 33, 2683-2686.
12. Ma, Y; Qiu, J-B; Cao, Y-A; Guan, Z-S; Yao, J-N. Photocatalytic Activity of TiO<sub>2</sub> Films Grown on Different Substrates. *Chemosphere* **2001**, 44, 1087-1092.
13. Park, J; Privman, V; Matijevic, E. Model of Formation of Monodispersed Colloids. *Journal of Physical Chemistry B* **2001**, 105, 11630-11635.
14. Sugimoto, T. Formation of Monodispersed Nano- and Micro-Particles Controlled in Size, Shape, and Internal Structure. *Chemical Engineering and Technology* **2003**, 26, 313-321.
15. Cossement, D; Plumier, F; Delhalle, J; Hevesi, L; Mekhalif, Z. Electrochemical Deposition of Polypyrrole Films on Organosilane-Modified ITO Substrates. *Synthetic Metals* **2003**, 138, 529-536.
16. Grant, C D; Schwartzberg, A M; Smestad, G P; Kowalik, J; Tolbert, L M; Zhang, J Z. Optical and Electrochemical Characterization of Poly(3-undecyl-2'-bithiophene) in Thin Film Solid State TiO<sub>2</sub> Photovoltaic Solar Cells. *Synthetic Metals* **2003**, 132, 197-204.
17. Clifford, J N; Palomares, E; Nazeeruddin, M K; Thampi, R; Grätzel, M; Durrant, J R. Multistep Electron Transfer Processes on Dye Co-sensitized Nanocrystalline TiO<sub>2</sub> Films. *Journal of the American Chemical Society* **2004**, 126, 5670-5671.

18. Jasieniak, J; Johnston, M; Waclawik, E R. Characterization of a Porphyrin-Containing Dye-Sensitized Solar Cell. *Journal of Physical Chemistry B* **2004**, 108, 12962-12971.
19. Zhang, D; Ito, S; Wada, Y; Kitamura, T; Yanagida, S. Nanocrystalline TiO<sub>2</sub> Electrodes Prepared by Water-Medium Screen Printing Technique. *Chemistry Letters* **2001**, 10, 1042-1043.
20. Zhang, J; Jiang, D; Weisenel, L; Greil, P. Binary Solvent Mixture for Tape Casting of TiO<sub>2</sub> Sheets. *Journal of the European Ceramic Society* **2004**, 24, 147-155.
21. Burnside, S; Winkel, S; Brooks, K; Shklover, V; Grätzel, M; Hinsch, A; Kinderman, R; Bradbury, C; Hagfeldt, A; Pettersson, H. Deposition and Characterization of Screen-Printed Porous Multi-Layer Thick Film Structures From Semiconducting and Conducting Nanomaterials for Use in Photovoltaic Devices. *Journal of Materials Science: Materials in Electronics* **2000**, 11, 355-362.
22. Zaban, A; Aruna, S T; Tirosh, S; Gregg, B A; Mastai, Y. The Effect of the Preparation Condition of TiO<sub>2</sub> Colloids on their Surface Structures. *Journal of Physical Chemistry B* **2000**, 104, 4130-4133.
23. Carotta, M C; Ferroni, M; Guidi, V; Martinelli, G. Preparation and Characterization of Nanostructured Titania Thick Films. *Advanced Materials* **1999**, 11, 943-946.
24. Yusuf, M M; Imai, H; Hirashima, H. Preparation of Mesoporous TiO<sub>2</sub> Thin Films by Surfactant Templating. *Journal of Non-Crystalline Solids* **2001**, 285, 90-95.
25. Patil, K R; Sathaye, S D; Khollam, Y B; Deshpande, S B; Pawaskar, N R; Mandale, A B. Preparation of TiO<sub>2</sub> Thin Films by Modified Spin-Coating Method Using an Aqueous Precursor. *Materials Letters* **2003**, 57, 1775-1780.
26. Nazeeruddin, M K; Pechy, P; Renouard, T; Zakeeruddin, S M; Humphry-Baker, R; Comte, P; Liska, P; Cevey, L; Costa, E; Shklover, V; Spiccia, L; Deacon, G B; Bignozzi, C S; Grätzel, M. Engineering of Efficient Panchromatic Sensitizers for Nanocrystalline TiO<sub>2</sub>-Based Solar Cells. *Journal of the American Chemical Society* **2001**, 123, 1613-1624.
27. Bertoz, M. The opaque paste 142op is the same as the transparent screen-printing paste 148, but that 20% of the titania is of 400 nm particles. *Dyesol Ltd.* **2006**, (October)
28. Wang, Z-S; Kawauchi, H; Kashima, T; Arakawa, H. Significant Influence of TiO<sub>2</sub> Photoelectrode Morphology on the Energy Conversion Efficiency of N719 Dye-Sensitized Solar Cell. *Coordination Chemistry Reviews* **2004**, 248, 1381-1389.
29. Stipkala, J M; Castellano, F N; Heimer, T A; Kelly, C A; Livi, K J T; Meyer, G J. Light-Induced Charge Separation at Sensitized Sol-Gel Processed Semiconductors. *Chemistry of Materials* **1997**, 9, 2341-2353.
30. Zaki, M I; Hasan, M A; Al-Sagheer, F A; Pasupulety, L. *In Situ* FTIR Spectra of Pyridine Adsorbed on SiO<sub>2</sub>-Al<sub>2</sub>O<sub>3</sub>, TiO<sub>2</sub>, ZrO<sub>2</sub> and CeO<sub>2</sub>: General Considerations for the Identification of Acid Sites on Surfaces of Finely Divided Metal Oxides. *Colloids and Surfaces A: Physicochemical and Engineering Aspects* **2001**, 190, 261-274.
31. Adams, L K; Lyon, D Y; Alvarez, P J J. Comparative Eco-Toxicity of Nanoscale TiO<sub>2</sub>, SiO<sub>2</sub> and ZnO Water Suspensions. *Water Research* **2006**, 40, 3527-3532.
32. Nazeeruddin, M K; Kay, A R, I; ; Humphry-Baker, R; Muller, E; Liska, P; Vlachopoulos, N; Grätzel, M. Conversion of Light to Electricity by Cis-X<sub>2</sub>Bis(2,2'-Bipyridyl-4, 4'-Dicarboxylate)Ruthenium(II) Charge-Transfer Sensitizers (X=Cl<sup>-</sup>, Br<sup>-</sup>, I<sup>-</sup>, CN<sup>-</sup>, and SCN<sup>-</sup>) on Nanocrystalline TiO<sub>2</sub> Electrodes. *Journal of the American Chemical Society* **1993**, 115, 6382-6390.
33. Zhang, H; Banfield, J F. Kinetics of Crystallization and Crystal Growth of Nanocrystalline Anatase in Nanometer-Sized Amorphous Titania. *Chemistry of Materials* **2002**, 14, 4145-4154.
34. Legrand-Buscema, C; Malibert, C; Bach, S. Elaboration and Characterization of Thin Films of TiO<sub>2</sub>

Prepared by Sol-Gel Process. *Thin Solid Films* **2002**, 418, 79-84.

35. Burnside, S D; Shklover, V; Barbe, C; Comte, P; Arendse, F; Brooks, K; Grätzel, M. Self-Organization of TiO<sub>2</sub> Nanoparticles in Thin Films. *Chemistry of Materials* **1998**, 10, 2419-2425.

36. Yang, J; Mei, S; Ferreira, J M F. Hydrothermal Synthesis of TiO<sub>2</sub> Nanopowders from Tetraalkylammonium Hydroxide Peptized Sols. *Materials Science and Engineering C* **2001**, 15, 183-185.

37. O'Regan, B; Moser, J; Anderson, M; Grätzel, M. Vectorial Electron Injection into Transparent Semiconductor Membranes and Electric Field Effects on the Dynamics of Light-Induced Charge Separation. *Journal of Physical Chemistry* **1990**, 94, 8720-8726.

38. Shin, H; Jung, H S; Hong, K S; Lee, J-K. Crystal Phase Evolution of TiO<sub>2</sub> Nanoparticles with Reaction Time in Acidic Solutions Studied via Freeze-Drying Method. *Journal of Solid State Chemistry* **2005**, 178, 15-21.

39. Wang, C-C; Ying, J Y. Sol-Gel Synthesis and Hydrothermal Processing of Anatase and Rutile Titania Nanocrystals. *Chemistry of Materials* **1999**, 11, 3113-3120.

40. Yang, J; Mei, S; Ferreira, J M F; Norby, P; Quaresma, S. Fabrication of Rutile Rod-Like Particle by Hydrothermal Method: an Insight into HNO<sub>3</sub> Peptization. *Journal of Colloid and Interface Science* **2005**, 283, 102-106.

41. Scolan, E; Sanchez, C. Synthesis and Characterization of Surface-Protected Nanocrystalline Titania Particles. *Chemistry of Materials* **1998**, 10, 3217-3223.

42. Eiden-Assmann, S; Widoniak, J; Maret, G. Synthesis and Characterization of Porous and Nonporous Monodisperse Colloidal TiO<sub>2</sub> Particles. *Chemistry of Materials* **2004**, 16, 6-11.

43. Barringer, E A; Bowen, K. High-Purity, Monodisperse TiO<sub>2</sub> Powders by Hydrolysis of Titanium Tetraethoxide. 1. Synthesis and Physical Properties. *Langmuir* **1985**, 1, 414-420.

44. Pottier, A; Sophie, C; Chaneac, C; Villain, F; Tronc, E; Jolivet, J-P. Size Tailoring of TiO<sub>2</sub> Anatase Nanoparticles in Aqueous Medium and Synthesis of Nanocomposites. Characterization by Raman Spectroscopy. *Journal of Materials Chemistry* **2003**, 13, 877-882.

45. Shklover, V; Nazeeruddin, M-K; Zakeeruddin, S M; Barbe, C K, A; ; Haibach, T; Steurer, W; R., H; Nissen, H, -U; ; Grätzel, M. Structure of Nanocrystalline TiO<sub>2</sub> Powders and Precursor to their Highly Efficient Photosensitizer. *Chemistry of Materials* **1997**, 9, 430-439.

46. Zhang, Q-L; Du, L-C; Weng, Y-X; Wang, L; Chen, H-Y; Li, J-Q. Particle-Size-Dependent Distribution of Carboxylate Adsorption Sites on TiO<sub>2</sub> Nanoparticle Surfaces: Insights into the Surface Modification of Nanostructured Materials. *Journal of Physical Chemistry B* **2004**, 108, 15077-15083.

47. Berger, T; Sterrer, M; Diwald, O; Knozinger, E; Panayotov, D; Thompson, T L; Yates, J T J. Light-Induced Charge Separation in Anatase TiO<sub>2</sub> Particles. *Journal of Physical Chemistry B* **2005**, 109, 6061-6068.

48. Toyoda, T; Tsuboya, I. Apparent Band-Gap Energies of Mixed TiO<sub>2</sub> Nanocrystals with Anatase and Rutile Structures Characterised with Photoacoustic Spectroscopy. *Review of Scientific Instruments* **2003**, 74, 782-784.

49. Chappel, S; Grinis, L; Ofir, A; Zaban, A. Extending the Current Collector into the Nanoporous Matrix of Dye Sensitized Electrodes. *Journal of Physical Chemistry B* **2005**, 109, 1643-1647.

50. Sakai, N; Prasad, G K; Ebina, Y; Takada, K; Sasaki, T. Layer-by-Layer Assembled TiO<sub>2</sub> Nanoparticle/PEDOT-PSS Composite Films for Switching of Electric Conductivity in Response to Ultraviolet and Visible Light. *Chemistry of Materials* **2006**, 18, 3596-3598.

51. Goh, G K L; K., D S; Pallathadka, P K. Cracking and Orientation of Solution-Deposited Rutile TiO<sub>2</sub>

Films. *Chemistry of Materials* **2004**, 16, 2857-2861.



## 5. *TOWARDS THE SELF-ASSEMBLY OF TITANIA USING SMALL MOLECULES*

### 5.1. *Introduction*

The self-assembly of titania nanoparticles upon a conductive substrate would circumvent the need to sinter Grätzel cell electrodes. Rather than heating the electrode in order to form physical and electrical connectivity between adjacent particles and the substrate, linkage using small molecules could provide the necessary rigidity and electron conduction pathways. The construction of flexible and inexpensive plastic electrodes for Grätzel cells may then be a possibility.

Self-assembly of molecular and nanosized species demands a high affinity between the respective components, which in this case are titania, the linker species, sensitizer dyes and the substrate.<sup>1</sup> The use of polymeric materials has been reported in the lamellar deposition of nanoparticles, including titania, but small molecules are of interest as there is the potential to have greater control over particle ordering in the system. It may then be possible to mimic the ordering found in opaline materials. In order to form an ideal, ‘opal-like’ assembly of titania particles that may be used in a similar way to ‘standard’ mesoporous, nanocrystalline electrodes, several criteria must be fulfilled. The first is that the titania must be of dimensions small enough to be tethered to each other and to the substrate in a robust manner by covalent or electrostatic interactions *via* molecular ‘linker’ materials. The second is that the titania surface must be able to be sensitized by dyes. The third is that the ‘linker’ must be a fully conjugated species to facilitate the transfer of charge through the particulate array to the substrate.<sup>2</sup>

To allow the self-assembly of material into an ‘opal-like’ formation, dispersed, discrete nanoparticles are required to allow chemical and electrostatic interactions to direct assembly. The size limitation upon dispersed, discrete, particles for assembly by chemical assistance using small molecules is demonstrated in the case of silica opal formation using micron-sized colloids bearing either carboxylic or amine functionality. There did not appear to be any contribution to the packing or lattice stability of opals which could be ascribed to salt formation between complementary beads, as opposed to the simple close-packing of particles.<sup>3, 4</sup> Another advantage of using nanoparticles,

rather than larger colloids, is the increased surface area and shorter electron diffusion length. The maximum dye loading and collection of injected electrons from excited-state dyes are then increased. However, a disadvantage is that increased number of intergrain boundaries raises the probability of charge recombination between electrons injected by the dye with titania defects.<sup>5,6</sup>

The self-assembly of titania nanoparticles onto a surface involves the deposition of an organic layer for binding of the first layer of particles, then the adhesion of subsequent particulate layers. Either covalent bonding or electrostatic interactions may be used in the formation of particulate arrays, using polymers or small molecules.

## **5.2. *Surface Functionalisation and Particle Binding***

The functionalisation of surfaces to bind organic or inorganic species has been studied for a number of substrates and particulate or solvated species, as illustrated below. While there are instances of particle deposition without the aid of chemically-modified surfaces, as is the case of opals, to encourage the deposition and self-assembly of nanoparticles the use of organic species to bind the target material is more frequent. Electrostatic and covalent interactions can be used in concert, with multiple surface modifications prior to binding of the target species.

Techniques of surface modification that employ electrostatic interactions include simply altering the surface charge to self-assemble nanoparticles, as in the case of the deposition of multiple bilayers of anionic silica and cationic titania onto glass. Judicious adjustment of the pH of nanoparticle suspensions was used to layer silica and titania. The respective particle diameters of 22 and 7 nm were small enough to perhaps imitate point charges, and so permit electrostatic interactions to direct particle assembly.<sup>7</sup> Another example involved polyelectrolytes in the layering of anionic titania 16 nm in diameter with cationic poly(diallyldimethylammonium chloride) by repeated dip-coating of glass coated with fluoride-doped tin oxide (FTO).<sup>8</sup>

The use of covalent bonds to functionalise surfaces is often done to ensure the rigidity and permanence of the first deposited layer. For instance, silicon has been grafted by

reaction with an alkene, forming a Si-C bond, to present a thiolated surface.<sup>9</sup> Another example is glass coated with indium-doped tin oxide (ITO) treated with silane species, such as octyltrimethoxysilane, to covalently bind a monolayer of alkane chains.<sup>10</sup> Similarly, glassy carbon electrodes have been functionalised by amines *via* the electrochemical formation of a C-N bond. A greater surface coverage was obtained with primary amines, rather than with secondary or tertiary amines, due to less steric hindrance at the nitrogen atom.<sup>11-13</sup> The formation of covalent bonds has been well documented in the binding of amines and thiols onto gold. The stronger affinity of thiols over amines for gold, permits the facile exchange of amines for thiols to pattern modified surfaces.<sup>14-16</sup> Polymers have been used to covalently bind 10 nm colloidal gold to gold nanorods using dithiolated poly(ethyleneglycol).<sup>17</sup> However, electrostatic repulsion between nanoparticles resulted in incomplete substrate coverage, despite favourable interaction between the substrate and particle. This was shown by the binding of citrate-chelated gold colloids *via* salt formation with a surface bearing amine functionality.<sup>18</sup>

The ‘overgrafting’ of organic species onto functionalised substrates has been well studied and can employ a combination of electrostatic and covalent interactions. For instance, a gold surface functionalised with 16-mercaptohexadecanoic acid has been used to bind an amine-derivative of poly(4-phenylenevinylene) *via* salt formation and hydrogen-bonding.<sup>19</sup> Surfaces have been overgrafted by the formation of covalent bonds, as in the case of silica substrates condensed with 1-mercaptopropyltrimethoxysilane to present a thiolated surface. A thioester was then formed to produce a bromine-terminated species, which acted as a radical initiator to polymerise styrene.<sup>20</sup> Similarly, amine groups tethered to silica by the condensation of reactive aminoalkylsilanes have been condensed with species such as diisocyanates and diamines or 4-nitrobenzaldehyde. New functionalities such as copolymers and nitro groups were covalently bound *via* the respective formation of urea and imine linkages.<sup>21, 22</sup> Upon ITO condensed with (3-aminopropyl)triethoxysilane, hexylferrocenephosphonic acid can be ‘overgrafted’ *via* salt formation or hydrogen-bonding. In this case, the amino functionality presented by the modified substrate restricted the adsorption of acid to a monolayer, while adsorption of the acid upon bare ITO produced multilayers of disordered material.<sup>23</sup>

The formation of bulk composite materials of linkers and nanoparticles include the covalent linkage of titania and silica nanoparticles *via* a bifunctional molecule.<sup>24</sup> At one terminus the linker sported an alkoxy silane, while the other was a phosphonate ester. First, silica was bound by condensation with the alkoxy silane and then the hybrid material was treated to deprotect the phosphonic acid and bind titania (Fig. 5.1). Another example of a bulk composite is the linkage of cadmium sulfide to titania *via* mercaptoacetic acid. Again, colloids of relatively small diameters were used, in this case 2 nm for cadmium sulfide and 7 nm for titania.<sup>25</sup> A sol-gel method has been reported where the small linker species also sensitises titania for visible light absorption. In this case, a derivatised sexithiophene with terminal alkoxy silane functionalities is present during the condensation of tetraethylorthosilicate and titanium isopropoxide to form a composite material *in situ* within the sol-gel (Fig. 5.2).<sup>26</sup>

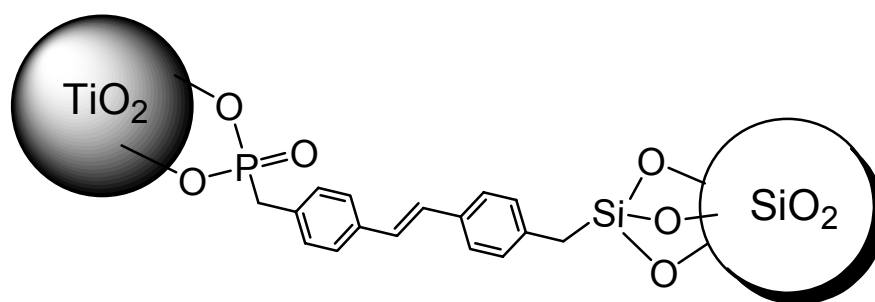


**Figure 5.1.** A cartoon of the base unit of the composite material described by R. Frantz *et al.* 2004.<sup>24</sup>

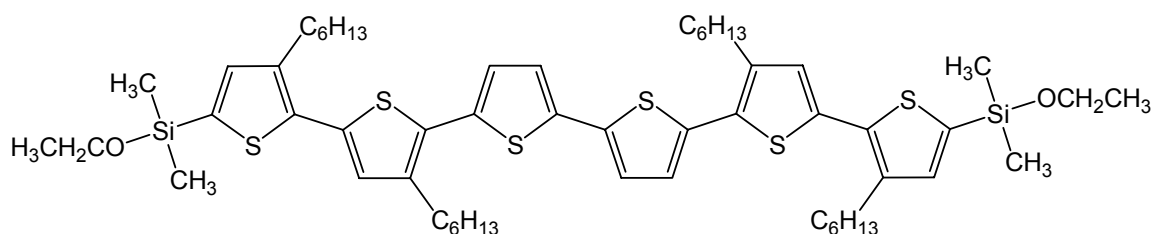


**Figure 5.2.** A dye used in the sol-gel preparation of a composite material for testing within Grätzel cells, as described by C. L. Lin *et al.* 2006.<sup>26</sup>

The advantage of covalent bonding in the formation of mono- or multilayers upon a substrate include more robust adhesion, though depending on the system there may be rearrangement within the layer, as found with scanning tunnelling microscopy (STM) studies of alkylthiols bound to gold.<sup>27</sup> Advantage may be taken of relatively weak binding between linker species, nanoparticles and the substrate, as this may allow the system to 'relax' into a more desirable formation. For example, in the binding of gold nanoparticles, the use of a substrate presenting amine groups, rather than thiols, permits the thermal rearrangement of gold into an array with closer packing.<sup>18</sup> However, by using only electrostatic interactions to bind species to ITO, it is possible that there may be diffusion off the surface, causing instabilities in the nanoparticle lattice.

The chemically-assisted self-assembly of titania arrays requires either a monolayer or thin film of an organic molecule upon the chosen substrate of ITO glass. Issues that need to be addressed include the nature and extent of dye binding to ITO and titania, in addition to whether adsorption is uniform and if material has aggregated. The stability and mechanical strength of any nanoparticle superlattice will depend upon the integrity of the first layer of organic material bound to the substrate. If the monolayer is unstable, incomplete or binds ineffectively to titania then the whole array will be weak.

### **5.3. *The Functionalisation of ITO Electrodes***

ITO is a reasonably robust and conductive surface that may be applied upon glass or plastic substrates such as Mylar. Before ITO glass may be functionalised it is necessary to prepare the surface for binding. Cleaning and priming techniques include the use of detergents, ultrasonication within solvents, chelating agents and the use of basic and oxidising solutions. Piranha solutions and mixtures such as a 1 : 4 : 20 v/v solution of ammonia to hydrogen peroxide to water have been used to ensure a fully hydroxylated surface.<sup>10, 28, 29</sup> Treatment may also be done with air- or oxygen-plasma cleaning and etching with hydrofluoric acid in order to strip the surface of ITO.<sup>30</sup> Cleaning of ITO with Piranha solution, combined with treatment with the chelating agent ethylenediaminetetraacetic acid (EDTA) has been used to remove contaminants, such as weakly bound indium hydroxide species. As a result of such treatment, a complete

monolayer of adsorbates like ferrocenemonocarboxylic acid were bound directly to the surface of ITO.<sup>31</sup> Surface-bound indium can be removed by reaction with carboxylic acids.<sup>32</sup> However, caution must be used, as ITO glass is produced by sputter coating or spray pyrolysis and consequently the quality of the material varies between batches and manufacturers. The reported work function for ITO, while typically around 4.4 to 4.7 eV ranges between 4.1 and 5.5 eV. The variation in work function may also be due to agents that ITO was exposed to prior to use, as acid treatments increase the work function and basic media reduce the work function.<sup>33-35</sup> For instance, treatment with a 15 mM solution of phosphoric acid shifted the work function of ITO from 4.4 to 5.2 eV, while soaking in a 5 mM solution of tetra-*t*-butylammonium hydroxide gave a value of 3.8 eV.<sup>36</sup>

The mode of binding of adsorbates on ITO is analogous to that of silica, titania, zirconia and hafnia, as ITO bears both metal oxide and surface hydroxyl functionalities. In the functionalisation of metal oxide surfaces the most common agents include silane species, which are thought to condense with Lewis acid sites of metal oxides to form covalent bonds.<sup>37</sup> ITO has been functionalised with (3-aminopropyl)silane and (3-mercaptopropyl)silane to present amine and thiol moieties, through which citrate-stabilised gold nanoparticles were bound. A non-close packed array of particles 15 to 120 nm in diameter resulted, appearing as a “continuous red-violet film”.<sup>38</sup> However, the presence of a silicon atom would prevent complete electronic conjugation between tethered particles and the substrate. This was illustrated with oligo(disilanylene(thienylene)), for which the  $sp^3$  hybridised silicon atoms effectively interrupt the  $\pi$ -bond conjugation of the thienylene units.<sup>2, 39, 40</sup> As a consequence, adsorbates that were investigated in this chapter have binding groups that are either amines or carboxylic acids. It has been reported that acids bind to ITO *via* both electrostatic interactions and covalent bonding. The binding of carboxylic acids to ITO glass has been proposed to be *via* hydrogen bonding or by the chelation of cation defect sites by carboxylate species, in a fashion similar to the binding of acids to titania.<sup>32, 41</sup> An instance of ITO functionalised with carboxylic acids is that of terthiophene derivatives. The interaction is strong enough to permit the further overgrafting of 2,4-ethylenedioxythiophene-type species, which may then be polymerised.<sup>42</sup> Acidic species have been chemisorbed onto ITO by interaction between the acidic adsorbate and hydroxylated surface, such as 4-chlorobenzoylchloride, 4-chlorobenzenesulfonyl

chloride and 4-chlorophenyldichlorophosphate.<sup>43</sup>

Dry solvents are necessary for the adsorption of material onto ITO and it has been noted that immersion of the substrate is necessary, rather than simply spraying a solution of the adsorbate onto the surface.<sup>44</sup> Adsorbates such as ferrocenyl species bearing amine or carboxylic acid functionality have been bound to ITO by soaking at room temperature in solvents such as methanol, ethanol and diethyl ether. Mixed solvents, by increasing the adsorbate concentration of the solution, have been used to improve surface coverage. One such example is the deposition of 7-ferrocenylheptanoic acid from a 5% v/v solution of 1,4-dioxane in hexane.<sup>45</sup> The concentration of adsorbate solutions vary from 0.01 mM to 5 mM, while the soaking time ranges from 1 minute to overnight. A typical protocol involves the soaking of ITO in a 1 mM solution for 10 to 30 minutes, followed by a rinsing step.<sup>23, 31</sup> For instance, di(3-aminopropylviologen) was adsorbed after soaking ITO for 24 hours within a 5 mM methanolic solution, followed by rinsing in methanol (Fig. 5.3).<sup>46</sup> However, the stronger interaction of carboxylic acids with ITO, in comparison to amines,<sup>45</sup> permits the adsorption of 3-thiopheneacetic acid after soaking for 20 minutes within a 1 mM ethanolic solution, then rinsing in acetonitrile.<sup>31</sup> Similarly, acid chlorides, sulfonyl chlorides and chlorophosphates have been adsorbed onto ITO by immersion for 30 minutes in 1 mM solutions using dichloromethane, followed by rinsing.<sup>43</sup>

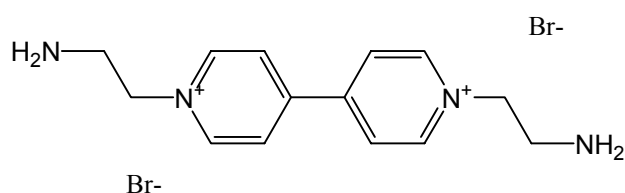


**Figure 5.3.** Di(3-aminopropyl)viologen, as described by K. H. Hyung, 2003.<sup>46</sup>

The pH value of solutions used to deposit and modify species adsorbed on ITO has influence over both the binding equilibrium and ordering of the adsorbate. For instance, the respective treatment of monolayers terminated by amine and carboxylic acid functionalities by acid or base results in a suppression of ionisation. By reduction of the

electrostatic repulsion between adjacent molecules, a smoother film resulted.<sup>14</sup> Similarly, the use of protonated ITO to improve electrostatic interactions with the tertiary amine 4,4'-bis(*N*-naphth-1-yl-*N*-phenylamine)-1,1'-biphenyl (Fig. 5.4) produced smoother films by chemical vapour deposition.<sup>33</sup> Interaction between non-bonding portions of the adsorbate may also influence coverage and alignment upon the substrate. For instance, the alignment and reproducible adsorption of species such as 7-ferrocenylheptanoic acid and 1,12-diaminododecane upon ITO appears to be aided by interaction between adjacent alkyl chains. It has been suggested that greater than 8 carbon atoms are required in the alkyl chain to induce alignment and prevent the flexing of the adsorbate into a 'hairpin' configuration.<sup>45, 47</sup>

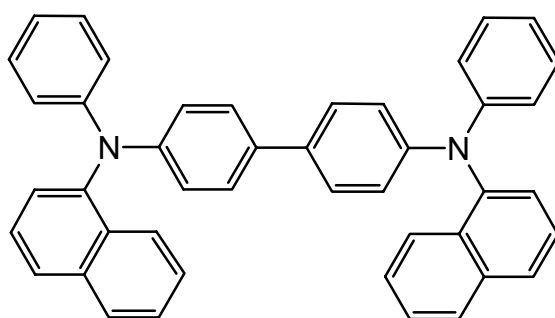


**Figure 5.4.** 4,4'-bis(*N*-naphth-1-yl-*N*-phenylamine)-1,1'-biphenyl, as described by Q. T. Lee *et al.* 2000.<sup>33</sup>

#### 5.4. *The Binding of Amines and Carboxylic Acids to ITO*

This work involves two sets of experiments in the investigation of the binding of amines and carboxylic acids to ITO. The first set involved the treatment of ITO with small aromatic molecules, including 4-aminobenzoic acid and 4-phenylenediamine, on the premise that once adsorption was confirmed, then either overgrafting or binding of larger conjugated molecules would be possible. While amine functionalities bind with less strength to ITO, the diamine species was an attractive candidate for the functionalisation of the surface, as the free amine may be used to react with other organic species to directly or indirectly bind titania nanoparticles. This method may involve the production of an imine, amino or C-N bond. An intervening layer involving

either covalent or electrostatic interactions could play a role in the indirect binding of nanoparticulate titania. The use of a dicarboxylic acid would have been better, as the linker could then have directly bound titania to ITO. However, species such as 1,4-benzenedicarboxylic acid and 2,6-naphthalenedicarboxylic acid (Fig. 5.5) are practically insoluble in the solvents of interest, which included water, alcohols, tetrahydrofuran and 1,4-dioxane.

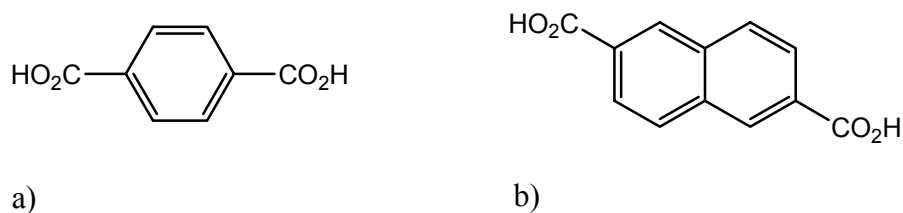
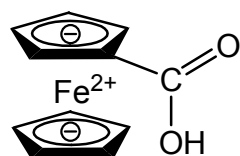
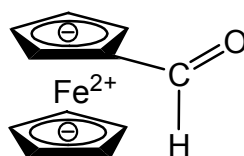


**Figure 5.5.** a) 1,4-benzenedicarboxylic acid. b) 2,6-naphthalenedicarboxylic acid.

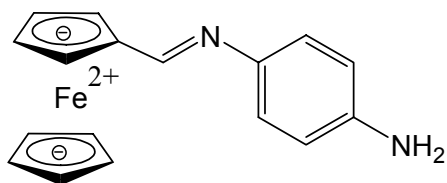
The detection of the species such as 4-aminobenzoic acid and 4-nitrobenzoic acid proved to be difficult, so the second set of experiments utilised ferrocenyl species, in order to introduce a redox-active centre and a relatively strong chromophore. Ferrocene moieties were attached to ITO either by overgrafting onto adsorbed species *via* the formation of an imine or by direct adsorption of ferrocenyl species derived to bear carboxylic acid or amine functionality. Ferrocenyl derivatives used to determine the surface coverage of ‘linker’ species on ITO glass include ferrocenemonocarboxylic acid (**5.1**), ferrocenemonocarboxaldehyde (**5.2**), the imine (Schiff base) *N*-(ferrocenylmethylidene)-4-phenylenediamine (**5.3**) and 2-(4-aminophenyl)ethenyl-ferrocene (**5.4**).



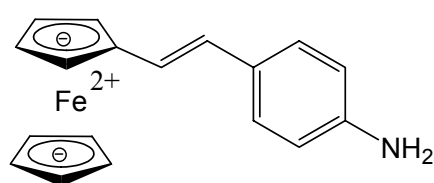
5.1



5.2



5.3



5.4

Probe **5.3** was synthesised from 4-phenylenediamine and **5.2** using an adaptation of methods found in the literature.<sup>48, 49</sup> In short, **5.2** dissolved in 2,2'-dimethoxypropane was dropped into a stirred solution of 4-phenylenediamine in methanol. The solution was stirred for one and a half hours at 45°C, after which black-brown solids of poly(4-phenylenediamine) were filtered off and the filtrate was concentrated by rotary evaporation. Solids that crystallised from the concentrated filtrate were separated and rinsed with a few millilitres of methanol, while the supernatant solution was reserved. Recrystallisation from the supernatant was repeated to collect six fractions, which despite varying in colour from light orange to brown was the same product. The rationale for using this process of fractional recrystallisation was to remove unreacted 4-phenylenediamine from the mono-imine base. In addition, the four-times molar excess of the diamine should have ensured that the di-imine, *N,N'*-di(ferrocenylmethylidene)-4-phenylenediamine, if present, would be a minor product.

An alternative approach to using ferrocenyl species was to create a coordination compound using carbonyl(5',10',15',20'-tetraphenylporphyrinato)ruthenium(II) and the amine 4-(*trans*-2-(4-pyridinyl)ethenyl)benzoic acid (Fig. 5.6). Provided that the pyridine derivative was bound to ITO *via* the acid functionality, it was plausible that a

coordination compound formed by interaction between the amine and the ruthenium cation would permit indirect detection of 4-(*trans*-2-(4-pyridinyl)ethenyl)benzoic acid *via* spectroscopy and voltammetry. However, the coordination compound proved to be fragile and experienced decomposition during purification by chromatography. In addition, the compound was only weakly bound to sintered screen-printed titania and was easily removed by rinsing with solvent.

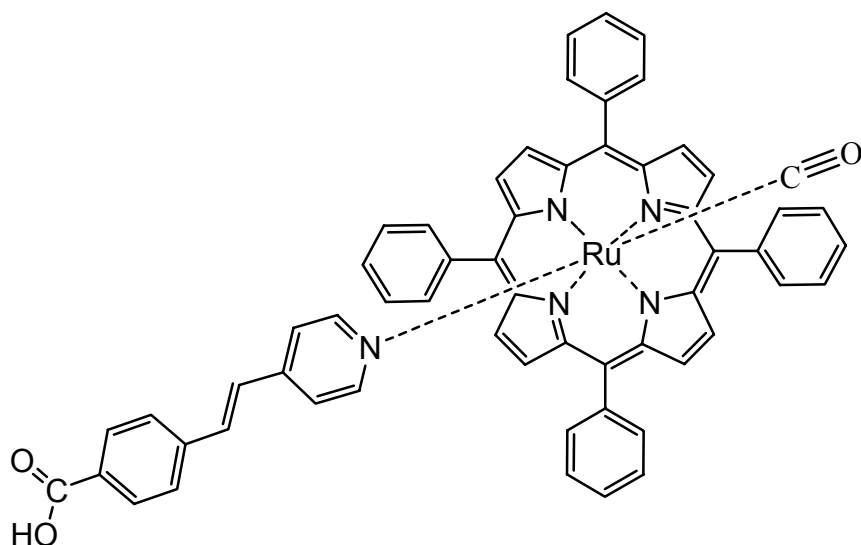


**Figure 5.6.** The coordination compound of 4-(*trans*-2-(4-pyridinyl)ethenyl)benzoic acid and carbonyl(5',10',15',20'-tetraphenylporphyrin)ruthenium(II).

### 5.5. *The Adsorption of Small Aromatic Molecules*

For use in this chapter, ITO glass was cleaned prior to use by washing with detergent, rinsing and then ultrasonication within a 1 : 1 : 5 v/v solution of 30% hydrogen peroxide to 28% ammonia to water. Next, ITO was washed by ultrasonication within acetone, water, then 95% v/v ethanol before drying in air. Typical adsorption conditions were to immerse ITO glass within a solution of the adsorbate using a concentration in the range of 1 to 10 mM. The solvents used included 2,2'-dimethoxypropane, 1,4-dioxane and mixtures of 1,4-dioxane in hexane. Given the same piece of ITO glass, it was verified that the sample may be rescanned to give UV-Vis absorbance spectra with an error of  $\pm 0.001$ . Care was taken to subtract from each sample spectrum the blank spectrum of

that piece of ITO. This was to account for variability between pieces of ITO. Broad signals were produced on the subtraction of the blank spectrum of a different piece of ITO (Fig. 5.7).

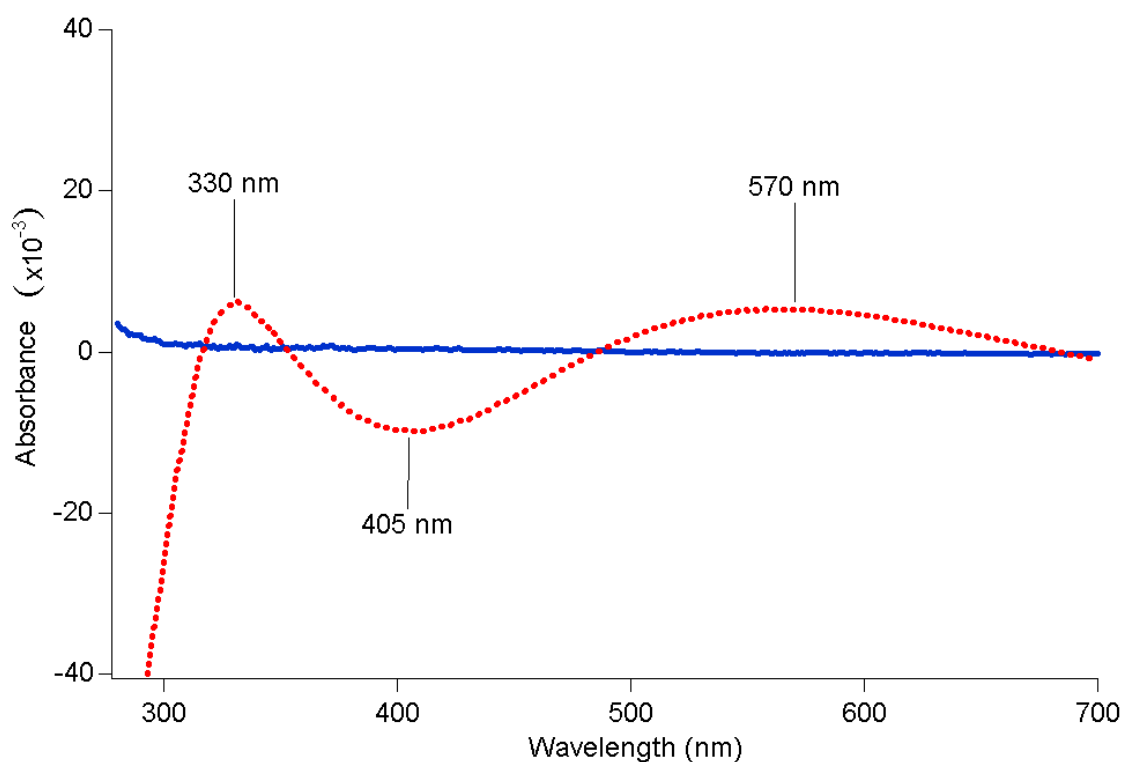


**Figure 5.7.** In order to obtain useful UV-Vis spectra, it is essential to subtract the blank (reference) spectrum of the same piece of ITO glass as used for each adsorption experiment. The spectrum of piece 1, after subtraction of an earlier scan of the same piece of ITO produces the expected, featureless resultant (—). However, the spectrum of piece 1, after subtraction of a scan of a different piece of ITO creates an artificial result (.....).

The small, aromatic and electronically conjugated species used for adsorption onto ITO include 4-phenylenediamine, 4-aminobenzoic acid and 4-nitrobenzoic acid (Table 5.1). The spectra of drop-dried 4-nitroaniline and 4-phenylenediamine both show low absorbance and broad signals centred at 400 nm and 420 nm, respectively (Fig. 5.8). It is possible that aggregation of deposited species produced the shift in peak maximum and signal broadening. However, it is curious that for 4-nitroaniline the signal at 300 nm is weak in comparison to what should be the  $\pi - \pi^*$  transition at 400 nm.

**Table 5.1.** UV-Vis absorption of aromatic species used in absorption studies.

Small, aromatic species	UV-Vis absorbance (nm)	Solvent
4-aminobenzoic acid <sup>50</sup>	266, 288.	Water Isopropanol
4-phenylenediamine	325	1,4-dioxane
4-nitroaniline	230, 350	Dichloromethane
Benzoic acid*	230, 270	Water
Aniline*	230, 280	Water
1,4-dioxane*	Below 215	1,4-dioxane

\*51

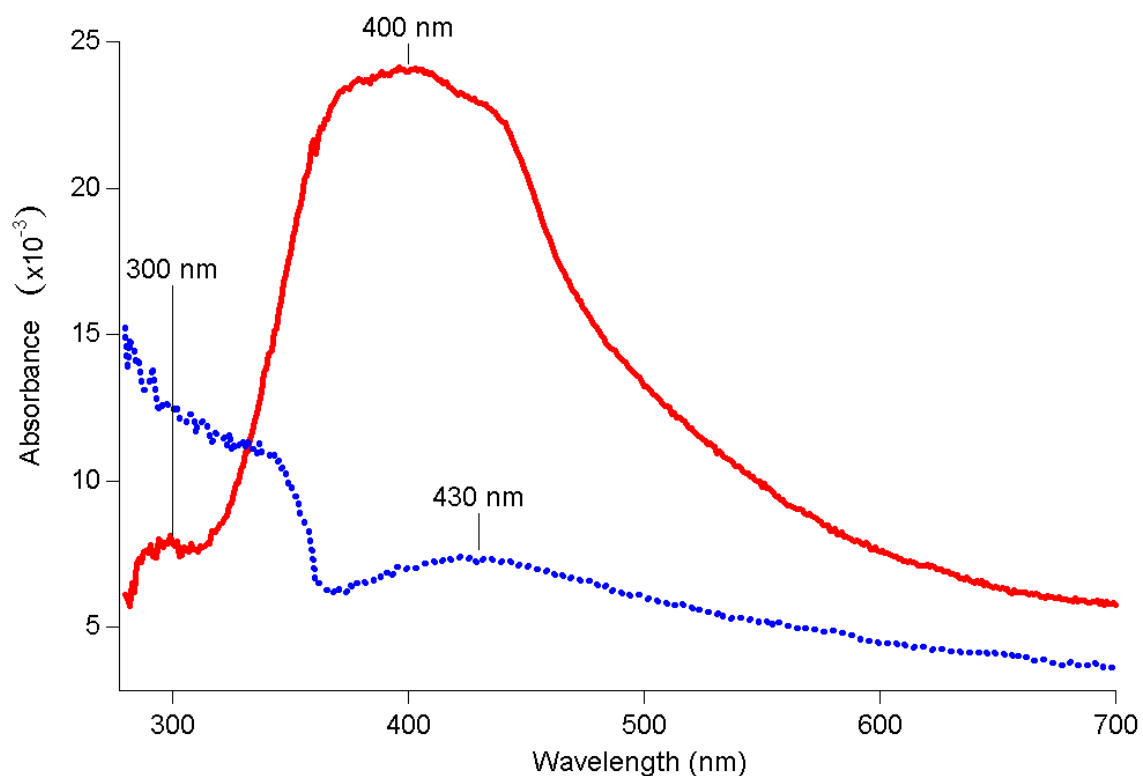


**Figure 5.8.** UV-Vis spectra of ITO glass with drop-dried: 4-nitroaniline (—), 4-phenylenediamine (.....).

The first lot of adsorption experiments included the immersion of ITO glass within 1 mM solutions of 4-phenylenediamine, 4-nitroaniline and 4-aminobenzoic acid in 1,4-dioxane, for 4 days at 70°C. The UV-Vis spectra all appear similar, with low absorbance values, a small peak at 300 nm and a broad signal centred at 430 nm (Fig. 5.9). Spectra of treated ITO showed a variation of  $\pm 0.001$  absorbance units, which is up to 10% of the signal intensity. Such low UV-Vis absorption intensities on the order of 0.003 have been reported for the electropolymerisation of a cyclopentadithiophene species upon ITO.<sup>52</sup> While a peak shift of 10 to 20 nm is significant and it is tempting to ascribe the shift and broadening to aggregation of the adsorbed material, the signal is very broad. The broad signal is not due to the degradation of 1,4-dioxane, as aged 1,4-dioxane shows a gradual increase in absorbance at higher energies, rather than a peak centred around 430 nm (Fig. 5.10). As the absorbance is so low, there is the potential that the spectra are simply an instrumental artifact.

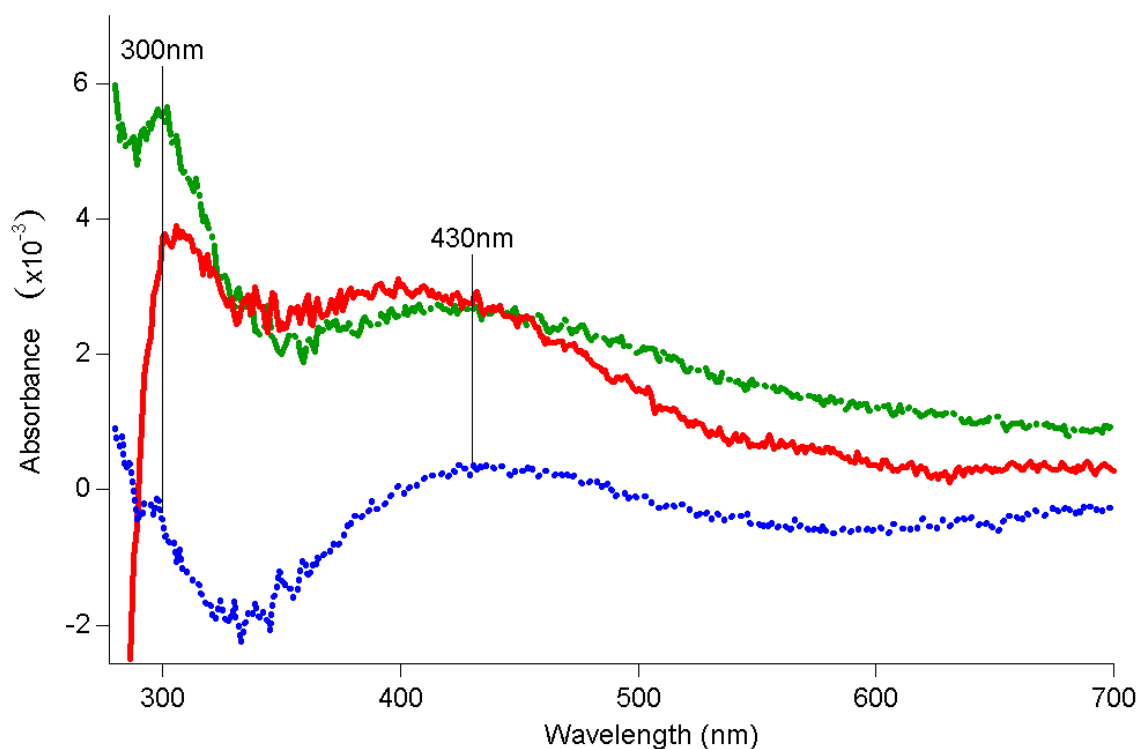


**Figure 5.9.** UV-Vis spectra of species adsorbed onto ITO glass from 1 mM solutions in 1,4-dioxane: 4-phenylenediamine (—), 4-nitroaniline (.....) and 4-aminobenzoic acid (---). Glass absorbs below 300 nm, which produces a marked effect in subtracted spectra.

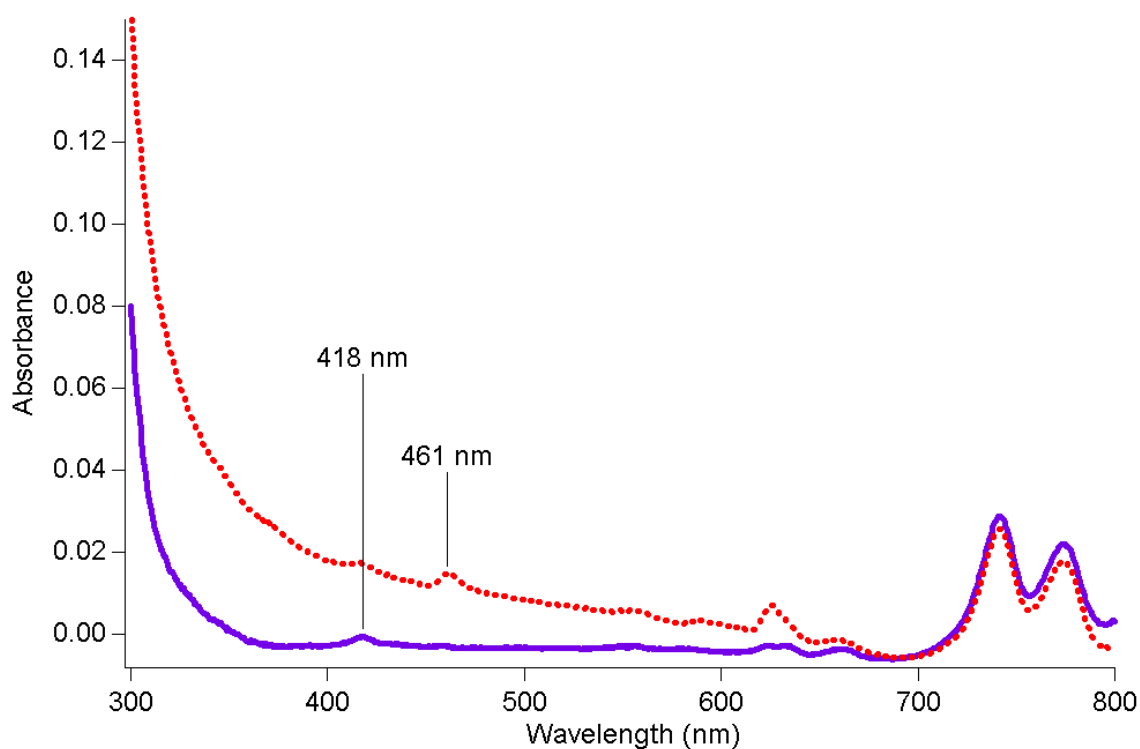


**Figure 5.10.** UV-Vis absorption for fresh 1,4-dioxane (—) and for 1,4-dioxane heated at 80°C for two days (····).

For instance, 4-phenylenediamine does oxidise and decompose under elevated temperature, as evidenced by UV-Vis spectroscopy with a new, broad feature in the region of 430 nm (Fig. 5.11). The spectra of ITO glass treated with 4-phenylenediamine and 4-aminobenzoic acid are not due to polymerised material, as the peak positions of polymeric species reported in the literature differ significantly. For instance, poly(aniline-*co*-2-aminobenzoic acid) displays the  $\pi - \pi^*$  transition of the benzene ring at the shorter wavelength of 320 to 340 nm and a broad absorbance below 550 nm due to the conjugated backbone (Table 5.2). As it was both difficult to detect adsorbed species and to reproduce samples, it was not possible to confirm the binding of species such as 4-phenylenediamine to ITO. Consequently, species were modified to contain a ferrocenyl moiety to aid detection.

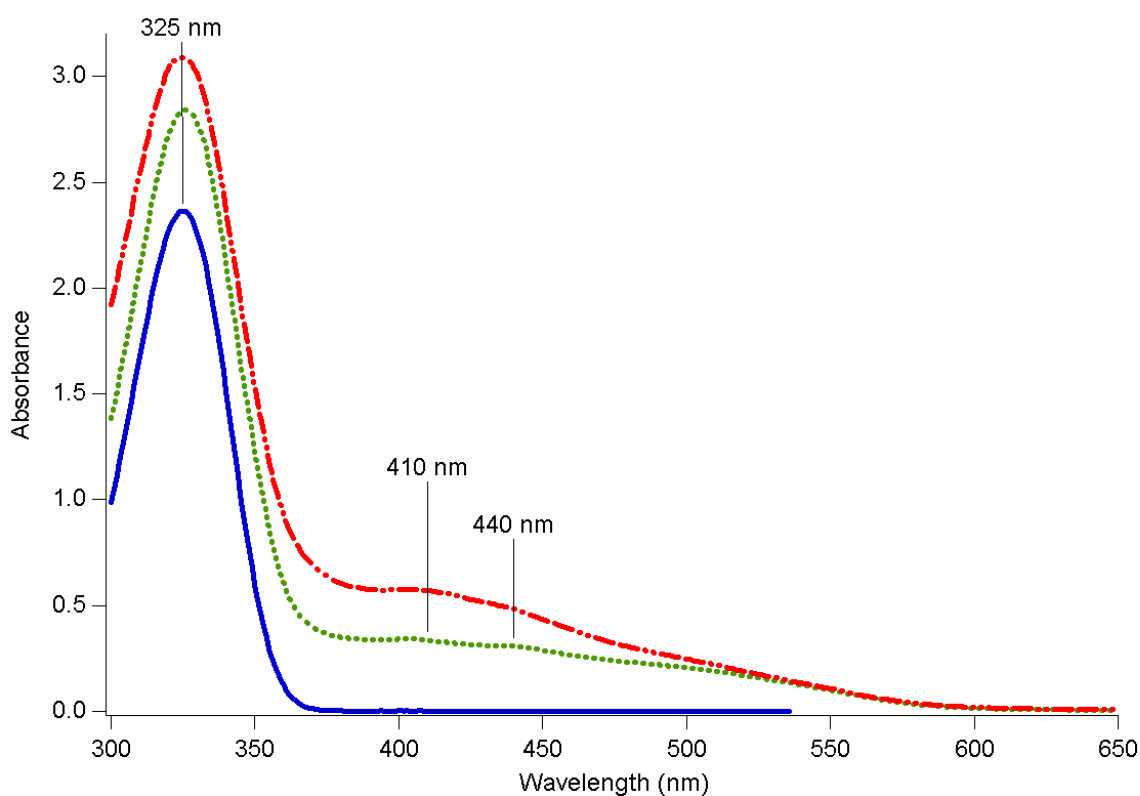


**Figure 5.11.** UV-Vis solution spectra of 4-phenylenediamine kept within 1,4-dioxane, at 80°C. Shown are spectra corresponding to the initial solution (—) and the solution after 21 hours (.....) and 4 days (---).

**Table 5.2.** UV-Vis absorbance peaks for polymeric material related to the probe species.

Species	n- $\pi^*$ transition (nm)	$\pi - \pi^*$ transition (nm)	Other UV-Vis absorbance peaks
Poly(4-phenylenevinylene) <sup>19</sup>	N/A	470	Extended conjugation shifts the $\pi - \pi^*$ transition to the lower energy.
<i>N,N'</i> -diphenyl-1,4-phenylenediamine <sup>53</sup>	N/A	387	551 nm for the monoprotonated form. 695 nm for the radical cation.
Poly(oligoaniline- <i>co</i> -4-phenylenediamine) <sup>54</sup>	N/A	330	A broad signal at 600 nm due to the polyaniline backbone
Poly(aniline- <i>co</i> -2-aminobenzoic acid) <sup>55</sup>	280 nm	320 to 340	A broad feature at 550 nm shifted to longer wavelengths with increased content of 4-aminobenzoic acid.

## 5.6. The Adsorption of Ferrocene Derivatives

Of the ferrocene derivatives used in this study, **5.1** and **5.2** were chosen as they are simple ferrocene derivatives, the latter may be used to further functionalise surfaces by overgrafting methods. For instance, a substrate bearing amine functionality may be condensed with an aldehyde to form an imine group, thus altering the surface presented to the environment. **5.3** was selected as an analogue of 4-phenylenediamine, which was used for experiments in Section 5.4.1. **5.4** is a more stable version of **5.3**, as the imine functionality is replaced by an alkene group.

### 5.6.1. UV-Vis Spectroscopy

The UV-Vis absorption peaks for these ferrocenyl species are listed in Table 5.3. As the adsorption of amines to ITO was investigated in Section 5.4.1, the imine **5.3** was tested first. Dioxane was the primary solvent for the treatment of ITO for adsorption studies, as opposed to alcohols or acetonitrile. This is as the use of relatively poor solvents may increase surface coverages closer to that of the maximum calculated, by effectively depositing the adsorbate from a saturated solution.<sup>23</sup> An illustration of the effect of the solvent is shown with the deposition of **5.4**. Samples were soaked for 3 days at 80°C in either 1,4-dioxane or acetonitrile, but only the sample treated in the less polar solvent produced a detectable signal (Fig. 5.12).

**Table 5.3.** UV-Vis absorption of solution spectra of ferrocenyl derivatives.

Ferrocenyl derivatives	Benzylic $\pi - \pi^*$ transition (nm)	Cyclopentadienyl $\pi - \pi^*$ transition (nm)	Iron d-d transition (nm)
Ferrocenemonocarboxylic acid ( <b>5.1</b> )	260	310	450
Ferrocenemonocarboxyaldehyde ( <b>5.2</b> )	270	340	460
<i>N</i> -(ferrocenylmethylidene)-4-phenylenediamine ( <b>5.3</b> )	280	310 to 360 solvachromatic	450
<i>N, N'</i> -bis(ferrocenylmethylidene)-4-phenylenediamine <sup>49</sup>	272	350 nm	460
<i>N</i> -(ferrocenylmethylidene)aniline <sup>49</sup>	281	309	448
2-(4-aminophenyl)ethenylferrocene ( <b>5.4</b> )	280	315	450
1-aryl-2-ferrocenylethylenes <sup>56</sup>	265	305	450

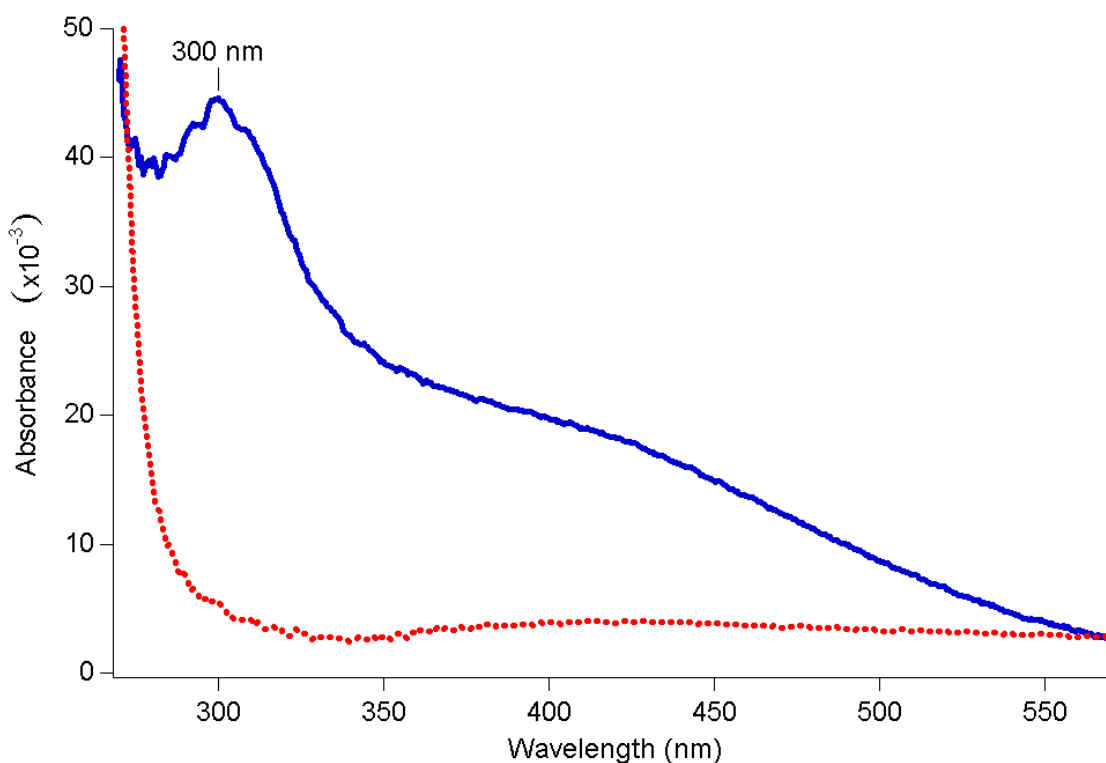


**Figure 5.12.** The effect of solvent on the deposition of **5.4** onto ITO glass: 1,4-dioxane (—), acetonitrile (.....).

There are notable differences between the solution spectrum and that of ITO glass bearing the imine (Fig. 5.13). Drop-drying of the imine upon ITO produced a UV-Vis spectrum with a large red shift of 50 nm, which is likely to be due to aggregation as a large excess of material was present. ITO glass was immersed for 2.5 days at 35°C in a 0.13 M solution of **5.3** in 2,2-dimethoxypropane, before being rinsed with 95% ethanol. Though the spectrum of drop-dried **5.3** should provide a reasonable comparison for the adsorption of **5.3** onto ITO glass, there is little similarity with the spectrum of **5.3** deposited on ITO by immersion. The absolute UV-Vis signal maxima of ITO with **5.3** drop-dried and deposited by immersion were 0.04 and 0.10, respectively.

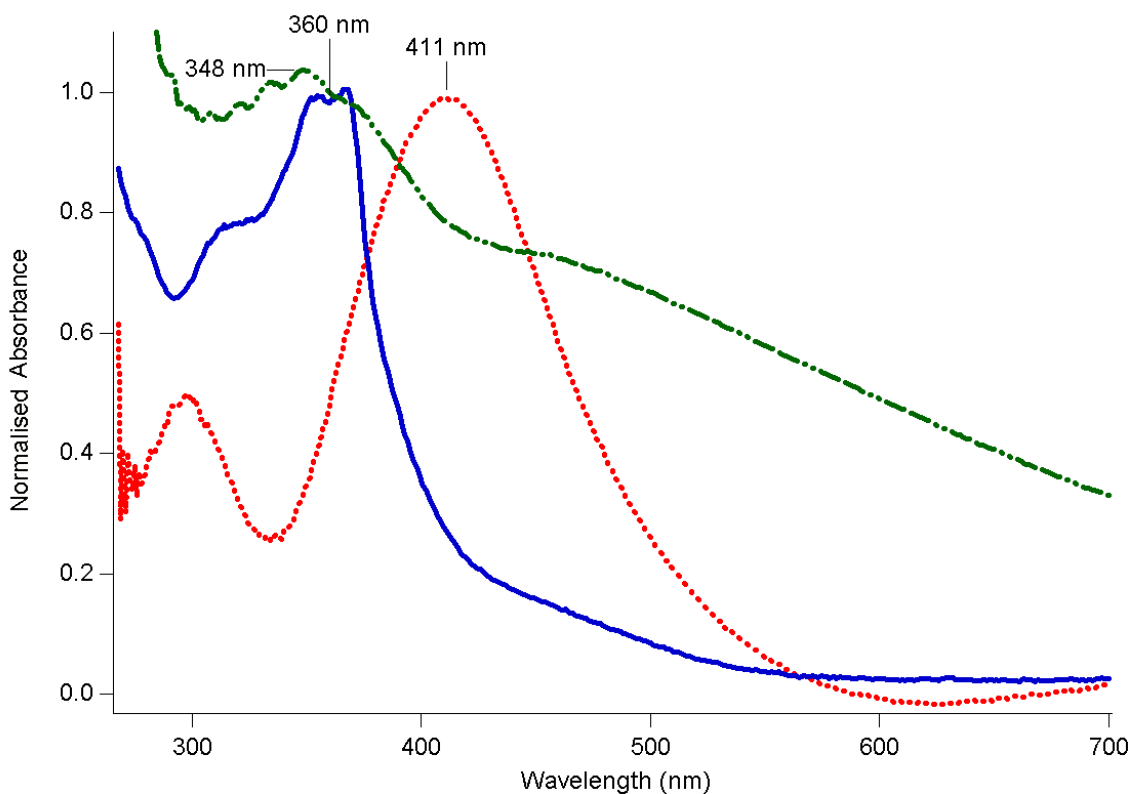


**Figure 5.13.** UV-Vis spectra of the imine **5.3** in methanol (—), drop-dried upon ITO glass (.....) and ITO glass treated by immersion from a 2 mM solution in 2,2-dimethoxypropane (-.-.).

In order to examine if a ferrocenyl species may be overgrafted onto ITO glass bearing a small molecule, ITO glass treated with 4-phenylenediamine was exposed to a solution of **5.2**. While the diamine was not detected on ITO glass, the overgrafting appears to have been successful, as after exposure to **5.2** a single absorbance at 360 nm was observed. This signal corresponds to the  $\pi - \pi^*$  transition of the cyclopentadiene ring of the imine **5.3** (Fig. 5.14).<sup>49</sup> The spectrum of the overgrafted sample resembled that of **5.3** in methanol and of ITO treated by immersion within a solution of **5.3**. However, the spectrum of overgrafted **5.3** is missing a broad shoulder at 450 to 500 nm and also differs markedly from that of drop-dried **5.3**, which has a maximum at 411 nm (Figure 5.14). As there is not a great similarity in spectrum profiles, this raises the possibility that Figure 5.14 shows only **5.2**, rather than an overgrafted imine. In the presence of water or metal cations, any imine formed may have decomposed during the overgrafting step to produce amines and the aldehyde **5.2**.<sup>57</sup> To circumvent the decomposition of the

imine functionality of **5.3**, species **5.4** was employed as a more stable probe for adsorption onto ITO glass.

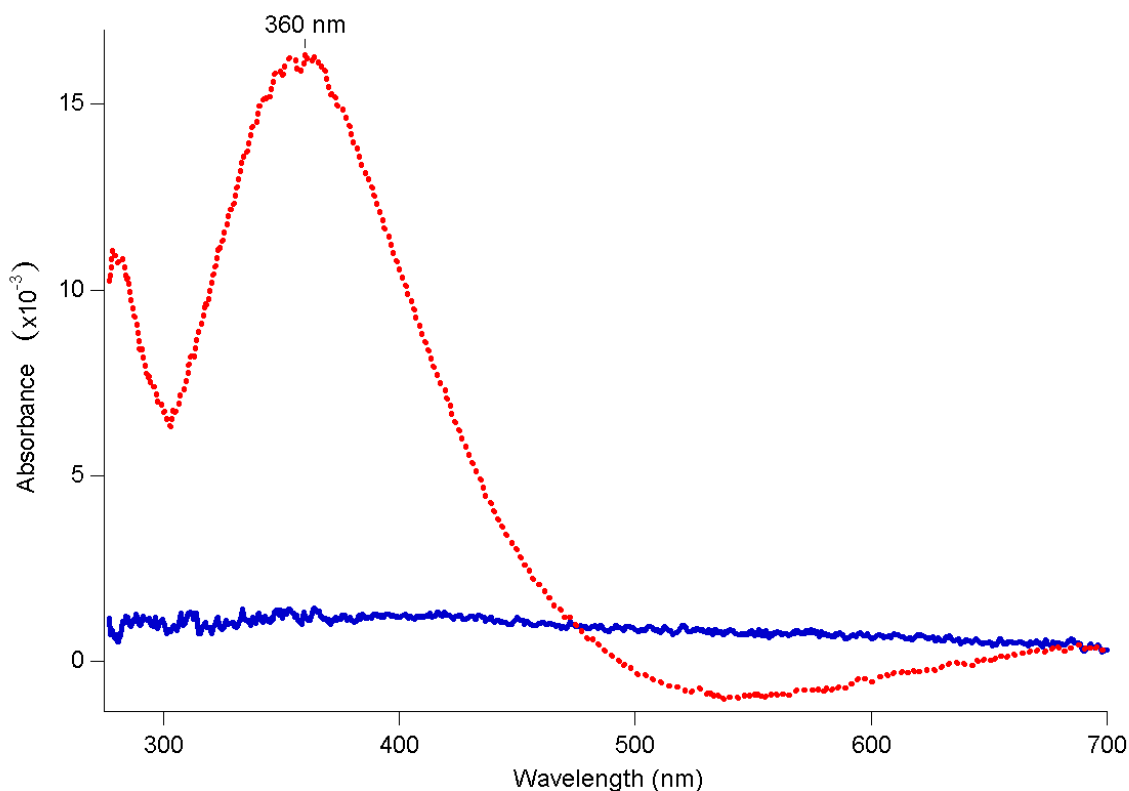


**Figure 5.14.** UV-Vis absorption spectra of ITO glass treated with 4-phenylenediamine (—), then with **5.2** (.....) to yield the overgrafted sample.

Species **5.4** was deposited onto ITO glass by soaking for 2 hours at room temperature in a 2 mM solution of **5.4** in a solvent of 6% v/v 1,4-dioxane in hexane. The sample was then rinsed in a 5% v/v solution of 1,4-dioxane in hexane. Unlike the imine **5.3**, there is a resemblance between the UV-Vis spectra of ITO treated by drop-drying and immersion (Fig. 5.15). Both signals due to the  $\pi - \pi^*$  transition of the cyclopentadiene rings and the d-d transition of iron display a blue peak shift for ITO treated by immersion, while there is a red shift for the drop-dried sample. The absolute absorbance for the  $\pi - \pi^*$  transition of the cyclopentadiene ring of ITO with **5.4** drop-dried and deposited by immersion were 0.28 and 0.01, respectively.

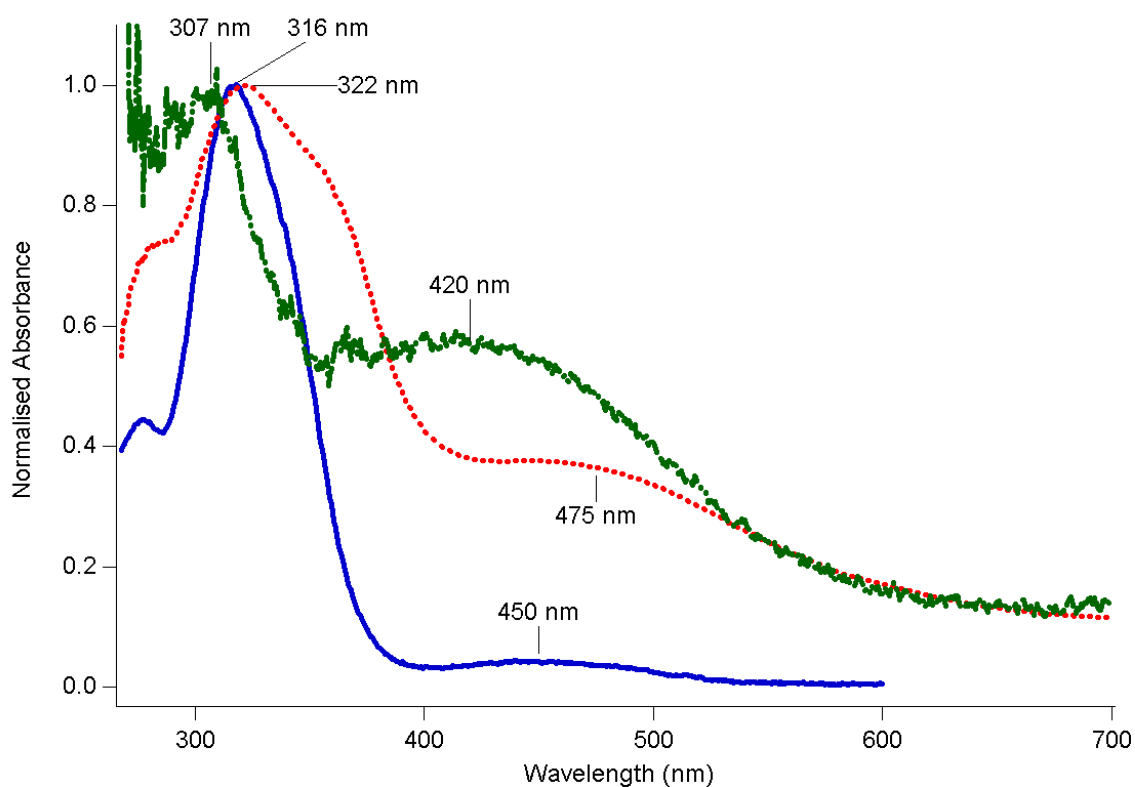


**Figure 5.15.** UV-Vis spectra of **5.4** in solution (—), drop-dried upon ITO glass (.....) and ITO glass treated by immersion from a 2 mM solution (---).

Similar UV-Vis spectra were obtained from ITO treated by immersion for an hour within either a 3 mM solution of ferrocenemonocarboxylic acid (**5.1**) or a 10 mM solution of 2-(4-aminophenyl)ethenylferrocene (**5.4**). The respective solvents were 6% of dry ethanol in hexane and 10% of 1,4-dioxane in hexane (Fig. 5.16). This confirms that both carboxylic acids and amines bind to ITO and that the larger species **5.4** as well as **5.1** can be bound.

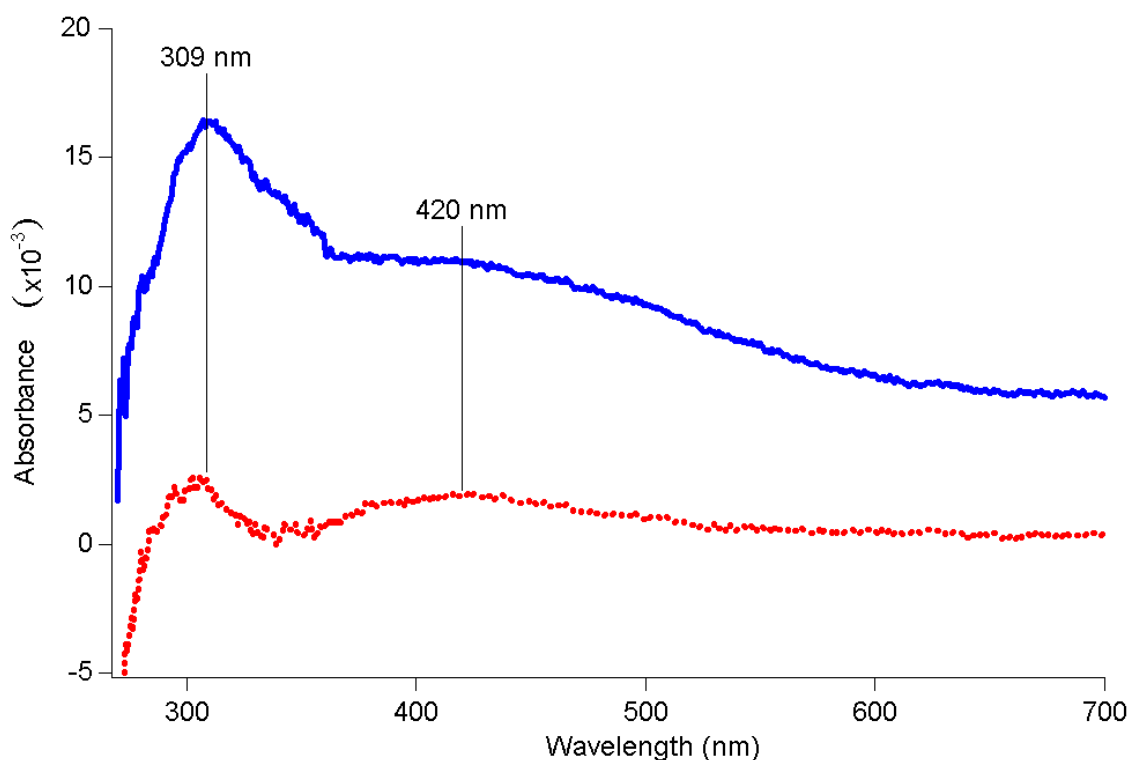


**Figure 5.16.** UV-Vis spectra of ITO glass treated by immersion within a 10 mM solution of **5.4** (—) and a 5 mM solution of **5.1** (.....).

### 5.6.2. Voltammetry

Voltammetry can be used to detect adsorbed species using both positive and negative responses by the presence and absence of signals. In the case of an electroactive material, electrodeposition causes an increase in film thickness, which should be accompanied by an increase in peak charge.<sup>58</sup> While an ideal electrode should display a peak-to-peak separation of zero,<sup>59</sup> narrow redox signals indicate homogenous oxidation and reduction processes.<sup>60</sup> It must be noted that bare ITO electrodes have a degree of interfacial capacitance, which is shown as a hysteresis in cyclic voltammetry that increases with the scan rate.<sup>61</sup> In addition, signal broadening of species adsorbed upon ITO may be attributed to interfacial capacitance charging.<sup>61</sup> If the adsorbed material is stable under voltage cycling, a linear relationship between peak current and scan rate may be used to indicate that a redox-active species is bound to the electrode surface.<sup>59</sup> The presence of pre- or post-peaks associated with oxidation and reduction processes of

the solution species can also be ascribed to adsorbed material.<sup>62</sup>

Positive voltammetric responses include redox activity of species directly or indirectly bound to the electrode surface. For instance, a porphyrinic species covalently attached to ITO,<sup>63</sup> and phosphomolybdic acid adsorbed to an amine-functionalised surface<sup>47</sup> have been detected by voltammetry. The presence of an underlying adsorbate has been inferred by a positive response, as documented by the detection of redox-active polyoxometalates ('Keggin salts') adsorbed on an ITO surface treated with a diamine.<sup>46</sup> One terminus of the diamine is bound to ITO, while the other is free to bind Keggin salts from solution. Through measurement of the voltammetric response of the Keggin salt phosphomolybdic acid, adsorbed onto an underlying layer of 1,12-diaminododecane, an estimated surface coverage for the diamine was obtained.<sup>47, 64</sup> Negative voltammetric responses include the loss of signal due to blocking of the electrode by non-conductive species. An example is the decreased signal of hexacyanoferrate in solution, due to coverage of the electrode by species such as polyimides or 6-(1-pyrrolyl)-*n*-hexyltrichlorosilane.<sup>65, 66</sup> Another instance is the electrodeposition of 4-aminobenzoic acid which reduced the Faradaic current of the oxidation signal,<sup>12</sup> while the electroactivity of ITO is reduced by the attachment of octyltrichlorosilane.<sup>10</sup>

In this work, the use of voltammetry for the indirect detection of the small molecule 4-phenylenediamine by adsorption of the Keggin salt phosphomolybdic acid was complicated by a number of issues. The complications included that to prevent degradation of phosphomolybdic acid, the solution used to deposit the Keggin salt onto ITO treated with 4-phenylenediamine contained 0.1 M hydrochloric acid. The additional acid may have protonated the diamine and resulted in desorption of 4-phenylenediamine from ITO. Also, despite a statement in the literature, the amount of the Keggin salt present proved to be sensitive to the rinsing step that was necessary to remove excess phosphomolybdic acid from the sample. This may indicate that the amine-acid interaction is weak, that the amine functional groups did not project out from the substrate or that the stability of 4-phenylenediamine on ITO is poor.<sup>12</sup> As a consequence, ferrocenyl species were employed in adsorption studies for examination by cyclic voltammetry in this chapter.

To confirm that a functional group such as a carboxylic acid is necessary to bind species to ITO, ITO glass was treated by immersion for an hour within a 2 mM solution of either ferrocene or **5.1** in a solvent of 6% of dry ethanol in hexane. The samples were rinsed in a 5% v/v solution of 1,4-dioxane in hexane, prior to voltammetry in acetonitrile containing the electrolyte tetrabutylammonium perchlorate (TBAP) at a concentration of 0.1 M (Fig. 5.17). ITO treated by ferrocene displayed only the hysteresis due to interfacial capacitance, while **5.1** produced a half-wave potential of 0.39 V<sub>SCE</sub>, which is significantly more negative than the literature potential of 0.58 V<sub>SCE</sub> for adsorbed **5.1**. This may be compared to the reported value of 0.62 V<sub>SCE</sub> for free **5.1**. The broad signals for ITO treated with **5.1** have been reported to be due to strong intermolecular interactions, while the decreasing current of subsequent scans may be due to the oxidation of **5.1** to amorphous ferric oxide<sup>45</sup> or simply diffusion of **5.1** off ITO (Fig. 5.18).

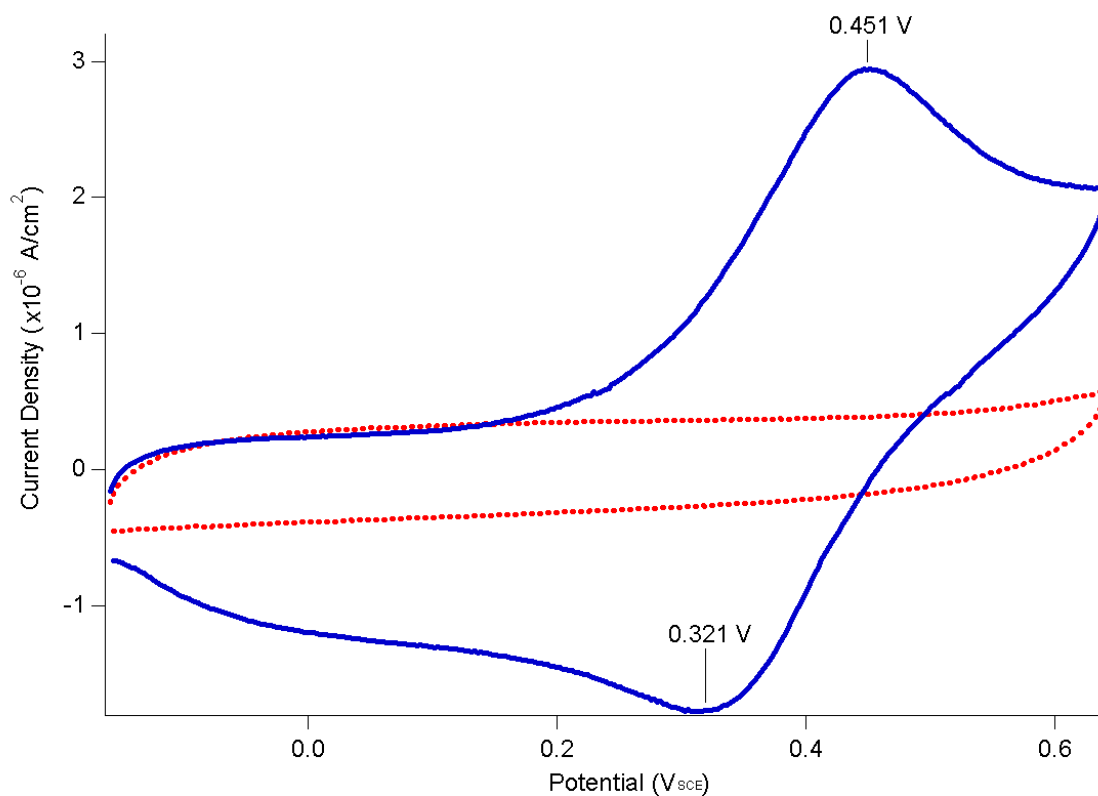


**Figure 5.17.** Cyclic voltammetry of within ITO glass was treated by immersion for an hour within a 2.5 mM solution in a 6% v/v solution of dry ethanol in hexane of either **5.1** (—) or ferrocene (.....). The sample was rinsed in a 5% v/v solution of 1,4-dioxane in hexane prior to voltammetry. The scans were done at 50 mV s<sup>-1</sup> in acetonitrile.

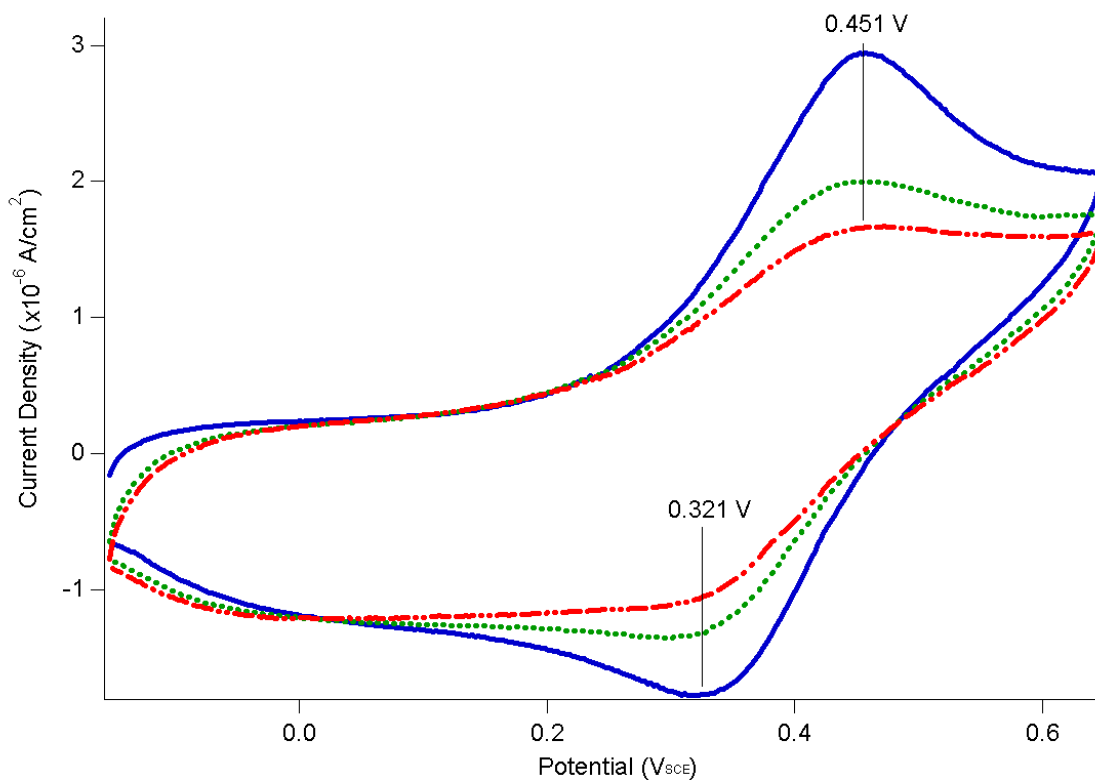


**Figure 5.18.** The diffusion or degradation of adsorbed **5.1** off ITO glass over sequential cyclic voltammetry scans. Scan 1 (—), Scan 2 (⋯), Scan 3 (---). The scans were done at  $50 \text{ mV s}^{-1}$  in acetonitrile.

The cyclic voltammetry of **5.3** in solution shows irreversible oxidation processes and the reversible ferrocene/ferrocenium couple with a half-wave potential of  $0.52 \text{ V}_{\text{SCE}}$ . However, the cyclic voltammetry plots for ITO glass treated by immersion within a  $2 \text{ mM}$  solution of the imine in acetonitrile, soaked for 3 days at  $40^\circ\text{C}$ , are different from that of the solution species (Fig. 5.19). The adsorbed species appears to have two ill-defined, irreversible oxidations at  $0.55$  and  $0.84 \text{ V}_{\text{SCE}}$ . 1,4-dioxane appears to be a better solvent for the deposition of the imine onto ITO, as cyclic voltammetry shows a larger current, though there appears to be only one oxidation signal at  $+0.74 \text{ V}_{\text{SCE}}$  which is irreversible (Fig. 5.20). Two small, irreversible reduction processes are also present at  $0.27 \text{ V}_{\text{SCE}}$  and  $0.45 \text{ V}_{\text{SCE}}$ , which are not observed in voltammetry of the solution species, which may indicate that the decomposition of **5.3** occurred. The shift in peak position may also be explained by the presence of water, which in the case of ferrocene tethered *via* thiols onto a gold substrate results in a shift of redox potentials to more

negative values.<sup>67</sup> In the case of ITO treated with **5.3** from 1,4-dioxane, another explanation for the signal at 0.74 V<sub>SCE</sub> may be the oxidation of the amino group to a radical cation species. Such an assignment has been made for the signal at +0.73 V<sub>Ag/Ag+</sub> of 4-aminobenzoic acid electrodeposited onto glassy carbon.<sup>12, 13</sup> Alternatively, the peaks may correspond to oxidation of the imine group. For instance, the imines *N*-(ferrocenylmethylidene)aniline and *N,N'*-bis(ferrocenylmethylidene)-4-phenylenediamine both display a quasi-reversible oxidation between the half-wave potentials of 0.54 to 0.56 V<sub>SCE</sub> and the irreversible oxidation of the imine functionality at 0.82 V<sub>SCE</sub>, respectively.<sup>49</sup>

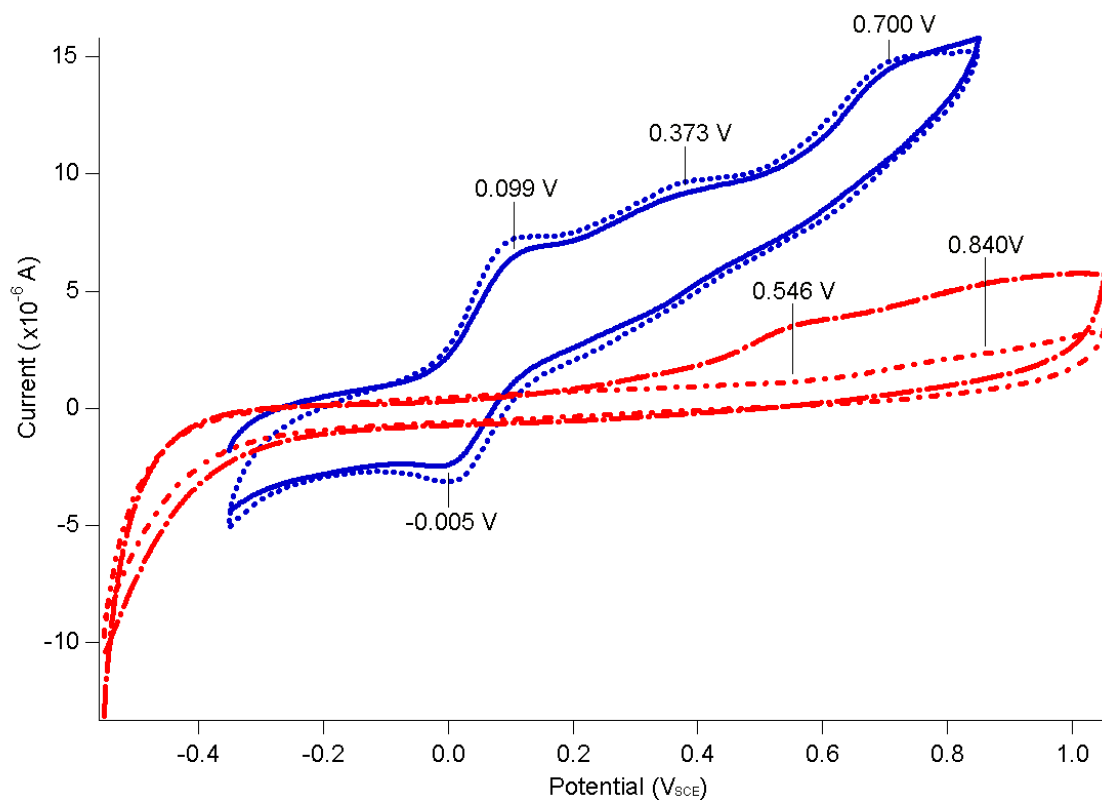


**Figure 5.19.** Voltammetric plots of **5.3** in solution and adsorbed onto ITO glass. In solution: Scan 1 (—), Scan 3 (⋯). On ITO: Scan 1 (—), Scan 3 (⋯). The scans were done at 100 mV s<sup>-1</sup> in acetonitrile.

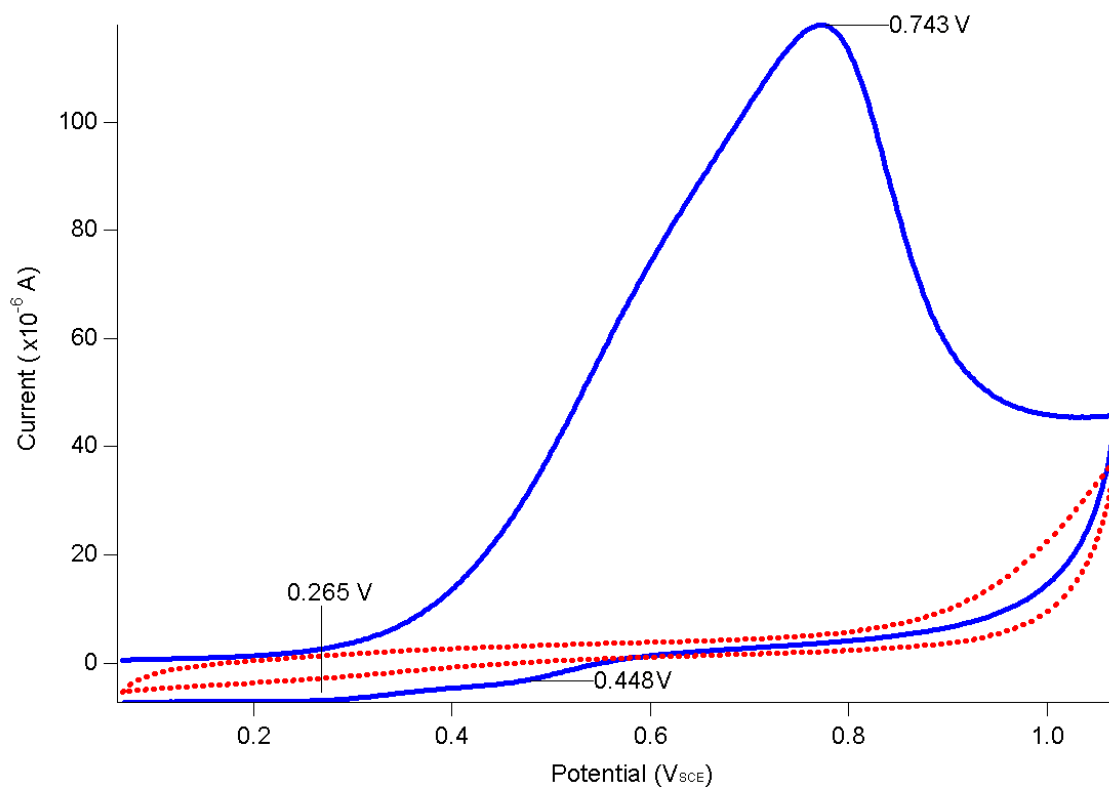


**Figure 5.20.** Cyclic voltammery showing **5.3** deposited onto ITO glass by immersion within a 0.1 mM solution in 1,4-dioxane, at 85°C for three days. Scan 1 (—), Scan 2 (---). The scans were done at 50 mV s<sup>-1</sup> in acetonitrile.

The altered profile of the deposited imine is not due to a polymerised species, as on prolonged potential cycling there is no increase in peak current that would indicate electropolymerisation within solution. This eliminates the possibility that the irreversible oxidation is due to the degradation of polymeric material, though at 0.62 V<sub>SCE</sub>, 4-phenylenevinylene has a lower oxidation potential than aniline, which oxidises above 0.8 V.<sup>68</sup> Given that ITO treated with **5.3** gave a poor response, it was not surprising that attempts to form the imine *in situ*, by the treatment of ITO with 4-phenylenediamine, then **5.2** did not produce any detectable current. The steady decrease in peak current of sequential scans for ITO treated with **5.4** may be rationalised by either desorption or degradation of the adsorbate.

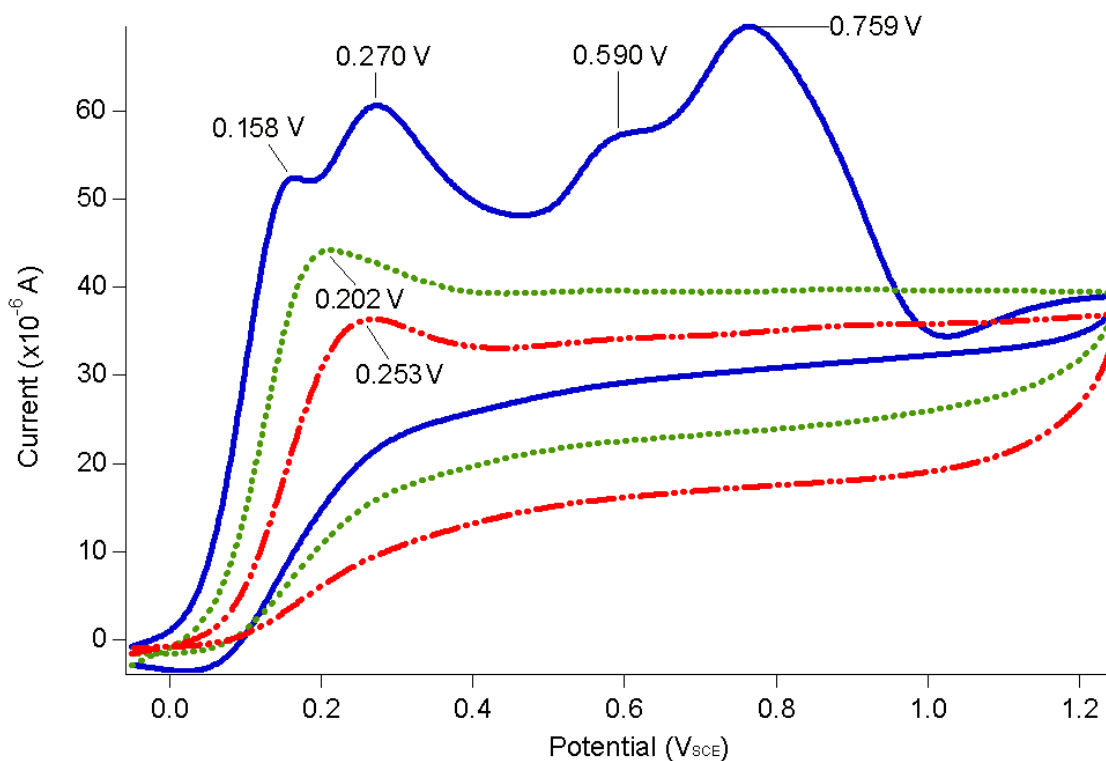


**Figure 5.21.** Cyclic voltammetry showing the irreversible oxidation of **5.4** from a 10 mM solution results in a contamination of the electrode, as evidenced by the decreased current. Scan 1 (—), Scan 2 (⋯), Scan 3 (---). The scans were done at  $50 \text{ mV s}^{-1}$  in acetonitrile.

As found for the imine analogue, electropolymerisation of **5.4** does not occur with the solution species, though the decreasing peak current with subsequent scans indicate that there is contamination of the electrode surface due to irreversible oxidation processes (Fig. 5.21). The cyclic voltammetry of **5.4** in solution shows irreversible oxidation processes and one reversible process. The oxidation at  $0.27 \text{ V}_{\text{SCE}}$  and a reduction at  $0.13 \text{ V}_{\text{SCE}}$  is due to the ferrocene/ferrocenium couple, as the signals are much lower than the oxidation potential of 4-phenylenevinylene (Fig. 5.22).<sup>68</sup> Cyclic voltammetry of ITO glass treated by immersion within **5.4** shows a significant shift in the signal position, which may be attributed to the presence of adsorbed species (Fig. 5.23).

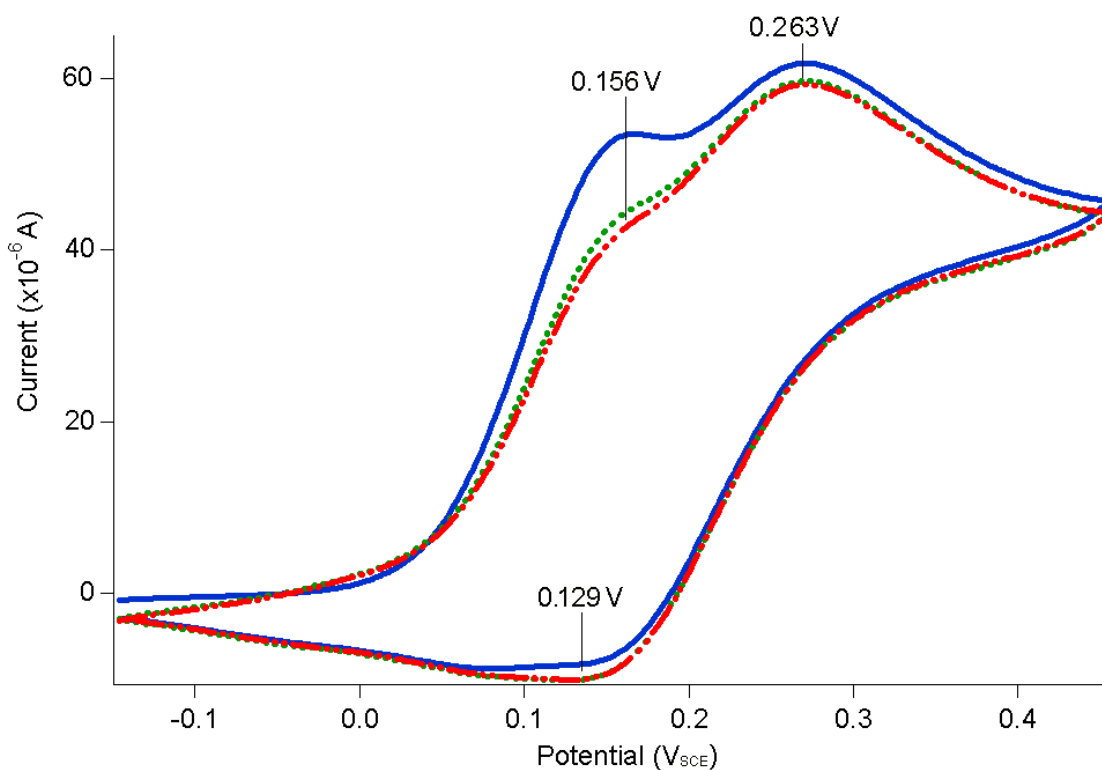


**Figure 5.22.** Cyclic voltammetry scans of a 10 mM solution of **5.4**. The half-wave potential for the reversible ferrocene/ferrocenium redox couple is 0.196 V<sub>SCE</sub>. Scan 1 (—), Scan 2 (⋯), Scan 3 (---). The scans were done at 50 mV s<sup>-1</sup> in acetonitrile.

It is possible that shifts in the oxidation and reduction potentials of **5.4** are due to adsorption on ITO. If the binding of ferrocenyl species results in extension of conjugation from the molecule to the surface, the electronic character of the alkene group that bridges the ferrocene moiety to ITO would be altered, which may then shift the redox potential of the ferrocene/ferrocenium couple. This is plausible as the reversible ferrocene/ferrocenium couple of species like those shown in Figures 5.24 and 5.25 is reported to vary with the bridging functionality, but be practically independent of the substituent on the other side of the bridge. For instance, in the case of ethynylferrocene species, the half-wave potential for the ferrocenyl signal appears between 0.15 to 0.16 V, while for ethynylferrocene derivatives, the signal is observed between 0.28 to 0.33 V<sub>SCE</sub>.<sup>69</sup> Similarly, the ferrocene/ferrocenium couple for 2-ferrocenylmethylidenimino-5-methylbenzoic acid is reported as 0.72 V<sub>SCE</sub>, while the analogous amine has a significantly lower oxidation potential (0.50 V<sub>SCE</sub>).<sup>57</sup>

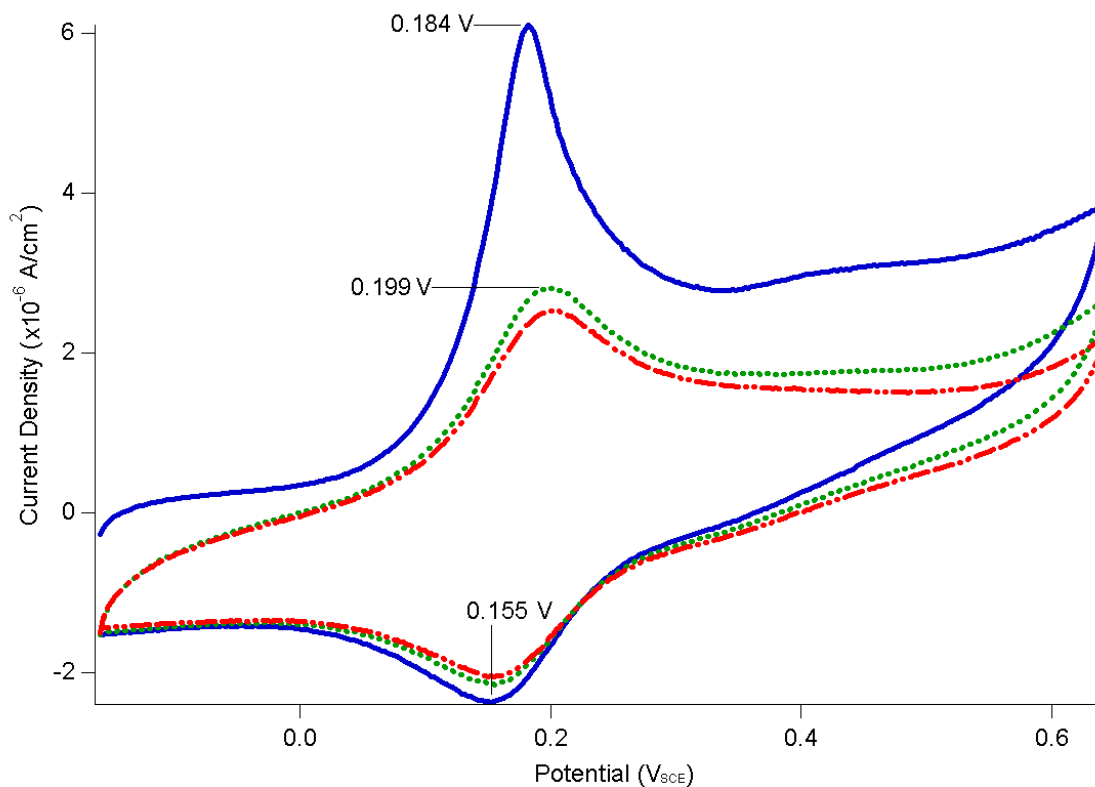


**Figure 5.23.** Cyclic voltammetry of **5.4** adsorbed upon ITO glass by immersion within a 2.3 mM solution, using 6% v/v 1,4-dioxane in hexane as the solvent. Scan 1 (—), Scan 2 (⋯), Scan 3 (---). The scans were done at 50 mV s<sup>-1</sup> in acetonitrile.

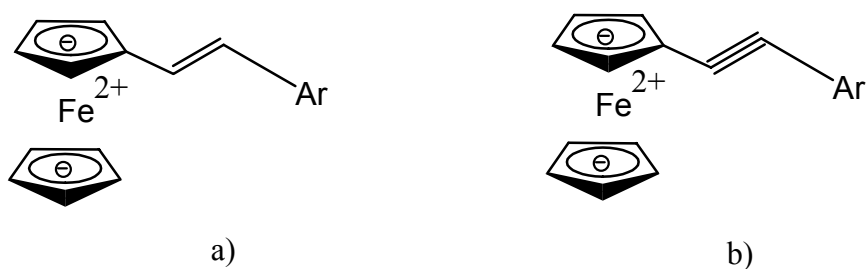


**Figure 5.24.** a) An ethenylferrocene and b) an ethynylferrocene, where ‘Ar’ represents aryl functionality, as described by L. Cuffe *et al.* 2005.<sup>69</sup>

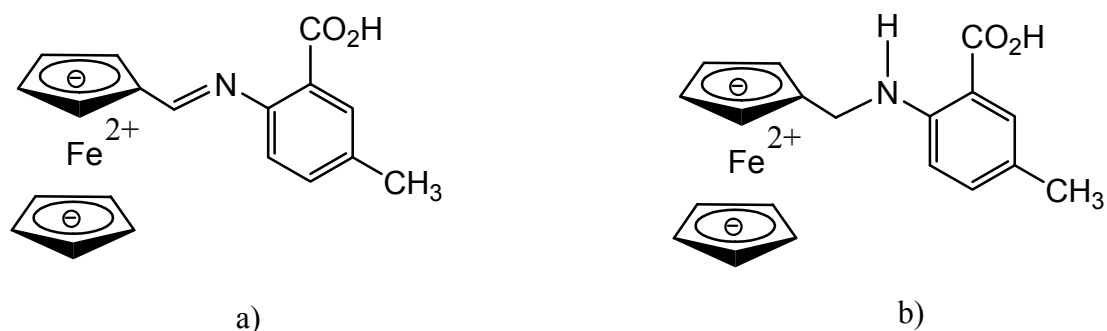


**Figure 5.25.** 2-ferrocenylmethylidenimino-5-methylbenzoic acid (a) and 2-ferrocenylmethylamino-5-methylbenzoic acid (b), as described by J. Cano *et al.* 1995.<sup>57</sup>

### 5.6.3. Surface Coverage Estimates

The surface coverage for **5.4** upon ITO was obtained by both voltammetry and UV-Vis spectroscopy. **5.4** was adsorbed onto ITO from a 2 mM solution in 10% v/v of 1,4-dioxane in hexane after soaking at room temperature for 30 minutes, followed by rinsing in a 5% v/v solution of 1,4-dioxane in hexane. The bracket of surface coverage values of **5.4** was calculated to be  $3.2 - 3.9 \times 10^{-10} \text{ mol cm}^{-2}$  for an ideal monolayer and was derived from minimum and maximum molecular ‘footprint’ areas of  $4.3$  and  $5.3 \times 10^{-19} \text{ m}^{-2}$  (Section 2.5.1). The experimental surface coverage given by voltammetry of  $5 \times 10^{-13} \text{ mol cm}^{-2}$  is an underestimate, due to the significant diffusion of the adsorbate off ITO during the experiment and to uncertainties in selection of the peak area to be integrated. However, from UV-Vis data, a surface coverage of  $5 \times 10^{-10} \text{ mol cm}^{-2} \pm 5\%$  was obtained, which is greater than the calculated maximum coverage value of  $3.9 \times 10^{-10} \text{ mol cm}^{-2}$ , but is comparable to the coverage of an ideal monolayer of hexylferrocenephosphonic acid ( $4.5 \times 10^{-10} \text{ mol cm}^{-2}$ )<sup>23</sup> and 1,12-diaminododecane upon ITO ( $6 - 9 \times 10^{-10} \text{ mol cm}^{-2}$ ).<sup>47</sup>

### 5.7. *Towards Chemically-Assisted Self-Assembled Titania Arrays*

It would be ideal to perform the self-assembly of such dye-sensitised solar cells in an anhydrous environment. Quantitative studies using ruthenium coordination compounds upon titania have found that water will quench up to 70% of excited molecules, while the remaining 30% of molecules are perhaps bound in the crevices of adjacent sintered particles of the nanocrystalline titania electrode and thus are sheltered from water.<sup>70</sup> However, practical limitations demand that aqueous or ethanolic systems are used, as the dispersible sol-gel titania used in Chapter 6 of this investigation has a hydrophilic surface.

To investigate the binding of titania to functionalised ITO, 4-aminobenzoic acid was used as the linker species. ITO glass was first cleaned by washing with detergent, then ultrasonication within acetone, water, ethanol and then allowed to air-dry. The substrate was treated by immersion within a 1 mM solution of 4-aminobenzoic acid in 1,4-dioxane at room temperature for 11 days. The sample was rinsed with ethanol then immersed within a suspension of acidified Degussa P25 titania with a pH value of 2, for 14 days. After rinsing by ethanol the sample appeared to be slightly opaque. The low pH of the solution was necessary to ensure that the particles, with an average diameter of 25 nm, remained dispersed. SEM and AFM images confirmed that a thin film of titania particles, rather than a monolayer was deposited. The force of the AFM tip, scanning in contact mode was sufficient to clear a small patch in the sample, providing an estimate of the film thickness at approximately 75 nm, with a root mean squared (RMS) roughness of the cleared area of 10 nm (Fig. 5.26). The bare ITO glass used in this work has a RMS roughness of 2 nm, which is comparable to the RMS roughness of 5 - 7 nm that has been reported for ITO.<sup>71</sup> This may indicate that either that particles were not completely removed by contact force AFM, or that loose material was simply dragged across the cleared portion of the ITO surface.

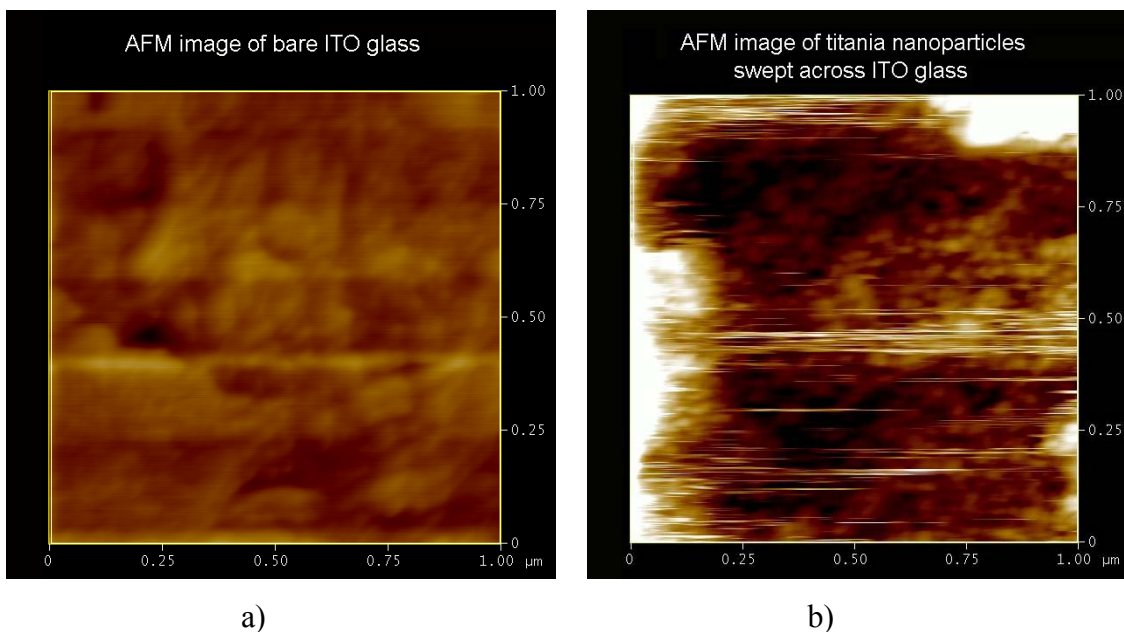


**Figure 5.26.** a) Bare ITO glass cleaned by washing with detergent, then ultrasonication within acetone, water and then ethanol. b) ITO glass treated with 4-aminobenzoic acid and Degussa P25 titania. A central area was swept clear of titania nanoparticles by the force of contact mode AFM.

## 5.8. Conclusions

ITO glass was functionalised by amines and carboxylic acids through what are likely to be electrostatic interactions. The use of adsorbates bearing a ferrocenyl moiety enabled estimates of surface coverage to be obtained from UV-Vis absorption and voltammetry data. Insufficient material was adsorbed to permit the determination of adsorbate binding modes on ITO glass by attenuated total internal reflectance FTIR spectroscopy; samples were both difficult to detect and reproduce. In addition, during voltammetric analysis ferrocenyl adsorbates were lost either by diffusion off the surface or degradation to  $\text{Fe}_2\text{O}_3$ .<sup>45</sup> The modified surfaces produced in this work proved to be less robust than for ITO with adsorbed 1,12-diaminododecane, which was claimed to be stable after immersion in a 0.1 M solution of hydrochloric acid, repeated cyclic voltammetry scans and prolonged exposure to air.<sup>46, 47</sup> It is possible that the bulky ferrocenyl adsorbates **5.1** to **5.4** form monolayers that are loosely packed, which could facilitate the displacement of adsorbed species by solvent molecules.<sup>72</sup>

It is possible that the use of EDTA treatment, by removal of weakly bound indium hydroxide species,<sup>31</sup> could have improved both the voltammetric response and UV-Vis absorption. The improvement would have been more pronounced for voltammetry, assuming that only adsorbed species contribute to the detected current. However, even if the concentration of adsorbates was increased by 50%, the voltammetric response would still be on the order of  $10^{-5}$  A cm<sup>-1</sup> and detection of adsorbates by FTIR spectroscopy would be unlikely.

While in this work, small molecules were adsorbed onto ITO glass *via* electrostatic interactions, complementary techniques for surface functionalisation include the use of polyelectrolytes and covalent bond formation. The layering of polyelectrolytes with nanoparticles is a common method in the literature for the production of stable structures upon surfaces, including gold,<sup>73</sup> silica,<sup>74, 75</sup> polystyrene<sup>76</sup> and cotton.<sup>77</sup> The formation of covalent bonds between adsorbate and substrate has been used to give robust monolayers of *n*-hexyltrichlorosilane on ITO glass<sup>66</sup> and to produce stable, robust films on surfaces other than ITO, such as silicon<sup>21</sup> and glassy carbon.<sup>11, 13</sup>

In this work, ITO glass was functionalised with 4-aminobenzoic acid in attempts to bind redispersed titania nanoparticles. Titania was weakly bound to the substrate, as the force of contact mode AFM was sufficient to remove particulate matter. This is in contrast to nanoparticle superlattices of gold upon ITO glass functionalised with organosilanes, which are stable when stored in solution and have been imaged by AFM.<sup>78</sup> In order to explore the formation of more robust titania arrays with small, molecular linkers, it was logical to study the binding mode of linker and dye species upon titania surfaces.

## 5.9. References

1. Leung, K C-F; Mendes, P M; Magonov, S N; Northrop, B N; Kim, S; Patel, K; Flood, A H; Tseng, H-R; Stoddart, J F. Supramolecular Self-Assembly of Dendronized Polymers: Reversible Control of the Polymer Architectures Through Acid-Base Reactions. *Journal of the American Chemical Society* **2006**, 128, 10707-10715.
2. Tang, H; Zhu, L; Harima, Y; Yamashita, K; Ohshita, J; Kunai, A. Photophysical Properties of  $\sigma$ - $\pi$ -Conjugated Alternating Oligothiénylene-Oligosilylene Polymers. *Journal of Polymer Science Part B: Polymer Physics* **1999**, 37, 1873-1880.
3. Masuda, Y; Itoh, T; Itoh, M; Koumoto, K. Self-Assembly Patterning of Colloidal Crystals Constructed from Opal Structure or NaCl Structure. *Langmuir* **2004**, 20, 5588-5592.
4. Okubo, T; Kimura, H; Hase, H; Yamaguchi, K; Taniguchi, T; Nagai, K. Colloidal Crystals of Cationic Spheres. *Colloid and Polymer Science* **2004**, 282, 250-255.
5. Grätzel, M. Solar Energy Conversion by Dye-Sensitized Photovoltaic Cells. *Inorganic Chemistry* **2005**, 44, 6841-6851.
6. Nakade, S; Makimoto, Y; Kubo, W; Kitamura, T; Wada, Y; Yanagida, S. Roles of Electrolytes on Charge Recombination in Dye-Sensitized TiO<sub>2</sub> Solar Cells (1): the Case of Solar Cells Using the I<sup>-</sup>/I<sub>3</sub><sup>-</sup> Redox Couple. *Journal of Physical Chemistry B* **2005**, 109, 3480-3487.
7. Lee, D; Omolade, D; Cohen, R E; Rubner, M F. pH-Dependent Structure and Properties of TiO<sub>2</sub>/SiO<sub>2</sub> Nanoparticle Multilayer Thin Films. *Chemistry of Materials* **2007**, 19, 1427-1433.
8. Agrios, A G; Cesar, I; Comte, P; Nazeeruddin, M K; Grätzel, M. Nanostructured Composite Films for Dye-Sensitized Solar Cells by Electrostatic Layer-by-Layer Deposition. *Chemistry of Materials* **2006**, 18, 5395-5397.
9. Bocking, T; Salomon, A; Cahen, D; Gooding, J J. Thiol-Terminated Monolayers on Oxide-Free Si: Assembly of Semiconductor-Alkyl-S-Metal Junctions. *Langmuir* **2007**, 23, 3236-3241.
10. Hillebrandt, H; Tanaka, M. Electrochemical Characterisation of Self-Assembled Alkylsiloxane Monolayers on Indium-Tin-Oxide (ITO) Semiconductor Electrodes. *Journal of Physical Chemistry B* **2001**, 105, 4270-4276.
11. Downard, A J; Garrett, D J; Tan, E S Q. Microscale Patterning of Organic Films on Carbon Surfaces Using Electrochemistry and Soft Lithography. *Langmuir* **2006**, 22, 10739-10746.
12. Liu, J; Cheng, L; Liu, B; Dong, S. Covalent Modification of a Glassy Carbon Surface by 4-Aminobenzoic Acid and Its Application in Fabrication of a Polyoxometalates-Consisting Monolayer and Multilayer Films. *Langmuir* **2000**, 16, 7471-7476.
13. Deinhammer, R S; Anderegg, J W; Porter, M D. Electrochemical Oxidation of Amine-Containing Compounds: A Route to the Surface Modification of Glassy Carbon Electrodes. *Langmuir* **1994**, 10, 1306-1313.
14. Wang, H; Chen, S; Li, L; Jiang, S. Improved Method for the Preparation of Carboxylic Acid and Amine Terminated Self-Assembled Monolayers of Alkanethiolates. *Langmuir* **2005**, 21, 2633-2636.
15. Hiramatsu, H; Osterloh, F E. A Simple Large-Scale Synthesis of Nearly Monodisperse Gold and Silver Nanoparticles with Adjustable Sizes and with Exchangable Surfactants. *Chemistry of Materials* **2004**, 16, 2509-2511.
16. Fleming, M S; Walt, D R. Stability and Exchange Studies of Alkanethiol Monolayers on Gold-Nanoparticle-Coated silica Microspheres. *Langmuir* **2001**, 17, 4836-4843.

17. Pierrat, S; Zins, I; Breivogel, A; Sonnichsen, C. Self-Assembly of Small Gold Colloids with Functionalised Gold Nanorods. *Nano Letters* **2007**, 7, 259-263.
18. Sato, T; Brown, D; Johnson, B F G. Nucleation and Growth of Nano-Gold Colloidal Lattices. *Chemical Communications* **1997**, 1007-1008.
19. Liang, Z; Cabarcos, O M; Allara, D L; Wang, Q. Hydrogen-Bonding-Directed Layer-by-Layer Assembly of Conjugated Polymers. *Advanced Materials* **2004**, 16, 823-827.
20. El Harrak, A; Carrot, G; Oberdisse, J; Eychenne-Baron, C; Boue, F. Surface-Atom Transfer Radical Polymerisation from Silica Nanoparticles with Controlled Colloidal Stability. *Macromolecules* **2004**, 37, 6376-6384.
21. Kohli, P; Blanchard, G J. Applying Polymer Chemistry to Interfaces: Layer-by-Layer and Spontaneous Growth of Covalently Bound Multilayers. *Langmuir* **2000**, 16, 4655-4661.
22. Moon, H H; Kim, J H; Kim, K-J; Kang, T-H; Kim, B; Kim, C-H; Hahn, J H; Park, J W. Absolute Surface Density of the Amine Group of the Aminosilylated Thin Layers: Ultraviolet-Visible Spectroscopy, Second Harmonic Generation, and Synchrotron-Radiation Photoelectron Spectroscopy Study. *Langmuir* **1997**, 13, 4305-4310.
23. Vercelli, B; Zotti, G; Zecchin, S. Adsorption of Hexylferrocene Phosphonic Acid on Indium-Tin Oxide Electrodes. Evidence of Strong Interchain Interactions in Ferrocene Self-Assembled Monolayers. *Langmuir* **2003**, 19, 9351-9356.
24. Frantz, R; Durand, J-O; Granier, M; Lanneau, G F. Triisopropoxysilyl-Functionalized Oxide Nanoparticles Using a Di-tert-butyl Phosphonate Ester as the Surface Grafting Agent. *Tetrahedron Letters* **2004**, 45, 2935-2937.
25. Lawless, D; Kapoor, S; Meisel, D. Bifunctional Capping of CdS Nanoparticles and Bridging to TiO<sub>2</sub>. *Journal of Physical Chemistry* **1995**, 99, 10329-10335.
26. Lin, C-L; Yeh, M-Y; Chen, C-H; Sudhakar, S; Luo, S-J; Hsu, Y-C; Huang, C-Y; Ho, K-C; Luh, T-Y. Silica-Titania-Based Organic-Inorganic Hybrid Materials for Photovoltaic Applications. *Chemistry of Materials* **2006**, 18, 4157-4162.
27. Wakamatsu, S; Fujii, S; Akiba, U; Fujihira, M. Motions of Single Molecules Inserted in a Self-Assembled Monolayer Matrix of a Bicyclo[2.2.2]octane Derivative on Au(111). *Nanotechnology* **2003**, 14, 258-263.
28. Wang, M; Leichti, K M; Wang, Q; White, J M. Self-Assembled Silane Monolayers: Fabrication with Monoscale Uniformity. *Langmuir* **2005**, 21, 1848-1857.
29. Besbes, S; Ltaief, A; Reybier, K; Ponsonnet, L; Jaffrezic, N; Davenas, J; Ben Ouada, H. Injection Modifications by ITO Functionalization with a Self-Assembled Monolayer in OLEDs. *Synthetic Metals* **2003**, 138, 197-200.
30. Marrikar, F S; Brumbach, M; Evans, D H; Paler-Lebron, A; Pemberton, J E; Wysocki, R J; Armstrong, N R. Modification of Indium-Tin Oxide Electrodes with Thiophene Copolymer Thin Films: Optimising Electron Transfer to Solution Probe Molecules. *Langmuir* **2007**, 23, 1530-1542.
31. Armstrong, N R; Carter, C; Donley, C; Simmonds, A; Lee, P; Brumbach, M; Kippelen, B; Domercq, B; Yoo, S. Interface Modification of ITO Thin Films: Organic Photovoltaic Cells. *Thin Solid Films* **2003**, 445, 342-352.
32. Carter, C; Brumbach, M; Donley, C; Hreha, R D; Marder, S R; Domercq, B; Yoo, S; Kippelen, B; Armstrong, N R. Small Molecule Chemisorption on Indium-Tin Oxide Surfaces: Enhancing Probe Molecule Electron-Transfer Rates and the Performance of Organic Light-Emitting Diodes. *Journal of Physical Chemistry B* **2006**, 110, 25191-25202.

33. Le, Q-T; Forsythe, E W; Nuesch, F; Rothberg, L J; Yan, L; Gao, Y. Interface Formation between NBP and Processed Indium Tin Oxide. *Thin Solid Films* **2000**, 363, 42-46.
34. Bisquert, J; Cahen, D; Hodes, G; Ruhle, S; Zaban, A. Physical Chemical Principles of Photovoltaic Conversion with Nanoparticulate, Mesoporous Dye-Sensitized Solar Cells. *Journal of Physical Chemistry B* **2004**, 108, 8106-8118.
35. Nuesch, F; Rothberg, L J; Forsythe, E W; Le, Q T; Gao, Y. A Photoelectron Spectroscopy Study on the Indium Tin Oxide Treatment by Acids and Bases. *Applied Physics Letters* **1999**, 74, 880-882.
36. Le, Q T; Nuesch, F; Rothberg, L J; Forsythe, E W; Gao, Y. Photoemission Study of the Interface between Phenyl Diamine and Treated Indium-Tin-Oxide. *Applied Physics Letters* **1999**, 75, 1357-1359.
37. Fadeev, A Y; Helmy, R; Marcinko, S. Self-Assembled Monolayers of Organosilicon Hydrides Supported on Titanium, Zirconium, and Hafnium Dioxides. *Langmuir* **2002**, 18, 7521-7529.
38. Doron, A; Katz, E; Willner, I. Organization of Au Colloids as Monolayer Films onto ITO Glass Surfaces: Application of the Metal Colloid Films as Base Interfaces to Construct Redox-Active Monolayers. *Langmuir* **1996**, 11, 1313-1317.
39. Tanaka, K; Ago, H; Yamabe, T. Electronic Structures of Organosilicon Polymers Containing Thienylene Units. *Organometallics* **1994**, 13, 3496-3501.
40. Ohshita, J; Kumai, A. Polymers with Alternating Organosilicon and  $\pi$ -Conjugated Units. *Acta Polymerica* **1998**, 49, 379-403.
41. Hedges, D H P; Richardson, D J; Russell, D A. Electrochemical Control of Protein Monolayers at Indium Tin Oxide Surfaces for the Reagentless Optical Biosensing of Nitric Oxide. *Langmuir* **2004**, 20, 1901-1908.
42. Zotti, G; Zecchin, S; Vercelli, B. Surface-Initiated Polymerisation of Thiophene and Pyrrole Monomers on Poly(terthiophene) Films and Oligothiophene Monolayers. *Chemistry of Materials* **2005**, 17, 3681-3694.
43. Khodabakhsh, S; Sanderson, B M; Nelson, J; Jones, T S. Using Self-Assembling Dipole Molecules to Improve Charge Collection in Molecular Solar Cells. *Advanced Functional Materials* **2006**, 16, 95-100.
44. VanderKam, S K; Bocarsly, A B; Schwartz, J. Enhanced Bonding of Poly(ethylene-co-acrylic acid) to Oxides Through Surface-Bound Alkoxyzirconium Complex Surfaces. *Chemistry of Materials* **1998**, 10, 685-687.
45. Zotti, G; Schiavon, G; Zecchin, S; Berlin, A; Pagani, G. Adsorption of Ferrocene Compounds on Indium-Tin-Oxide Electrodes. Enhancement of Adsorption by Decomposition of Ferrocenium Molecules by Oxygen. *Langmuir* **1998**, 14, 1728-1733.
46. Hyung, K-H; Han, S-H. Formation of Self-Assembled Monolayers of Di-(3-aminopropyl)-viologen as Electron Acceptor in ITO Surface. *Synthetic Metals* **2003**, 137, 1441-1442.
47. Oh, S-Y; Yun, Y-J; Hyung, K-H; Han, S-H. Self-Assembled Monolayers of Diamine Molecules and Phosphomolybdic Acid on an ITO Surface. *New Journal of Chemistry* **2004**, 28, 495-501.
48. Base, T; Cisarova, I; Stepnicka, P. Acid-Catalyzed Self-Alkylation of FcCH<sub>2</sub>NHPh. Solid-State Structures of FcCH<sub>2</sub>NHPh and (FcCH<sub>2</sub>)NPh. *Inorganic Chemistry Communications* **2002**, 5, 46-50.
49. Pal, S K; Alagesan, K; Samuelson, A G; Pebler, J. Synthesis and Characterization of Novel Charge Transfer Complexes formed by *N, N'*-bis(ferrocenylmethylidene)-*p*-phenylenediamine and *N*-(ferrocenylmethylidene)aniline. *Journal of Organometallic Chemistry* **1999**, 575, 108-118.
50. O'Neil, M J; Smith, A; Heckelman, P E. *The Merck Index: an Encyclopedia of Chemicals, Drugs and Biologicals*. 13<sup>th</sup> ed, Merck & Co. Inc.: New Jersey, USA, **2001**.

51. Silverstein, R M; Bassler, G C; Morrill, T C. *Spectrometric Identification of Organic Compounds*. 5<sup>th</sup> ed, John Wiley & Sons, Inc.: **1991**.
52. Zotti, G; Schiavon, G; Zecchin, S; Berlin, A; Canavesi, A; Pagani, G. Self-Assembly and Electropolymerization of Pyrrole- and Bithiophene-*n*-hexyl-ferrocene Molecules on ITO Electrodes. *Synthetic Metals* **1997**, 84, 239-240.
53. de Santana, H; Quillard, S; Fayad, E L, G;. *In Situ* UV-Vis and Raman Spectroscopic Studies of the Electrochemical Behaviour of *N,N'*-diphenyl-1,4-phenylenediamine. *Synthetic Metals* **2006**, 156, 81-85.
54. Chao, D; Ma, X; Lu, X; Cui, L; Mao, H; Zhang, W; Wei, Y. Electroactive Hyperbranched Polyamide Synthesized by Oxidative Coupling Polymerisation within an A<sub>2</sub> + B<sub>3</sub> Strategy. *Macromolecular Chemistry and Physics* **2007**, 208, 658-664.
55. Salvagione, H J; Acevedo, D F; Miras, M C; Motheo, A J; Barbero, C A. Comparative Study of 2-Amino and 3-Aminobenzoic Acid Copolymerization with Aniline Synthesis and Copolymer Properties. *Journal of Polymer Science: Part A: Polymer Chemistry* **2004**, 42, 5587-5599.
56. Toma, S; Gaplovsky, A; Elecko, P. Synthesis and Electronic Spectra of 1-aryl-2-ferrocenylethylenes. *Chemical Papers* **1985**, 39, 115-124.
57. Cano, J; Benito, A; Martinez-Manez, R; Soto, J P, Jordi ; Lloret, F; Julve, M; Marcos, M D; Sinn, E. Ferrocene Containing Chelating Ligands 3. Synthesis, Spectroscopic Characterization, Electrochemical Behaviour and Interaction With Metal Ions of New Ligands Obtained by Condensation of Ferrocenecarboxaldehyde With 2-aminobenzoic Acid Derivatives. Crystal Structures of 2-ferrocenylmethylamino-5-methylbenzoic Acid and 2-bis(ferrocenylmethyl)ammonium-5-methylbenzoic Acid Perchlorate. *Inorganica Chimica Acta* **1995**, 231, 45-56.
58. Raffa, D L; Battaglini, F. Novel Conducting Polyaniline Bearing Functional Groups. *Journal of Electroanalytical Chemistry* **2001**, 504, 120-124.
59. VanderKam, S K; Gawalt, E S; Schwartz, J; Bocarsly, A B. Electrochemically Active Surface Zirconium Complexes on Indium Tin Oxide. *Langmuir* **1999**, 15, 6598-6600.
60. Wei, L; Syomin, D; Loewe, R S; Lindsey, J S; Zaera, F; Bocian, D F. Structural and Electron-Transfer Characteristics of Carbon-Tethered Porphyrin Monolayers on Si(100). *Journal of Physical Chemistry B* **2005**, 109, 6323-6330.
61. Morkrani, C; Fatisson, J; Guerente, L; Labbe, P. Structural Characterization of (3-mercaptopropyl)sulfonate Monolayer on Gold Surfaces. *Langmuir* **2005**, 21, 4400-4409.
62. Bard, A J; Faulkner, L R. *Electrochemical Methods: Fundamentals and Applications*. 2<sup>nd</sup> ed, John Wiley & Sons Inc: **2001**.
63. Cho, Y-J; Ahn, T K; Song, H; Kim, K S; Lee, C Y; Seo, W S; Lee, K; Kim, S K; Kim, D; T;, P J. Unusually High Performance Photovoltaic Cell Based on a [60]Fullerene Metal Cluster-Porphyrin Dyad SAM on an ITO Electrode. *Journal of the American Chemical Society* **2005**, 127, 2380-2381.
64. Oh, S-Y; Yun, Y-J; Kim, D-Y; Han, S-H. Formation of a Self-Assembled Monolayer of Diaminododecane and a Heteropolyacid Monolayer on the ITO Surface. *Langmuir* **1999**, 15, 4690-4692.
65. Zhu, Y; Xing, W; Li, Y; Ding, M; Sun, G; Gou, D; Lu, T. Direct Deposition and Characterization of Langmuir-Blodgett Monolayers of Soluble Polyimides. *Thin Solid Films* **1997**, 303, 282-286.
66. Cossement, D; Plumier, F; Delhalle, J; Hevesi, L; Mekhalif, Z. Electrochemical Deposition of Polypyrrole Films on Organosilane-Modified ITO Substrates. *Synthetic Metals* **2003**, 138, 529-536.
67. Zhang, X G; Shi, Y L; Li, H L. The Effect of the Water Content of Acetonitrile on the Electrochemistry of Ferrocenyl Thiol Self-Assembled Monolayers. *Journal of Colloid and Interface Science* **2002**, 246, 296-301.

68. Desilvestro, J; Scheifele, W. Morphology of Electrochemically Prepared Polyaniline. *Journal of Materials Chemistry* **1993**, 3, 263-272.
69. Cuffe, L; Hudson, R D A; Gallagher, J F; Jennings, S; McAdam, C J; Connelly, R B T; Manning, A R; Robinson, B H; Simpson, J. Synthesis, Structure, and Redox Chemistry of Ethenyl and Ethynyl Ferrocene Polyaromatic Dyads. *Organometallics* **2005**, 24, 2051-2060.
70. Delgadillo, A; Arias, M; Leiva, A M; Loeb, B; Meyer, G J. Interfacial Charge-Transfer Switch: Ruthenium-dppz Compounds Anchored to Nanocrystalline TiO<sub>2</sub>. *Inorganic Chemistry* **2006**, 45, 5721-5723.
71. Koh, S E; McDonald, K D; Holt, D H; Dulcey, C S; Chaney, J A; Pehrsson, P E. Phenylphosphonic Acid Functionalization of Indium Tin Oxide: Surface Chemistry and Work Functions. *Langmuir* **2006**, 22, 6249-6255.
72. Karsi, N; Lang, P; Chehimi, M; Delamar, M; Horowitz, G. Modification of Indium Tin Oxide Films by Alkanethiol and Fatty Acid Self-Assembled Monolayers: A Comparative Study. *Langmuir* **2006**, preprint.
73. Chirea, M; Garcia-Morales, V; Manzanares, J A; Pereira, C; Gulaboski, R; Silva, F. Electrochemical Characterization of Polyelectrolyte/Gold Nanoparticle Multilayers Self-Assembled on Gold Electrodes. *Journal of Physical Chemistry B* **2005**, 109, 21808-21817.
74. Hao, E; Yang, B; Ren, H; Qian, X; Xie, T; Shen, J; Li, D. Fabrication of Composite Film Comprising TiO<sub>2</sub>/CdS and Polyelectrolytes Based on Ionic Attraction. *Materials Science and Engineering C* **1999**, 10, 119-122.
75. Sun, Y; Hao, E; Zhang, X; Yang, B; Shen, J; Chi, L; Fuchs, H. Buildup of Composite Films Containing TiO<sub>2</sub>/PbS Nanoparticles and Polyelectrolytes Based on Electronic Interaction. *Langmuir* **1997**, 13, 5168-5174.
76. Yap, H P; Quinn, J F; Ng, S M; Cho, J; Caruso, F. Colloid Surface Engineering via Deposition of Multilayered Thin Films from Polyelectrolyte Blend Solutions. *Langmuir* **2005**, 21, 4328-4333.
77. Hyde, K; Rusa, M; Hinestroza, J. Layer-by-Layer Deposition of Polyelectrolyte Nanolayers on Natural Fibres: Cotton. *Nanotechnology* **2005**, 16, S422-S428.
78. Shipway, A N; Lahav, M; Willner, I. Nanostructured Gold Colloid Electrodes. *Advanced Materials* **2000**, 12, 993-998.



## 6. THE BINDING OF DYE TO TITANIA

### 6.1. Introduction

In this chapter, the mode of dye binding on titania has been studied as part of the effort to draw general relationships between dye structure and performance within Grätzel cells. Sensitiser dyes may then be designed for Grätzel cells with greater confidence that optimal efficiencies will be obtained.<sup>1-3</sup>

An intimate association between dye and titania is essential for Grätzel cell performance and it has been suggested that an overlap of dye  $\pi^*$  and titanium 3d orbitals permits the efficient injection of electrons into titania.<sup>4</sup> The mode of dye binding will dictate the conformation and 'footprint' area of the dye, influencing packing and thus the maximum concentration of dye that may be loaded onto titania electrodes. If dyes are bound so that the dye footprint area is decreased, the maximum dye loading will increase, which can contribute to an improved Grätzel cell efficiency.<sup>5</sup> Knowledge of how dyes bind to titania will therefore aid rational design of sensitiser dyes. Strong bonding to the surface is also necessary to reduce the quenching effect of solvents on the electron injection rate of dyes to titania.<sup>6</sup> In addition, adsorbed species modify the electronic properties of titania.<sup>4, 7</sup> This study employs spectroscopic methods to determine the binding mode of adsorbed dye on titania and the nature of dye binding.

### 6.2. Dye Adsorption on Titania for Grätzel Cells

The binding of adsorbates to titania is characterised by the preference of  $\text{Ti}^{4+}$  for coordination with hard bases, such as oxygen and nitrogen atoms. Species adsorbed on titania typically bind *via* Brønsted acids and Lewis bases, such as carboxylic and phosphonic acids or cyano groups, to titanium atoms with a coordination number less than 6, which is the preferred value.<sup>8</sup> Dyes that are bound to titania as a carboxylate include the porphyrin dye cyano-3-(2'-(5',10',15',20'-tetraphenylporphyrinato zinc(II))yl)acrylic acid and the 'N3' dye, di(thiocyanato)-bis(2,2'-bipyridyl-4,4'-dicarboxylate) ruthenium(II).<sup>9,10</sup> 1,3-Propanediphosphonic acid and acetonitrile are two examples of adsorbates bound *via* phosphonic acids and a cyano moiety.<sup>11, 12</sup> A simple

cyano-containing species such as acetonitrile can bind either *via* the nitrogen atom to undercoordinated  $\text{Ti}^{4+}$  Lewis acid sites or by hydrogen bonding to titanol (Ti-OH) functionality.<sup>13, 14</sup>

### 6.2.1. *The Binding of Carboxylic Acids to Titania*

The binding of fully conjugated sensitizer dyes *via* carboxylic acid groups currently produce Grätzel cells with the highest performance.<sup>15, 16</sup> The anchoring geometry may play a significant role in the efficiency of electron injection from excited-state dyes into titania, as dyes bound to titania by more than one carboxylic acid group produce higher Grätzel cell efficiencies than dyes bound by a single acid.<sup>17</sup> Carboxylic acids may bind in a monodentate or bidentate fashion, the latter of which may bridge or chelate titania atoms (Fig. 6.1).<sup>18, 19</sup> A distinction is made between the pseudo-ester form (Fig. 6.1.a) and the other monodentate carboxylate forms. A well-cited reference is the work of Deacon *et al.*<sup>20</sup> who examined published data on a range of coordination compounds. Empirical evidence was used to draw correlations between structure and features of FTIR spectra. A ‘rule of thumb’ guide was developed for the wavenumber difference ( $\Delta\nu$ ) between the asymmetric carboxylate ( $\nu(\text{CO}_2^-)_{\text{asym}}$ ) and symmetric carboxylate ( $\nu(\text{CO}_2^-)_{\text{sym}}$ ) stretching frequencies to indicate the mode of binding. A  $\Delta\nu$  value larger than  $200\text{ cm}^{-1}$  may indicate a pseudo-ester monodentate binding (Fig. 6.1.a), though the monodentate carboxylate form (Fig. 6.1.b) is a more likely structure. Smaller  $\Delta\nu$  values are typical of carboxylate forms that involve bridging (Fig. 6.1.c, e, f) or chelation (Fig. 6.1.d, f).<sup>21, 22</sup> Simple species, such as acetylacetone and formic acid have been studied as models for more complex carboxylic acids such as coordination compounds.<sup>23</sup> The general consensus on the binding of carboxylic acids to titania is that a bidentate carboxylate form is involved and is either a chelating<sup>15, 16</sup> or a bridging<sup>24, 25</sup> mode, as reported for ruthenium coordination compounds and porphyrinic dyes. However, the unidentate pseudo-ester form has also been reported for the adsorption of coordination compounds, as well as smaller species such as acetic acid, on titania.<sup>26-28</sup>

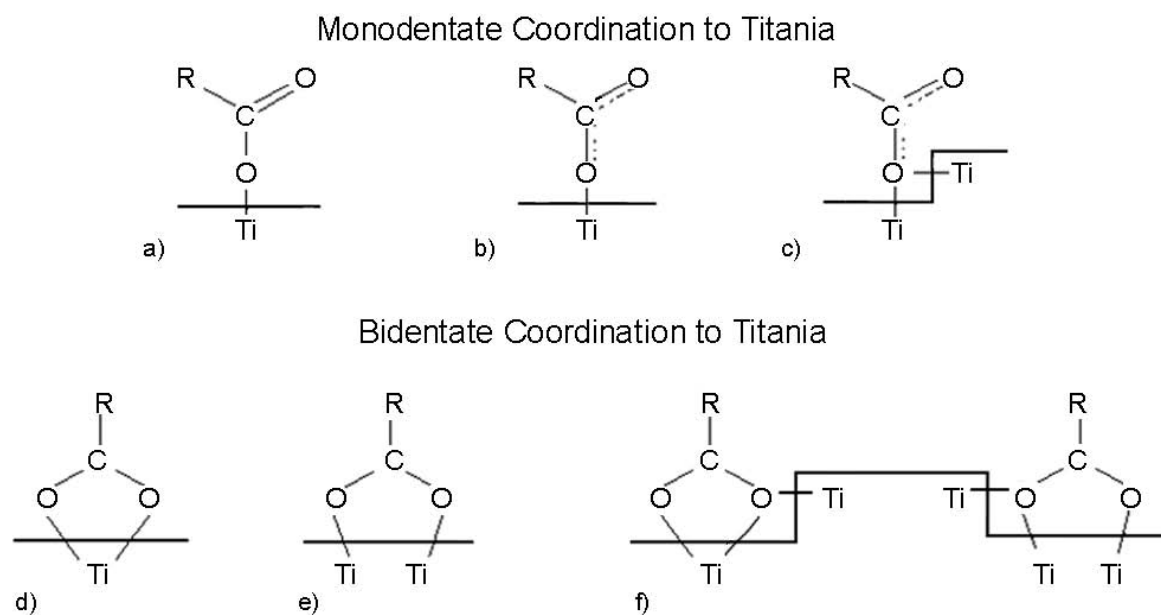


**Figure 6.1.** Plausible binding modes of an adsorbate *via* carboxylic acid functionality to titania. Monodentate forms: a) pseudo-ester; b) carboxylate; c) bridging carboxylate. Bidentate forms: d) chelating; e) bridging; f) chelating and bridging.

Both the surface structure of titania and the environment influence the binding of species. Materials processing affects adsorptive properties of the substrate, as documented with the weaker binding of acetonitrile to Merck P25 titania than to Degussa P25 titania.<sup>14</sup> Hydration of titania surfaces has an impact on the mode of acid binding, as illustrated by computational studies and experimental data for the adsorption of formic acid and sodium formate. On a dry anatase surface, formic acid was found to bind *via* hydrogen bonding in a monodentate pseudo-ester mode, but upon hydrated titania may bind either as a bidentate bridging species or as a pseudo-ester stabilised by hydrogen-bonding with titanol groups. While the formate species was predicted to bind *via* bidentate *bridging* coordination on both dry and hydrated anatase, bidentate *chelating* structures are not energetically favoured for either the formate anion or formic acid. To complicate matters, while molecular formic acid binds *via* hydrogen bonding upon dry anatase, formic acid binds as a pseudo-ester on a rutile surface.<sup>19</sup> The degree of crystallinity and relative abundance of surface defects may determine the mode of binding by carboxylic acids. For instance, carboxylic acids bind either as a pseudo-ester or a carboxylate upon titania particles smaller than 6 nm, as a pseudo-ester on particles greater than 6 nm and by simple adsorption for particles greater than 50 nm in size.<sup>28</sup>

By X-ray absorbance near-edge spectroscopy (XANES) it was observed that as particle size decreased from 50 to 2 nm in size titanium atoms in the particle displayed a change from 6 to 5 in the average coordination number.<sup>29</sup> As particle size decreases, the number of facets and step defects is expected to increase with the greater lattice strain, reducing the average coordination number.<sup>30</sup>

### 6.3 Dye Aggregation, Solvent and Concentration Effects

The extent of dye aggregation must be addressed in the analysis of dye adsorption as there are implications for the performance of sensitised electrodes in terms of Grätzel cell efficiency. Aggregation can result in a shift and broadening of UV-Vis absorption features and is solvent dependent or may be complicated by specific dye-solvent interactions.<sup>31</sup> Molecules may aggregate in poor solvents, as in the case of oligothiophenes end-capped by oligoethylene oxide, which have a lower solubility in *n*-butanol than in chloroform or tetrahydrofuran.<sup>32</sup>  $\pi$ -Conjugated species may form ‘J- and H-type’ aggregates, which exhibit red (bathochromic) and blue (hypsochromic) UV-Vis shifts, respectively. In planar systems, H-aggregates can be envisioned as stacking in a plane-to-plane (‘side to side’) fashion, and J-aggregates as layered (‘head to tail’) stacking (Fig. 6.2). Consequently, H-type aggregates have a better intermolecular overlap of the conjugated system and so have improved charge-transport properties between molecules.<sup>33,34</sup>

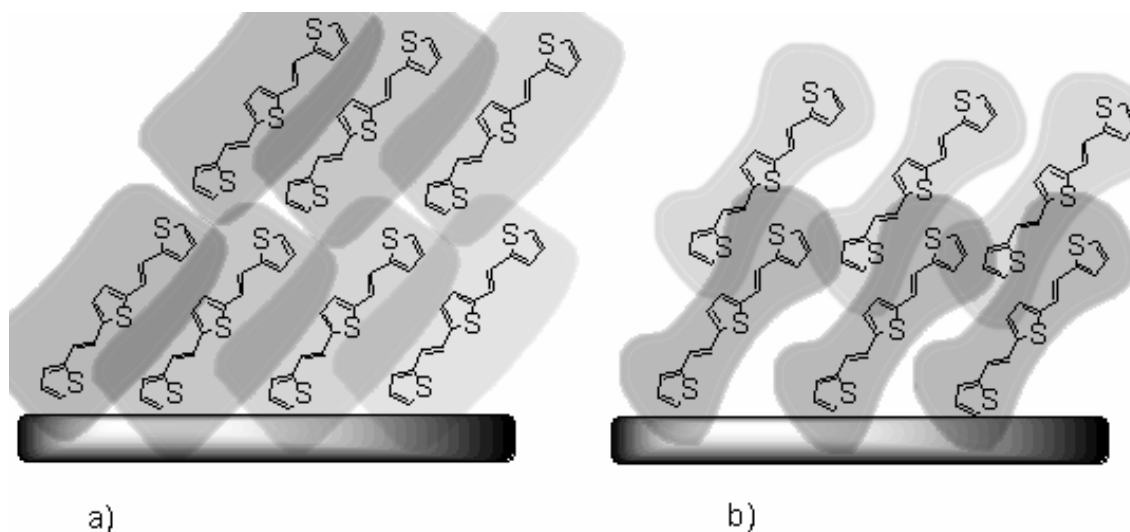


**Figure 6.2.** A cartoon of a) H-aggregation and b) J-aggregation of di(thienylenevinylene)thiophene.

The association of dye molecules in aggregates produces new electronic transition states from the interaction of molecular transition dipoles (Fig. 6.3). The angle  $\theta$ , which describes the ‘slip angle’ between molecules, is ideally  $90^\circ$  for H-aggregates and less than  $90^\circ$  for J-aggregates. Of the excited electronic transition states only one is allowed. As the higher energy excited state is allowed for H-aggregates, while the lower energy state is permitted for J-aggregates, respective blue and red shifts in absorption result.<sup>35, 36</sup>

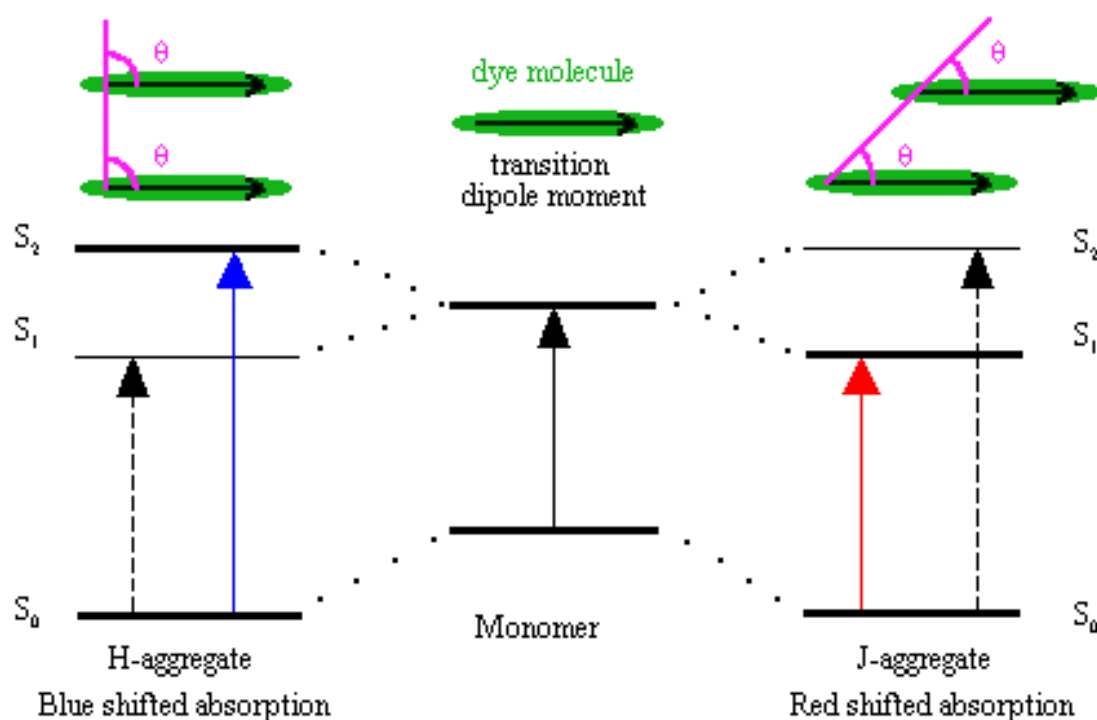


**Figure 6.3.** The origin of blue and red shifts in absorption on the formation of H- and J-aggregates as described by Mishra *et al.* 2000.<sup>36</sup> The interaction between the electronic transition dipole moments of associated molecules results in additional excited states. Only one of the excited states is permitted, which for H-aggregates is that of higher energy and for J-aggregates is of lower energy.

The H-aggregation of dyes results in an efficiency decrease of Grätzel cells, as found with coumarin dyes (Fig. 6.4). The species bearing a side ring on the alkene chain (Fig. 6.4.a) showed a higher Grätzel cell performance and only a small blue shift in UV-Vis

absorbance that indicated a lack of dye aggregation. The corresponding species without the side ring formed H-aggregates, as inferred from a 50 nm blue shift of absorbance.<sup>37</sup> However, a contrasting case is that of merocyanine dyes,<sup>38</sup> where the formation of J-aggregates by the alignment of molecules *via* a long substituent alkyl chain gave an improved Grätzel cell performance.

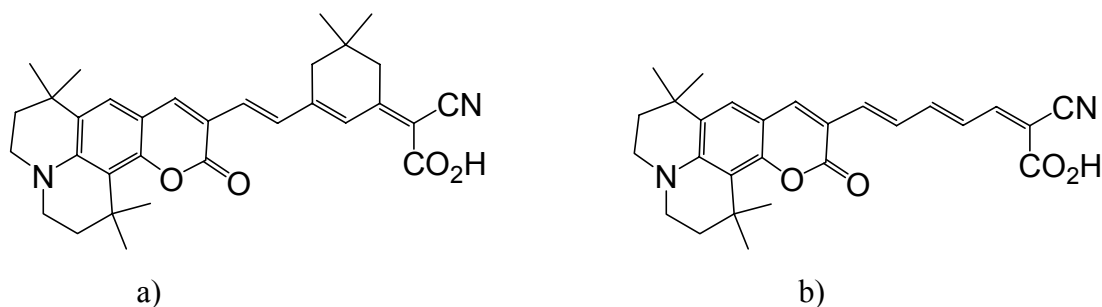


**Figure 6.4.** Coumarin dyes as described by Z. S. Wang *et al.* 2005.<sup>37</sup> a) Cyano(5,5-dimethyl-3-[2-(1,1,6,6-tetramethyl-10-oxo-2,3,5,6-tetrahydro-1*H*,4*H*,10*H*-11-oxa-3a-aza-benzo[de]anthracen-9-yl)vinyl]cyclohex-2-enylidene)acetic acid, which bears a side ring on the alkene chain and prevents aggregation. b) The analogous material, which is without a side ring and forms H-aggregates.

Solvent effects are a significant factor and have been investigated for species such as formic acid and the hexacyanoferrate ion. Within an alcoholic environment, the formate anion favours a more asymmetric mode of bidentate coordination than when in water.<sup>19, 25</sup> Similarly, time-dependent density-functional theory estimates that the bidentate coordination of the hexacyanoferrate ion is favoured in vacuum, while monodentate coordination is stabilised by the presence of water molecules.<sup>39</sup> Even with free species such as the coordination compound  $[(\text{NH}_3)_5\text{Ru-CN-Fe}(\text{CN})_6]^-$  a large solvent dependency is found for the stretching vibrations of the bridging and *trans* cyano groups.<sup>40</sup>

Concentration effects are a consequence of equilibrium dye binding between adsorbed and solution species. Equilibrium binding on titania is illustrated by the free acid, half-salt and full-salt forms of *cis*-dithiocyanatobis(2,2'-bipyridine-4,4'-

dicarboxylate)ruthenium(II), the ‘N3’ dye.<sup>4</sup> Though dyes such as ruthenium polypyridine coordination compounds bind well when anchored through carboxylic acid groups, basic conditions cause desorption from titania.<sup>2</sup> Ethylenediaminetetraacetic acid (EDTA) has also been documented to compete in adsorption on titania with ruthenium dyes bound by carboxylic acid groups.<sup>41</sup> Equilibrium binding in solvents such as dimethylsulfoxide has been used to tune the surface coverage of hemin (Fig. 6.5) upon titania.<sup>42</sup> The concentration of the adsorbate may also influence the mode of binding, as is the case with glutamic acid (Fig. 6.6). As studied by ATR-FTIR, on increasing the concentration of the solution above the ATR crystal, the conformation of glutamic acid changed from binding *via* both acid groups, to binding by one terminal only. By FTIR, it was shown that there may be two forms of carboxylate species, one solvated and one bound to titania.<sup>43</sup>

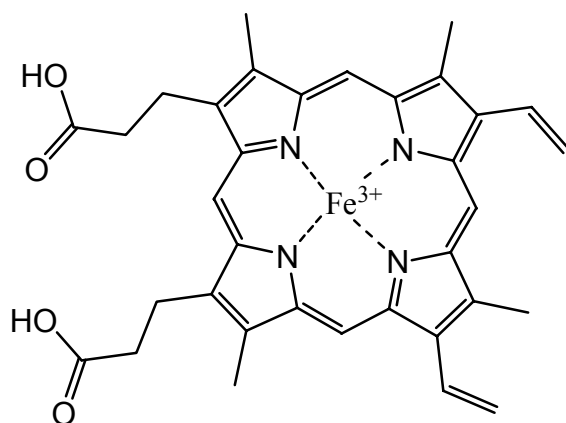


**Figure 6.5.** Hemin, the  $\text{Fe}^{3+}$  analogue of heme.

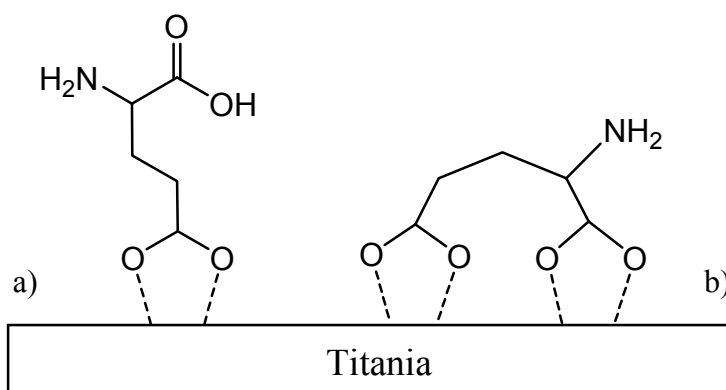
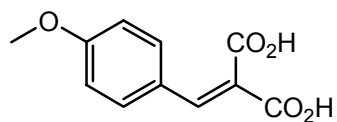


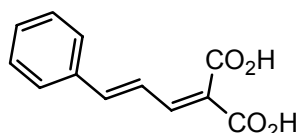
**Figure 6.6.** Glutamic acid as described by A. D. Roddick-Lanzilotta *et al.* 2000.<sup>43</sup> Glutamic acid bound to titania by a) a single acid group and b) both acid functionalities.

#### 6.4. Carboxylic Acid Probe Dyes

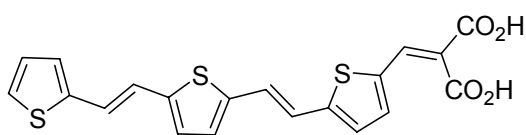
To investigate dye binding to titania, monocarboxylic and malonic acids were used, as the best Grätzel cell performance has been obtained from dyes that bear carboxylic acid groups.<sup>44</sup> 4-Methoxybenzylidenemalonic acid (**6.1**) and cinnamylidenemalonic acid (**6.2**) were the two simple malonic acids chosen as probe species, in addition to ter(thienylenevinylene)malonic acid (**6.3**), ter(thienylenevinylene)cianoacetic acid (**6.4**), 8,15-dicyanoter(thienylenevinylene)malonic acid (**6.5**) and ter(thienylenevinylene)rhodanine acetic acid (**6.6**). Spectral characteristics of the probe dyes are shown in Table 6.1; supplementary information is supplied in Section 8.2, Table 8.2. The UV-Vis absorbance of dyes in the solid state were collected from samples drop-dried on glass; as the peaks are low and broad, the mid-point of the absorbance range is quoted. While the spectral coverage of **6.1** and **6.2** are low, these dyes were selected as their simple structure means that <sup>1</sup>H-NMR spectra are easier to analyse than that of **6.3** to **6.6**. Ter(thienylenevinylene) derivatives were used as in terms of solubility and structure, they approach the complexity of porphyrinic dyes.



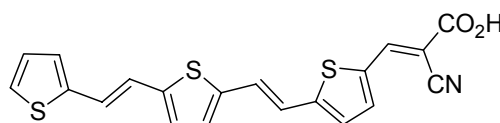
**6.1**



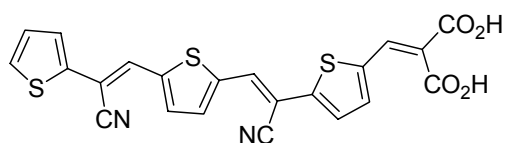
**6.2**



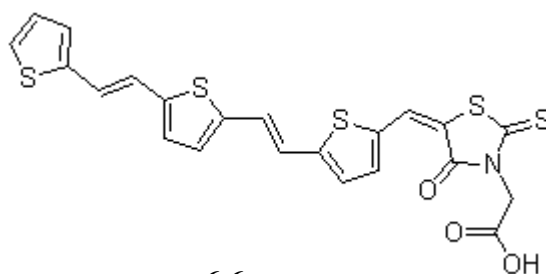
**6.3**



**6.4**



**6.5**



**6.6**

**Table 6.1.** Spectral properties of carboxylic acid probe dyes.

Dye	Colour of dye in the solid state	$\lambda_{\max}(\text{solid})$		Colour of dye in tetrahydrofuran (0.2 mM in THF)	$\lambda_{\max}(\text{THF})$	
		(nm)	( $\text{cm}^{-1}$ )		(nm)	( $\text{cm}^{-1}$ )
6.1	Cream-yellow	450	22,220	Colourless	310	32,260
6.2	Bright yellow	450	22,220	Colourless	328	30,490
6.3	Red-orange	500	20,000	Gold	458	21,840
6.4	Red-orange	500	20,000	Dark orange	465	21,510
6.5	Brick-red	500	20,000	Light orange	477	20,970
6.6	Purple-green	500	20,000	Red	507	19,720

### 6.5. Spectroscopic Analysis of Adsorbed Dyes & Dye Adsorption

To examine the nature of the interaction between adsorbed dyes and a titania surface, spectroscopic techniques were used to analyse probe dyes bound *via* carboxylic acid groups. Dye loading and aggregation was investigated with UV-Vis spectroscopy, while the mode of dye binding was determined by FTIR spectroscopy. Raman and fluorescence spectroscopy confirmed that dye interacts with titania from the quenching of excited-state dye. Samples were also examined by  $^1\text{H-NMR}$  spectroscopy to document changes in the electronic character of dyes after binding to titania.

The titania substrates used in this chapter were sintered crystalline titania and dispersed sol-gel titania, prepared as described in Sections 4.3 and 4.4. The sintered titania used for the bulk of this work was transparent Dyesol screen-printing material, which was crystalline, dehydrated and closely resembled the pre-formed titania plates used for Grätzel cell testing in our laboratories. The surface of crystalline titania is terminated by hydroxyl groups bound to  $\text{Ti}^{4+}$  sites, which act as Brønsted acids.<sup>45</sup> In addition, the sintered material was aggregated and could be used either as a powder or as a semi-transparent film supported by glass. The separation of dyed titania from free dye was then trivial, by decantation of dye solution and rinsing with solvent.

Dispersed sol-gel titania presents a distinctly different surface from that of sintered material and has a hydrated, acidic and amorphous character. As the environment of a dye molecule in solution will differ from that adsorbed on a substrate, dispersed sol-gel titania was used to investigate whether any intermediary states between non-aggregated solvated dyes and dyes aggregated upon a bulk surface exist. A concern regarding the use of acidic sol-gel titania was that the protonated surface would prevent dye binding. While basic dyes would form a salt within the acidic solution, acidic dyes could experience electrostatic repulsion on approach to the titania surface. However, an advantage of using acidic titania may be an improved efficiency of dye-sensitised solar cells (DSSCs). It has been suggested that protonated titanol sites may reduce the recombination of electrons that are injected into titania with the oxidized dye or electrolyte.<sup>46, 47</sup> In addition, the acidic environment may stabilise the binding of acidic dyes, which desorb from titania under alkaline conditions, such as polypyridyl ruthenium complexes anchored *via* a phosphonic acid moiety.<sup>48</sup> The nanoparticle size may also affect the mode of dye binding, as it has been reported that as the size of titania nanoparticles falls from 50 to 1 nm the material changes from crystalline to amorphous.<sup>28</sup> The corresponding drop in titanium coordination number from 6 to 4 resulted in less physisorbed material and in a greater proportion of chemically bound species. The use of sol-gel titania enabled examination of adsorbed dyes with solution-state spectroscopy. Contrast and comparison of dye binding modes upon dry, crystalline titania and amorphous, acidic titania surfaces were then drawn.

In order to gauge the efficacy of dye binding, an estimate of the surface coverage was required. To do this, molecular 'footprint' areas of the dyes and the surface area of the titania substrates were obtained. As  $\pi$ - $\pi$  stacking of the conjugated dyes is a strong possibility, a rectangular footprint was used to account for the possible aggregation of dyes. The footprint areas are derived from the width of the aromatic ring (5 Å), multiplied by the length of the molecule when anchored *via* carboxylic acid functionality. Dye footprint areas were calculated on the assumption that as the carboxylic acid binding groups are at a terminal position, dyes would be 'upright' on the surface. The anchoring geometry alters the dye footprint area, as reported for bis-((4,4'-dicarboxy-2,2'-bipyridine)(thiocyanato)) ruthenium(II), which has a 9% difference in footprint area between dye bound 'upright' by one carboxylic group ( $8.6 \times 10^{-19} \text{ m}^2$ ) and dye bound 'flat' by four carboxylic groups ( $1.3 \times 10^{-18} \text{ m}^2$ ) to titania.<sup>49</sup>

For all dyes except **6.2**, the rotational conformer where both potential binding groups are presented to the surface provides the larger footprint. Dye **6.4** has been shown with the cyano functionality pointing towards the surface, as a polyene-diphenylaniline dye with a cyanoacetic binding group has been shown to have the cyano nitrogen atom in close proximity to the titania surface.<sup>50</sup> For dyes **6.1**, **6.3** to **6.6**, when bound by a single acid group the footprint area decreased, increasing the number of molecules of dye required for a monolayer. Dimensions were estimated with ChemDraw<sup>®</sup> 8.0 and Chem3D<sup>®</sup> Ultra 9.01. Dye footprints are the same whether a ball-and-stick or van der Waals radius model was used; the former are shown for clarity (Figs 6.7, 6.8, Table 6.3).

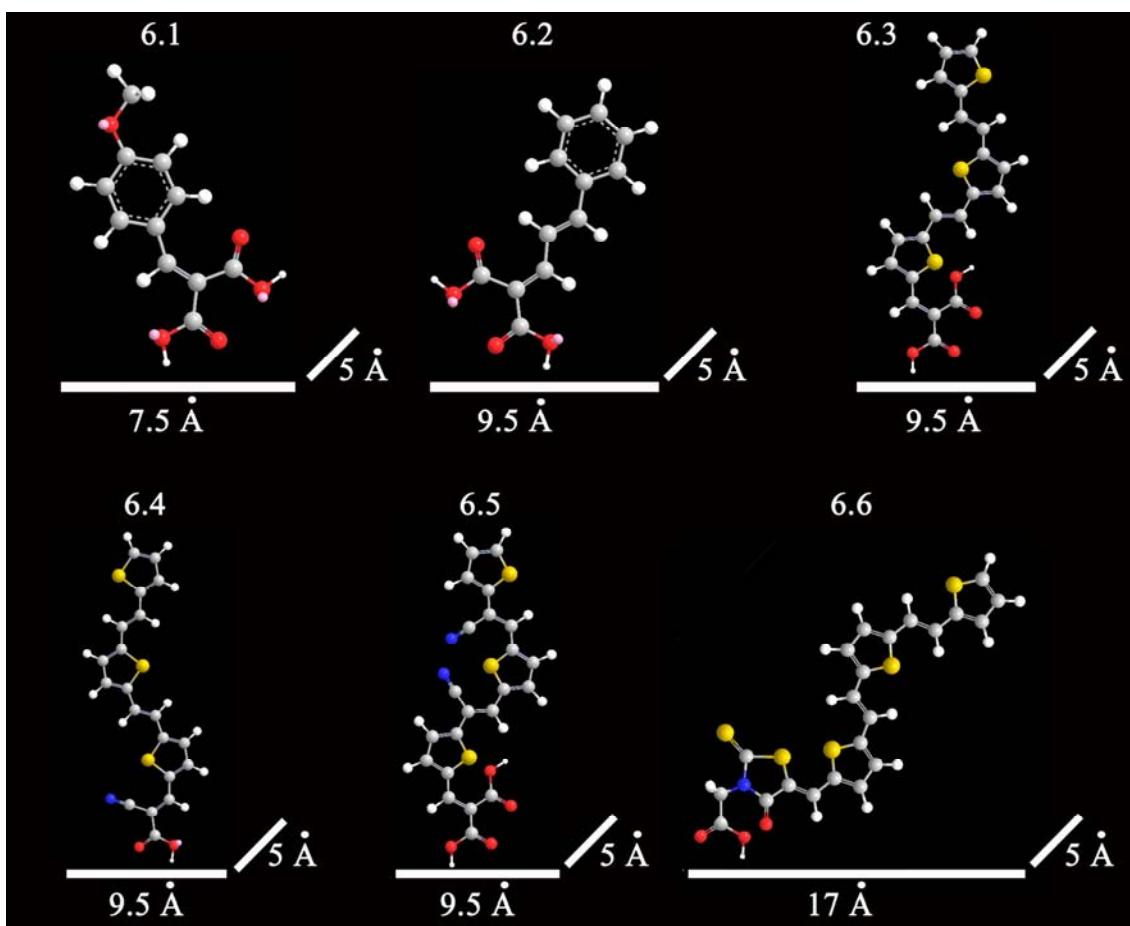


**Figure 6.7.** Chem3D<sup>®</sup> representations of **6.1** to **6.6** with estimates of the rectangular footprint area for dyes bound by only one carboxylic group.

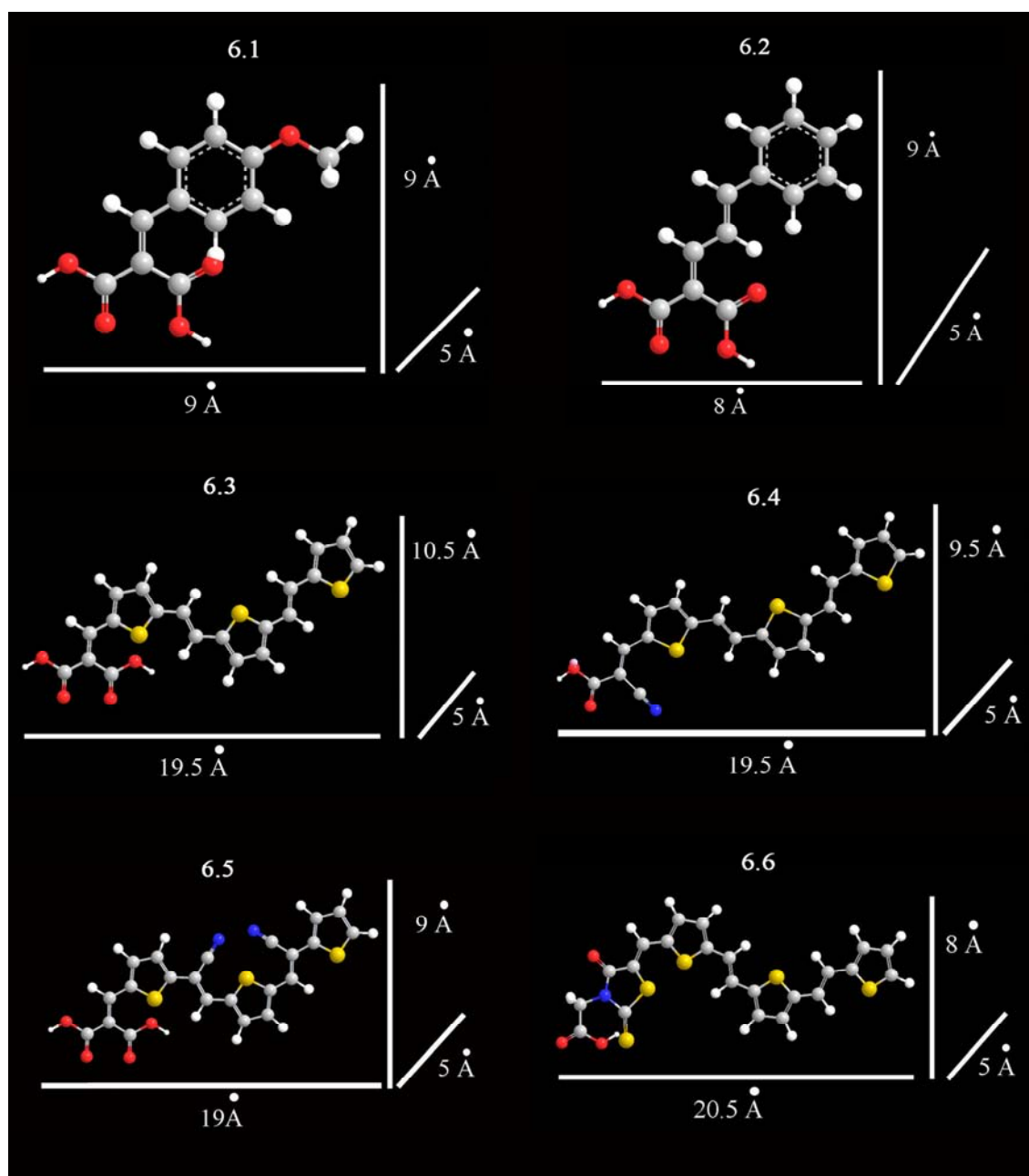


**Figure 6.8.** Chem3D<sup>®</sup> representations of **6.1** to **6.6** with estimates of the rectangular footprint area for bound dye with potential binding groups towards the surface.

The surface area of titania substrates were obtained experimentally for sintered titania from Brunauer-Emmett-Teller (BET) isotherm nitrogen sorption experiments ( $P/P_0$  of 0.3) and estimated from dynamic light scattering (DLS) particle sizing measurements for native sol-gel titania. It was not possible to measure the surface area of native sol-gel titania by BET nitrogen sorption, due to the acidic and hygroscopic surface.

Sintered transparent Dyesol titania was used for dye loading studies, as sol-gel titania produced erratic results due to large variations in the surface area between sintered powder and sintered film (Table 6.2).

**Table 6.2.** Surface area of titania from nitrogen sorption data, unless otherwise stated.

<b>Titania</b>	<b>Surface area (m<sup>2</sup>g<sup>-1</sup>)</b>
Titania colloids (300 nm in diameter) <sup>51</sup>	35
Sintered sol-gel titania film*	38
Sintered Degussa P25 titania powder <sup>52,53</sup>	55
Sintered opaque Dyesol titania film*	60
Sintered transparent Dyesol titania film*	83
Sintered titania film from 14 nm particles <sup>54</sup>	90
Sintered Showa Denko titania powder <sup>55</sup>	94
Sintered titania film (formed by MOCVD) <sup>56</sup>	130
Sintered sol-gel titania powder*	187
Porous titania colloids (1 μm diameter) <sup>51</sup>	300
Anatase nanoparticles (10 nm diameter) <sup>57</sup>	395
Native amorphous sol-gel titania (3.5 nm diameter) <sup>58</sup>	433
Native sol-gel titania (2 nm diameter)* <sup>s</sup>	698

\*This work. <sup>s</sup>Derived from DLS data.

The hydrodynamic diameter of native sol-gel titania was measured by DLS to give a number-average diameter of 2.6 nm with a standard deviation of 20%. As one standard deviation in the diameter of titania gives a range from 2.1 to 3.1 nm, a small diameter of 2 nm was used to estimate dye coverage, because the minimum conditions for monolayer coverage are of interest in this study. It was then reasonable to use a ‘worst-case scenario’ of a 2 nm particle diameter to give a lower boundary for the dye to titania ratio required for monolayer formation. If the real particle size is larger than 2 nm, then submonolayer coverage would be the result. While the 1.5 nm Ti<sub>18</sub>O<sub>22</sub> oxide core of anatase titanium-organo-oxo clusters are composed of distorted octahedra,<sup>59</sup> to simplify calculations the shape of the amorphous sol-gel titania was taken to be spherical.

Spheres 2 nm in diameter have a surface area of 12.57 nm<sup>2</sup> per particle; by using the bulk density of titania (4.3 g cm<sup>-3</sup>) for that of titania nanoparticles,<sup>60</sup> a molar mass of 10847 g mol<sup>-1</sup> was derived. The molar mass was used to calculate a value of 698 m<sup>2</sup> g<sup>-1</sup> for the surface area of totally dehydrated sol-gel titania.

Calculated values for dye coverage were obtained by dividing the surface area of titania by the dye footprint (Table 6.3). A bracket of dye loading values on titania were calculated from the minimum and maximum dye footprints (Section 8.2, Tables 8.3 - 8.8). While the surface area of sintered titania was obtained using the BET adsorption isotherm, which permits multiple layers of adsorbate, a Langmuir model was applied to simplify calculations. The Langmuir model assumes that adsorption is limited to a monolayer, that the surface is uniform and that the probability of adsorption on any given site is independent of the state of all other sites. While dye coverage is best described in terms of moles of dye per gram of substrate for sintered titania, experiments involving native dispersed sol-gel titania were described with mole ratios of dye to titania particles.

**Table 6.3.** Range of the rectangular footprint areas of probe dyes (Figs 6.7, 6.8) and monolayer coverage values for dye upon sintered transparent Dyesol titania and native sol-gel titania.

<b>Dye</b>	<b>Rectangular footprint of the dye (x 10<sup>-19</sup> m<sup>2</sup>)</b>	<b>Sintered Dyesol titania n(dye) / m(TiO<sub>2</sub>) (x 10<sup>-4</sup> mol g<sup>-1</sup>)</b>	<b>Native sol-gel titania Molecules of dye per 2 nm TiO<sub>2</sub> particle</b>
<b>6.1</b>	3.8 - 4.5	3.0 - 3.6	28 - 33
<b>6.2</b>	4.0 - 4.8	2.9 - 3.4	26 - 31
<b>6.3</b>	4.8 - 9.8	1.4 - 2.9	13 - 26
<b>6.4</b>	4.8 - 9.8	1.4 - 2.9	13 - 26
<b>6.5</b>	4.8 - 9.5	1.4 - 2.9	13 - 26
<b>6.6</b>	8.5 - 10	1.3 - 1.6	13 - 15

### 6.5.1. UV-Vis Spectroscopy

#### 6.5.1.1. Dye Loading on Titania

Dye loading studies were done to determine what proportion of the titania substrates was available for dye adsorption. The assumptions made include that the surface area of the transparent Dyesol titania plates is constant at  $82.6 \text{ m}^2 \text{ g}^{-1}$  and that the surface area measured by BET nitrogen sorption is accessible by the probe dyes. As the concentration of dye solutions used to prepare titania plates for Grätzel cell testing in our laboratories is  $0.2 \text{ mM}$ , another assumption was that similar or greater concentrations would be sufficient to ensure total coverage of the substrate from the equilibrium dye binding. Dye adsorption experiments involved the immersion of titania plates in dye solution, while the dye uptake was monitored by UV-Vis spectroscopy. As illustrated by Figure 6.9, in which titania plates were immersed in a  $0.2 \text{ mM}$  solution of **6.3** in tetrahydrofuran, the probe dyes show a rapid rate of dye adsorption with no significant increase in dye uptake after 80 minutes. While the plot appears to show a slight decrease after that time, the data is derived from subtraction spectra, with the absolute absorbance of **6.3** above 2.0 after the first 15 minutes of immersion. As the amount of transmitted light is less than 1% for an absorbance greater than 2, the apparent decrease in absorption may be due to noise in the collected spectra.

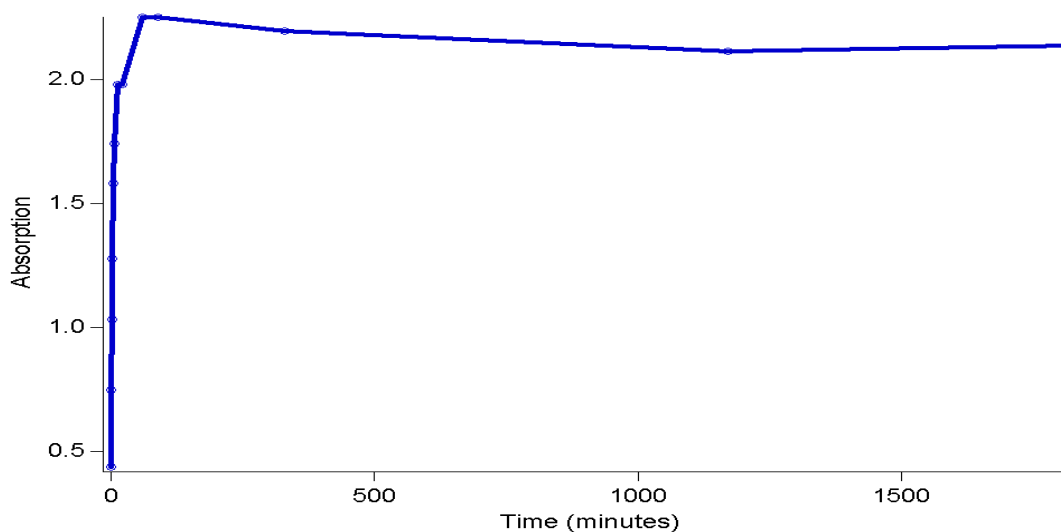


**Figure 6.9.** UV-Vis absorbance over time for the 410 nm peak of **6.3** adsorbed onto sintered Dyesol titania plates from a  $2 \text{ mM}$  solution in tetrahydrofuran (—). The x-axis error bars are for  $\pm 1$  minute, the y-axis error bars are for  $\pm 0.001$  absorbance units.

Dyes **6.1** and **6.2** were tested for adsorption onto sintered Dyesol screen-printed titania. Dye may be adsorbed in three different ways: chemical binding, physisorption to titania or physisorption to a dye monolayer. In the case of chemical binding by the formation of a pseudo-ester, bridging carboxylate or chelating carboxylate, dye is not expected to desorb easily. In contrast, as binding by physisorption may be an equilibrium process, desorption can be expected, more so for crystalline than for amorphous titania.<sup>28</sup> As illustrated in Figure 6.10, both the adsorption of **6.2** from a 2.3 mM methanolic solution and desorption into fresh methanol are relatively fast, with no further change after 80 and 60 minutes, respectively. Both plots have profiles that reveal an approach to an adsorption equilibrium and resemble that of a Langmuir adsorption isotherm.<sup>61</sup> The experimental bracket of dye coverage was 9 to 11% of the calculated value for monolayer formation. The low surface coverage of **6.1** and **6.2** may be a result of using a protic solvent, which may displace the carboxylic acids from titania, as shown by desorption studies of **6.1** and **6.2** in methanol. The dye desorbed from titania substrates that first were rinsed and blotted to remove excess dye, was 6 to 8%, a solution concentration of 1.0 to 1.3  $\mu\text{M}$ . The adsorption and desorption data for **6.1** and **6.2** could be consistent with either the release of loosely bound dye or an equilibrium situation. In the former was true, this would indicate that a mixture of physi- and chemisorbed material was present, with the loss of physisorbed material on immersion in fresh solvent. If only physisorbed material was present, dye would be released from titania until the equilibrium surface concentration was achieved. Either scenario would result in the profile of the plots shown in Figure 6.10.

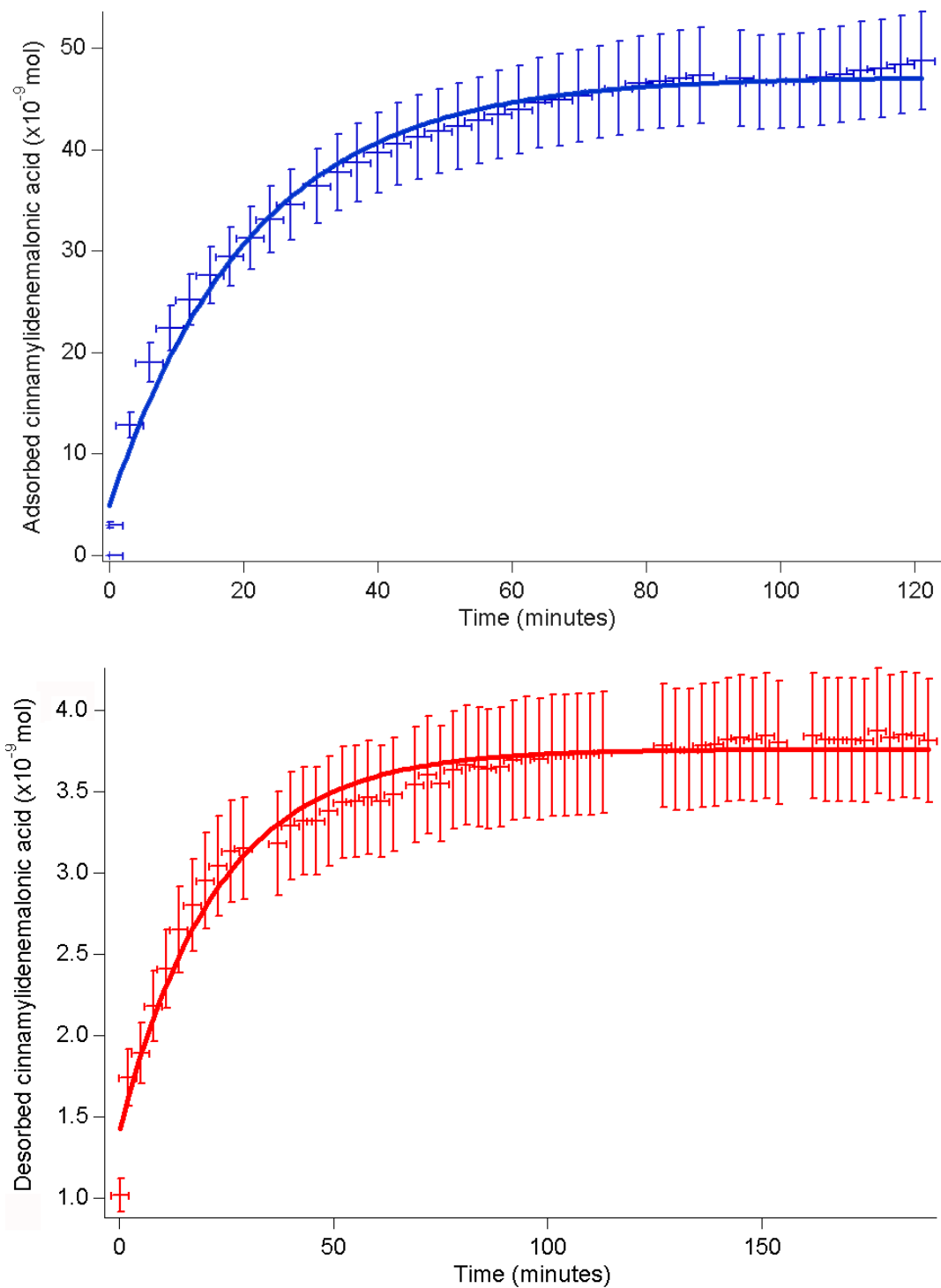


**Figure 6.10.** Adsorption of **6.2** onto sintered Dyesol titania powder from a 2.3 mM methanolic solution (—) and desorption in dry methanol (.....). Data was collected for the UV-Vis maximum at 330 nm, the error bars are for conservative values of a  $\pm 10\%$  uncertainty for the calculated number of moles of **6.2** and  $\pm 2$  minutes of time. Similar data was obtained for **6.1**.

The low surface coverage of **6.1** and **6.2** is not due to the titania surface, as adsorption studies of ter(thienylenevinylene) dyes show a higher dye loading. Coverage values for **6.3** and **6.4** were calculated from UV-Vis data of sintered Dyesol titania plates immersed in 0.15 mM solutions in tetrahydrofuran for a period of 20 hours. The uncertainty in these calculations is  $\pm 10\%$ , which accounts for error in the weighed mass of Dyesol titania, the concentration of dye, BET surface area measurements and the calibration plots used to correlate solution UV-Vis absorbance with dye concentration. The bracket of dye loading values obtained for **6.3**, **6.4** and **6.5** were 55 to 115%, 63 to 150% and 55 to 130%, respectively. The dye loading bracket is from  $1.4$  to  $2.9 \times 10^{-4}$  mol g<sup>-1</sup>, which is comparable to that for 4-(2'-(5',10',15',20'-tetraphenylporphyrinato zinc(II)yl)butadienylmalonic acid ( $3.3 \times 10^{-5}$  mol g<sup>-1</sup>) and 4-(2'-(5',10',15',20'-tetraxylylporphyrinato zinc(II)yl)butadienylmalonic acid ( $4.5 \times 10^{-5}$  mol g<sup>-1</sup>).<sup>62</sup> Similar surface coverage values of  $1.2 \times 10^{-5}$  mol g<sup>-1</sup> for 5,10,15,20-tetra(3-ethynyl(4-triethylammoniumcarboxyphenyl)phenyl)porphyrinato zinc(II) and  $2.7 \times 10^{-5}$  mol g<sup>-1</sup> for 5,10,15,20-tetra(4-triethylammoniumcarboxyphenyl)porphyrinato zinc(II) have been reported.<sup>63</sup>

### **6.5.1.2 Aggregation Studies**

#### **6.5.1.2.1. Introduction**

Dye may aggregate either as a monolayer or multiple layers upon a substrate. UV-Vis peak shape and position may be used to distinguish between monolayer and multilayer dye aggregation. While both H- and J-aggregates can form multilayers,<sup>34</sup> dye loading studies of **6.1** to **6.5** showed that the amount of adsorbed material is on the order of a monolayer or less (Section 6.5.1). Multilayer dye aggregates result in broadened signals, as reported for multilayer Langmuir-Blodgett films of a porphyrin dye; also observed was a progressive UV-Vis red shift due to increased ordering of the porphyrin from interlayer interactions.<sup>64</sup> However, broadened UV-Vis absorbance for perylene dyes on titania have also been reported for submonolayer coverage.<sup>65</sup>

#### 6.5.1.2.2. *Overview of UV-Vis Signal Shifts*

The aggregation of dyes was studied upon both sintered and non-sintered titania to enable the collection of UV-Vis spectra of dye adsorbed onto both dry and solvated substrates. Sintered screen-printed transparent Dyesol titania plates and acidic dispersed sol-gel titania were the substrates used for transmission UV-Vis spectroscopy. Dye aggregation studies were done using the ter(thienylenevinylene) dyes **6.3** to **6.6**. Use of the small malonic acids **6.1** and **6.2** were restricted to solution spectra with relatively low concentrations of sol-gel titania as the absorption maxima of the dyes are at higher energies than the titania absorption onset. The absorption cut-off for screen-printed Dyesol titania is approximately 400 nm, while dilute dispersions of sol-gel titania absorb light at wavelengths less than 330 nm. Increasing the concentration of sol-gel dispersions extends the apparent absorption onset of nanoparticulate titania towards longer wavelengths. The absorption onset of the titania used in this study are similar to reported values of 382 nm for bulk titania and 370 nm with a maxima at 322 nm for nanoparticulate titania.<sup>66, 67</sup>

A summary of UV-Vis absorption maxima for the probe dyes in a pure solution, in acidified solution, adsorbed on dispersed sol-gel titania and adsorbed on sintered Dyesol titania plates is shown in Table 6.5; supplementary data is shown in Section 8.3, Table 8.9. UV-Vis spectra of the pure dyes were collected in polar solvents, such as tetrahydrofuran and methanol. For comparison with spectra of dyes with the acidic sol-gel titania, spectra of dye acidified with hydrochloric acid were collected. UV-Vis spectra of dyes with amorphous acidic dispersed sol-gel titania were collected primarily in tetrahydrofuran. Sol-gel titania was titrated with solutions of dye and the mole ratios of dye to titania were calculated as outlined in Section 6.5. Spectra of dye adsorbed on sintered Dyesol titania were recorded following the immersion of screen-printed plates in 0.2 mM solutions of dye.

The probe dyes show a strong absorbance due to the  $\pi$ - $\pi^*$  electronic transition, which for **6.3** to **6.6** are at longer wavelengths than the absorbance of titania. It must be noted that the UV-absorption peaks are relatively broad, spanning approximately 150 nm. Following adsorption on sintered and sol-gel titania the UV-Vis signals are shifted, with some peak broadening for dyes **6.2** to **6.5** (Table 6.4). The full-width half-maximum

(FWHM) of adsorbed **6.1** was not able to be collected due to the absorbance of titania. While dyes **6.2** to **6.4** display increased FWHM values on titania, as **6.6** displays the largest increase when adsorbed on sintered titania this indicates that if multilayer aggregation is present, then it is most likely to have occurred for **6.6**. In contrast, for **6.5** the increase in FWHM in the presence of titania is similar to that of the dye in acidic solution, which together with shifts in UV-Vis absorption indicates monolayer dye aggregation.

**Table 6.4.** FWHM values for UV-Vis absorption signals of the probe dyes in tetrahydrofuran (THF) and on both dispersed sol-gel and sintered Dyesol titania.

Dye	Dye in THF (nm)	Dye with 35 $\mu$ M HCl in THF (% increase)	On sol-gel titania in THF (% increase)	On sintered Dyesol titania (% increase)
<b>6.2</b>	61	8	21	#
<b>6.3</b>	106	0	21	32
<b>6.4</b>	103	6	20	17
<b>6.5</b>	108	5	6	8
<b>6.6</b>	109	3	6	48

#Dye absorbance masked by that of titania. FWHM values have an uncertainty of  $\pm 5\%$ .

#### 6.5.1.2.3. Probe Dyes on Sol-Gel Titania

In the presence of sol-gel titania, a red UV-Vis shift is observed, which is greatest for ter(thiophenylenevinylene) dyes and may indicate the formation of J-aggregates. While deprotonation of a polyene-diphenylaniline dye in methanol was reported to give a 30 nm red shift in the UV-Vis,<sup>68</sup> acidification of dyes **6.1** to **6.6** with hydrochloric acid produced both red and blue shifts result, relative to pure dye (Table 6.5). However, dyes that were red-shifted with acid were shifted further with sol-gel titania. Similar UV-Vis red shifts of 10 to 20 nm have been published for *cis*-bis(isothiocyanato)bis(2,2'-bipyridyl-4,4'-dicarboxylato)ruthenium(II) adsorbed on acidic dispersed sol-gel titania particles 1 to 2 nm in diameter.<sup>27</sup> The adsorption of all-

*trans*-retinoic acid (ATRA) upon acidic dispersed sol-gel titania 12 to 13 nm in diameter also results in UV-Vis shifts to the red, similar to that seen for **6.1** to **6.6**.<sup>69</sup> In the presence of sol-gel titania, two signals were observed for ATRA, red-shifted by 39 and 72 nm. The former was attributed to protonated ATRA, the latter to partly deprotonated ATRA, both of which were adsorbed to titania. In the same manner that a red shift of UV-Vis absorption is observed after the carboxylation of oligothiophenes,<sup>70</sup> a red shift may also indicate that bound dyes have extended delocalisation of the conjugated system of the dye to surface sites of titania.<sup>37</sup> The extension of the electronic system could occur *via* hybridisation of the  $\pi^*$  orbital of adsorbed dye and titanium 3d orbitals of the nanoparticle.<sup>27</sup>

#### **6.5.1.2.4. Probe Dyes on Dyesol Titania**

In contrast to sol-gel titania, dyes adsorbed from solution onto dry sintered screen-printed Dyesol titania show a blue shift in dye absorption, with the exception of **6.6**. While a blue shift may be due to H-aggregation, a blue shift of 32 nm has been reported for a polyene-diphenylaniline dye bound to titania *via* a cyanoacetic functionality and was attributed to either interaction with the surface or deprotonation of the dye.<sup>68</sup> Dye **6.1** was used as a representative of the probe dyes for the effect of deprotonation on UV-Vis shifts (Fig. 6.11). The tetra-*n*-butylammonium salts of **6.1** with a 1 : 1 and 2 : 1 molar ratio of tetra-*n*-butylammonium hydroxide to **6.1** show no UV-Vis shift from that of the pure dye for the former and a 12 nm shift for the latter. Similarly, ATRA deprotonated by triethylamine shows a 9 nm blue shift in the UV-Vis.<sup>71</sup> This could indicate that on sintered titania, dyes are adsorbed as a carboxylate. The different UV-Vis shifts displayed by dyes upon sintered titania, compared to sol-gel titania, may owe more to the difference between the titania surfaces than to dye aggregation.

**Table 6.5.** UV-Vis absorption of pure dyes in THF and on both dispersed sol-gel and sintered Dyesol titania.

Dye	Dye in THF		Dye with 35 $\mu$ M HCl in THF		On sol-gel titania in THF		On sintered Dyesol titania	
	(nm)	( $\text{cm}^{-1}$ )	(nm)	( $\text{cm}^{-1}$ )	(nm)	( $\text{cm}^{-1}$ )	(nm)	( $\text{cm}^{-1}$ )
<b>6.1</b>	310	32,260	308	32,470	316*	31,650*	#	#
<b>6.2</b>	328	30,490	327	30,580	340*	29,410*	#	#
<b>6.3</b>	458	21,840	447	22,370	475	21,050	425	23,530
<b>6.4</b>	465	21,510	485	20,620	500	20,000	432	23,150
<b>6.5</b>	477	20,970	450	22,220	480	20,830	463	21,600
<b>6.6</b>	507	19,720	514	19,460	522	19,160	510	19,610

\*Spectra subtracted for sol-gel titania. #Dye absorbance masked by that of titania.

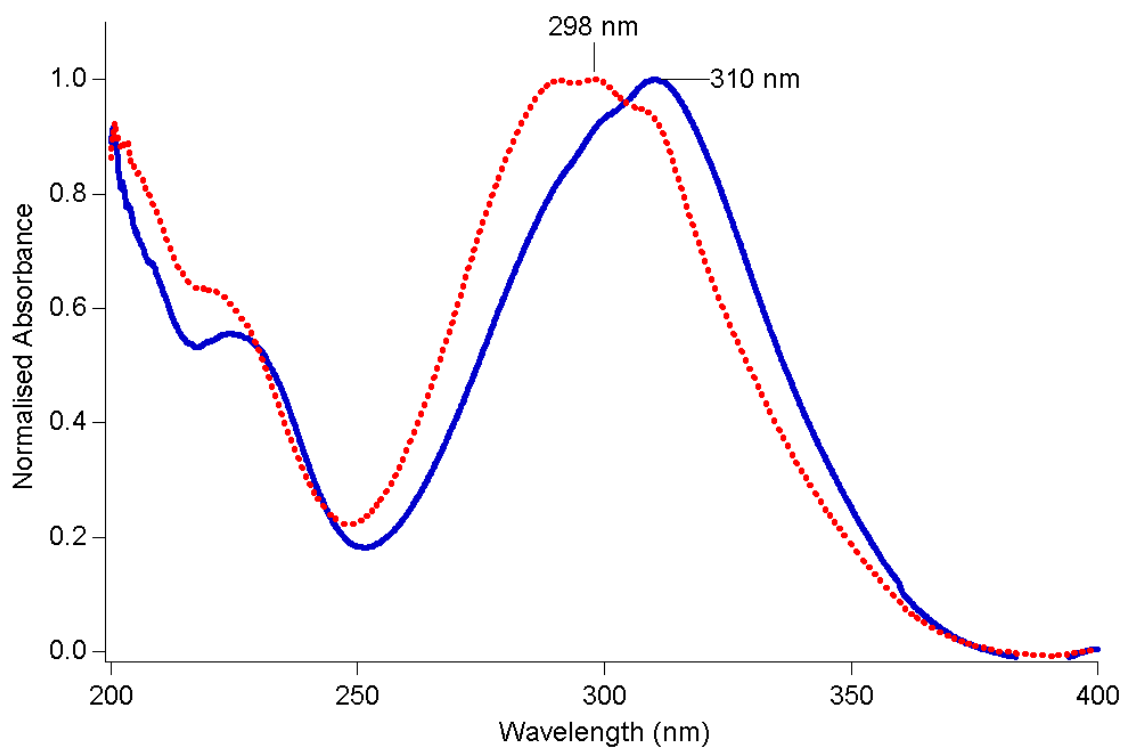


**Figure 6.11.** UV-Vis spectra of a 1 : 1 (—) and a 2 : 1 (⋯) molar ratio of tetra-*n*-butylammonium hydroxide to **6.1** in methanol.

#### 6.5.1.2.5. Solvent Effects

Solvent effects complicate the spectral analysis. The UV-Vis spectra of **6.1** and **6.2** do not display solvent dependency, but ter(thienylenevinylene) dyes display a negative solvatochromatic effect (Table 6.6).

**Table 6.6.** UV-Vis absorption of pure dyes and dyed titania in solvent A.

Dye	Dye in A		Dye with 35 $\mu$ M HCl in A		On sol-gel titania in A	
	(nm)	( $\text{cm}^{-1}$ )	(nm)	( $\text{cm}^{-1}$ )	(nm)	( $\text{cm}^{-1}$ )
<b>6.3</b>	457	21,880	450	22,220	464	21,550
<b>6.4</b>	454	22,030	482	20,750	496	20,160
<b>6.5</b>	446	22,420	450	22,220	498	20,080

A is a 1 : 5 v/v solution of tetrahydrofuran to 95% ethanol.

The negative solvatochromatic effect experienced by ter(thienylenevinylene) dyes also affects the validity of comparison between spectra of dry and solvated samples. For instance, the spectrum of dry sintered titania dyed with **6.5** is red shifted in relation to solution spectra of **6.5** in a 1 : 5 v/v solution of tetrahydrofuran to 95% ethanol, rather than blue shifted (Fig. 6.12). A similar effect is seen when dry sintered titania dyed with **6.5** is reimmersed in a solution of dye in tetrahydrofuran (Fig. 6.13). The same amount of dye was present between wet and dry scans, as confirmed on integration of the UV-Vis absorbance (Section 8.2, Fig. 8.1). For the sake of argument, if the UV-Vis shifts are due to dye aggregation, this may indicate that solvent molecules stabilise the formation of H-aggregates on titania that reform as J-aggregates on solvent loss. The interconversion of H- and J-aggregates of a rhodanine dye adsorbed on sintered titania has been reported to occur on alteration of the solvent vapour composition above the sample.<sup>31</sup> However, it is more likely to be a dielectric effect as air is displaced by solvent within the titania plate. The apparent drop in absorption intensity is due to an increase in the dispersion of transition energies, due to dye aggregation following solvent loss, as reported for phthalocyanine dyes.<sup>72</sup>

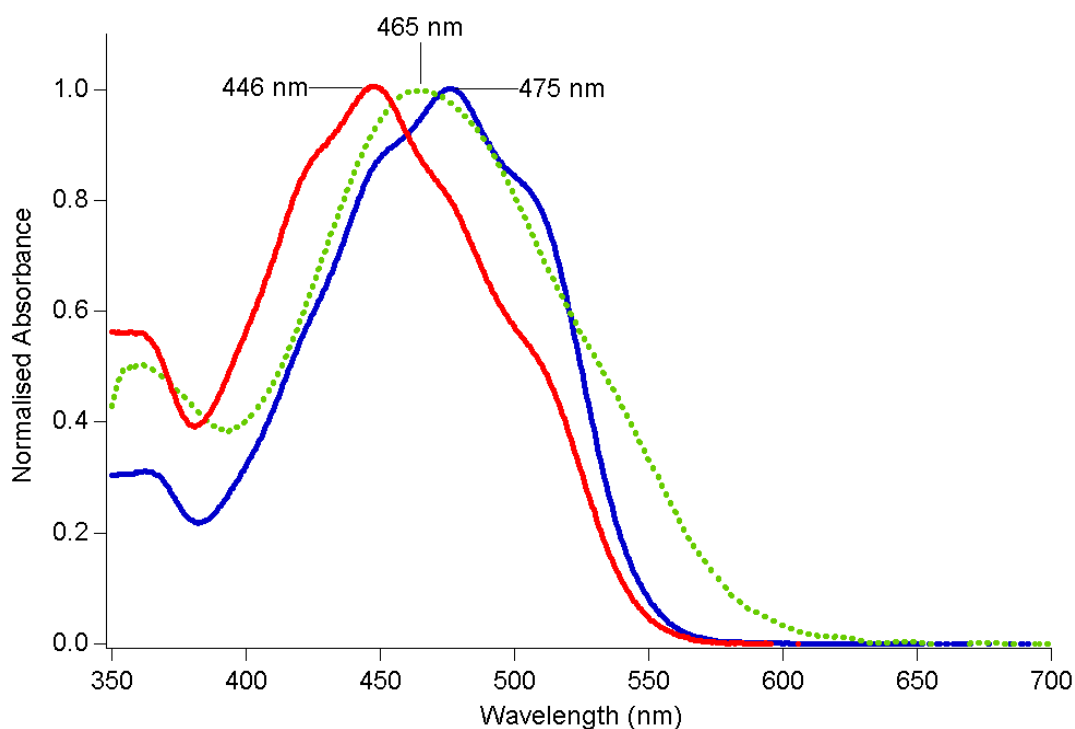


**Figure 6.12.** UV-Vis spectra of **6.5** in tetrahydrofuran (—) in a 1 : 5 v/v solution of tetrahydrofuran to 95% ethanol (—) and adsorbed onto sintered titania plates (•••••).

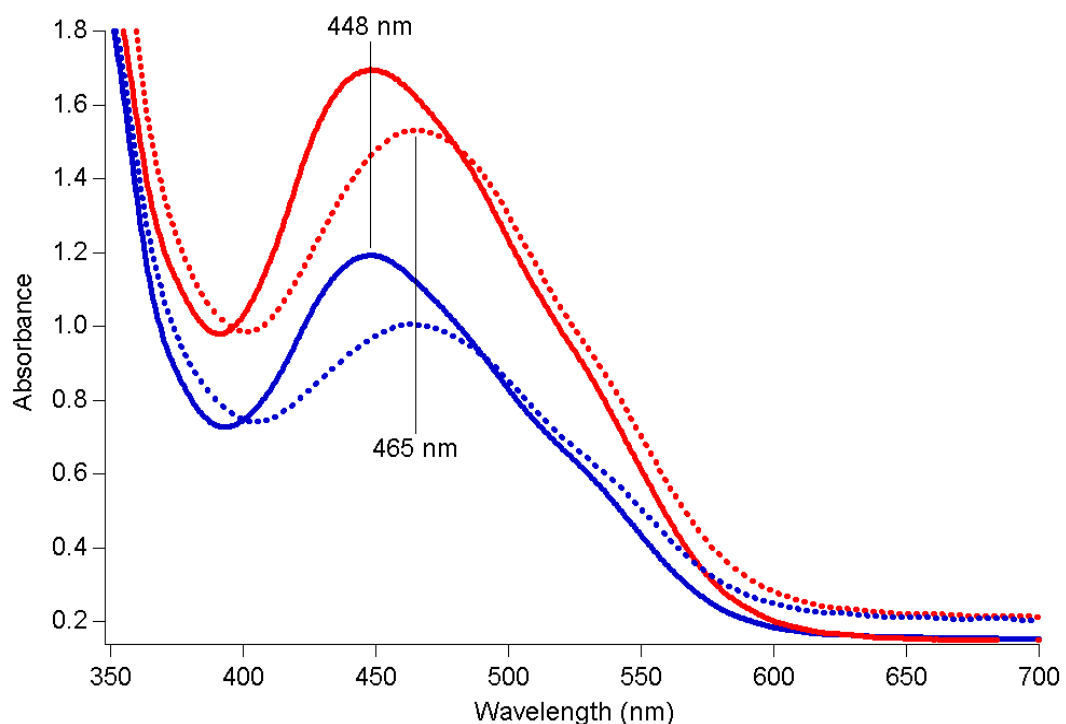


**Figure 6.13.** A red shift of UV-Vis absorbance is observed when a titania plate dyed with **6.5** is wet with tetrahydrofuran (—) is dried (•••••). The effect is reproducible as shown by further immersion of the plate in a solution of **6.5** (—) and subsequent drying (•••••). The spectra are not subtracted for the titania blank in order to show that the wet plate is more transparent than the dry plate.

Despite the solvatochromism of ter(thienylenevinylene) dyes, there is no solvatochromic effect of dyes adsorbed on sol-gel titania. For instance, the peak maximum for pure dye **6.4** is different in methanol, tetrahydrofuran and a 1 : 5 v/v solution of tetrahydrofuran to 95% ethanol, yet is always near 500 nm in the presence of sol-gel titania (Fig. 6.14). This indicates that when bound, dye molecules experience an environment that is independent of the solvent used to disperse the sol-gel titania.

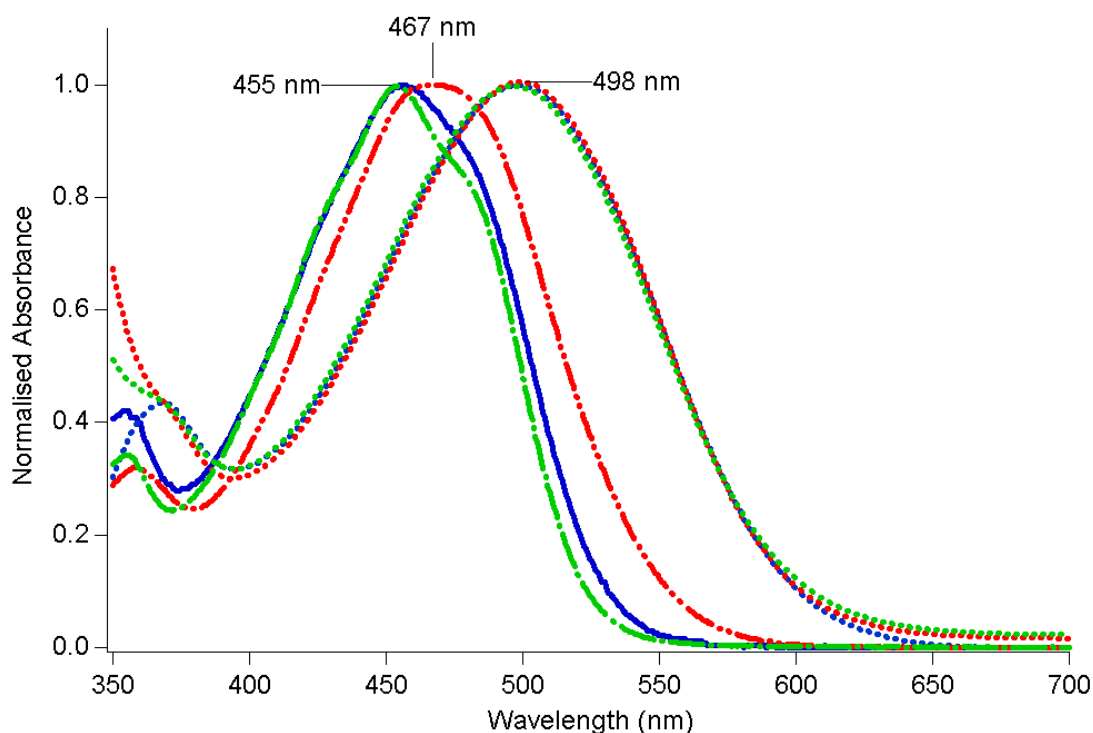


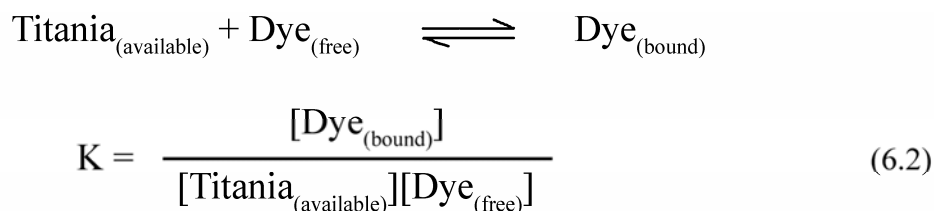
**Figure 6.14.** UV-Vis spectra of **6.4** in methanol (—), tetrahydrofuran (---), in a 1 : 5 v/v solution of tetrahydrofuran to 95% ethanol (solvent A) (—) and with sol-gel titania in methanol (.....), tetrahydrofuran (.....) and solvent A (.....).

#### 6.5.1.2.6. Support for Equilibrium Dye Binding

Two scenarios exist for the adsorption of dye on titania: irreversible and equilibrium binding. In the case of irreversible binding, two signals corresponding to free and bound dye should be observed, which may occur either as distinct peaks or as a shoulder upon the other signal. For an excess of titania, the UV-Vis absorption by free

dye would decrease to complement the growth of a new absorption due to the bound species.

If dye binding is an equilibrium process, near equilibrium conditions both free and bound dye should be present. An averaged signal would then be observed due to the rapid exchange of free and bound dye. If only the relationship between free and bound dye is considered (Eq. 6.1), then the ratio between the two is expected to be constant and the position of the averaged signal would not change. However, if the concentration of the available titania binding sites is taken into account (Eq. 6.2), then as sol-gel titania is added to dye the ratio of free to bound dye will drop. In this case, a shift in the position of the averaged signal may be anticipated.



Titration of **6.4** with dispersed sol-gel titania gave an averaged signal and a gradual red shift in dye absorbance as the system was changed from an excess of dye to an excess of titania (Fig. 6.15). A slight peak broadening was observed, which could be caused by either dye aggregation on titania or a slow exchange of free and bound dye. Despite the signal broadening, a single peak was observed without distinct peaks or shoulder signals, which supports the equilibrium binding of dye on sol-gel titania. The shift in position of the averaged signal also gives evidence for the participation of the available titania binding sites in the equilibrium binding of dye.

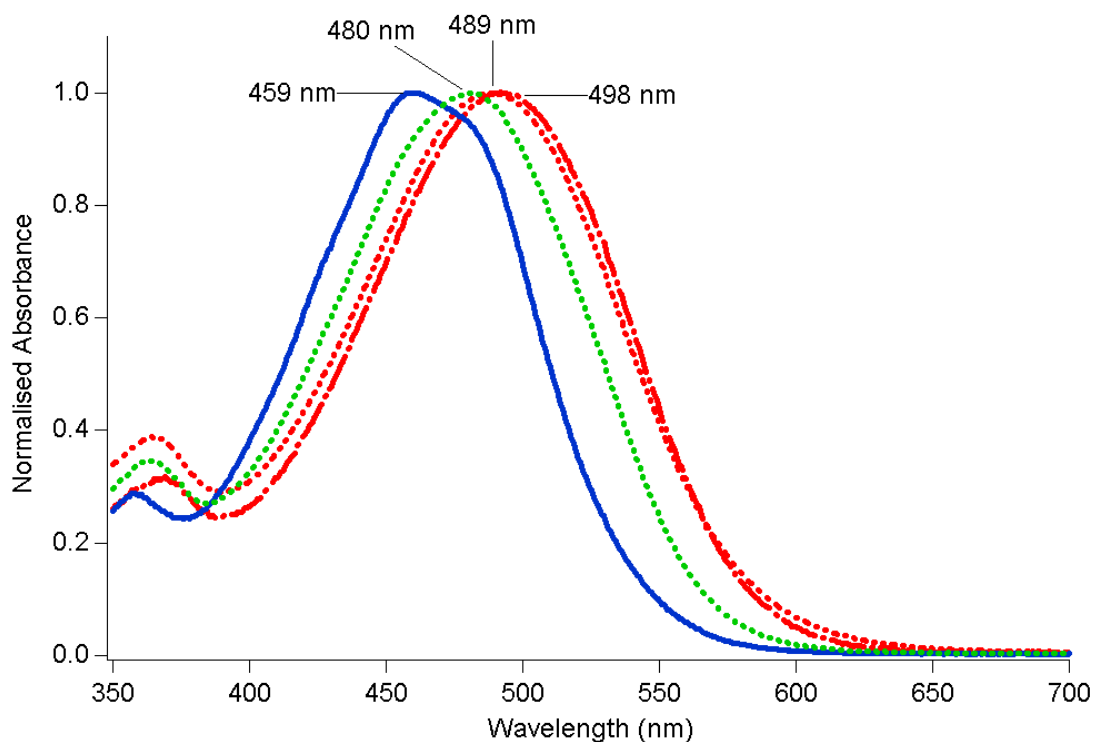


**Figure 6.15.** UV-Vis spectra of **6.4**, showing an absence of signal shoulders on titration with sol-gel titania in ethanol. Pure dye (—), a 339 : 1 (·····), a 21 : 1 (·····), and a 1 : 1 (---) mole ratio of dye to titania. The FWHM values are 99 nm, 109 nm, 114 nm and 113 nm, respectively, with an uncertainty of 3%.

#### 6.5.1.2.7. *Impact of Structure on Dye Aggregation*

The impact of dye structure on the ability of dyes **6.1** to **6.6** to aggregate upon titania is illustrated by the difference in the magnitude of dye absorption shifts between **6.1** and **6.2** (Figs. 6.16, 6.17). Due to the absorbance of titania, the spectra of **6.1** and **6.2** on sintered titania plates were unable to be collected. While both dyes are malonic acids, the methoxy group on the benzene ring of **6.1** is free to rotate and provide steric hindrance to the close alignment of adjacent dye molecules. Compared to **6.2**, which has a planar and fully conjugated structure, **6.1** may be expected to form less closely packed dye aggregates than **6.2** and the ter(thienylenevinylene) dyes **6.3** to **6.6**. As **6.1** is less closely packed, the perturbation of the dye electronic transition moment is less, resulting in a smaller red shift in the UV-Vis spectrum.

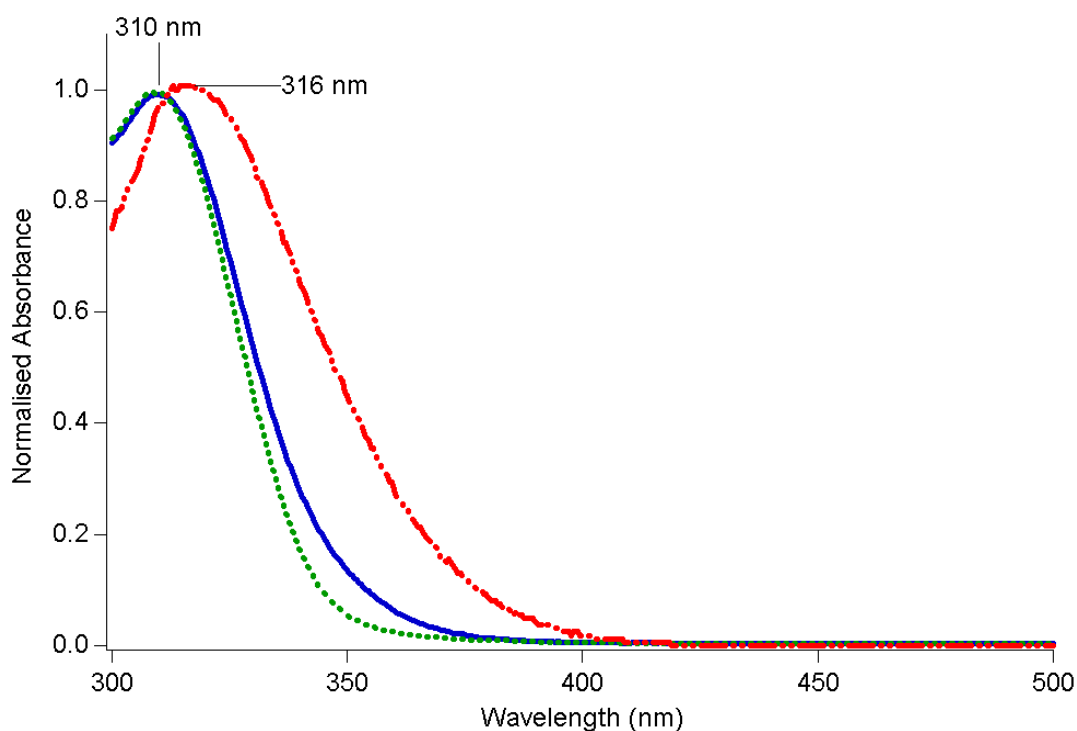


**Figure 6.16.** UV-Vis spectra of **6.1** in tetrahydrofuran (—), in acidic solution (.....), in solution with acidic sol-gel titania (---). The mole ratio of sol-gel titania spheres 2 nm in diameter to dye was 1 : 5.

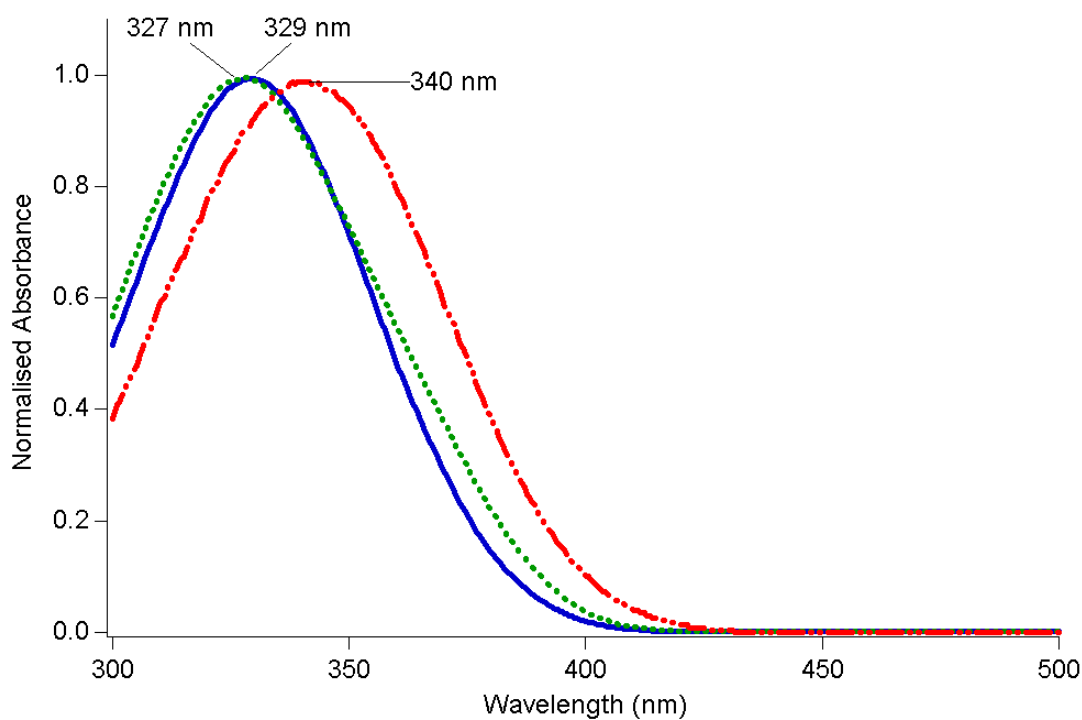


**Figure 6.17.** UV-Vis spectra of **6.2** in tetrahydrofuran (—), in acidic solution (.....), in solution with acidic sol-gel titania (---). The mole ratio of sol-gel titania spheres 2 nm in diameter to dye was 1 : 4.

There is a significant difference between the UV-Vis spectra of dyes adsorbed on dispersed sol-gel titania, when compared to dyes on sintered screen-printed titania. For instance, while both **6.3** and **6.4** with sol-gel titania show a red UV-Vis shift, on sintered screen-printed titania a blue-shift from that of the dye solution spectrum is seen (Table 6.5). Relative to the UV-Vis absorbance of pure dye in tetrahydrofuran, on sol-gel titania the absorbance of **6.3** and **6.4** are red shifted by 17 and 35 nm, respectively. On sintered Dyesol titania, both **6.3** and **6.4** both show a blue shift in absorbance of 33 nm. This confirms that the sintered and sol-gel titania surfaces are quite different environments for adsorbed dye.

The ability of **6.4** to pack closer together than for **6.3** may explain the larger blue and red UV-Vis shifts on binding to sintered and sol-gel titania, respectively (Figs. 6.18, 6.19). For comparison of **6.3** and **6.4** with dyes of a similar structure and the same binding groups, terthienylvinylmalonic acid and terthienylcyanoacrylic acid were also examined. Consistent with what was observed for **6.3** and **6.4**, a larger red-shift was observed for the cyanoacrylic species than for the malonic acid dye on sol-gel titania (Figs. 6.20 6.21). This indicates that the cyano functionality on **6.4** and terthienylcyanoacrylic acid has an impact upon the magnitude of the red UV-Vis shift either *via* interaction of the cyanoacetic group with titania or from dye aggregation effects. As the blue UV-Vis shift on sintered titania for both terthienylvinylmalonic acid and terthienylcyanoacrylic acid was less than that observed for **6.3** and **6.4**, this indicates that the size of the dye also has an effect on aggregation, as a result of packing size.

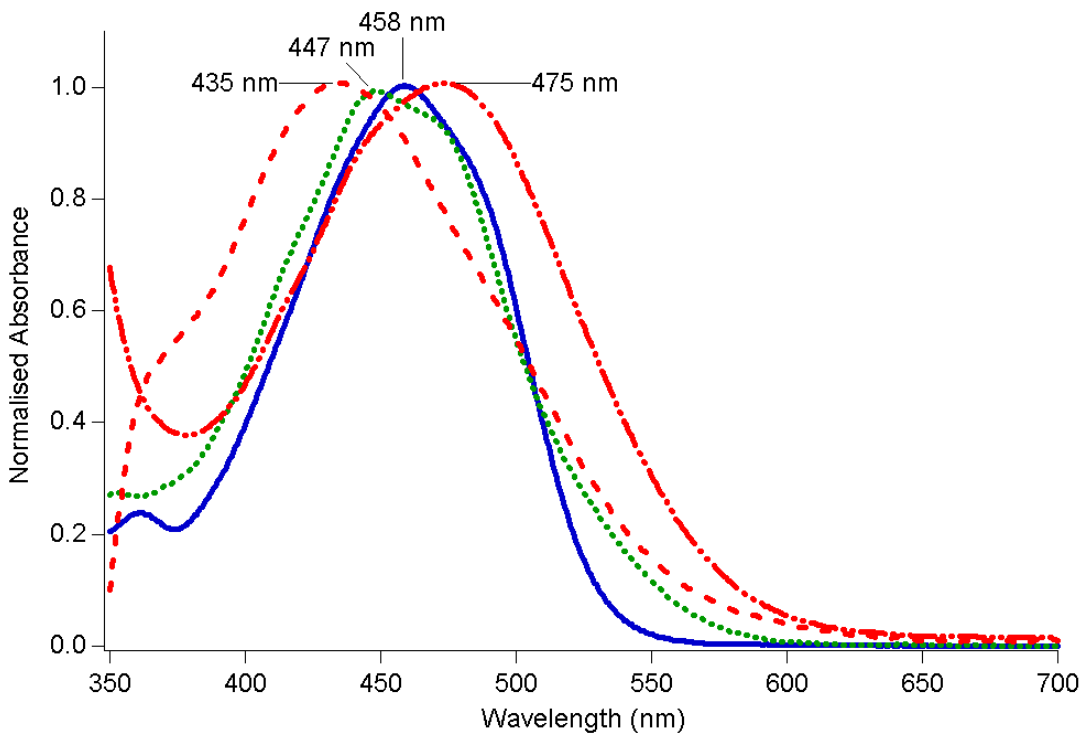


**Figure 6.18.** UV-Vis spectra of **6.3** in tetrahydrofuran (—), in acidic solution (.....), in solution with acidic sol-gel titania (---) and adsorbed onto sintered titania plates (-.-). The mole ratio of sol-gel titania spheres 2 nm in diameter to dye was 4 : 1.

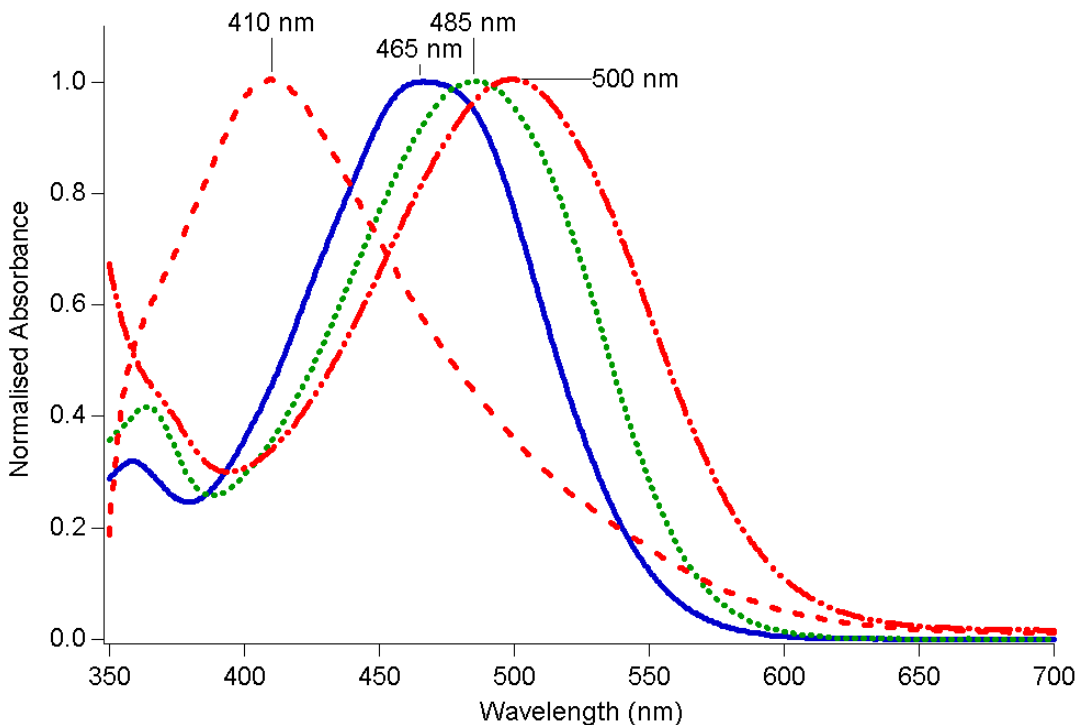


**Figure 6.19.** UV-Vis spectra of **6.4** in tetrahydrofuran (—), in acidic solution (.....), in solution with acidic sol-gel titania (---) and adsorbed on sintered titania plates (-.-). The mole ratio of sol-gel titania spheres 2 nm in diameter to dye was 4 : 1.

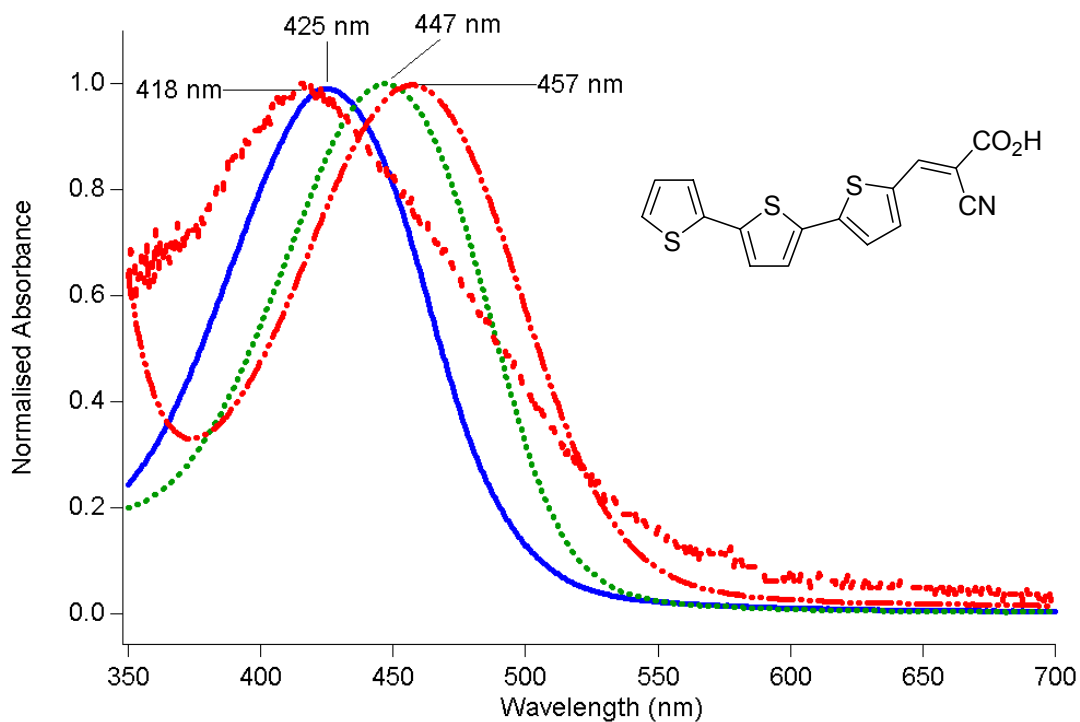


**Figure 6.20.** UV-Vis spectra of terthienylecyanoacrylic acid in tetrahydrofuran (—), in acidic solution (·····), in solution with acidic sol-gel titania (---) and adsorbed on sintered titania plates (-.-). n(sol-gel titania spheres 2 nm in diameter) : n(dye) of 3 : 1.

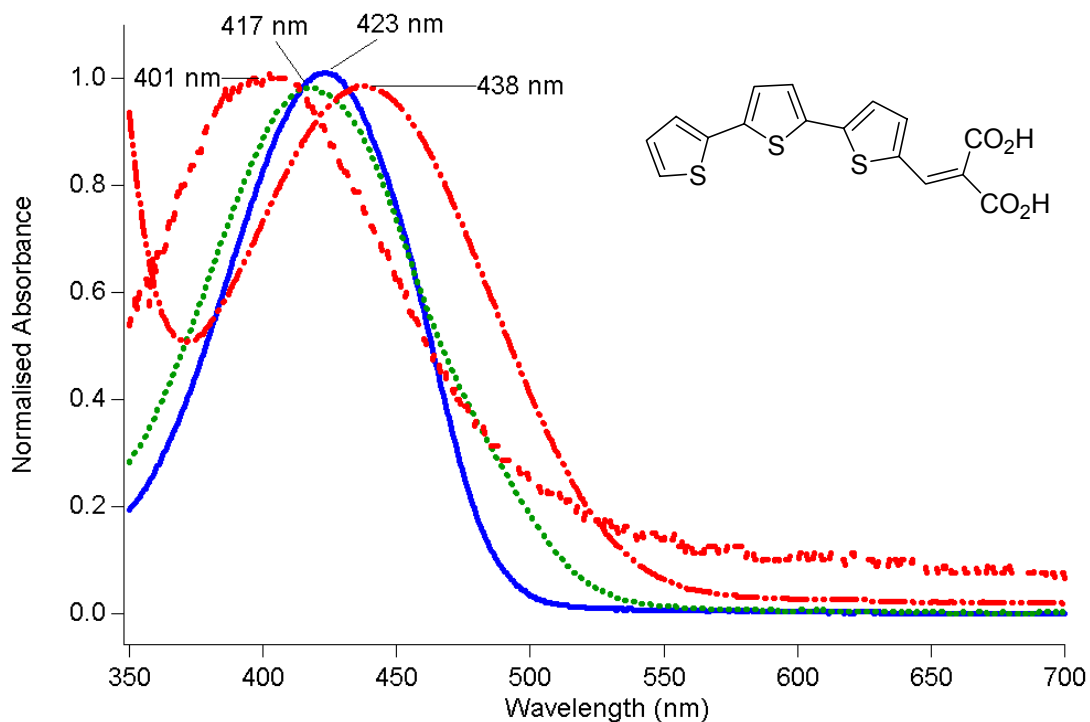


**Figure 6.21.** UV-Vis spectra of terthienylvinylmalonic acid in tetrahydrofuran (—), in acidic solution (·····), in solution with acidic sol-gel titania (---) and adsorbed on sintered titania plates (-.-). n(sol-gel titania 2 nm in diameter) : n(dye) of 3 : 1.

A possible difference in dye packing between **6.3** and **6.4** may be due to binding *via* a single group, as opposed to *via* two groups. As FTIR studies show that the cyano functionality of **6.4** is not directly involved in binding to titania and that malonic acids, such as **6.3** bind to titania *via* both carboxylic acid groups (Section 6.5.3), the two dyes could have different molecular footprint areas. If **6.4** is bound by only one group, whether it is the carboxylic acid or the cyano functionality,<sup>73</sup> closer packing and greater interaction of adjacent molecules also is possible than for species such as **6.3**. While the footprint area for **6.3** bound by only one carboxylic acid group is the same as for **6.4** bound by only the carboxylic acid, when **6.3** is bound by both binding groups staggered with respect to each other the dye is less closely packed (Figs. 6.22, 6.23).

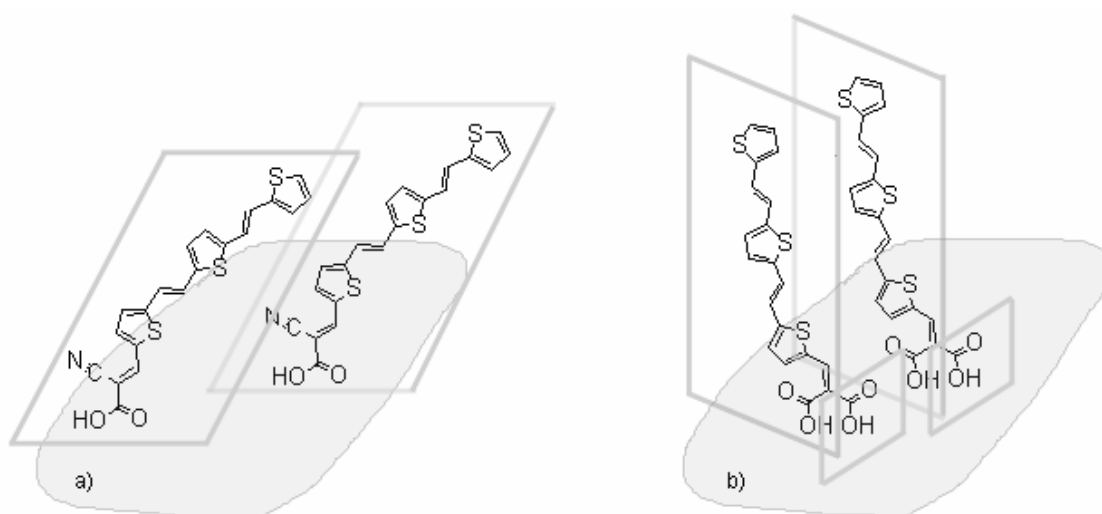


**Figure 6.22.** A cartoon of possible aggregation and packing of a) **6.4** and b) **6.3** upon titania.

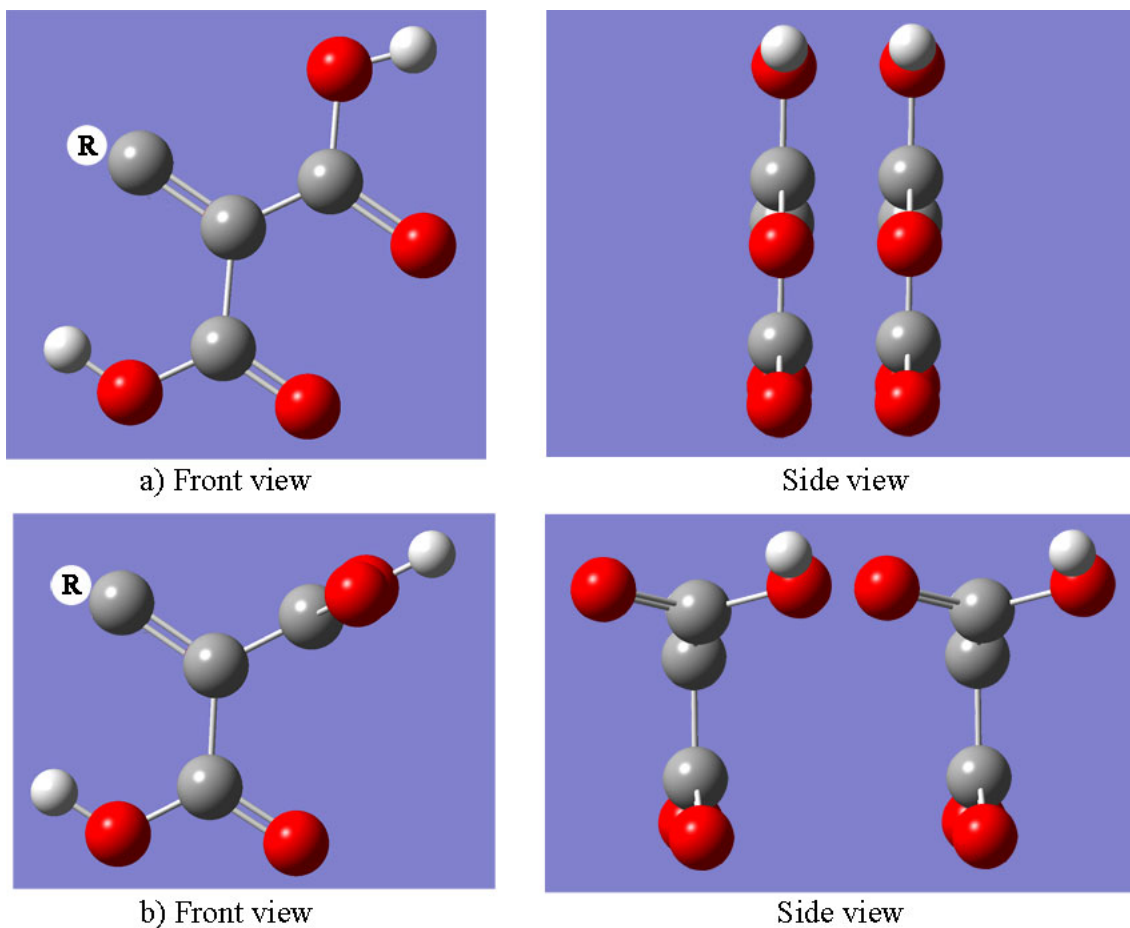


**Figure 6.23.** A depiction of the packing of a malonic acid with the binding groups a) parallel and b) staggered with respect to each other. The carbon atom labelled ‘R’ denotes the rest of the molecule.

While dyes **6.1** to **6.5** exhibit a blue shift in the UV-Vis when adsorbed on sintered titania, dye **6.6** shows a small red shift (Fig. 6.24). A slight red shift and signal broadening has been reported for dyes bound *via* a rhodanine group to titania,<sup>74</sup> which was attributed to a combination of non-aggregated dye and J-aggregates on the surface.<sup>75</sup> A possible explanation for the red shift is either that the interaction with the surface or aggregation effects of the rhodanine group of **6.6** are similar for both sintered and sol-gel titania. To use the argument of aggregation, comparison of the structures of **6.5** and **6.6** allows the difference in behaviour of the dyes on sintered titania to be rationalised. On adsorption to titania, the UV-Vis shifts of **6.5** are greater than that of **6.6**, but less than that of **6.3** (Fig. 6.25). The cyano functionality on the backbone of **6.5**

increases the electron-donating character of the dye and possibly prevents **6.5** from packing closer to adjacent molecules than **6.3**, as smaller UV-Vis shifts are observed on adsorption to titania. That **6.5** produces larger UV-Vis shifts than **6.6** could be due to the rhodanine group of **6.6**, as both **6.3** and **6.5** bind to titania *via* a malonic acid moiety. The larger binding group of **6.6** may mean that the ter(thienylenevinylene) backbone is unable to pack closely and that enough tilt is introduced between adjacent molecules so that ‘side to side’ H-type aggregation and a UV-Vis blue shift is not observed. The possibility that **6.6** may pack with a smaller ‘slip angle’ between molecules than **6.3** to **6.5** is shown with one extreme of dye conformation where the ter(thienylenevinylene) group lies parallel to the surface on binding (Figure 6.26). The spectral red shift of **6.6** on sintered Dyesol titania can be attributed to J-aggregation.

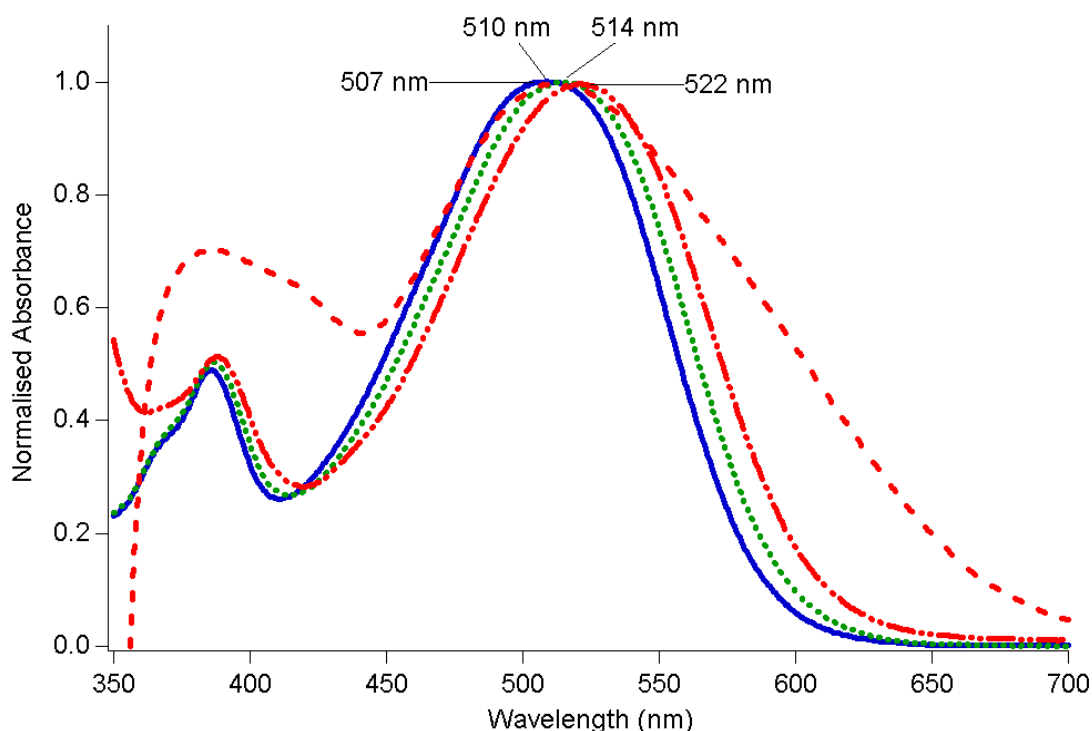


**Figure 6.24.** UV-Vis spectra of **6.6** in tetrahydrofuran (—) (507 nm), in acidic solution (.....) (514 nm), in solution with acidic sol-gel titania (---) (522 nm) and adsorbed onto sintered titania plates (-.-) (510 nm). The mole ratio of sol-gel titania spheres 2 nm in diameter to dye was 4 : 1.

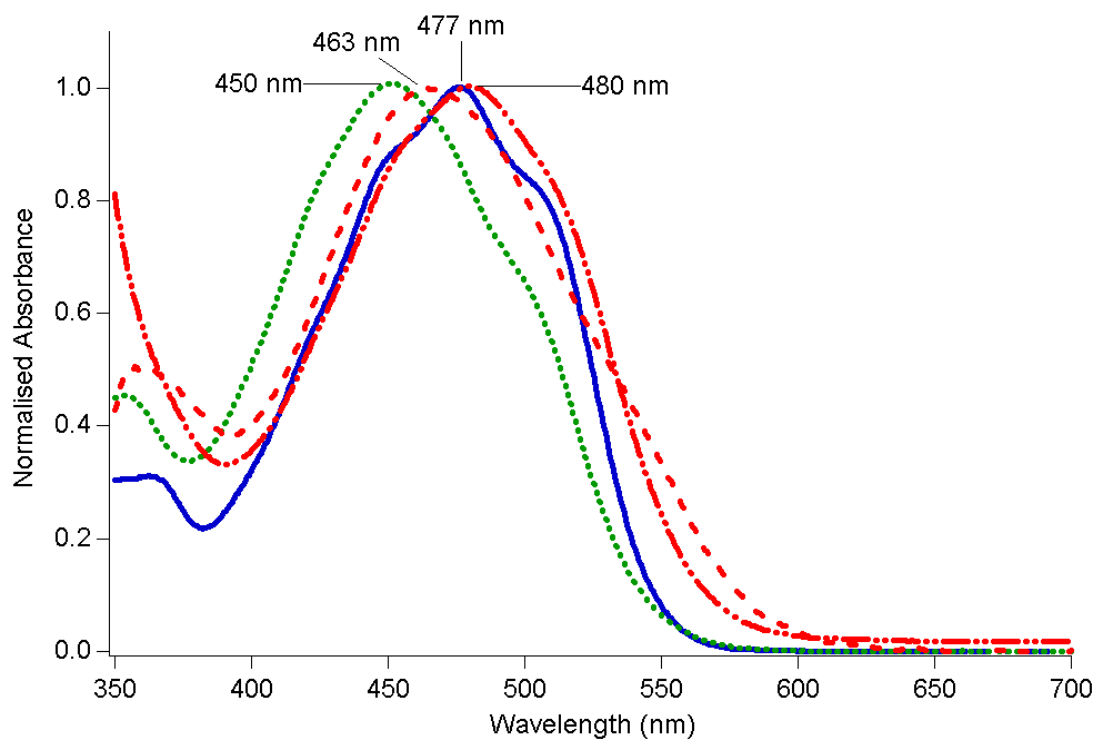


**Figure 6.25.** UV-Vis spectra of **6.5** in tetrahydrofuran (—), in acidic solution (.....), in solution with acidic sol-gel titania (---) and adsorbed onto sintered titania plates (-.-). The mole ratio of sol-gel titania spheres 2 nm in diameter to dye was 4 : 1.

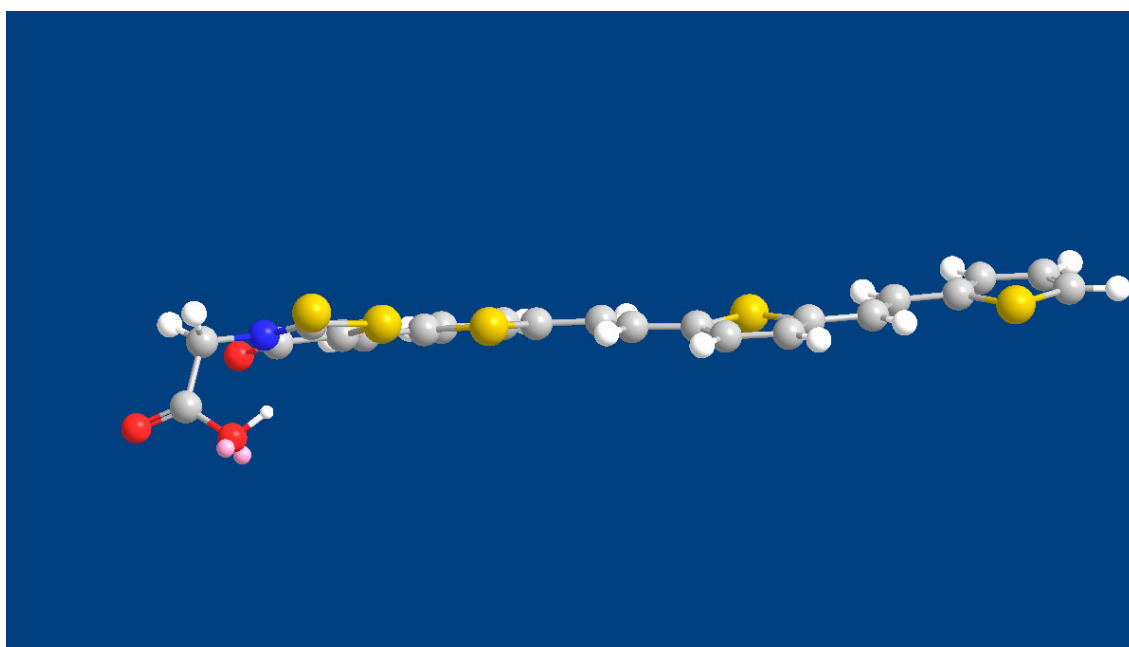
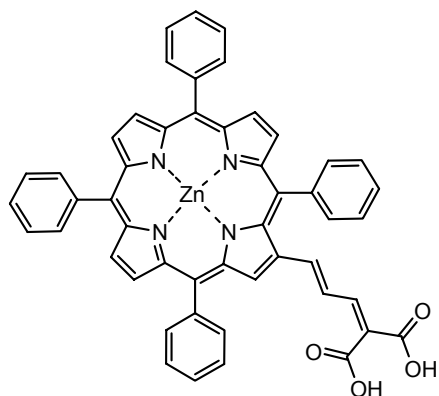


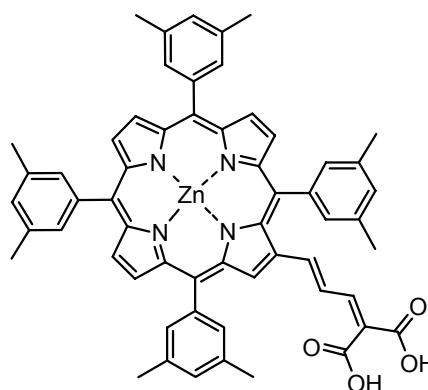
**Figure 6.26.** An extreme conformation of **6.6**, where the ter(thienylenevinylene) group lies parallel to the surface.

### 6.5.1.2.8. Aggregation of Porphyrinic Dyes

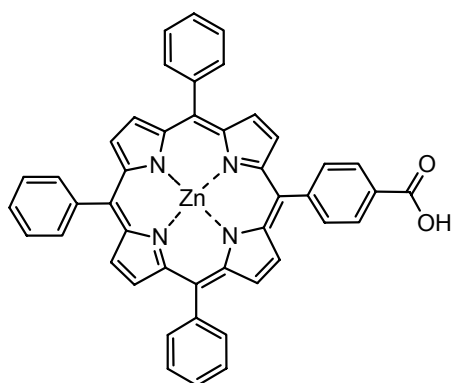
In order to compare the effect of dye structure of  $\pi$ -conjugated systems larger than **6.1** to **6.6**, the dye aggregation of porphyrinic dyes **6.7** to **6.11** upon sintered screen-printed titania was also investigated (Table 6.7). The aggregation of porphyrin dyes is well documented, for instance 5',10',15',20'-tetra(4-pyridyl)porphyrinato zinc(II) forms crystals of J-aggregated dye when injected into an aqueous surfactant solution.<sup>76</sup> The porphyrin dyes all use mono-carboxylic or malonic acid groups to bind to titania, while the structure of the dye distant from the binding group was altered to either encourage or prevent aggregation. The porphyrin dyes show monolayer coverage when adsorbed onto opaque Dyesol titania plates.<sup>62</sup> The structure of **6.8** and **6.10** should prevent the formation of dye aggregates, as the xyllyl and mesitylyl groups will be further twisted from the plane of the porphyrin core than the plain phenyl substituents of **6.7** and **6.9**.<sup>77</sup> The porphyrin **6.11** is designed to aggregate, as the octyl-functionalised benzene rings should encourage alignment through interactions of the long alkyl chains.



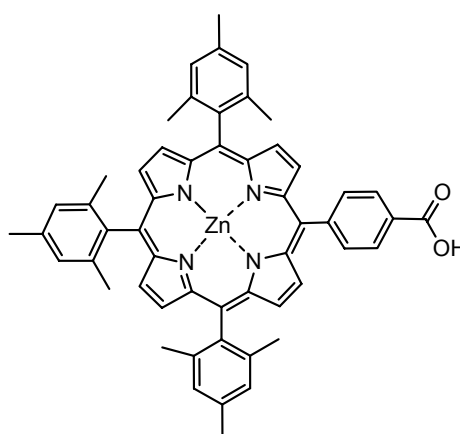
**6.7**



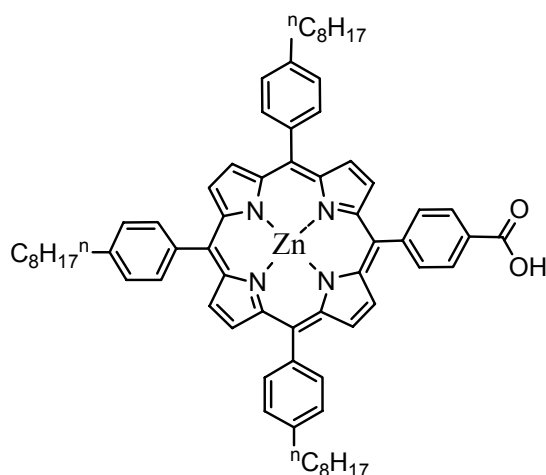
**6.8**



**6.9**



**6.10**



**6.11**

**Table 6.7.** Porphyrin-based dyes used in dye aggregation studies.

Dye	Name
<b>6.7</b>	4-(2'-(5',10',15',20'-tetraphenylporphyrinato zinc(II)yl)butadienylmalonic acid
<b>6.8</b>	4-(2'-(5',10',15',20'-tetraxylylporphyrinato zinc(II)yl)butadienylmalonic acid
<b>6.9</b>	(5'-(10',15',20'-triphenylporphyrinato zinc(II))-4-benzoic acid
<b>6.10</b>	(5'-(10',15',20'-trimesitylporphyrinato zinc(II))-4-benzoic acid
<b>6.11</b>	(5'-(10',15',20'-tri-(4- <i>n</i> -octylphenyl)porphyrinato zinc(II))-4-benzoic acid

Dyes **6.7** to **6.11** were adsorbed onto Dyesol titania plates by immersion within 0.2 mM solutions in tetrahydrofuran. As plates are dyed overnight for solar cell testing, UV-Vis subtraction spectra were collected of plates dried after short immersion times to record spectra for titania with submonolayer dye coverage. There are no clear blue or red shifts in dye adsorption that would indicate H- or J-aggregation with any of the dyes, including **6.7**, **6.9** and **6.11**, which are expected to aggregate (Figs. 6.27 to 6.31). However as less than 1% of light is transmitted for an absorbance above 2, peak broadening for such signals may owe more to noise than to aggregation, as evident for the subtraction spectra of **6.11** after 10 minutes of immersion (Fig. 6.29). It has been reported in a study of a range of porphyrin species, that while all of the dyes formed H-aggregates, not all produced a blue shift of the Soret band on aggregation in solution.<sup>35</sup>

While a broadened absorption rather than a signal shift with increased dye loading might be expected if both H- and J-aggregates of dye are formed, the large absorption of **6.7** to **6.11** after short immersion times means that noise cannot be ruled out as a cause of signal broadening.

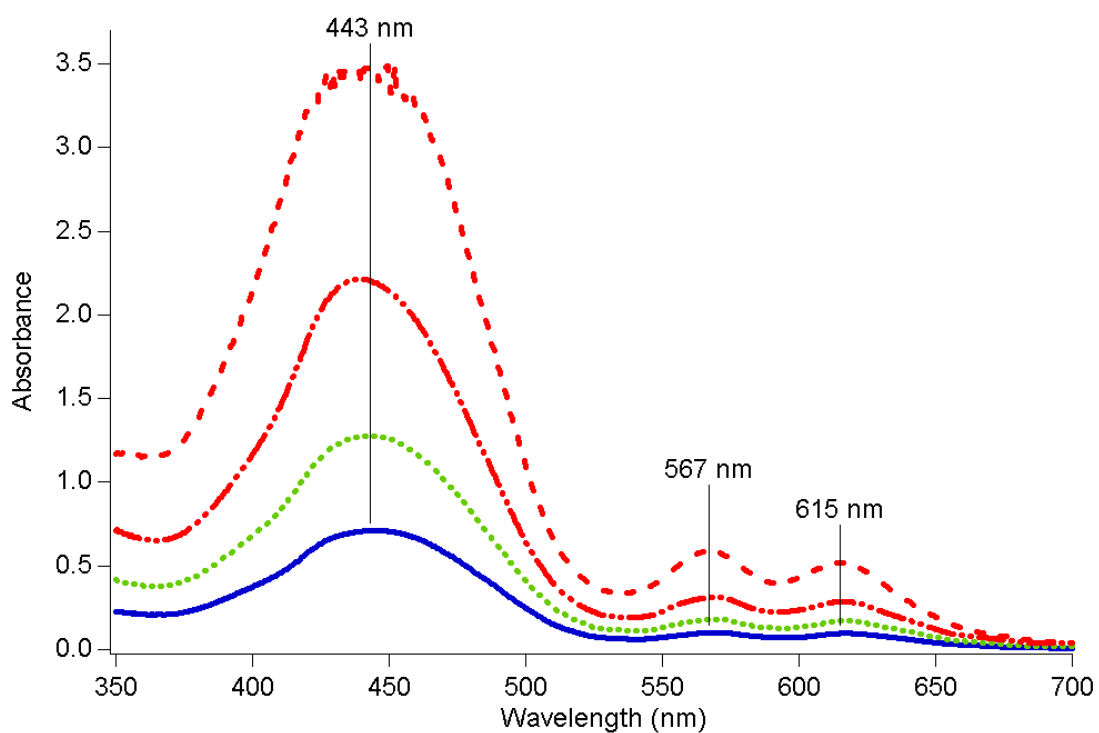


**Figure 6.27.** UV-Vis spectra of sintered Dyesol titania dyed with **6.7** from a 0.2 mM solution in tetrahydrofuran. The dye absorbance increases with progressive immersion times of 2 min (—), 4 min (⋯), 12 min (---) and 99 min (-.-).

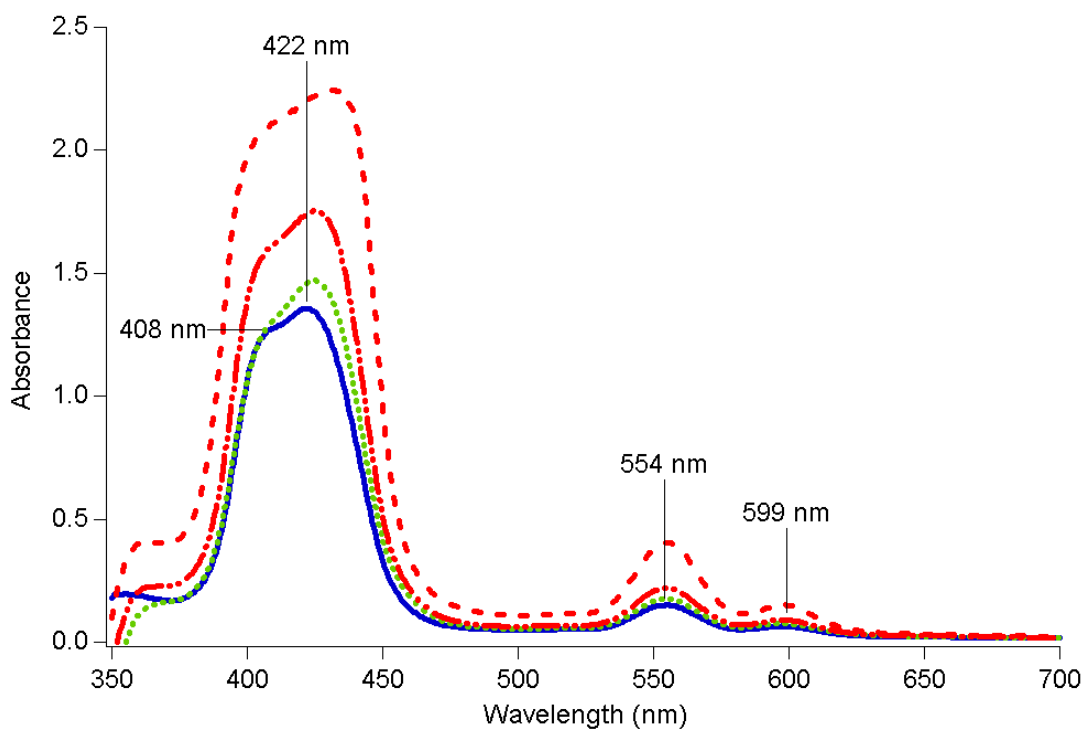


**Figure 6.28.** UV-Vis spectra of sintered Dyesol titania dyed with **6.9** from a 0.2 mM solution in tetrahydrofuran. The dye absorbance increases with progressive immersion times of 2 min (—), 4 min (·····), 8 min (---) and 50 min (-.-.).

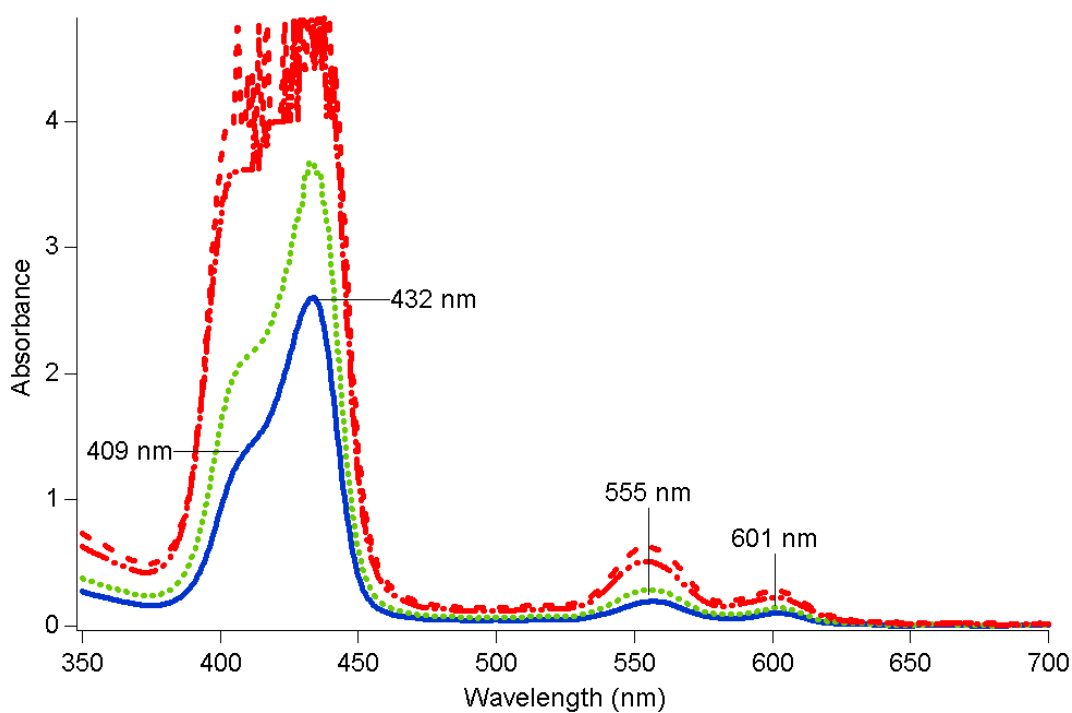


**Figure 6.29.** UV-Vis spectra of sintered Dyesol titania dyed with **6.11** from a 0.2 mM solution in tetrahydrofuran. The dye absorbance increases with progressive immersion times of 2 min (—), 4 min (·····), 10 min (---) and 60 min (-.-.).

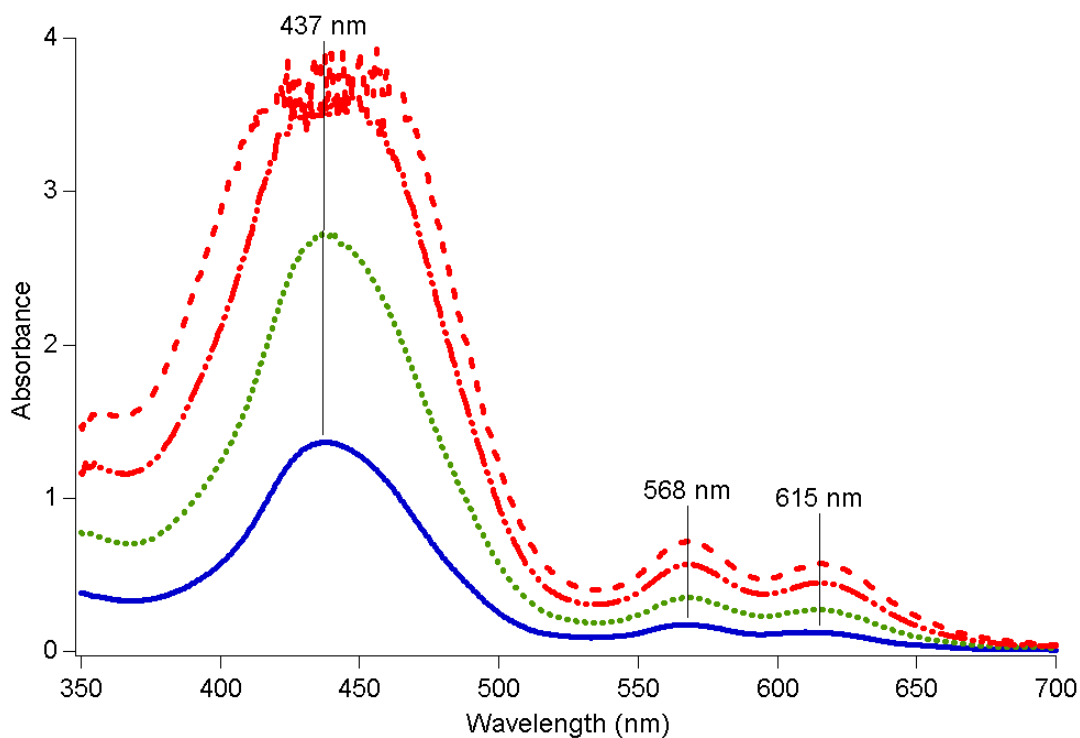


**Figure 6.30.** UV-Vis spectra of sintered Dyesol titania dyed with **6.8** from a 0.2 mM solution in tetrahydrofuran. The dye absorbance increases with progressive immersion times of 2 min (—), 4 min (⋯), 13 min (---) and 90 min (-.-).

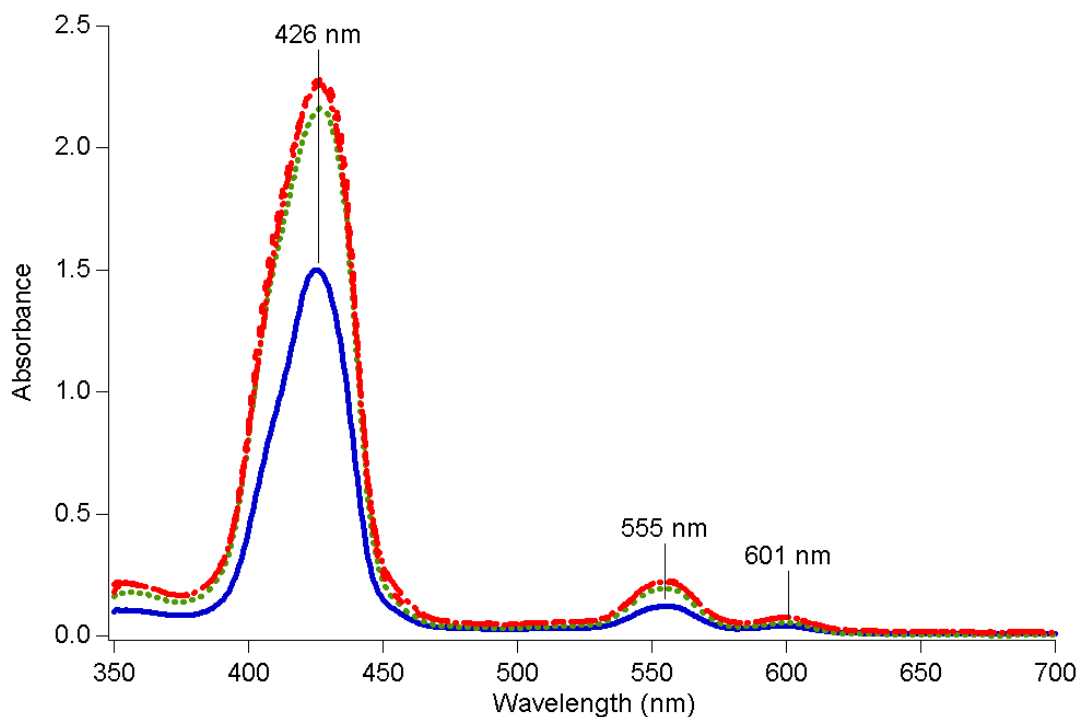


**Figure 6.31.** UV-Vis spectra of sintered Dyesol titania dyed with **6.10** from a 0.2 mM solution in tetrahydrofuran. The dye absorbance increases with progressive immersion times of 2 min (—), 4 min (⋯), 12 min (---) and 99 min (-.-).

#### **6.5.1.2.9. Summary**

Dye loading experiments with the probe dyes **6.1** and **6.2** gave submonolayer coverage, which may be due to displacement by solvent, while dyes **6.3** and **6.4** gave a bracket of dye loading values ranging from 55 - 150 %, which indicates that monolayer coverage is possible. Support for the equilibrium binding of the small probe dyes **6.1** and **6.2** was found, which is consistent with reports of reversible binding for larger coordination compounds on titania.<sup>4</sup> The binding of dye to both sintered crystalline titania and sol-gel titania resulted in signal shifts that are likely to result from the formation of H- and J- dye aggregates.<sup>36</sup> Similar peak shifts in UV-Vis spectra have been reported for H- and J-aggregates of coumarin dyes.<sup>37</sup> The difference in the magnitude of the signal shifts for dye adsorbed on titania may be rationalised by examination of molecular structure, as shown for dyes **6.5** and **6.6**. Aggregation is expected for porphyrin dyes adsorbed on titania,<sup>35</sup> but in this study was not observed on sintered Dyesol titania plates.

#### **6.5.3. FTIR Spectroscopy**

##### **6.5.3.1. Introduction**

Attenuated total internal reflection FTIR (ATR-FTIR) spectroscopy was used to distinguish whether the binding mode of dyes to titania is a carboxylate or pseudo-ester form. In the case of either screen-printed Dyesol titania or sintered sol-gel titania, despite the strongly coloured appearance of the dyed titania, data with reasonable signal intensity was unable to be collected. This may be due to the lower surface area of sintered material in comparison to non-sintered sol-gel titania, presenting a reduced concentration of dye available for detection. As a consequence, non-sintered amorphous sol-gel titania was used for the collection of ATR-FTIR spectra (Fig. 6.32). The sol-gel titania show signals attributed to lattice (Ti-O-Ti) vibrations below  $950\text{ cm}^{-1}$  and a broad peak centred at  $3200\text{ cm}^{-1}$  originating from water or titanol groups.<sup>13</sup> The titanol  $\nu(\text{Ti-OH})$  stretch has been reported to appear in the water  $\nu(\text{O-H})$  stretch region at  $3300\text{ cm}^{-1}$ , while at the lower energy of  $3570\text{ cm}^{-1}$  is the bridging (Ti-OH-Ti) stretching.<sup>22</sup> Titanol groups experiencing hydrogen bonding show a broad absorbance

from 2900 to 3600  $\text{cm}^{-1}$ , while titanol groups free of hydrogen-bonding show signals at the lower frequencies of 3730 and 3670  $\text{cm}^{-1}$ .<sup>66</sup> Present are sharp peaks at 1004 and 1124  $\text{cm}^{-1}$ , of which the latter may be attributed to titania.<sup>78</sup> Sharp spectral features from 400 to 700  $\text{cm}^{-1}$  have been reported to be due to titanium alkoxide  $\nu(\text{Ti-OR})$  stretching, which was not observed in this case due to the lower limit of 675  $\text{cm}^{-1}$  of the germanium ATR crystal.<sup>79, 80</sup>

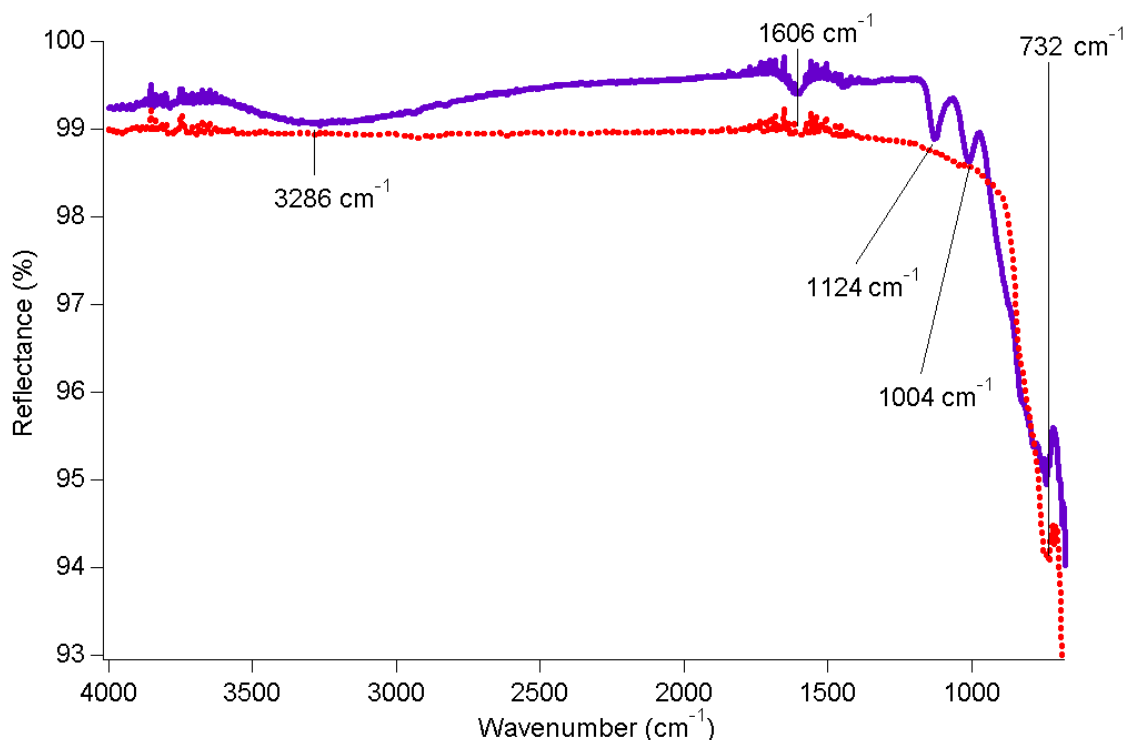


**Figure 6.32.** ATR-FTIR spectra of native sol-gel titania (—) and a sintered Dyesol titania plate (.....). The fine structure in the spectra at 3700 and 1606  $\text{cm}^{-1}$  are due to residual water.

### 6.5.3.2. Computer Modelling and Experimental Results

To interpret the experimental spectra of the free and adsorbed dyes, normal coordinate analysis from density functional theory (DFT) calculations have been employed to provide simulated vibrational data. Molecular modelling was done by Dr. Mark Waterland using the hybrid functional B3LYP with the basis set 6-31G. The orientations modelled for 6.2 in vacuum include the asymmetric form (a) and two

symmetric forms, **(b)** and **(c)** (Fig. 6.33). Selected vibrational modes are displayed in Figures 6.34 to 6.36. Vibrational modes that may be considered to be diagnostic of aliphatic carboxylic acids include  $\nu(\text{C=O})_{\text{sym}}$  and  $\nu(\text{C=O})_{\text{asym}}$  stretching signals, which are replaced by peaks due to  $\nu(\text{CO}_2^-)_{\text{sym}}$  and  $\nu(\text{CO}_2^-)_{\text{asym}}$  on deprotonation and the formation of a salt species. However, as the probe dyes **6.1** to **6.5** are fully conjugated, the vibrational frequencies of the carboxylic acid group are coupled to those of the rest of the molecule. As a consequence, isolated carbonyl and carboxylate stretches are not observed in the calculated spectra. For the same reason, the  $\delta(\text{C-H})$  bending of the diene backbone should also be strongly perturbed on adsorption. Provided that the dye is fully deprotonated on adsorption, the  $\delta(\text{O-H})$  bend should be absent in spectra of dyed titania. The calculated frequencies have not been scaled to fit experimental data and have been used to provide simulated spectra (Figs. 6.37 to 6.39). Solvent effects have not been included in the molecular models. The asymmetric form **(a)** is slightly more favoured than **(b)** and **(c)** by  $29 \text{ kJ mol}^{-1}$  and  $33 \text{ kJ mol}^{-1}$ , respectively. The doubly-deprotonated equivalents of **(a)** to **(c)** were also modelled. The calculated spectra of the deprotonated forms show impure  $\nu(\text{C=O})$  stretches, rather than carboxylate vibrations as the models were done without a counter-ion species. Modelling of the disalt of **6.2** with  $\text{TiCl}_4$  was attempted, but the calculation failed. While none of the configurations **(a)** to **(c)** have pure  $\nu(\text{C=O})$  stretching frequencies, the calculated  $\nu(\text{C=O})$  stretches and diene  $\delta(\text{C-H})$  bends may be used to aid interpretation of experimental data.

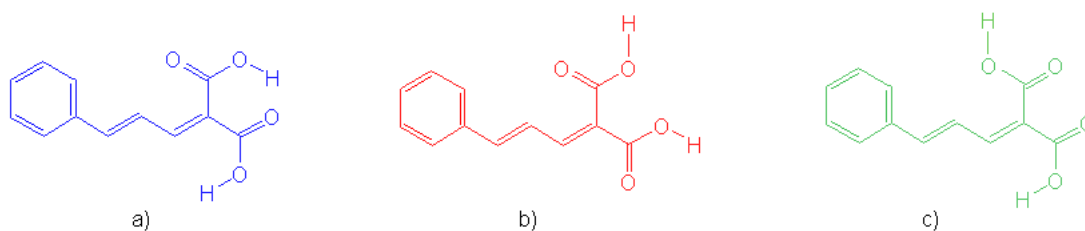


**Figure 6.33.** Illustration of the two configurations **(a)** and **(b)** of **6.2** that were modelled for *ab initio* calculations.

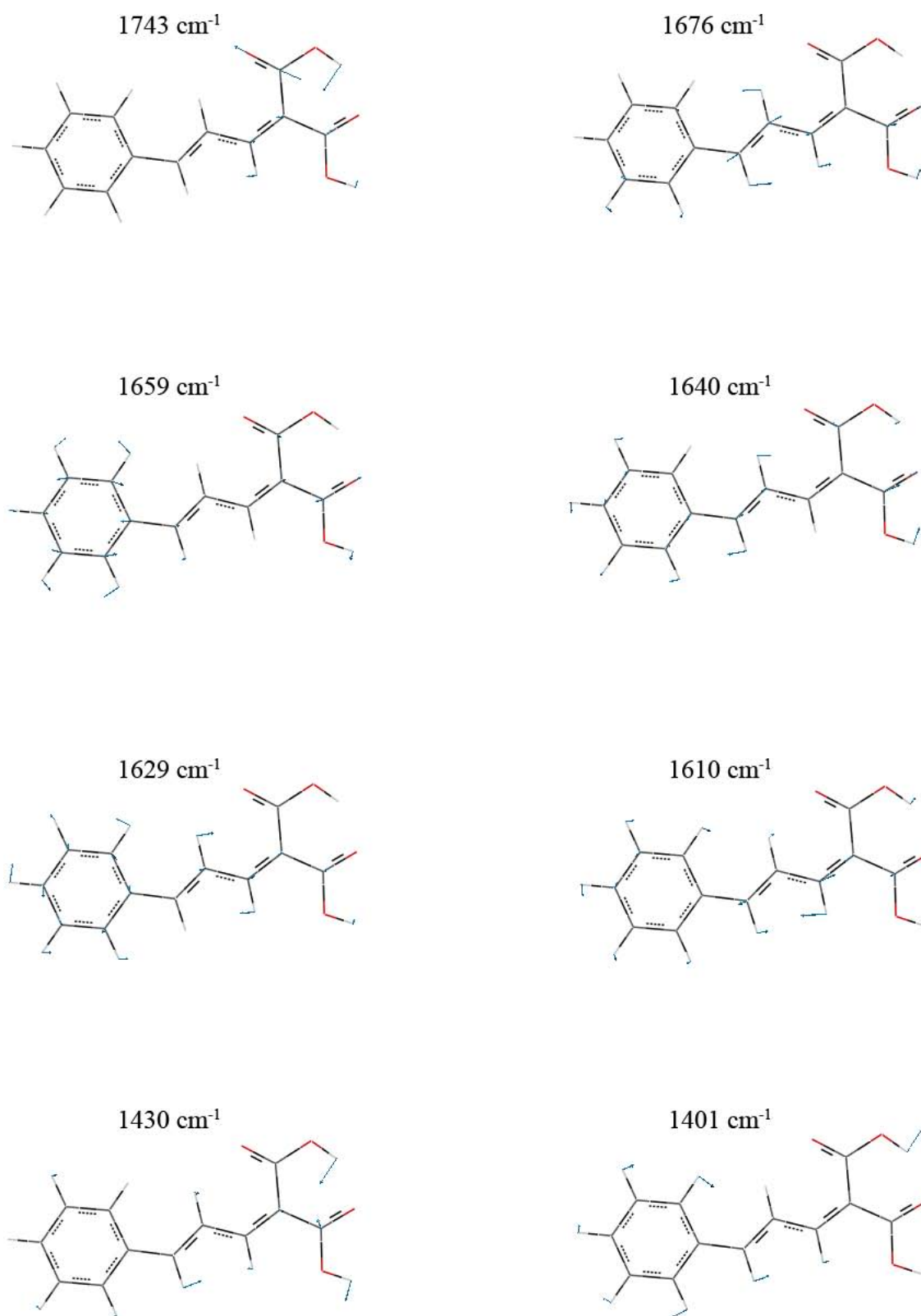


**Figure 6.34.** Calculated vibrational data for configuration (a) of 6.2.

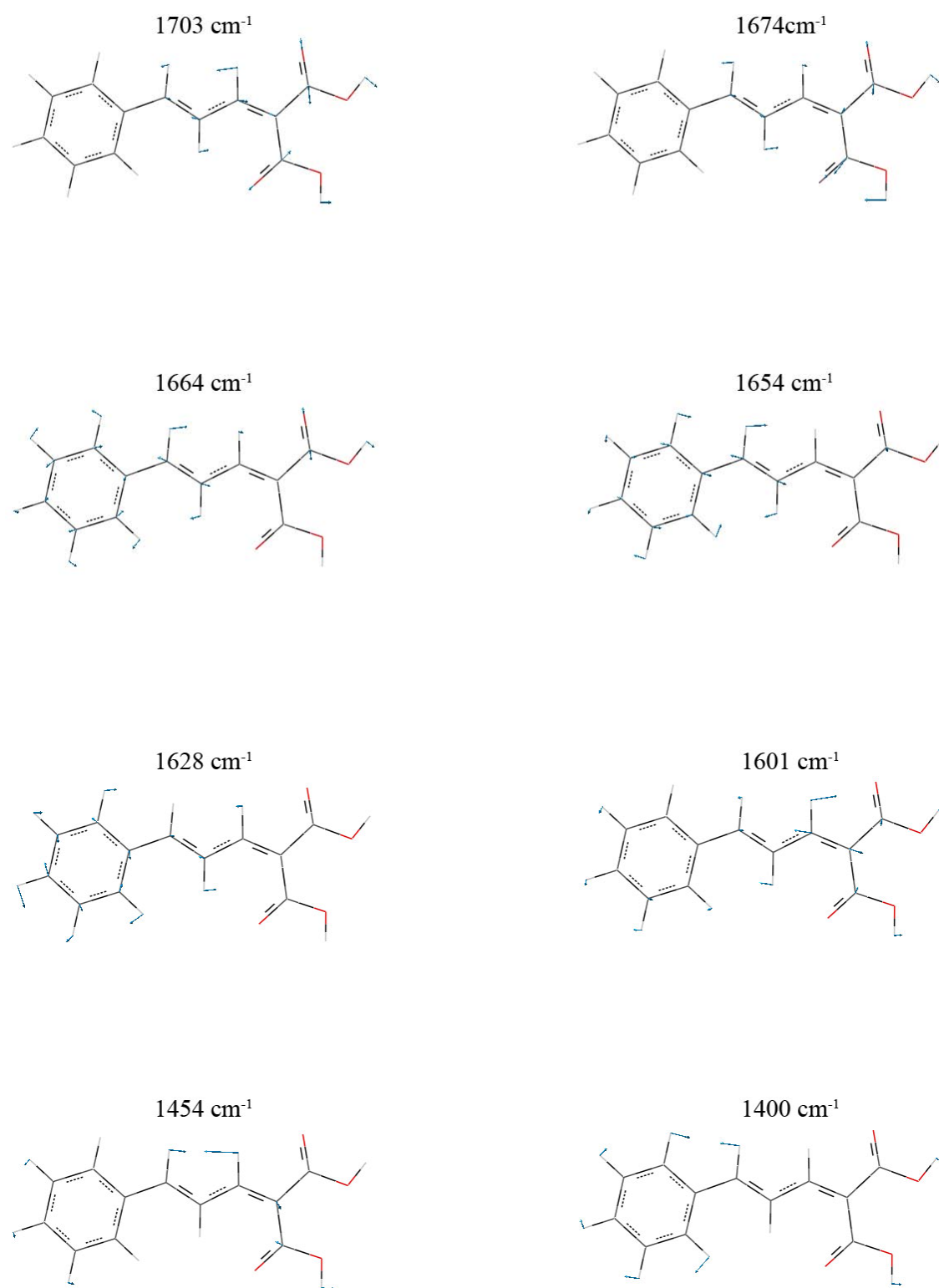


**Figure 6.35.** Calculated vibrational data for configuration (b) of 6.2.

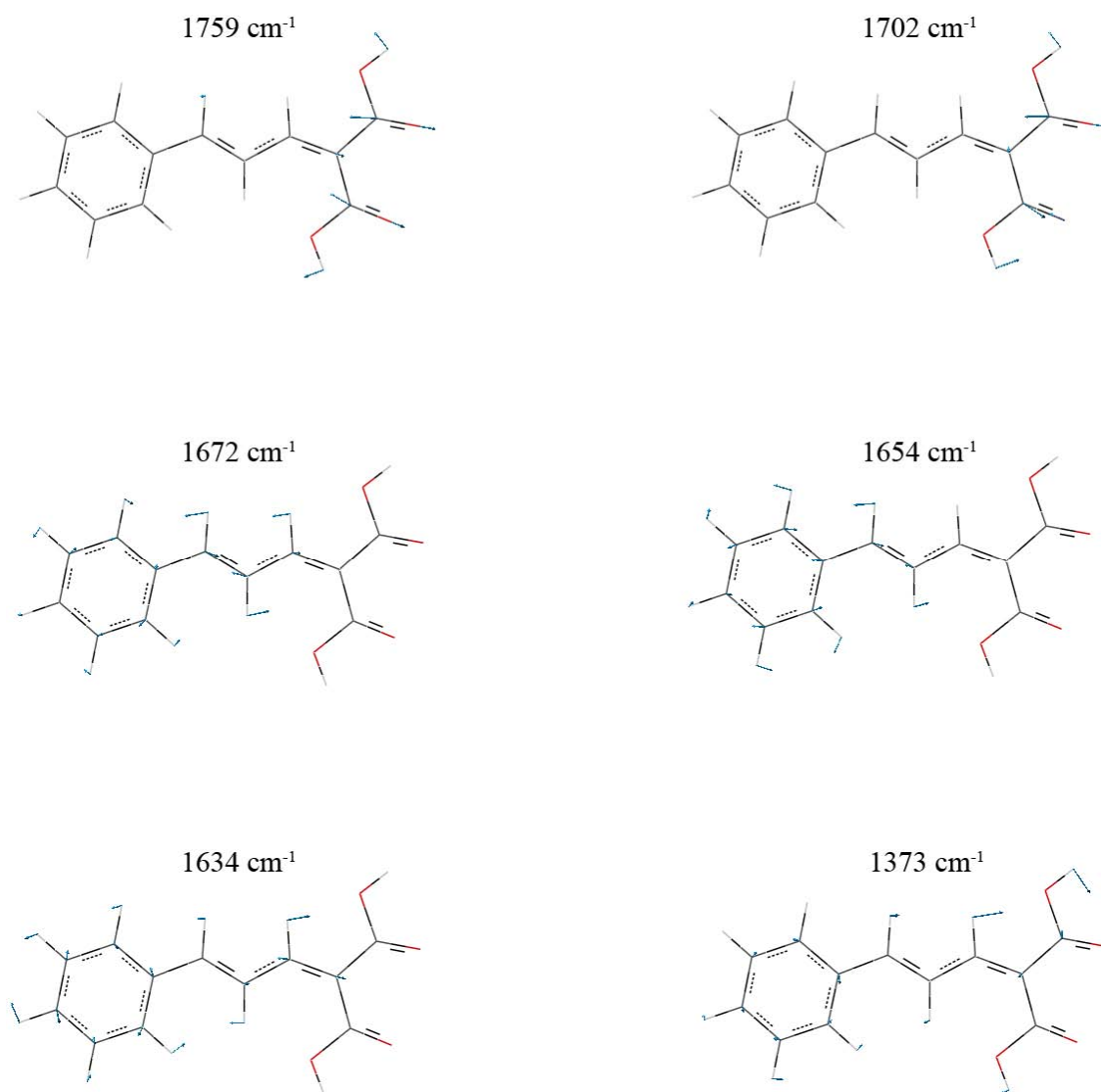


**Figure 6.36.** Calculated vibrational data for configuration (c) of **6.2**.

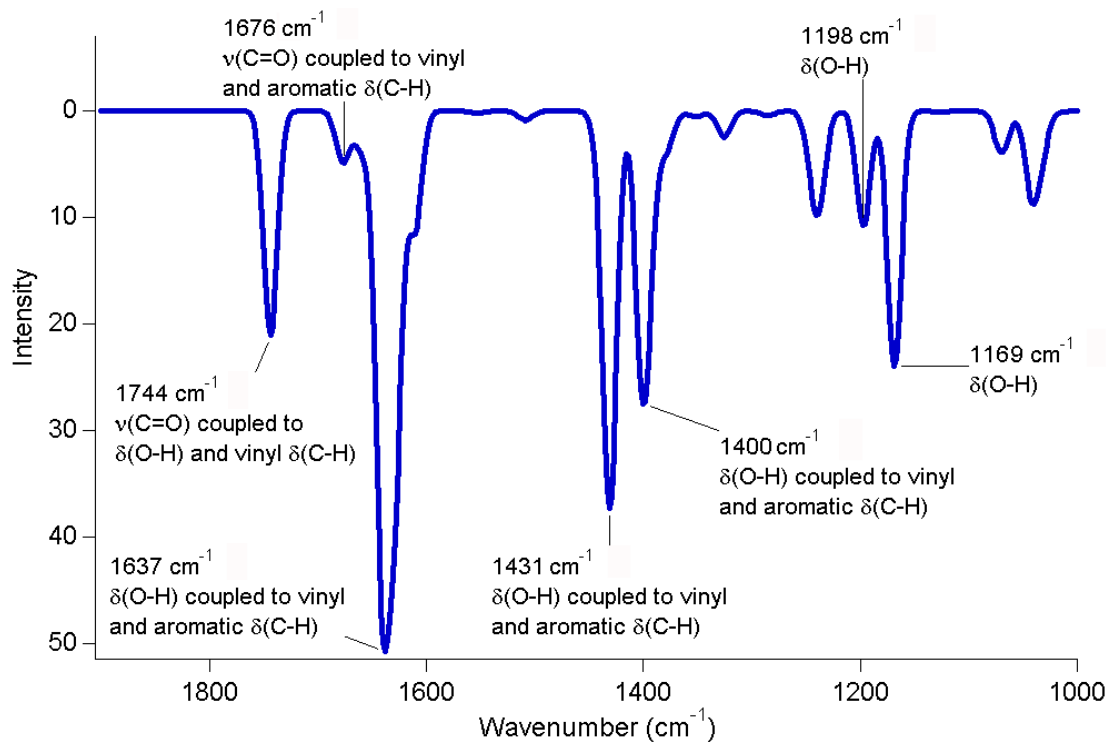


**Figure 6.37.** Calculated FTIR spectra for configuration (a) of 6.2 in vacuo.

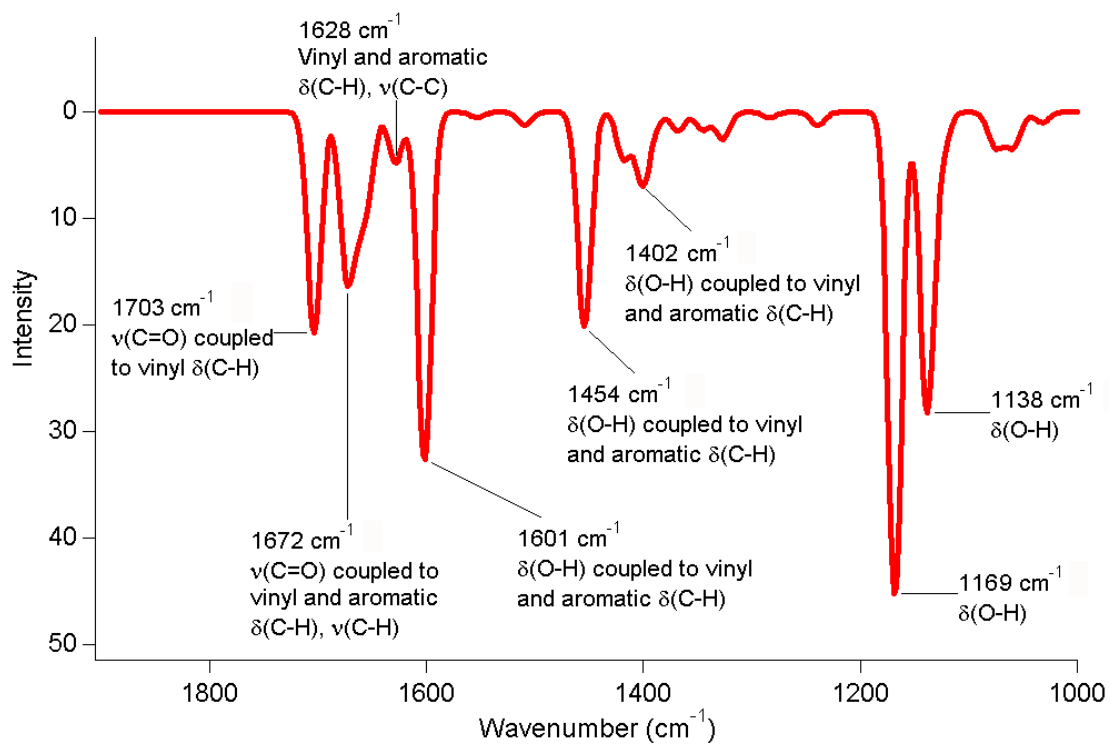


**Figure 6.38.** Calculated FTIR spectra for configuration (b) of 6.2 in vacuo.

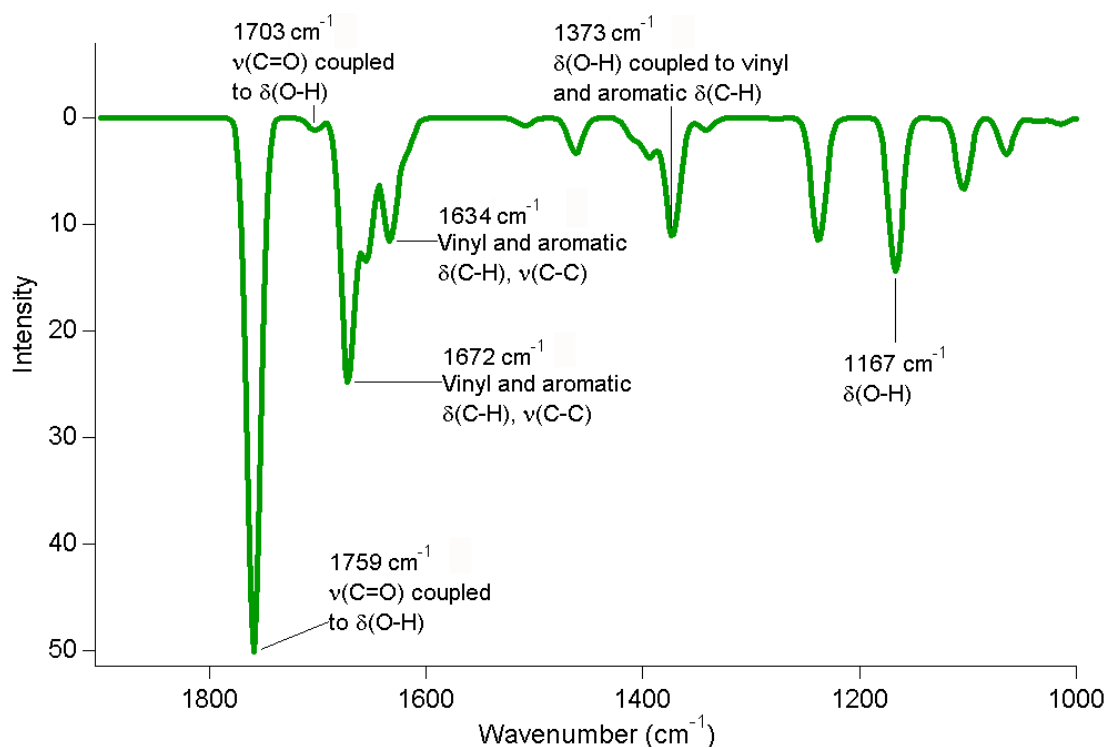


**Figure 6.39.** Calculated FTIR spectra for configuration (c) of **6.2** *in vacuo*.

The *ab initio* models of **6.2** show that in the case of conjugated malonic acids, the stretching of the carboxylic acid group is strongly influenced by the stretching vibrations of the alkene backbone. This may indicate that any generalisations using the calculated spectra will only be appropriate for malonic acids that have both a conjugated diene and an aromatic substituent. For pure **6.1** and **6.2**, signals due to carbonyl stretching are observed in the region of 1630 to 1720  $\text{cm}^{-1}$  (Figs. 6.40, 6.41). A broad, shallow band over 3000 to 2700  $\text{cm}^{-1}$  characteristic of carboxylic acid dimers is also present, which may indicate the presence of free dye.<sup>81</sup> Dye **6.1** has a vibration at 1592  $\text{cm}^{-1}$  that corresponds to the aromatic stretch of the benzene ring, while for **6.2** the signal at 1602  $\text{cm}^{-1}$  may be assigned to the asymmetric diene stretch  $\nu(\text{C}=\text{C}-\text{C}=\text{C})$  that typically appears in the region of 1577 to 1603  $\text{cm}^{-1}$ . The  $\nu(\text{C}=\text{C}-\text{C}=\text{C})$  stretch would be enhanced by conjugation to the aromatic ring and shifted to lower frequency by the carbonyl group.<sup>81</sup> The calculated spectrum for configuration (b) of **6.2** is a better fit for the experimental data for dyes **6.1** and **6.2**. In particular, the  $\nu(\text{C}=\text{O})$  stretching signals of **6.1** are closer in frequency to that of configuration (b).

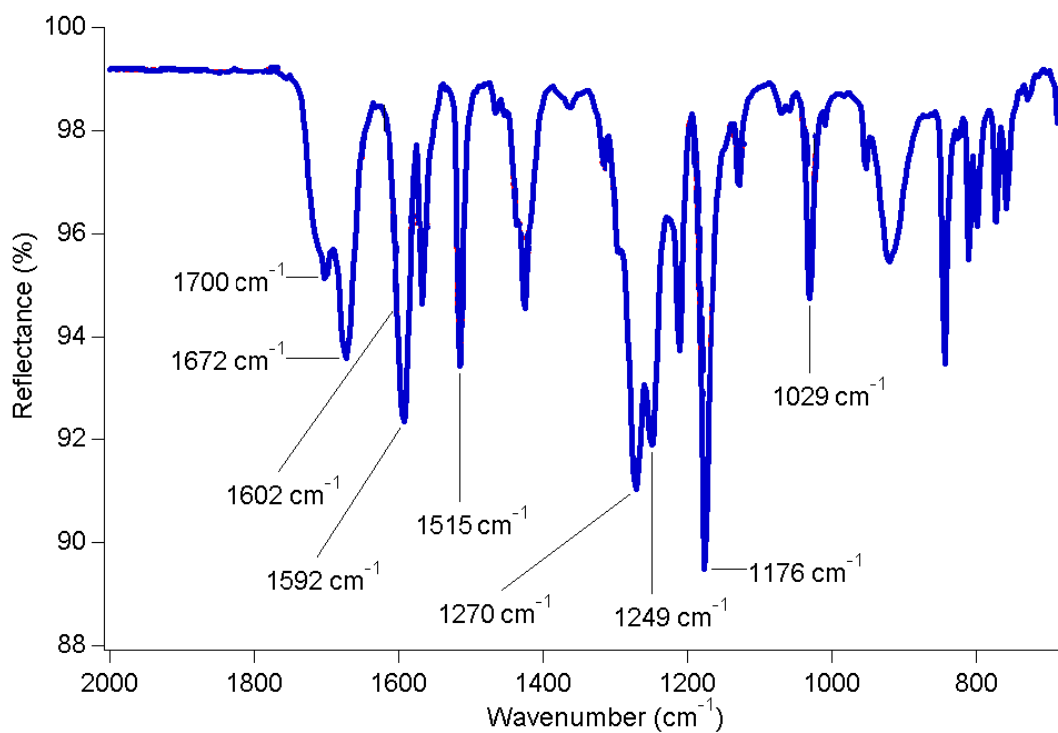


**Figure 6.40.** Experimental ATR-FTIR data for pure **6.1**.

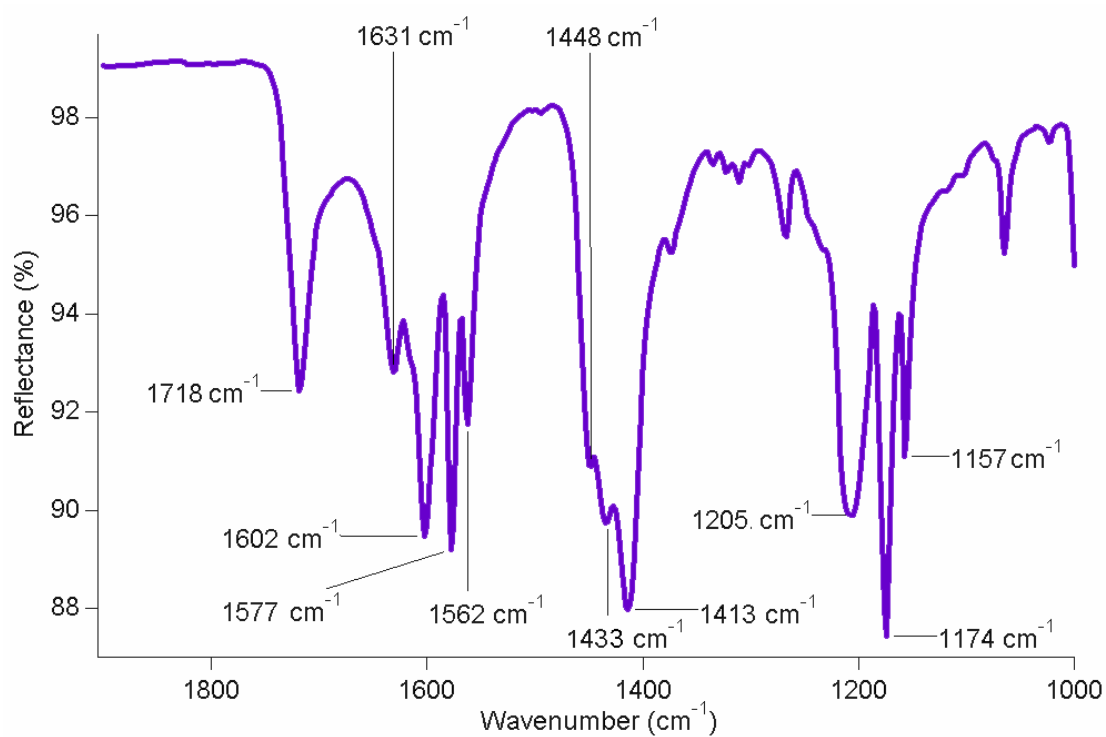


**Figure 6.41.** Experimental ATR-FTIR data for pure **6.2**.

On adsorption to titania, provided that the dyes are bound in a carboxylate form, it is expected that the carbonyl signals are replaced by carboxylate signals. On deprotonation, the calculated spectra of the forms (a) to (c) of **6.2** all minimise to the same conformation, with staggered carboxylate groups (Fig. 6.42). Selected vibrational modes are illustrated in Figure 6.43. The calculated spectrum for the doubly-deprotonated form of **6.2** show a replacement of  $\nu(\text{C}=\text{O})$  vibrations by  $\nu(\text{CO}_2^-)$  stretching frequencies and no  $\delta(\text{O}-\text{H})$  bends, as expected (Fig. 6.44). As no counter-ion was used in the modelling of the doubly-deprotonated form of **6.2**, a good fit with experimental data of adsorbed dye could indicate that carboxylic acids bind in an electrostatic manner. The adsorption of dyes onto sol-gel titania was done by suspension of titania in dye solution for submonolayer coverage, according to dye loading calculations. The dyed titania was then dried. ATR-FTIR spectra of **6.1** adsorbed on sol-gel titania show a large, broad peak centred at  $3151\text{ cm}^{-1}$  due to the  $\nu(\text{O}-\text{H})$  stretch of additional water adsorbed by the hygroscopic sol-gel titania during the process of dye adsorption (Fig. 6.45). The adsorption of water may account for the low surface coverage of sol-gel titania by **6.1** and **6.2** described in Section 6.5.1.

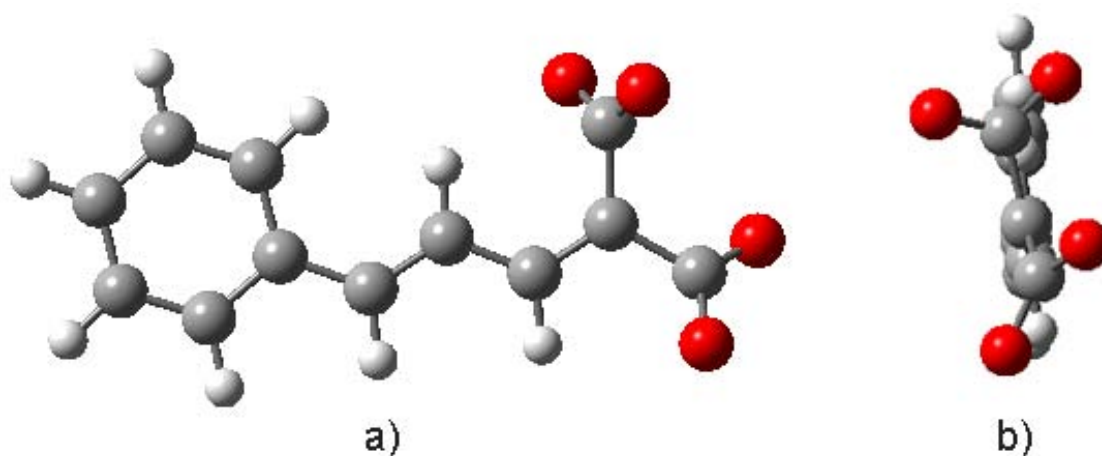


**Figure 6.42.** The minimised conformation of the doubly-deprotonated forms (a) to (c) of **6.2**.

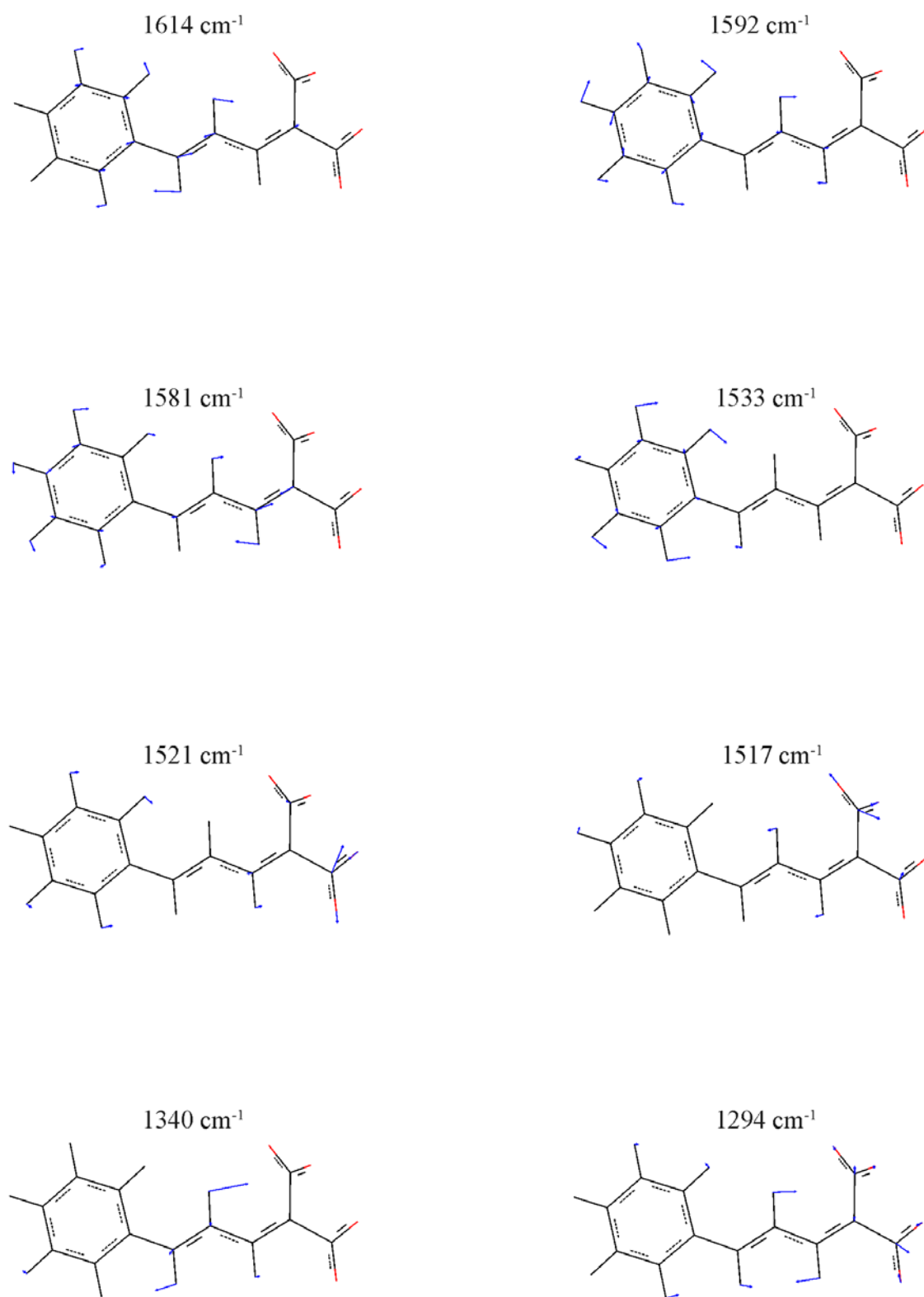


**Figure 6.43.** Calculated vibrational data for the doubly-deprotonated form of **6.2**.

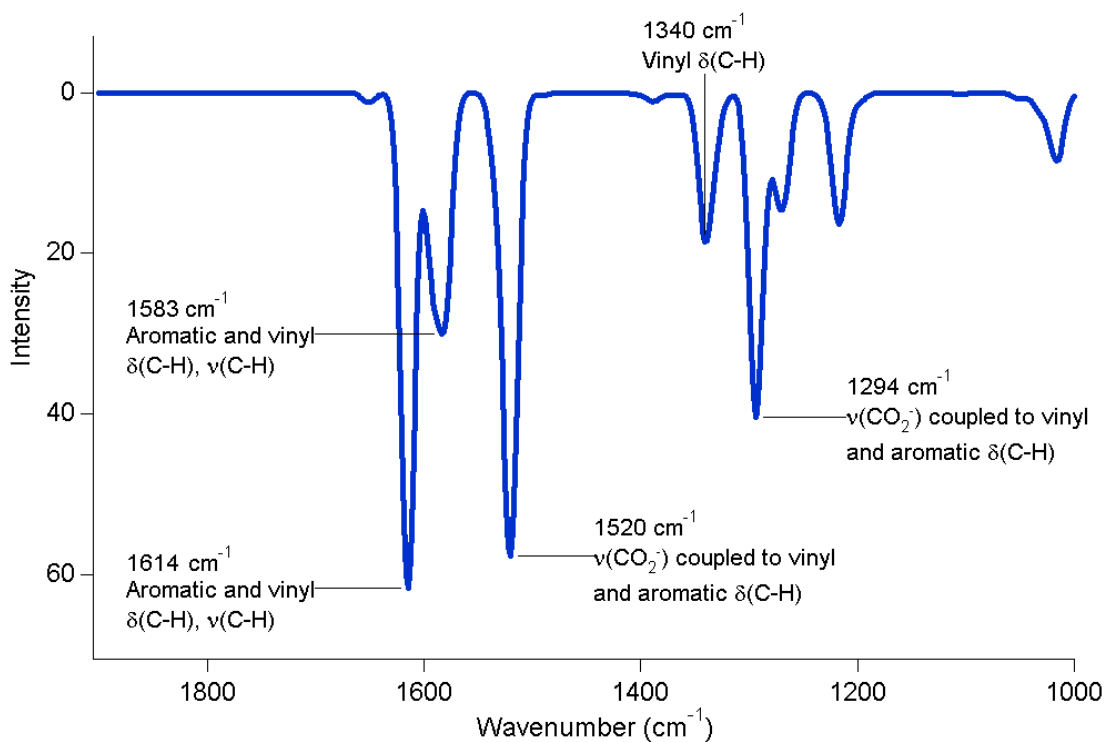


**Figure 6.44.** Calculated FTIR spectra of the doubly-deprotonated form of **6.2** *in vacuo*.

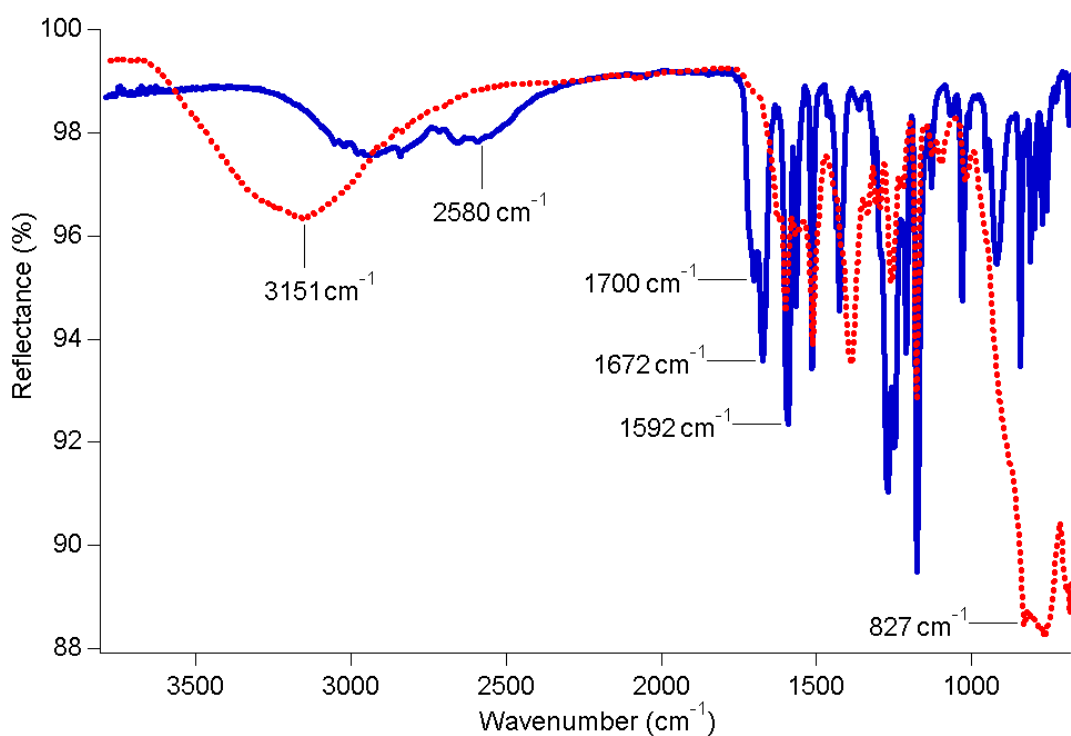


**Figure 6.45.** ATR-FTIR spectra of pure **6.1** (—) and the acid adsorbed onto native sol-gel titania in a 29 : 1 mole ratio of dye to 2 nm titania particles (.....).

The calculated spectrum for the doubly-deprotonated form of **6.2** shows a signal at 1520  $\text{cm}^{-1}$  due to  $\nu(\text{CO}_2^-)_{\text{asym}}$  stretching and a  $\nu(\text{CO}_2^-)_{\text{sym}}$  stretch frequency at 1294  $\text{cm}^{-1}$ . Both  $\nu(\text{CO}_2^-)$  stretching modes are coupled to vinyl and aromatic  $\delta(\text{C-H})$  bends. According to Deacon's 'rule-of-thumb' (Section 6.3), the  $\Delta\nu$  value of 226  $\text{cm}^{-1}$  indicates that the modelled carboxylate species has pseudo-ester character. A signal at 1340  $\text{cm}^{-1}$  in the calculated spectrum of doubly-deprotonated **6.2** originates from vinyl  $\delta(\text{C-H})$  bending. Similar low frequency stretches at 1630, 1530 and 1445  $\text{cm}^{-1}$  have been reported to appear on carboxylate binding of stearic acid to titania.<sup>82</sup> However, as the model was of the doubly-deprotonated species and not of a carboxylate salt, there is no guarantee that the calculated spectra will be directly comparable to experimental data. In an effort to obtain spectra of the carboxylate form of probe dyes, FTIR spectra of tetramethylammonium salts of dye **6.1** with a 1 : 1 and 2 : 1 mole ratio of tetramethylammonium hydroxide to **6.1** were collected. However, as the region of carbonyl and carboxylate stretching was masked by the absorption of tetramethylammonium hydroxide, the spectra could not be compared to that of adsorbed dyes.

Following the adsorption of **6.1** and **6.2** to titania, a signal is conserved at 1592 and 1602  $\text{cm}^{-1}$ , respectively (Figs. 6.46, 6.47). Adsorbed **6.1** and **6.2** both display vast reduction of the carbonyl  $\nu(\text{C=O})$  stretch signals at 1700 and 1672  $\text{cm}^{-1}$  and at 1718 and 1635  $\text{cm}^{-1}$ , respectively. New signals due to carboxylate  $\nu(\text{CO}_2^-)$  stretching vibrations appear at 1621 and 1388  $\text{cm}^{-1}$  for **6.1** and at 1587 and 1396  $\text{cm}^{-1}$  for **6.2**. While the calculated spectrum for doubly-deprotonated **6.2** places the vinyl  $\delta(\text{C-H})$  bend as the only strong vibration in the region of 1400  $\text{cm}^{-1}$ , the relative intensity of the  $\delta(\text{C-H})$  bend should be less than that of the calculated  $\nu(\text{CO}_2^-)_{\text{sym}}$  stretch. As the experimental data for **6.1** and **6.2** adsorbed on titania do not show a new and intense peak in the region of 1300  $\text{cm}^{-1}$ , it could mean that the strong signals near 1400  $\text{cm}^{-1}$  originate from  $\nu(\text{CO}_2^-)_{\text{sym}}$  stretching. That the calculated spectrum for doubly-deprotonated **6.2** is not a perfect fit for the experimental data of **6.1** and **6.2** on sol-gel titania indicates that dye is adsorbed in a manner other than electrostatic. The  $\delta(\text{O-H})$  signal at 1425 and 1411  $\text{cm}^{-1}$  for **6.1** and **6.2**, respectively, appears to be reduced to a shoulder of the lower frequency  $\nu(\text{CO}_2^-)$  stretch signal, which is further evidence for the formation of a carboxylate species upon titania. In both cases, a residual shoulder at 1720  $\text{cm}^{-1}$  remains after adsorption onto titania. This shows that while the malonic acids bind to titania in a

carboxylate or pseudo-ester mode, a proportion of free dye is still present. That the  $\nu(\text{C}=\text{O})$  stretch signals are so greatly reduced shows that both carboxylic acid groups are involved in binding. The use of Deacon's 'rule of thumb' with the new signals of **6.1** and **6.2** for  $\nu(\text{CO}_2^-)$  stretching, gives respective  $\Delta\nu$  values of 283 and 201  $\text{cm}^{-1}$ . This indicates that the binding of dye *via* a carboxylate form has a pseudo-ester character.<sup>20</sup> Such skewed pseudo-ester carboxylate bonding has also been reported for titanium lactate, where two sets of (Ti-O) distances are present for each chelating group.<sup>83</sup>

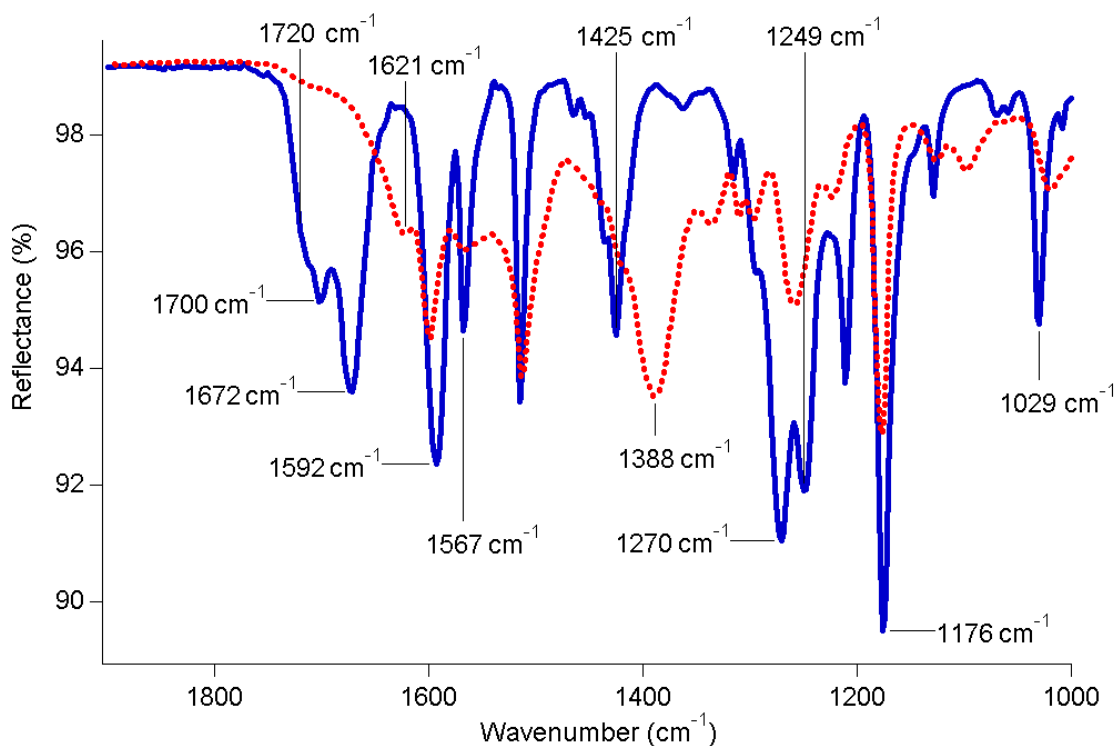


**Figure 6.46.** An expansion of Figure 6.43, of pure **6.1** (—) and the acid adsorbed onto native sol-gel titania in a 29 : 1 mole ratio of dye to 2 nm titania particles (.....).

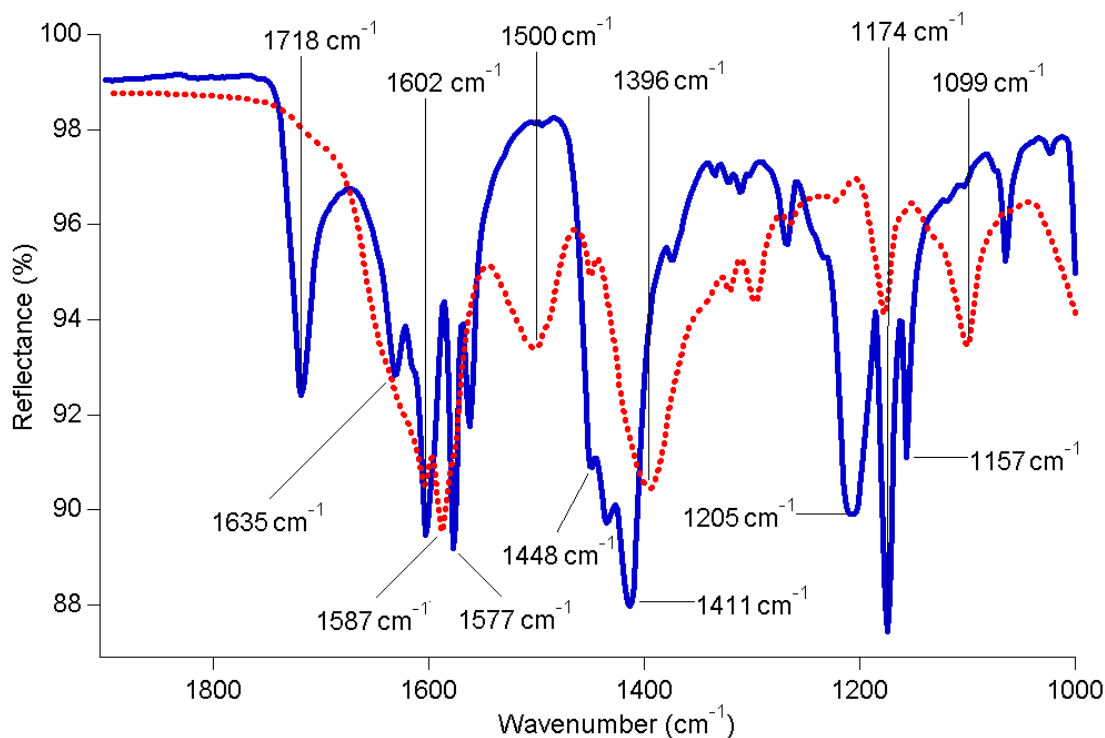


**Figure 6.47.** Experimental ATR-FTIR data for pure **6.2** (—) and the dye adsorbed onto sol-gel titania in a 15 : 1 mole ratio of dye to 2 nm titania particles (.....).

ATR-FTIR spectra collected of **6.3** and **6.4** show a relatively weak and broad  $\nu(\text{C}=\text{O})$  signal at 1710 and 1712  $\text{cm}^{-1}$ , respectively (Figs. 6.48, 6.49). Both **6.3** and **6.4** show a stronger and sharper signal, which may be a  $\nu(\text{C}=\text{O})$  stretch with respective peaks at 1564 and 1600  $\text{cm}^{-1}$ . On adsorption of **6.3** onto sol-gel titania, both  $\nu(\text{C}=\text{O})$  frequencies are reduced, though a broad band centred at 1564  $\text{cm}^{-1}$  remains. The reduction of intensity of the  $\nu(\text{C}=\text{O})$  stretches show that the majority of the dye is bound to the titania is present in a carboxylate form. The loss of the  $\nu(\text{C}=\text{O})$  stretch at 1700  $\text{cm}^{-1}$  and the appearance of broad bands centred at 1594  $\text{cm}^{-1}$  has been recorded for pyrene-isophthalic acid dyes on titania.<sup>84</sup> When bound to titania, **6.4** the cyano stretch signal at 2215  $\text{cm}^{-1}$  and the  $\nu(\text{C}=\text{O})$  stretch frequencies at 1700  $\text{cm}^{-1}$  and 1670  $\text{cm}^{-1}$  are greatly reduced. This may indicate that **6.4** is bound to the surface of titania by modes that affect both the cyano and carbonyl moieties. If a carboxylate was formed on binding of **6.4** to titania, this would account for the new absorbance at 1643  $\text{cm}^{-1}$ .

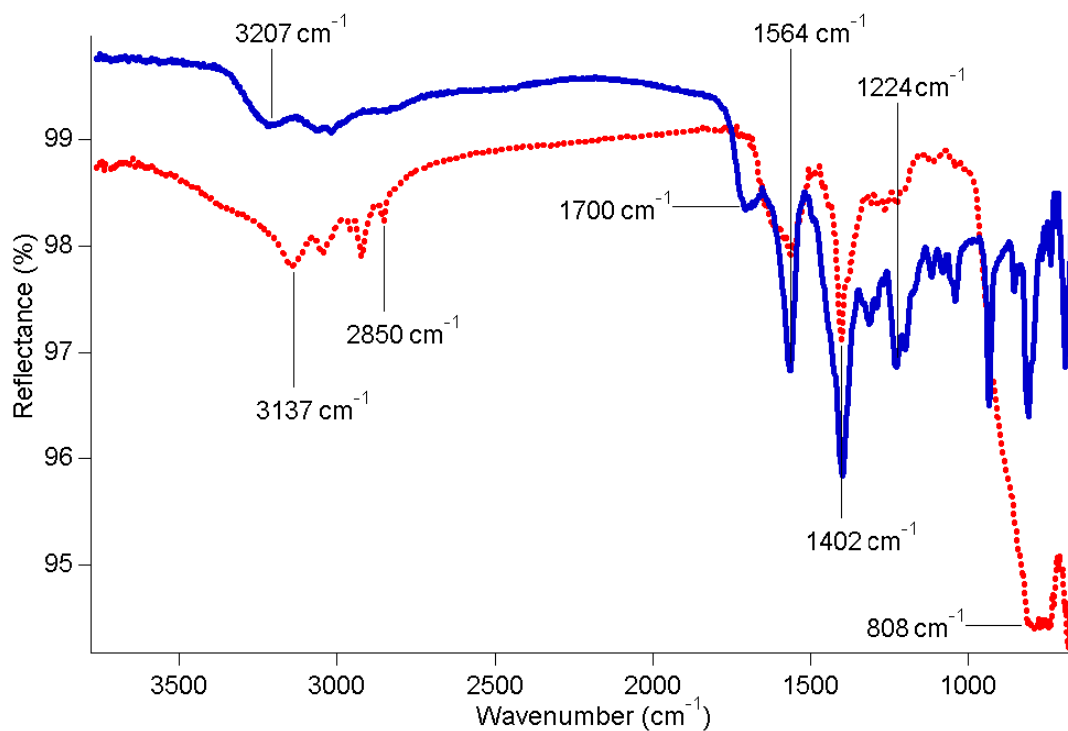


**Figure 6.48.** ATR-FTIR spectrum of pure **6.3** (—) and upon sol-gel titania in an 18 : 1 mole ratio of dye to titania 2 nm in diameter (.....).

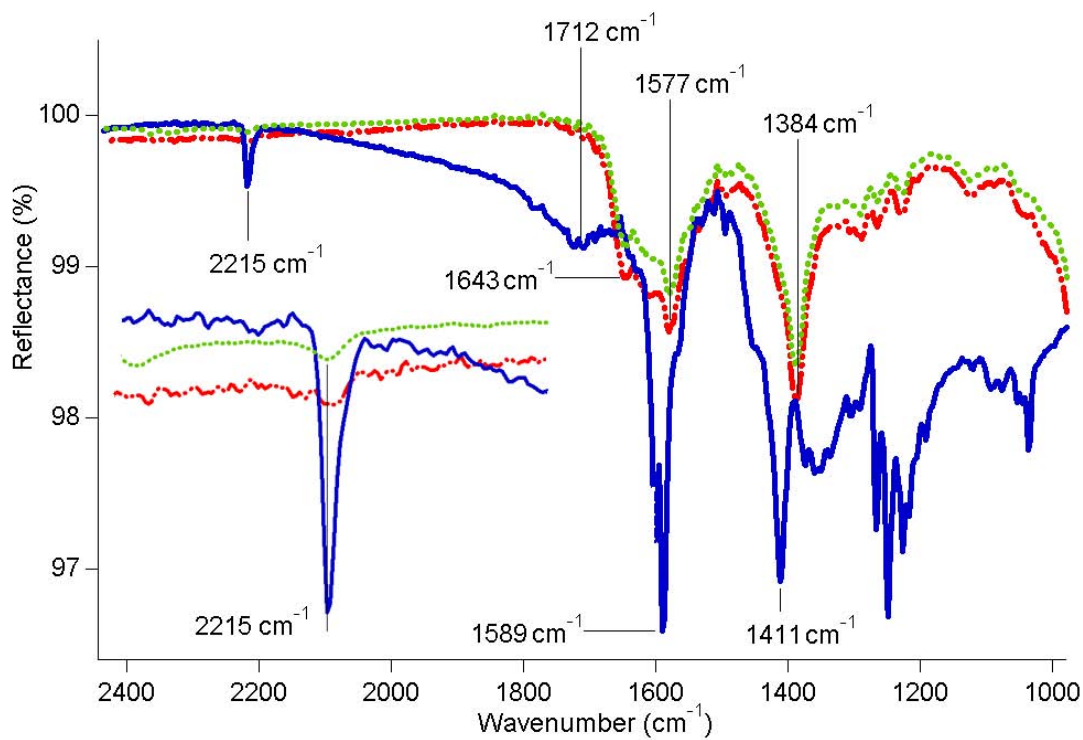


**Figure 6.49.** ATR-FTIR spectra of pure **6.4** (—) and the acid bound to sol-gel titania in an 18 : 1 (.....) and in a 21 : 1 mole ratio of dye to titania 2 nm in diameter (---).

### 6.5.3.3. *Summary*

Upon sol-gel titania the probe dyes **6.1** and **6.2** are bound as a carboxylate species, with pseudo-ester character. This is in accord with the carboxylate binding of dyes, such as mercaptosuccinic acid and the 'N3' ruthenium coordination compound, to a dry and crystalline titania surface.<sup>18, 85</sup> Carboxylate binding of glutamic and aspartic acid has also been reported on a solvated, amorphous titania film.<sup>43</sup> The FTIR spectrum of the malonic acid dye **6.3** shows a vast reduction of the carbonyl stretch signals, which indicates that only a small proportion of dye present is bound *via* a single carboxylic acid group. In the case of the cyanoacetic species **6.4**, the residual  $\nu(\text{C}=\text{O})$  signal that appears as a shoulder upon the stronger stretch frequency at  $1643\text{ cm}^{-1}$  is evidence for the presence of free dye in the sample.

### 6.5.4. *Raman and Fluorescence Spectroscopy*

#### 6.5.4.1. *Experimental Results*

Raman and fluorescence spectroscopy were used to probe whether dye was adsorbed on titania, by a loss of fluorescence intensity. In the case of dye bound to titania, excited dye then has available a non-radiative decay pathway *via* titania, which may be observed as a quenching of dye fluorescence.<sup>31</sup> The fluorescence of pyrene-isophthalic acid dyes has been reported to be completely quenched on binding to titania, with weak fluorescence from excimers of  $\pi$ -stacked dyes.<sup>84</sup> Ideally, the quenching of dye fluorescence would depend on the available surface area of sol-gel titania. If adsorbed dye is completely quenched and binding is irreversible, calculation of dye coverage values would be possible.

Ter(thienylenevinylene) dyes such as **6.3** and **6.4** display strong fluorescence. The emission for dyes **6.3** and **6.4** on excitation in tetrahydrofuran at 450 or 480 nm, respectively, occur at 535 and 595 nm. A solvent-related effect is also seen in fluorescence, as when dye **6.4** is excited at 455 nm in methanol, the resulting emission is observed at 590 nm. Excitation of **6.3** and **6.4** in 18  $\mu\text{M}$  hydrochloric acid in tetrahydrofuran did not shift the emission peak; at the low acid concentration it is

reasonable that only the carboxylic acid groups be protonated, rather than the thiophene moieties. The fluorescence of **6.4** was normalised to UV-Vis absorption in order to account for the effect of intensity losses due to absorption and scattering by the solute. However, the fluorescence of the free dye was shown to be non-linear with increasing concentration over the range of  $2 \times 10^{-6} \text{ mol L}^{-1}$  to  $5 \times 10^{-5} \text{ mol L}^{-1}$  with plots of normalised fluorescence intensity versus concentration (Section 8.2, Fig. 8.2). This was expected as fluorescence intensity was not corrected for signal loss due to scattering and reabsorption with increased dye concentration.

Quantitative studies of fluorescence quenching with titania involved the titration of **6.4** with sol-gel titania. The calculated mole ratio of dye to titania was done with the assumption that the sol-gel was composed of spheres 2 nm in diameter (Section 6.5). Solution-state fluorescence of dispersed sol-gel titania in methanol displayed Rayleigh scattering and a weak signal at 610 nm, which is likely to be due to contaminants. The fluorescence of 4 nm sol-gel titania particles capped with tri-*n*-octylphosphine oxide has been reported to be 370 nm in toluene.<sup>67</sup> On the addition of sol-gel titania to a solution of free dye, fluorescence signals show a gradual red shift of peak maxima, rather than showing a competition between a signal attributable to a bound species and the signal due to the free dye (Fig. 6.50). A contrary fluorescence blue shift of 45 nm was reported for ATRA adsorbed to acidic sol-gel titania.<sup>69</sup> The gradual shift in the position of the fluorescence maximum with an absence of signal shoulders is similar to what was seen in UV-Vis absorption studies and indicates irreversible rather than equilibrium dye binding. While there is a degree of quenching of organic materials bound to titania there was never a complete loss of fluorescence. To significantly quench the fluorescence of **6.4**, it was necessary to provide a vast excess of amorphous sol-gel titania particles. The persistent fluorescence indicates that either adsorbed dye is not fully quenched by titania, that free dye is still present or that dye excimers are formed.

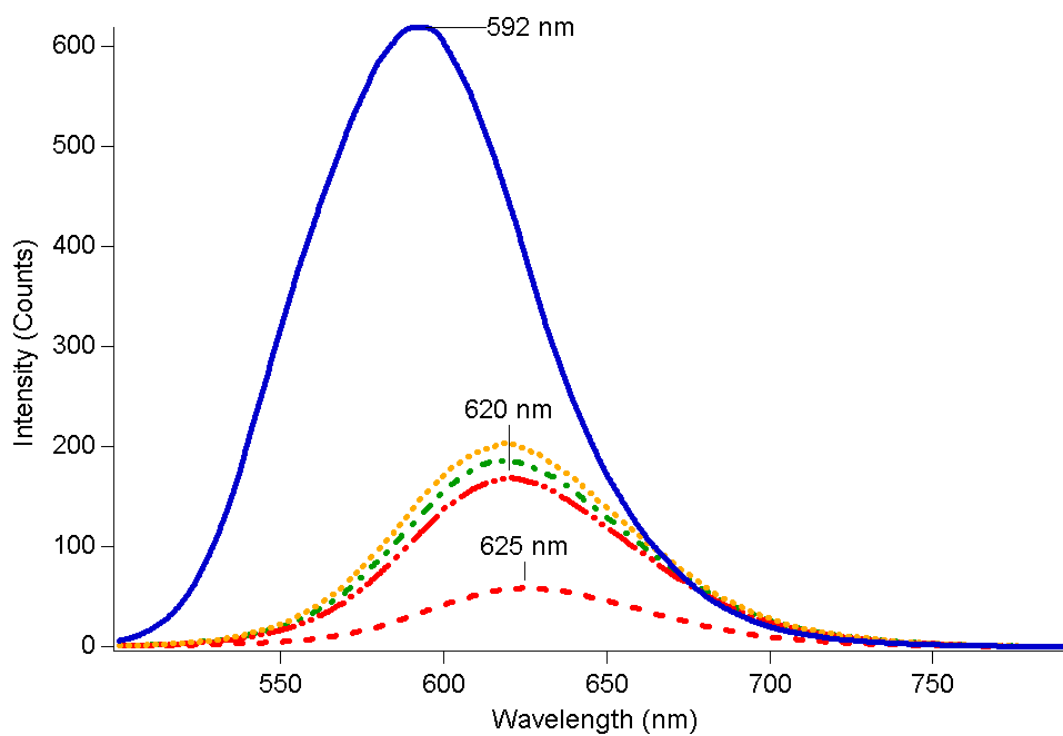


**Figure 6.50.** Fluorescence of **6.4** in methanol (—) and with a calculated mole ratio of dye to titania 2 nm in diameter of 39 : 1 (·····), 20 : 1 (·····), 10 : 1 (---) and 1 : 1 (---). The excitation wavelength was 455 nm.

As found in UV-Vis studies (Section 6.5.2), there is a non-linear relationship between fluorescence maximum and the mole ratio of dye to sol-gel titania 2 nm in diameter (Fig. 6.51).

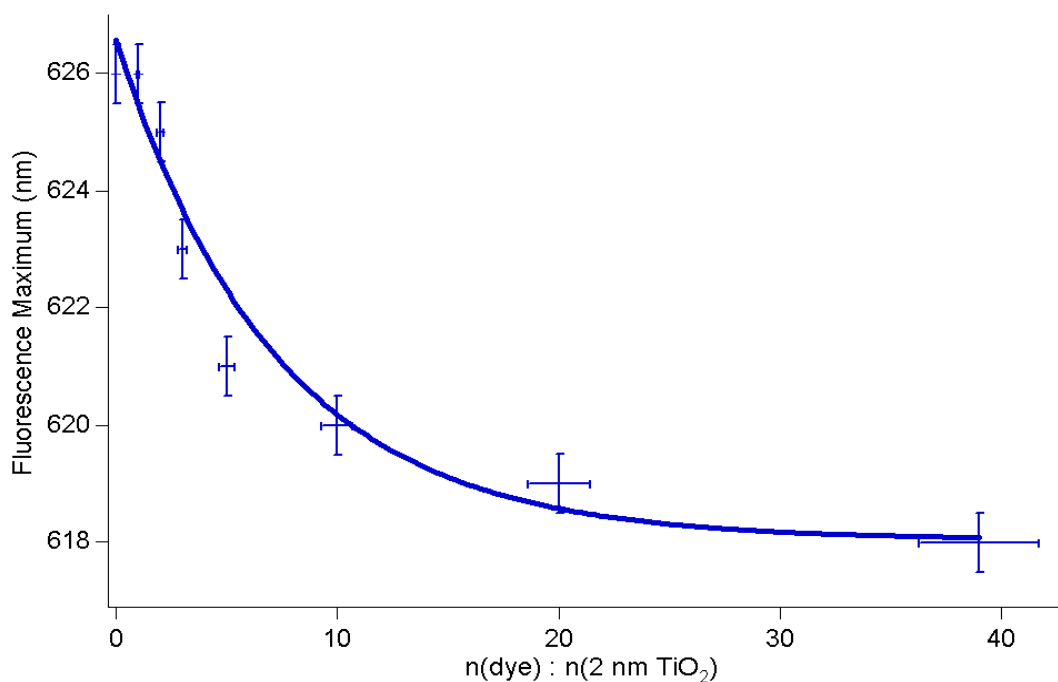


**Figure 6.51.** Fluorescence maximum of **6.4** in methanol versus the mole ratio of dye to titania particles 2 nm in diameter. The fluorescence maximum of pure **6.4** is 592 nm. The excitation wavelength was 455 nm. The error bars are for an uncertainty of  $\pm 0.5$  nm of the fluorescence signal and approximately  $\pm 7\%$  for the mole ratio of dye to 2 nm diameter titania.

Raman spectra of **6.1** and **6.2** were not used as they absorb in the blue region and only green-line lasers were available. The ter(thienylenevinylene) dye **6.4** was used as the available excitation line at 514 nm is very close to the absorbance maxima of the dye. Samples involved dye solutions and dispersed sol-gel titania, in order to avoid the specular reflections that the glass substrate of screen-printed titania would produce. The Raman spectrum of sol-gel titania in methanol displays a sloping, non-linear background, while the only sharp signals present are due to the solvent. Rutile has a broad Raman band centred at  $1600\text{ cm}^{-1}$  when excited at 458 nm.<sup>71</sup> While the free dye **6.4** produced too much fluorescence for the collection of Raman spectra, fluorescence was quenched in the presence of sol-gel titania. The titration of dye **6.4** into a methanolic solution of sol-gel titania turned the clear and colourless solution pink, which with more dye became a red colour. To reduce fluorescence from free **6.4**, the mole ratio of titania 2 nm in diameter to dye was kept high during the titration. A slight

shift in signal position was observed on decreasing the ratio of titania to dye from 1 : 0 to 12 : 1, to 6 : 1, to 4 : 1, and finally to a 3 : 1 ratio (Fig. 6.52). Though *ab initio* models of dye **6.4** were unable to be obtained for assignment of the vibrational modes, Raman spectroscopy has revealed that emission from **6.4** is quenched by titania, which indicates that **6.4** interacts with the titania surface.

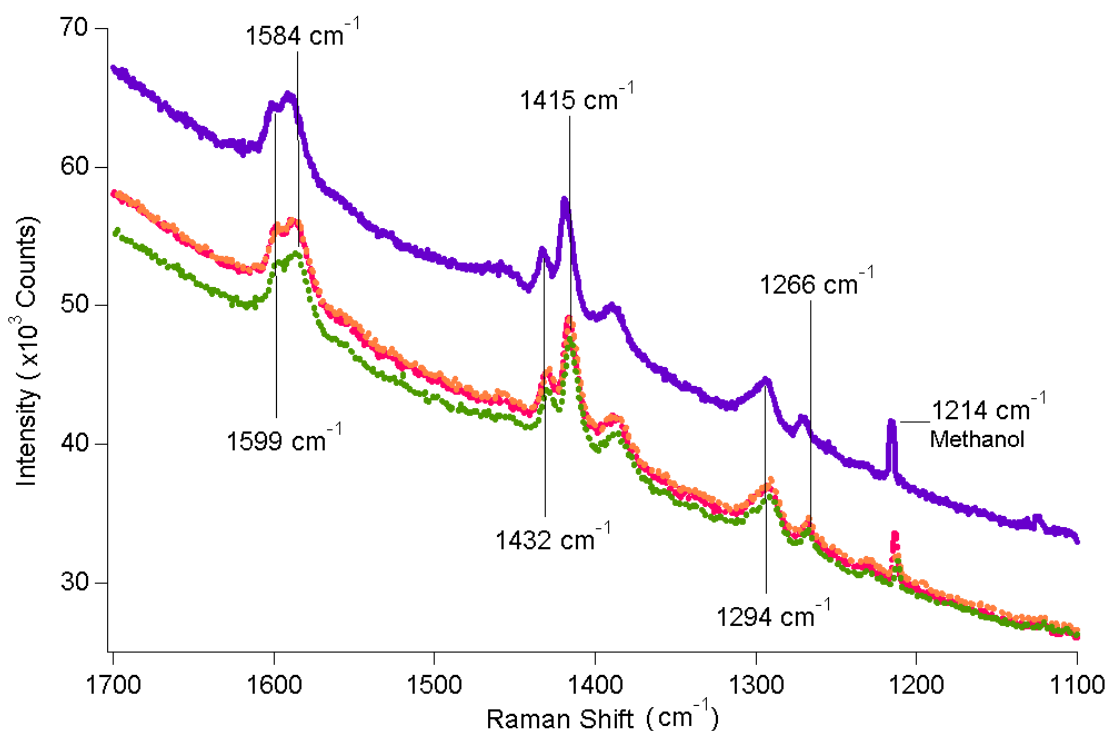


**Figure 6.52.** Raman spectra of a methanolic solution with a 12 : 1 (—), a 6 : 1 (.....), a 4 : 1 (.....) and a 1 : 3 mole ratio (---) of acidic, amorphous 2 nm sol-gel titania to dye **6.4**. The non-linear background has not been subtracted.

#### 6.5.4.2. Summary

It was expected that with a submonolayer ratio of **6.4** to titania that fluorescence of the dye would be quenched upon binding to titania. However, fluorescence persisted even in the presence of a large excess of titania, which indicates that either adsorbed dye is capable of fluorescence or that free dye remains. The persistent fluorescence may be due to intermolecular excimer formation from aggregated dyes, as reported for pyrene-based dyes bound to titania *via* carboxylic acid groups.<sup>84</sup>

## 6.5.5. NMR Spectroscopy

### 6.5.5.1. Introduction

$^1\text{H}$ -NMR spectroscopy was performed to investigate the altered environment experienced by dyes on binding to titania. While UV-Vis and FTIR studies provide information on the electronic transitions and molecular vibrations of dyes, respectively,  $^1\text{H}$ -NMR techniques offer information specific to chemically inequivalent atoms within the dye. Adsorption of dye on titania may result in a differential change in the chemical shifts depending on their proximity to the surface. A disadvantage of NMR spectroscopy is that relatively high concentrations are required on the order of 10 mM.<sup>86</sup>

Solid state NMR spectroscopy has been used to investigate the binding of species to nanoparticulate material and to titania. For instance,  $^{31}\text{P}$ -NMR spectroscopy has been used to confirm that Keggin units, such as the phosphomolybdic anion  $[\text{PMo}_{12}\text{O}_{40}]^{3-}$  and the analogous 12-tungstophosphoric acid, bind to aggregated and dry titania. A 0.5 to 0.9 ppm chemical shift of the signal was observed and attributed to adsorption of the intact Keggin unit.<sup>87, 88</sup>  $^1\text{H}$ -NMR of gold nanoparticles capped with mercaptoundecanoic phosphoric acid has found that the adsorbate is ordered due to intermolecular interactions between the acid groups. The increase in molecular ordering was reflected in an eight-fold decrease of the spin-lattice relaxation time,  $T_1$ .<sup>89</sup> Solid-state  $^{13}\text{C}$ -NMR has been used to investigate the conformation of carboxyalkylphosphonic acids bound onto zirconia and onto titania.<sup>11</sup> It was found that the methylene resonances of the alkyl chain broaden and shift downfield by 2 to 4 ppm. Solid-state  $^1\text{H}$ -NMR spectroscopy of dry titania colloids 50 to 400 nm in diameter has shown that in addition to the signal due to titanol groups at 1.3 ppm, water is bound in two different configurations, as indicated by signals at 3.8 and 6.1 ppm.<sup>51</sup> Similarly,  $^{13}\text{C}$ - and  $^{17}\text{O}$ -NMR spectroscopy has been used to confirm the replacement of ethoxide ligands of  $\text{Ti}_{16}\text{O}_{10}(\text{OCH}_2\text{CH}_3)_{32}$  clusters by carboxylic acid terminated dendrimers and that the titanium-oxo core remained intact.<sup>79</sup> The disadvantage of solid state NMR techniques is that if the signal-to-noise ratio is poor then a very large number of spectra must be acquired.

Solution phase  $^1\text{H}$ -NMR spectroscopy has been used to investigate opaque dispersions of rutile nanorods 15 nm in diameter and 40 to 100 nm in length. On functionalisation of titania with dopamine, 4-(2-aminoethyl)-1,2-benzenediol, a 0.04 ppm shift downfield relative to pure dopamine was recorded for all the aromatic protons.<sup>66</sup> Similarly,  $^1\text{H}$ - and  $^{17}\text{O}$ -NMR spectroscopy of titania clusters 2 to 3 nm in size have been used to confirm the chemical binding of 2,4-pentadione to the titanium-oxo core in both toluene solutions and in the solid state.<sup>23, 59</sup>  $^1\text{H}$ -NMR spectroscopy of dispersions of alkanethiols bound to gold and silver nanoparticles show both a downfield shift in signals and increased signal broadening for protons closer to the colloid surface, such that signals are lost for the methylene group next to the thiol.<sup>90</sup>

Line broadening may be expected if the sample population contains a range of different chemical or magnetic environments and if the spin-spin relaxation time,  $T_2$ , changes on binding. If dyes were adsorbed on titania nanoparticles with varied geometry and faults or if there was insoluble material, flocculation or coagulation, a range of different dye orientations and packing arrangements would result, with the slightly different  $^1\text{H}$ -NMR shifts resulting in a broadened line. For dyes adsorbed onto titania, peak broadening may be caused by inhomogeneities of the nanoparticles or by spin-spin relaxation. Spin-spin relaxation can be used to indicate whether dyes are intimately bound to titania nanoparticles, since in the presence of chemical binding of dyes to titania then the value of  $T_2$  should decrease.<sup>91</sup> The observed value of spin-spin relaxation,  $T_2^*$ , is a combination of true  $T_2$  and the effects of inhomogeneities of the applied magnetic field.<sup>61, 81</sup> In addition, if the sol-gel titania contains undercoordinated, paramagnetic  $\text{Ti}^{3+}$  sites, there will be broadened signals.

#### **6.5.5.2. Preliminary Experiments**

This study on the interaction of dyes with titania involved solution state  $^1\text{H}$ -NMR spectroscopy of dyes adsorbed on dispersed acidic sol-gel titania. Dyes **6.1** and **6.2** were employed, as they are small malonic acids with simple  $^1\text{H}$ -NMR spectra, containing sharp and discrete signals (Figs. 6.53, 6.54). Both dyes and sol-gel titania were soluble in deuteromethanol ( $\text{CD}_3\text{OD}$ ), so this solvent was used for most of the  $^1\text{H}$ -

NMR experiments. The hydrodynamic diameter of sol-gel titania, as measured by DLS number-average statistics, was 2.6 nm with a standard deviation of 20%. The adsorption of dye on titania results in a hydrophobic surface, which both reduced the hygroscopic character of the sol-gel titania and caused particle aggregation in aqueous media. However, provided that an organic solvent such as methanol was employed, DLS data showed that particle aggregation was circumvented, as the average diameter of titania did not increase on adsorption of **6.1** or **6.2**. As a representative of ter(thienylenevinylene) dyes, **6.3** was tested for use in  $^1\text{H-NMR}$  experiments (Fig. 6.55).

Probe dye **6.1**:

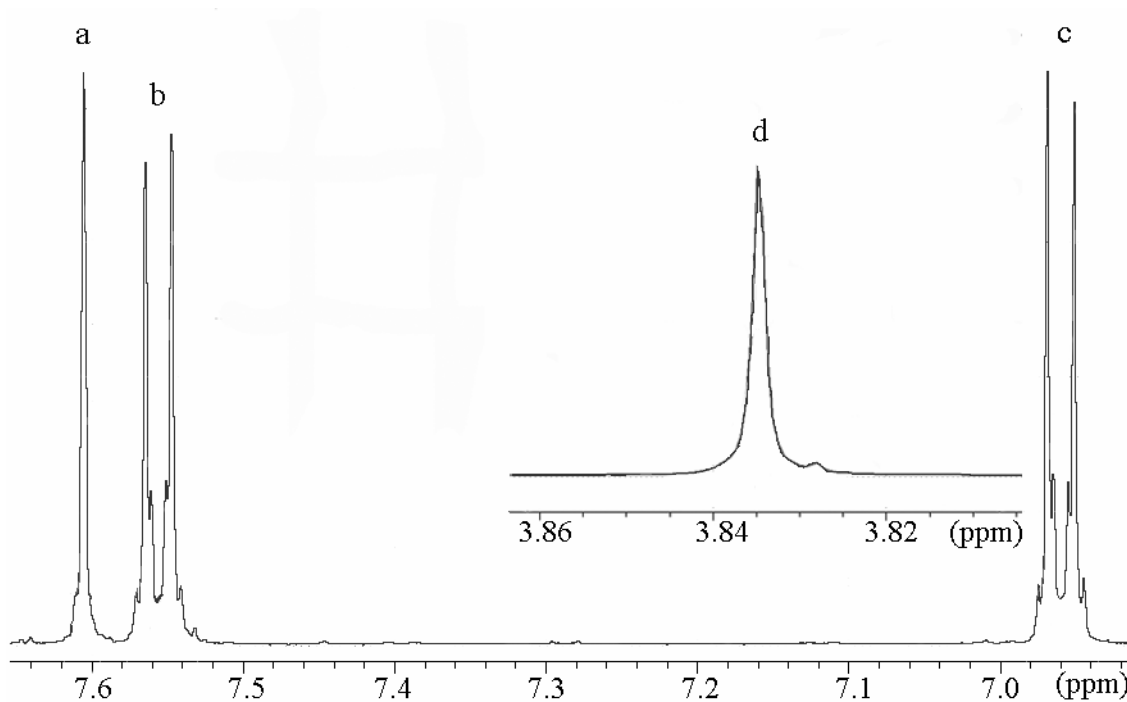
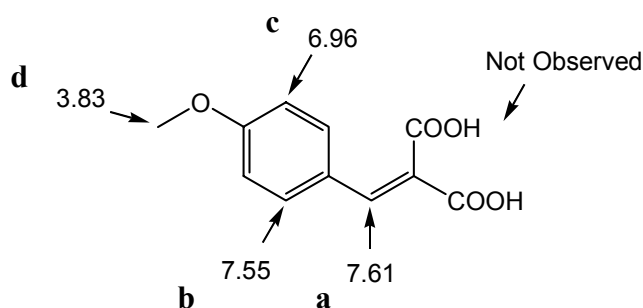


**Figure 6.53.**  $^1\text{H-NMR}$  spectrum of **6.1** in  $\text{CD}_3\text{OD}$ .

Probe dye **6.2**:

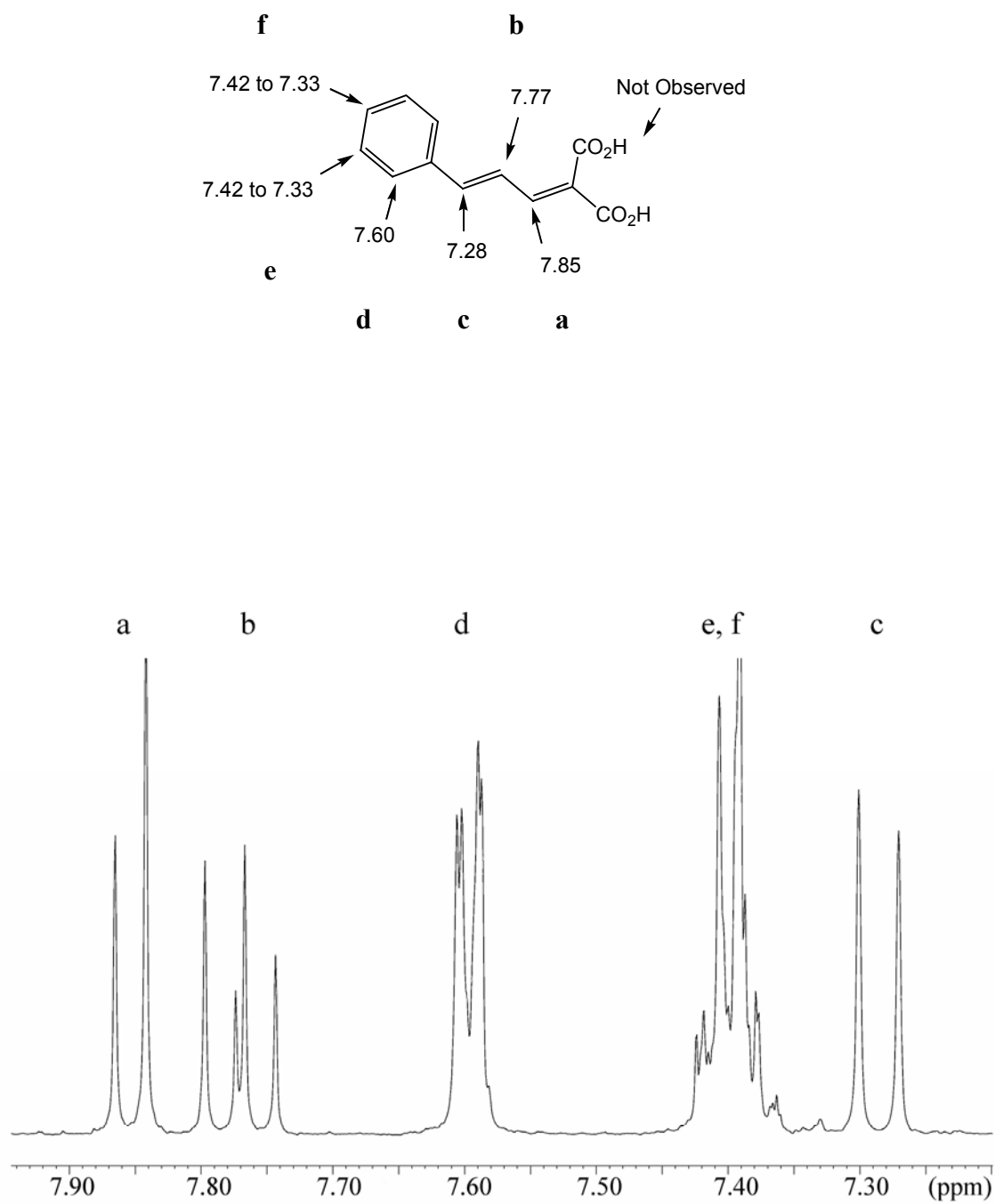


**Figure 6.54.** <sup>1</sup>H-NMR spectrum of **6.2** in CD<sub>3</sub>OD.

Probe dye **6.3**:

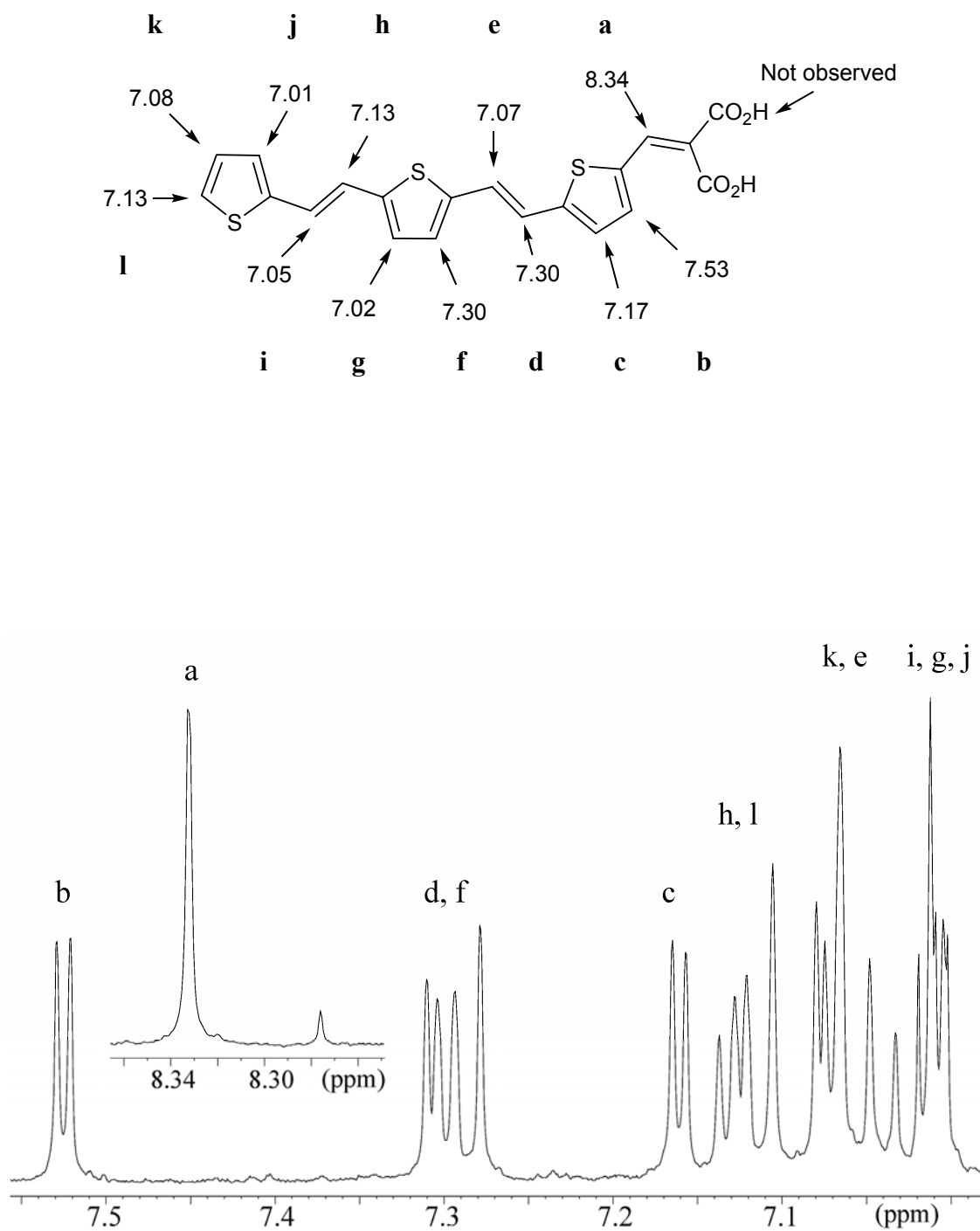


**Figure 6.55.**  $^1\text{H-NMR}$  spectrum of **6.3** in  $\text{CD}_3\text{OD}$ .

In order to distinguish whether changes in chemical shifts and signal broadening could be attributed to the adsorption of dye on titania, preliminary experiments were run. The first set of preliminary experiments was to obtain  $^1\text{H}$ -NMR spectra of salts of **6.1**. If dye **6.1** binds *via* a carboxylate form, then  $^1\text{H}$ -NMR spectra of the salts should bear a close resemblance to that of **6.1** adsorbed on titania. In addition, this experiment was used to confirm that signal broadening was not due to the formation of free salts of the dye in solution.  $^1\text{H}$ -NMR spectroscopy in  $\text{CD}_3\text{OD}$  of salts with a 1 : 1 and a 2 : 1 mole ratio of tetramethylammonium hydroxide to **6.1** show changes in chemical shifts, without peak broadening (Fig. 6.56). The greatest shift is that of the vinylic proton, which is closest to the deprotonated carboxylic group, with the signal at 7.61 ppm for the pure dye shifting to 7.52 and 7.06 ppm for the 1 : 1 and 2 : 1 salts, respectively.

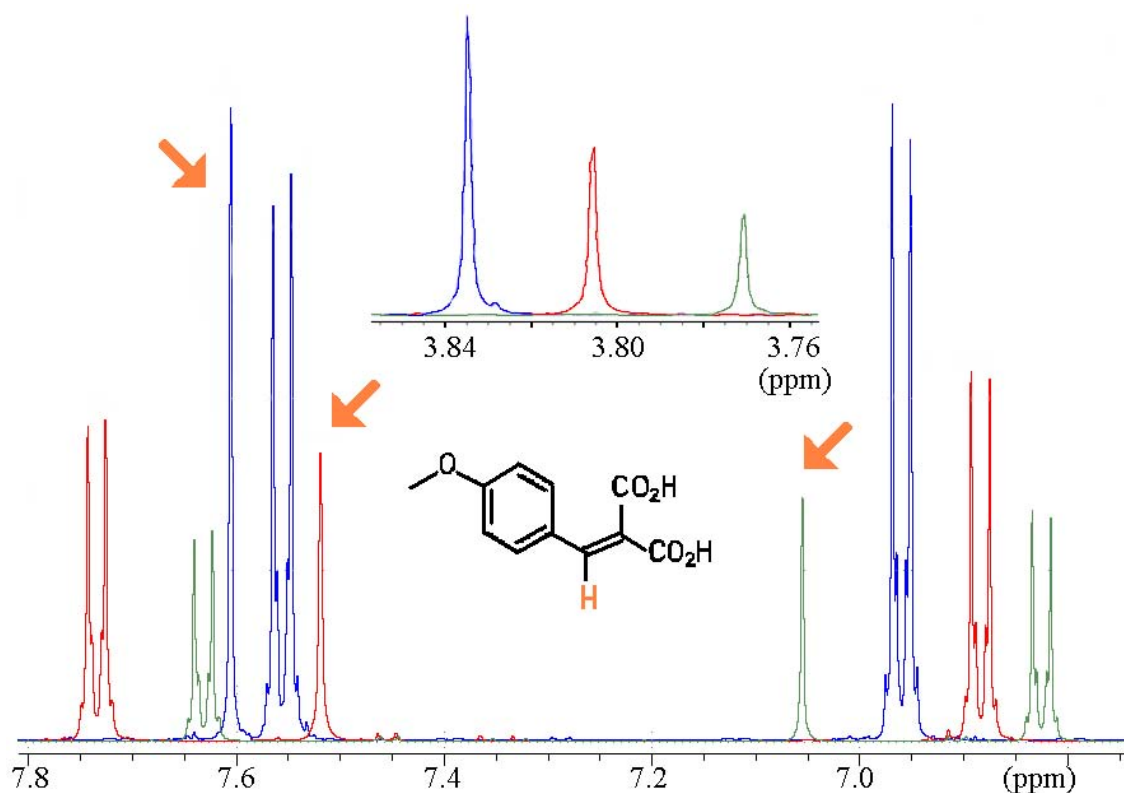


**Figure 6.56.**  $^1\text{H}$ -NMR spectra of the tetramethylammonium salt of **6.1** in  $\text{CD}_3\text{OD}$ . Pure **6.1** (—), a 1 : 1 mole ratio (—) and a 2 : 1 mole ratio of **6.1** to tetramethylammonium hydroxide (—).

Secondly, it was necessary to test that the simple presence of sol-gel titania was not the cause of signal broadening in  $^1\text{H-NMR}$  spectra. Furthermore, the possibility that changes in the spectra were due to the interaction of  $\pi$ -conjugated dyes with titania *via* dye  $\pi$  orbitals had to be ruled out. *Trans*-stilbene was chosen as like **6.1**, it is a  $\pi$ -conjugated species, but is not expected to bind to titania as it has no acidic or amine functionality. On the addition of sol-gel titania to *trans*-stilbene neither signal broadening nor shifts were observed. This confirmed that in the absence of a binding group on the dye that no change in  $^1\text{H-NMR}$  spectra should be expected on the addition of sol-gel titania. In addition, the lack of signal broadening for *trans*-stilbene in the presence of titania indicates that paramagnetic  $\text{Ti}^{3+}$  is not present in quantities that result in line broadening.

Finally, as the sol-gel titania is stabilised by hydrochloric acid, the probe dye used in  $^1\text{H-NMR}$  studies should show no change in chemical shift or signal broadening in the presence of hydrochloric acid. Direct titration of hydrochloric acid into solutions of probe dyes in  $\text{CD}_3\text{OD}$  showed that while **6.1** was unaffected by increased acidity, **6.2** and **6.3** showed chemical shifts of up to 0.05 ppm (Figs. 6.57, 6.58). Similar small changes in chemical shift have been reported for dopamine bound to rutile.<sup>66</sup> As shown in Figure 6.57, the effect of increased acidity is to alter the chemical shift of **6.2** from that of the pure dye, while the signals remain sharp. Figure 6.58 shows that while the change in chemical shift for **6.3** is a result of acidity, sol-gel titania causes broadened signals. The signals that are broadened for **6.3** with sol-gel titania are those that are closer to the binding group, such as the vinyl protons **a** and **d** and the thiophenyl protons **b** and **c**, but not protons such as **f**. Such signal broadening has been reported for alkanethiols bound to gold nanoparticles.<sup>90</sup> The higher solubility of **6.1** than ter(thienylenevinylene) dyes, such as **6.3**, in  $\text{CD}_3\text{OD}$  was another reason for using the smaller probe dye **6.1**. For instance, the higher concentration of **6.3** used for  $^1\text{H-NMR}$  experiments, than for UV-Vis experiments, results in the flocculation or coagulation of dye on the addition of sol-gel titania. The undesirable behaviour of **6.3** with acid and the low solubility, in comparison to **6.1** and **6.2** meant that ter(thienylenevinylene) dyes were not used in  $^1\text{H-NMR}$  experiments described later in this chapter.

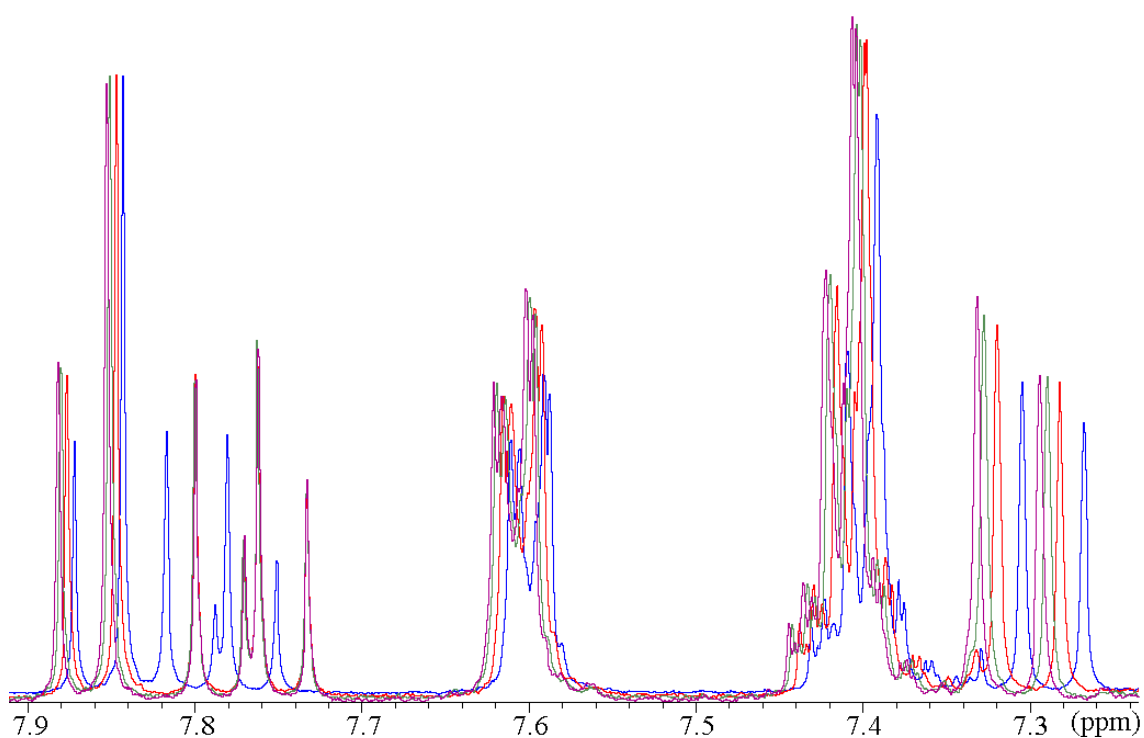


**Figure 6.57.**  $^1\text{H-NMR}$  spectra of a 12 M solution of **6.2** in  $\text{CD}_3\text{OD}$ , titrated with hydrochloric acid. A mole ratio of dye to hydrochloric acid of 1 : 0 (—), 1 : 45 (—), 1 : 89 (—) and 1 : 116 (—).

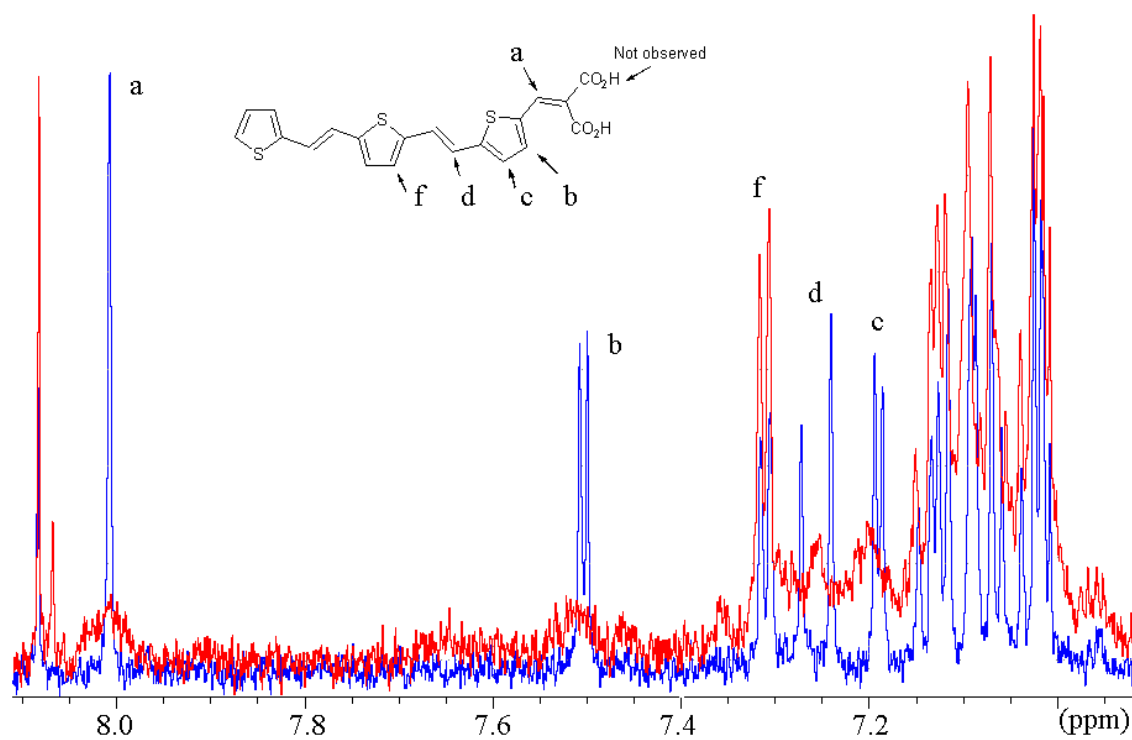


**Figure 6.58.**  $^1\text{H-NMR}$  spectra of **6.3** in  $\text{CD}_3\text{OD}$ , with a mole ratio of dye to hydrochloric acid of 1 : 124 (—) and with a mole ratio of dye to titania particles 2 nm in diameter of 19 : 1 (—).

### 6.5.5.3. Adsorption of Dye 6.1 on Sol-Gel Titania

Three techniques were used to obtain dyes bound to titania. The first was a direct titration of dye and titania into the NMR sample tube, the second was to drop-dry, wash then resuspend titrated material and the third, a solvent partition. As shown by UV-Vis experiments (Section 6.5.2, Fig. 6.14), dye binding on sol-gel titania is irreversible, so that direct titration of dye to titania should be able to produce submonolayer coverage with little free dye. From dye desorption studies using sintered titania, 6 to 8% of free dye will be present (Section 6.5.1); this range may indicate the likely amount of free dye present with dyed sol-gel titania. The second method involved the resuspension of dyed titania nanoparticles. A key assumption was that the washing stage removed all free dye from the bulk of the drop-dried material. Dye and sol-gel titania were first titrated within methanol to give less than the calculated monolayer coverage of dye for a titania sphere 2 nm in diameter. The solution was drop-dried onto glass, dried under high vacuum, then immersed within tetrahydrofuran to remove free dye. The film was redried, then immersed in methanol to solvate dyed titania. Supposing that bound dye is not removed from the titania surface on washing or resolution, the mole ratio of dye to titania should be that of the titration. However, the drop-drying process resulted in samples of which only approximately 80% was resuspendable. The final technique forms a solvent partition, by which free dye is separated from dyed titania nanoparticles (Fig. 6.59). Solvent partition experiments resemble that of direct titration, in that by using NMR solvents, sol-gel titania and dye may be reacted then examined by  $^1\text{H-NMR}$  spectroscopy without further treatment. Irreversible aggregation caused by sample drying, as in the resuspension technique, is then avoided. An advantage over direct titration is that the solvent partition method separates free and adsorbed dye on the basis of solubility.

As both sol-gel titania and the dyes are soluble in  $\text{CD}_3\text{OD}$ , the solvents used for the solvent partition method were deuterium oxide ( $\text{D}_2\text{O}$ ) and deuteriochloroform ( $\text{CDCl}_3$ ). Sol-gel titania dissolved in  $\text{D}_2\text{O}$  was slowly added to a saturated solution of dye in  $\text{CDCl}_3$  and left to sit. The diffusion of dye through the solvent interface was a limiting step, as stirring of the sample would form an emulsion. The experiment relies on dye diffusion, so the mole ratio of dye to titania that is used places an upper limit on dye coverage, but will not correspond to the actual concentration of adsorbed dye. Dyed

nanoparticles will only be found in the D<sub>2</sub>O phase if less than a monolayer of dye is adsorbed, so that the titania surface remains sufficiently hydrophilic. While both dyed and free nanoparticles are retained in the D<sub>2</sub>O phase, the excess of titania should ensure the adsorption of any free dye, even if dye binding was an equilibrium. Consequently, <sup>1</sup>H-NMR spectra of the D<sub>2</sub>O portion corresponds to that of dye adsorbed on titania. Dyed titania was apparent at the CDCl<sub>3</sub>-D<sub>2</sub>O interface, which was less than a tenth of the total volume, but was not sampled in order to eliminate both unbound dye and CDCl<sub>3</sub> from <sup>1</sup>H-NMR spectra of the D<sub>2</sub>O layer.

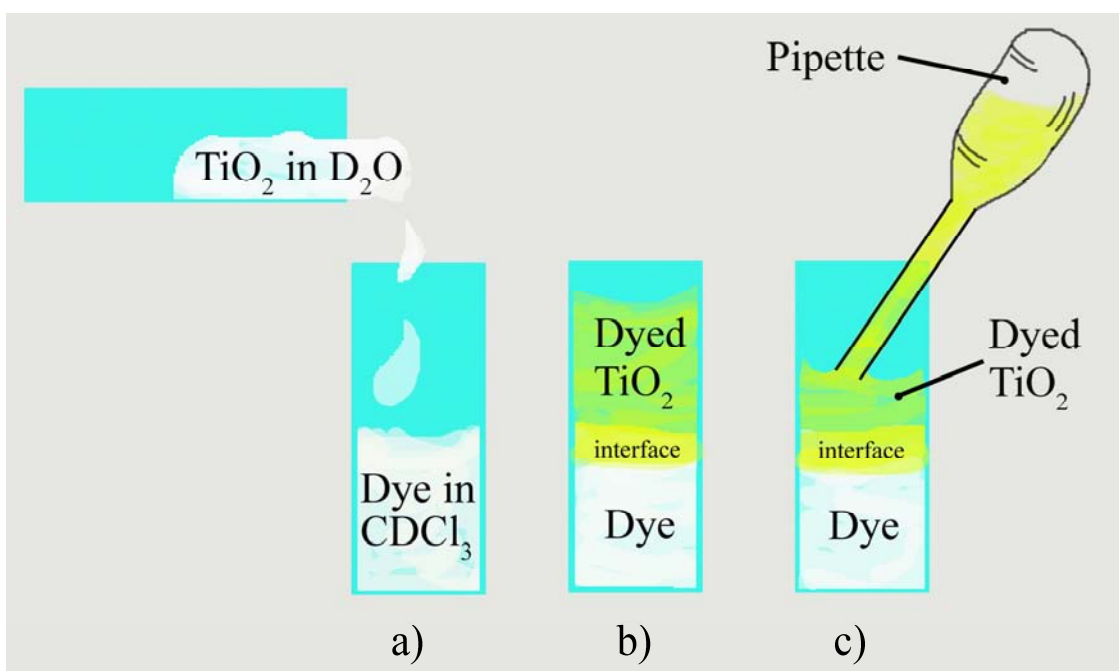


**Figure 6.59.** A cartoon of the solvent partition method. a) Sol-gel titania solvated in D<sub>2</sub>O is added to a saturated solution of dye in CDCl<sub>3</sub>. b) Dye diffuses through the solvent-solvent interface and binds to titania in the D<sub>2</sub>O layer. c) The D<sub>2</sub>O layer was removed by pipette for analysis by NMR spectroscopy.

Titration experiments of **6.1** with titania in CD<sub>3</sub>OD were done by the addition of dye to titania and by the titration of titania into dye. The same results were obtained, regardless of whether the dye or titania was the majority species at the beginning of the experiment. The spectra of **6.1** titrated directly with titania closely resembles that of pure dye, with no change in chemical shift, though signals sharpen on increasing the

ratio of dye to titania particles (Fig. 6.60). The signal broadening can be thus be attributed to bound dye. In addition, Figure 6.60 shows that  $^1\text{H-NMR}$  signals due to the vinyl and aromatic protons, which are located closer to the binding group, are broadened more than the distant methoxy group protons. It is interesting to note the lineshapes of the signals of protons **a** to **d** and the much smaller signals that have appeared on titration of dye with titania. As the signal-to-noise ratio of the solution state  $^1\text{H-NMR}$  spectra were already low, there was no benefit to be gained from solid state  $^1\text{H-NMR}$  spectroscopy, which would require far longer times to collect good spectra.

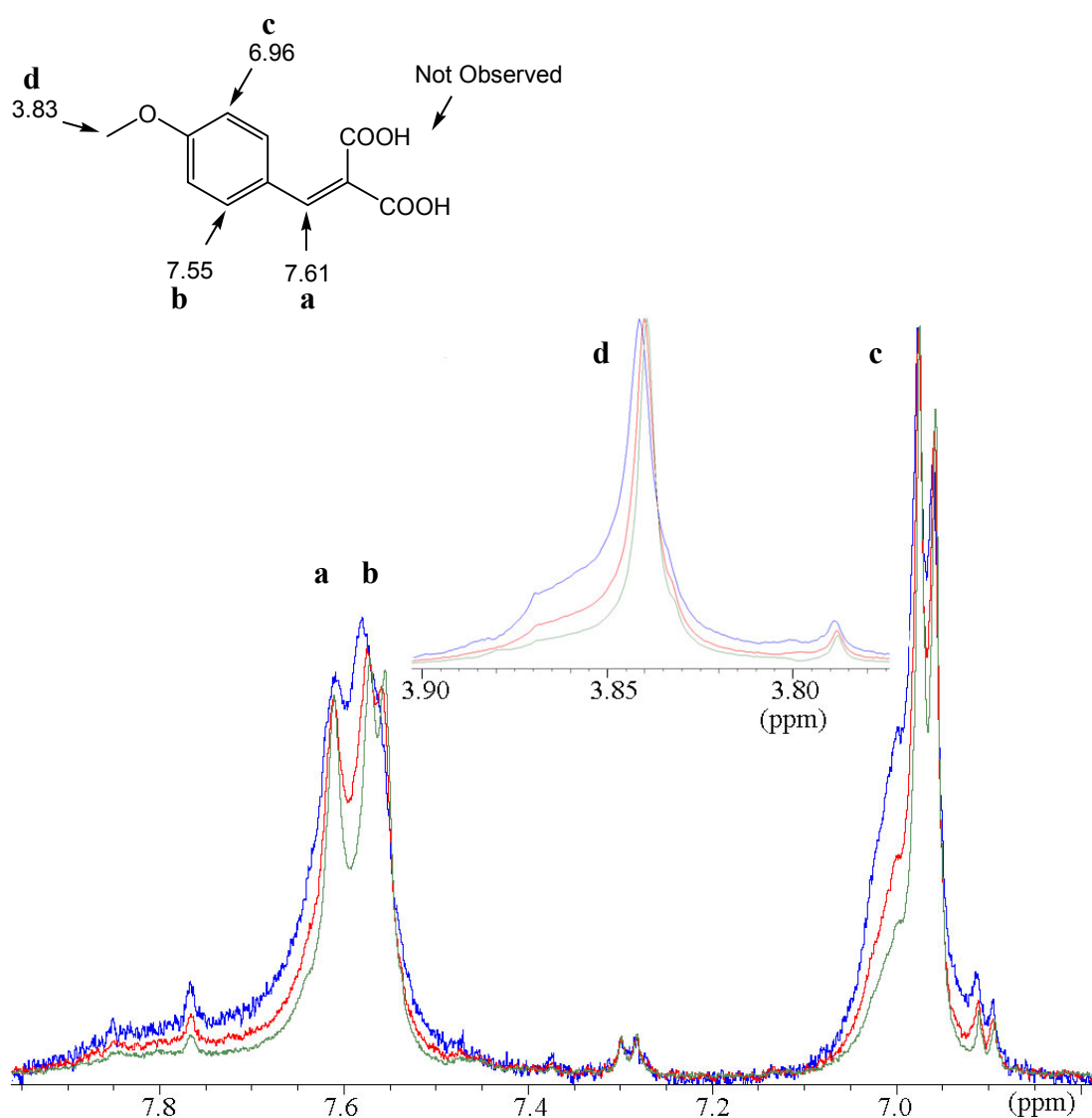


**Figure 6.60.**  $^1\text{H-NMR}$  spectra of the titration of **6.1** with acidic amorphous sol-gel titania in  $\text{CD}_3\text{OD}$ . An 8 : 1 (—), 12 : 1 (—) and a 17 : 1 mole ratio of **6.1** to titania particles 2 nm in diameter (—).

For resuspension experiments, samples were first titrated to have less than the calculated monolayer coverage of a 28 : 1 mole ratio of dye to titania. In the case of a sample with an 18 : 1 mole ratio, the methanol-soluble portion gave a clear, yellow solution with fine particles of titania with a  $^1\text{H-NMR}$  spectrum with both broad and sharp signals overlaid upon each other (Fig. 6.61). As the sharp signals have the same chemical shift as free dye, this indicates that free dye is present in addition to bound dye. As the broad signals originate from adsorbed dye, the sharp signals may be due to both physisorbed dye that was not removed by immersion of the drop-dried material in tetrahydrofuran and any dye desorbed from titania.

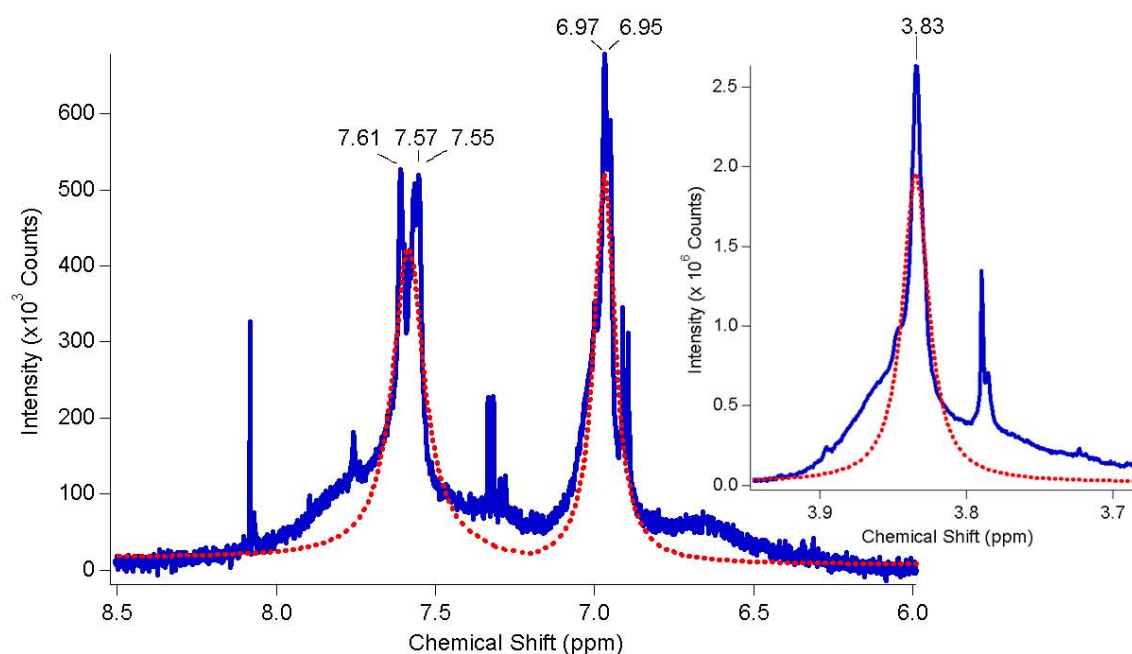


**Figure 6.61.**  $^1\text{H-NMR}$  spectrum of the methanol-soluble portion of a titania resuspension experiment. The mole ratio of **6.1** to 2 nm titania particles was 18 : 1. A crude indication of the position of sharp overlaid signals due to free dye (.....).

Solvent partition experiments would ideally use  $\text{D}_2\text{O}$  spiked with the sodium salt of 3-(trimethylsilyl)-1-propanesulfonic acid (DSS) to provide an internal standard for the calibration of chemical shifts. However, use of  $\text{D}_2\text{O}$  spiked with 1% wt/wt DSS resulted in the immediate flocculation of titania and salt formation of dye with DSS (Fig. 6.62), which could be confused with salt formation on the surface of titania. The

two new vinyl proton chemical shifts at 7.35 and 7.34 ppm indicate that two inequivalent forms of carboxylate salt are present. The two vinyl proton signals are due either to a mixture of mono- and di-salts or to a mono-salt positioned *cis*- and *trans*- to the aromatic ring (Fig. 6.63). If the  $^1\text{H}$ -NMR spectrum of the tetramethylammonium salt of 6.1 in  $\text{CD}_3\text{OD}$  is used as a guide (Fig. 6.56), then the signals at 7.35 and 7.34 ppm are due to the mono- and di-salt, respectively.

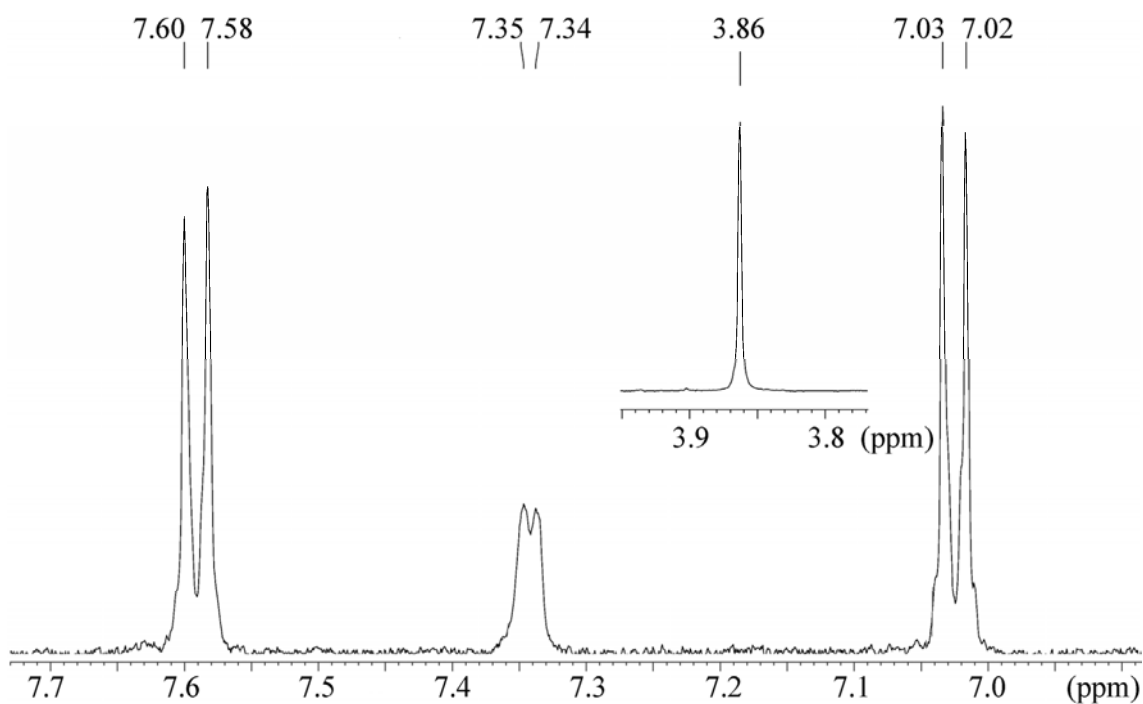


**Figure 6.62.**  $^1\text{H}$ -NMR spectrum of a 2 mM solution of **6.1** in  $\text{D}_2\text{O}$ -DSS.

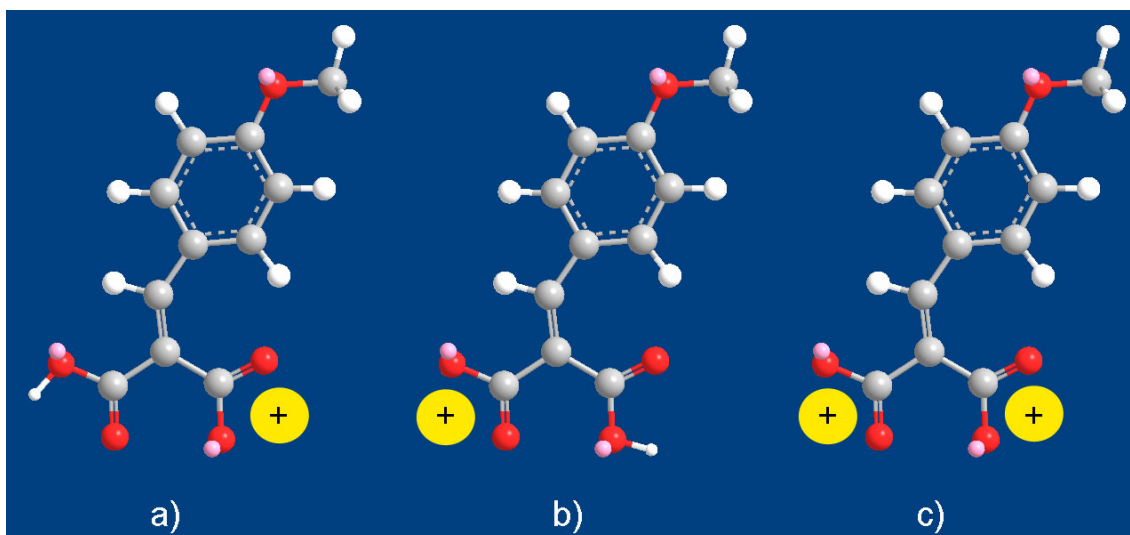


**Figure 6.63.** Representations of: (a) the *cis*- and (b) the *trans*- mono-salt forms and (c) the di-salt of **6.1**.

In a typical partition experiment procedure, a clear and colourless suspension of native sol-gel titania in  $D_2O$  was added atop a saturated, white and opaque suspension of **6.1** in  $CDCl_3$ . The interface became a bright, yellow colour, which is indicative of dye adsorption, as pure **6.1** gives a clear and colourless solution, while the dye is bright yellow in the solid state. While **6.1** is soluble in  $D_2O$ , given a saturated solution, the chemical shifts are sharp (Fig. 6.64), unlike that of **6.1** in the presence of sol-gel titania (Fig. 6.65). It is then simple to discriminate signals due to free dye from that of dye bound to titania.

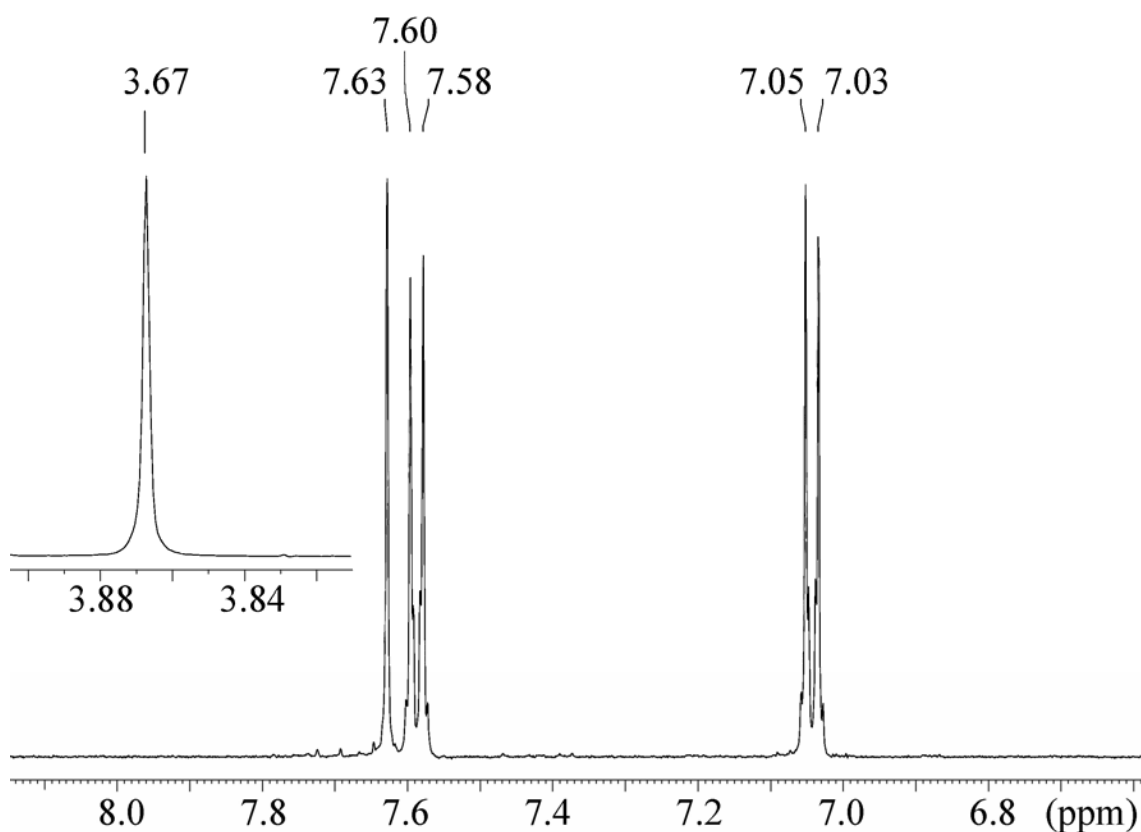


**Figure 6.64.**  $^1\text{H-NMR}$  spectrum of a saturated solution of **6.1** in  $\text{D}_2\text{O}$ .

First, a partition experiment containing an initial mole ratio of 12 : 1 of **6.1** to 2 nm titania particles was run with  $\text{D}_2\text{O}$  containing 0.7% wt/wt of DSS (Fig. 6.65). The bright, yellow  $\text{D}_2\text{O}$  layer was filtered through cotton-wool directly into NMR tubes. The  $^1\text{H-NMR}$  spectrum shows broad signals centred at 7.0 and 7.6 ppm, which correspond to the aromatic protons of **6.1**. Two chemical shifts of 7.16 and 7.26 ppm due to the vinyl proton indicate that two forms of carboxylate salt are present. A chemical shift of water of 4.76 ppm was used to calibrate the spectra of solvent partition experiments run in pure  $\text{D}_2\text{O}$ . The  $^1\text{H-NMR}$  spectrum of a typical partition experiment is shown in Figure 6.66, where sol-gel titania in  $\text{D}_2\text{O}$  was introduced to **6.1** in  $\text{CDCl}_3$  for an initial mole ratio of **6.1** to 2 nm titania particles of 17 : 1. By comparison with Figures 6.56, 6.62 and 6.65, it is clear that dye is not chemically bound to titania as a carboxylate species. While the signal to noise ratio was too low to permit the collection of a  $^1\text{H-COSY}$  spectrum to confirm peak assignments, the  $^1\text{H-NMR}$  spectrum of the  $\text{D}_2\text{O}$  layer shows broad signals that are due to adsorbed **6.1**.

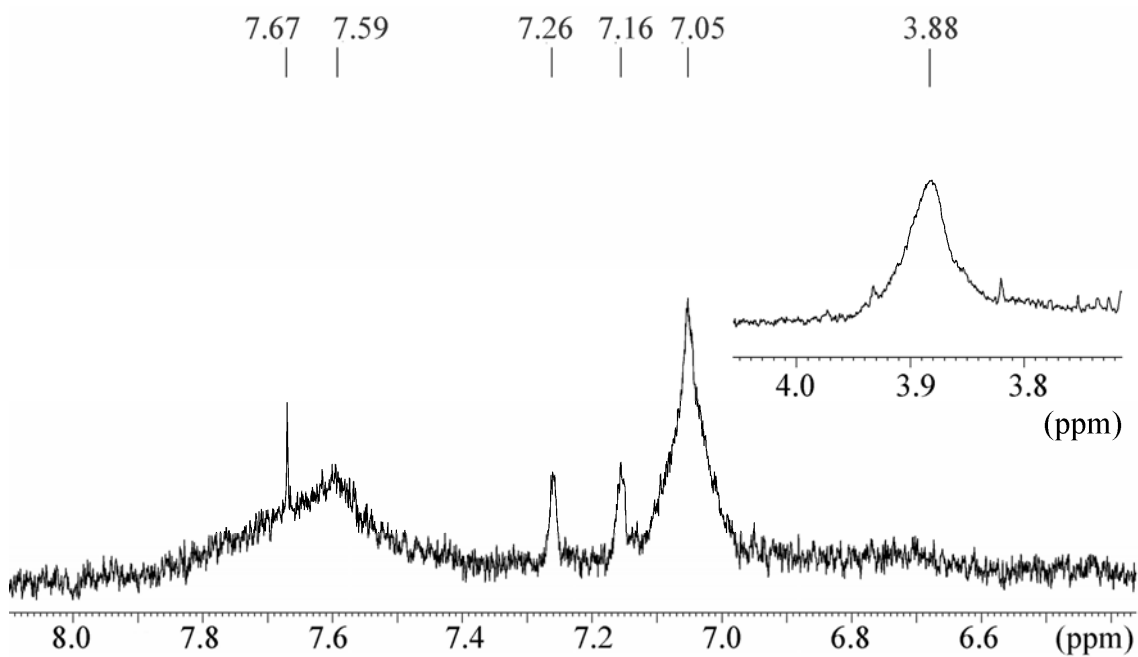


**Figure 6.65.**  $^1\text{H}$ -NMR spectrum of an initial 12 : 1 mole ratio of **6.1** to 2 nm titania particles in  $\text{D}_2\text{O}$ -DSS.

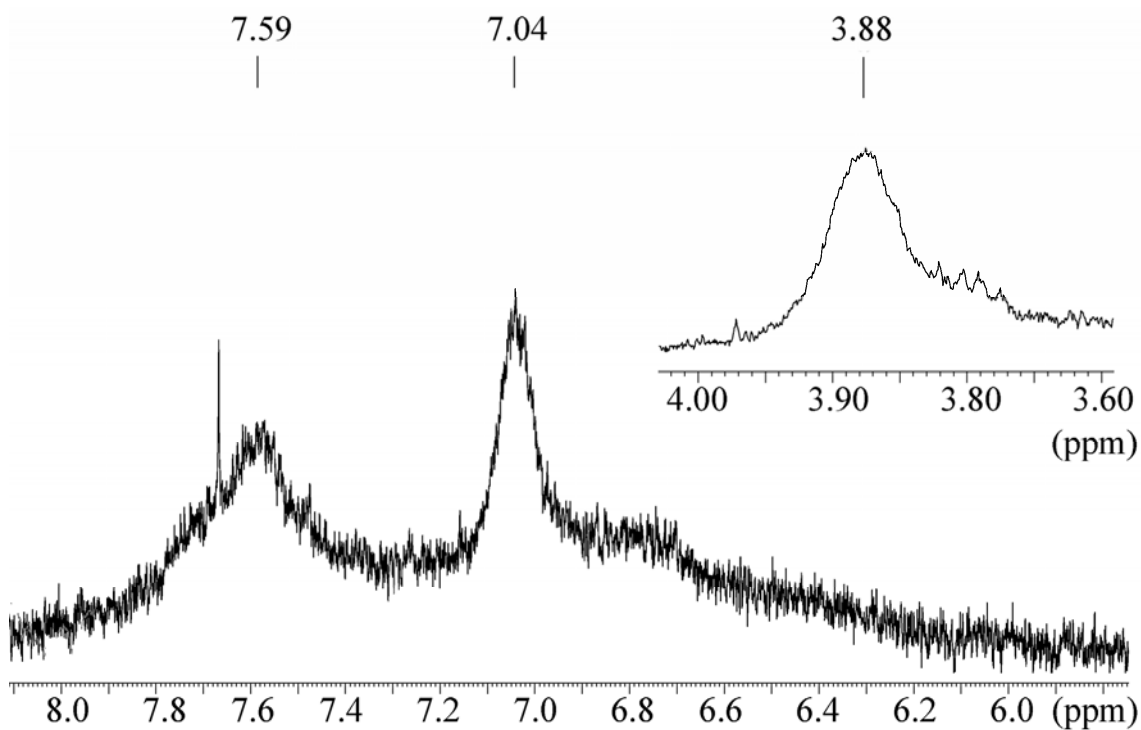


**Figure 6.66.**  $^1\text{H}$ -NMR spectrum of the  $\text{D}_2\text{O}$  layer of a partition experiment that used an initial 17 : 1 mole ratio of **6.1** to 2 nm titania particles.

It was necessary to confirm that the broad lineshapes observed in  $^1\text{H}$ -NMR spectra of solvent partition experiments is due to adsorbed dye, rather than to aggregation effects in  $\text{D}_2\text{O}$ . If aggregation is responsible for signal broadening, dilution in a suitable solvent, such as  $\text{CD}_3\text{OD}$ , will reduce aggregation and produce sharper signals.  $\text{CD}_3\text{OD}$  was chosen as the adsorption of dye results in a more hydrophobic surface than that of native sol-gel titania. Aggregation effects were suspected to contribute to line broadening, as the DLS number-average diameter of dyed titania nanoparticles of a  $0.7\ \mu\text{M}$  solution in water was 120 nm with a standard deviation of 30%. When the same sample was diluted in methanol, a diameter of 4.1 nm with a standard deviation of 13% was obtained, which is not much greater than that of native sol-gel titania in water. At similar concentrations, native sol-gel titania has an average particle size of 2.4 nm in water and 3.4 nm in methanol with respective standard deviations of 24% and 15%. To investigate aggregation effects,  $^1\text{H}$ -NMR spectra were collected of a solvent partition experiment run with neat  $\text{D}_2\text{O}$  and  $\text{CDCl}_3$ . An aliquot of the  $\text{D}_2\text{O}$  layer was diluted with  $\text{CD}_3\text{OD}$  to concentrations comparable to that of the DLS experiments, with a 3x and 10x dilutions giving approximately  $1.5\ \mu\text{M}$  and  $5.0\ \mu\text{M}$  solutions of titania, respectively. The  $^1\text{H}$ -NMR spectra of dilutions show broad signals similar to those observed in previous solvent partition experiments, without a reduction in FWHM on dilution from the 3x dilution to the 10x dilution (Fig. 6.67). The low signal-to-noise ratio gave a large uncertainty in FWHM measurements of  $^1\text{H}$ -NMR spectra, with values of  $1.6$  and  $1.3\ \text{ppm} \pm 20\%$  at the chemical shift of  $7.0\ \text{ppm}$  for the 3x and 10x dilutions, respectively. The lack of sharp chemical shifts that may be assigned to free **6.1** supports the argument that broadening of the probe dye  $^1\text{H}$ -NMR signals is due to binding of dye to the titania surface, rather than to particle aggregation.

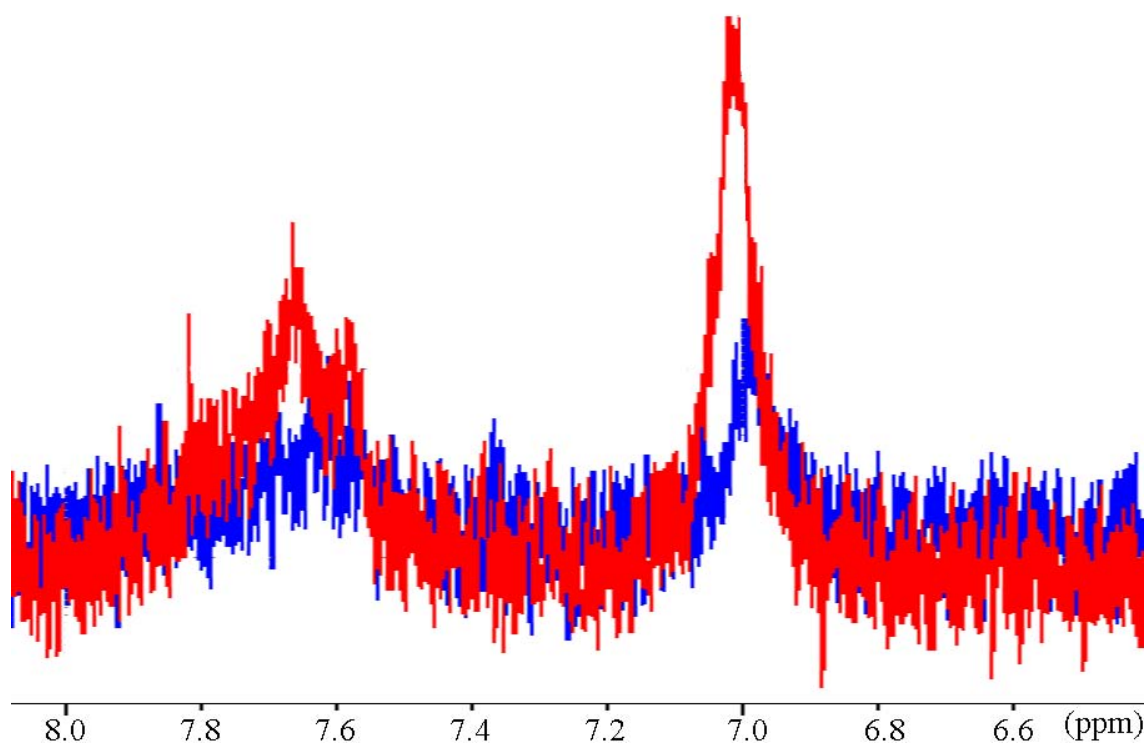


**Figure 6.67.**  $^1\text{H}$ -NMR spectra of the  $\text{D}_2\text{O}$  layer of a solvent partition experiment, which used an initial 12 : 1 mole ratio of **6.1** to 2 nm titania particles. A 3x (—) and a 10x (—) dilution in  $\text{CD}_3\text{OD}$ .

Supporting data is given by  $T_2$  relaxation times and diffusion data collected by Dr. Patrick Edwards for samples of **6.1** titrated with sol-gel titania for submonolayer coverage. Spin-spin  $T_2$  relaxation times for free and bound **6.1** were collected by direct measurement from a  $^1\text{H}$ -NMR Carr-Purcell-Meiboom-Gill (CPMG) spin echo experiment. The CPMG spin echo pulse sequence removes signal broadening effects due to inhomogeneities in the applied magnetic field and chemical shift variation as a consequence of non-uniformities in the binding of dye to nanoparticles by refocusing signals with a series of  $90^\circ$  and  $180^\circ$  magnetic pulses. 12 mM solutions of **6.1** in  $\text{CD}_3\text{OD}$  gave  $T_2$  values of 1.60 and 0.40 seconds, respectively, for pure dye and dye with a mole ratio of **6.1** to titania of 7 : 1. The smaller  $T_2$  value for **6.1** with sol-gel titania indicates that dye is bound to the surface. As the  $T_2$  values were calculated from the signal of the methoxy protons, which are furthest from the binding site, that the methoxy group is affected by adsorption to titania, this is good evidence for dye binding.

Diffusion coefficients for free and bound **6.1** were measured by <sup>1</sup>H-NMR spectroscopy using a pulsed field gradient and a simulated echo. The concentration of **6.1** used in diffusion experiments was 12 mM, while the mole ratio of dye to titania was 7 : 1. The measured diffusion coefficients for free **6.1** and **6.1** with sol-gel titania in CD<sub>3</sub>OD at 298K were 1 x 10<sup>-9</sup> m<sup>2</sup> s<sup>-1</sup> and 4 x 10<sup>-10</sup> m<sup>2</sup> s<sup>-1</sup>, respectively. The diffusion coefficient of dyed titania is less than half that of the free dye, which supports the argument that **6.1** is bound. The Stokes-Einstein relation may be used to derive the hydrodynamic radius from the diffusion coefficient, provided that the radius of the species is larger than that of the solvent.<sup>61, 91</sup> By using a value for (kT)/(6π $\eta$ ) of 3.9904 x 10<sup>-19</sup> m<sup>3</sup> s<sup>-1</sup> (Eq. 6.3), the calculated effective hydrodynamic radii for free and bound **6.1** were 0.4 and 1.0 nm, respectively. These values are in good agreement with calculated length of **6.1** of 0.9 nm (Section 8.3) and the measured diameter of 2.6 nm for the sol-gel titania, which is further evidence that **6.1** is adsorbed on the dispersed titania nanoparticles.

$$D = \frac{kT}{6\pi\eta r} \quad (6.3)$$

k - Boltzmann's constant. (1.3807 x 10<sup>-23</sup> J K<sup>-1</sup>)  
 T - temperature. (298K).  
 $\eta$  - viscosity of the solvent. (5.47 x 10<sup>-4</sup> kg m<sup>-1</sup> s<sup>-1</sup> for methanol at 298K)  
 r - radius of a spherical particle.

#### 6.5.5.4. Summary

Chemical shift broadening of <sup>1</sup>H-NMR signals, spin-spin T<sub>2</sub> relaxation times, measured diffusion coefficients and the calculated hydrodynamic radii indicate that the dye **6.1** is bound to the sol-gel titania. A decrease in T<sub>2</sub> relaxation time and an increase of the diffusion coefficient has been used as evidence for binding in the case of dispersed gold nanoparticles bearing a monolayer of the thiol tiopronin.<sup>91</sup> Signal broadening on the binding of carboxyalkylphosphonic acids to titania has also been observed with solid-state <sup>13</sup>C-NMR spectroscopy.<sup>11</sup> As the <sup>1</sup>H-NMR chemical shifts of **6.1** bound to dispersed sol-gel titania are identical to that of the free **6.1**, this indicates that in a solvated environment the carboxylic acid probe dye is bound in a form similar to that of the free dye, rather than as a carboxylate salt.

## 6.6. Section Summary

In summary, carboxylic acids are bound to titania.  $^1\text{H-NMR}$  data, including spin-spin relaxation and diffusion measurements, supports the intimate association of carboxylic acid dyes to sol-gel titania. Results from fluorescence and Raman spectroscopy were inconclusive as to whether dye was irreversibly bound or present as an equilibrium. Evidence from UV-Vis studies gives support for the equilibrium binding of carboxylic acids to titania, as reported for ruthenium coordination compound dyes.<sup>4</sup> UV-Vis spectra displayed a difference in dye aggregation that appeared to depend on the presence of solvent: probe dyes adsorbed on dry sintered crystalline surfaces gave H-aggregates, while on dispersed amorphous sol-gel titania the UV-Vis shifts corresponded to J-aggregate formation. However, it is possible that the underlying cause of the complementary UV-Vis shifts is the difference between the two titania surfaces.

Results from ATR-FTIR and  $^1\text{H-NMR}$  spectroscopy indicate that the binding mode of probe dyes upon sol-gel titania is dependent on the degree of solvation. ATR-FTIR studies show that in dry samples the carbonyl  $\nu(\text{C=O})$  stretch is absent or greatly reduced, implying that dyes are largely bound as a carboxylate species. This is in agreement with the reported carboxylate binding of species such as mercaptosuccinic acid upon dry, crystalline titania<sup>18</sup> and of glutamic acid on a solvated, amorphous titania film.<sup>43</sup> In contrast,  $^1\text{H-NMR}$  spectroscopy shows that though there is signal broadening following the adsorption of dyes, as observed for the binding of carboxyalkylphosphonic acids to titania powder,<sup>11</sup> no significant shift in line position was observed. This indicates that dye is bound in a form that resembles that of the free dye, which could be *via* electrostatic attraction or a pseudo-ester linkage, as opposed to a carboxylate species.

It is possible that while the binding of dye to titania may allow the displacement of dye from the surface, as shown by UV-Vis spectroscopy,  $^1\text{H-NMR}$  data appears to support the stabilisation of electrostatic or pseudo-ester binding of dye to titania. Conversely, as shown by ATR-FTIR spectroscopy, the loss of solvent appears to promote carboxylate binding as the dominant mode.

Further work is required with computer modelling to provide simulated spectra. Comparison of modelled and experimental data would aid the assignment of vibrational modes that are present after the binding of dye to titania. It is possible that surface-sensitive techniques, such as X-ray photoelectron spectroscopy could be used to determine the binding mode of dyes to titania *via* the oxidation state of organic and inorganic atoms at the point of dye binding.

## 6.7. References

1. Robertson, N. Optimising Dyes for Dye-Sensitized Solar Cells. *Angewandte Chemie International Edition* **2006**, 45, 2338-2345.
2. Galoppini, E. Linkers for Anchoring Sensitizers to Semiconductor Nanoparticles. *Coordination Chemistry Reviews* **2004**, 248, 1283-1297.
3. Tributsch, H. Dye Sensitization Solar Cells: a Critical Assessment of the Learning Curve. *Coordination Chemistry Reviews* **2004**, 248, 1511-1530.
4. Nazeeruddin, M K; Humphry-Baker, R; Liska, P; Grätzel, M. Investigation of Sensitizer Adsorption and the Influence of Protons on Current and Voltage of a Dye-Sensitized Nanocrystalline TiO<sub>2</sub> Solar Cell. *Journal of Physical Chemistry B* **2003**, 107, 8981-8987.
5. Campbell, W M; Burrell, A K; Officer, D L; Jolley, K W. Porphyrins as Light Harvesters in the Dye-Sensitized TiO<sub>2</sub> Solar Cell. *Coordination Chemistry Reviews* **2004**, 248, 1363-1379.
6. Schwarzburg, K; Emstorfer, R; Felber, S; Willig, F. Primary and Final Charge Separation in the Nano-Structured Dye-Sensitized Electrochemical Solar Cell. *Coordination Chemistry Reviews* **2004**, 248, 1259-1270.
7. Liu, Y; Scully, S R; McGehee, M D; Liu, J; Luscombe, C K; Frechet, J M J; Shaheen, S E; Ginley, D S. Dependence of Band Offset and Open-Circuit Voltage on the Interfacial Interaction Between TiO<sub>2</sub> and Carboxylated Polythiophenes. *Journal of Physical Chemistry B* **2006**, 110, 3257-3261.
8. Shriver, D F; Atkins, P W; Langford, C H. *Inorganic Chemistry*. Oxford University Press: Cambridge, **1990**.
9. Wang, Q; Campbell, W M; Bonfantani, E E; Jolley, K W; Officer, D L; Walsh, P J; Gordon, K; Humphry-Baker, R; Nazeeruddin, M K; Grätzel, M. Efficient Light Harvesting by Using Green Zn-Porphyrin-Sensitized Nanocrystalline TiO<sub>2</sub> Films. *Journal of Physical Chemistry B* **2005**, 109, 15397-15409.
10. Grätzel, M. Conversion of Sunlight to Electric Power by Nanocrystalline Dye-Sensitized Solar Cells. *Journal of Photochemistry and Photobiology A: Chemistry* **2004**, 164, 3-14.
11. Pawsey, S; Yach, K; Reven, L. Self-Assembly of Carboxyalkylphosphonic Acids on Metal Oxide Powders. *Langmuir* **2002**, 18, 5205-5212.
12. Zhuang, J; Rusu, C N; Yates, J T J. Adsorption and Photooxidation of CH<sub>3</sub>CN on TiO<sub>2</sub>. *Journal of Physical Chemistry B* **1999**, 103, 6957-6967.
13. Bulanin, K M; Lavalley, J C; Tsyganenko, A A. Infrared Study of Ozone Adsorption on TiO<sub>2</sub> (Anatase). *Journal of Physical Chemistry* **1995**, 99, 10294-10298.
14. Davit, P; Martra, G; Coluccia, S; Augugliaro, V; Garcia Lopez, E; Loddo, V; Marci, G; Palmisano, L; Schiavello, M. Adsorption and Photocatalytic Degradation of Acetonitrile: FT-IR Investigation. *Journal of Molecular Catalysis A: Chemical* **2003**, 204-205, 693-701.
15. Bae, E; Choi, W; Park, J; Shin, H S; Kim, S B; Lee, J S. Effects of Surface Anchoring Groups (Carboxylate vs Phosphonate) in Ruthenium-Complex-Sensitized TiO<sub>2</sub> on Visible Light Reactivity in Aqueous Suspensions. *Journal of Physical Chemistry B* **2004**, 108, 14093-14101.
16. Nazeeruddin, M K; Humphry-Baker, R; Officer, D L; Campbell, W M; Burrell, A K; Grätzel, M. Application of Metalloporphyrins in Nanocrystalline Dye-Sensitized Solar Cells for Conversion of Sunlight into Electricity. *Langmuir* **2004**, 20, 6514-6517.
17. Hara, K; Sugihara, H; Tachibana, Y; Islam, A; Yanagida, M; Sayama, K; Arakawa, H. Dye-

Sensitised Nanocrystalline TiO<sub>2</sub> Solar Cells Based on Ruthenium(II) Phenanthroline Complex Photosensitisers. *Langmuir* **2001**, 17, 5992-5999.

18. Angelome, P C; Aldabe-Bilmes, S; Calvo, M E; Crepaldi, E; Grosso, D; Sanchez, C; Soler-Illia, G J A A. Hybrid Non-Silica Mesoporous Thin Films. *New Journal of Chemistry* **2005**, 29, 59-63.

19. Vittadini, A; Selloni, A; Rotzinger, F P; Grätzel, M. Formic Acid Adsorption on Dry and Hydrated TiO<sub>2</sub> Anatase (110) Surfaces by DFT Calculations. *Journal of Physical Chemistry B* **2000**, 104, 1300-1306.

20. Deacon, G B; Phillips, R J. Relationships Between the Carbon-Oxygen Stretching Frequencies of Carboxylate Complexes and the Type of Carboxylate Coordination. *Coordination Chemistry Reviews* **1980**, 33, 227-250.

21. Nakamoto, K. *Infrared and Raman Spectra of Inorganic and Coordination Compounds*. 4<sup>th</sup> ed, John Wiley & Sons Inc.: **1986**.

22. Brownson, J R S; Tejedor-Tejedor, M I; Anderson, M A. Photoreactive Anatase Consolidation Characterized by FTIR Spectroscopy. *Chemistry of Materials* **2005**, 17, 6304-6310.

23. Scolan, E; Sanchez, C. Synthesis and Characterization of Surface-Protected Nanocrystalline Titania Particles. *Chemistry of Materials* **1998**, 10, 3217-3223.

24. Duffy, N W; Dobson, K D; Gordon, K C; Robinson, B H; McQuillan, A J. *In Situ* Infrared Spectroscopic Analysis of the Adsorption of Ruthenium(II) Bipyridyl Dicarboxylic Acid Photosensitisers to TiO<sub>2</sub> in Aqueous Solutions. *Chemical Physics Letters* **1997**, 266, 451-455.

25. Brownson, J R S; Tejedor-Tejedor, M I; Anderson, M A. FTIR Spectroscopy of Alcohol and Formate Interactions with Mesoporous TiO<sub>2</sub> Surfaces. *Journal of Physical Chemistry B* **2006**, 110, 12494-12499.

26. Rasko, J; Hancz, A; Erdohelyi, A. Surface Species and Gas Phase Products in Steam Reforming of Ethanol on TiO<sub>2</sub> and Rh/TiO<sub>2</sub>. *Applied Catalysis A: General* **2004**, 269, 13-25.

27. Murakoshi, K; Kano, G; Wada, Y; Yanagida, S; Miyazaki, H; Matsumoto, M; Murasawa, S. Importance of Binding States Between Photosensitizing Molecules and the TiO<sub>2</sub> Surface for Efficiency in a Dye-Sensitised Solar Cells. *Journal of Electroanalytical Chemistry* **1995**, 396, 27-34.

28. Zhang, Q-L; Du, L-C; Weng, Y-X; Wang, L; Chen, H-Y; Li, J-Q. Particle-Size-Dependent Distribution of Carboxylate Adsorption Sites on TiO<sub>2</sub> Nanoparticle Surfaces: Insights into the Surface Modification of Nanostructured Materials. *Journal of Physical Chemistry B* **2004**, 108, 15077-15083.

29. Weng, Y-X; Li, L; Liu, Y; Wang, L; Yang, G-Z. Surface-Binding Forms of Carboxylic Groups on Nanoparticulate TiO<sub>2</sub> Surface Studied by the Interface-Sensitive Transient Triplet-State Molecular Probe. *Journal of Physical Chemistry B* **2003**, 107, 4356-4363.

30. Chen, X; Burda, C. Photoelectron Spectroscopic Investigation of Nitrogen-Doped Titania Nanoparticles. *Journal of Physical Chemistry B* **2004**, 108, 15446-15449.

31. Nuesch, F; Moser, J E; V, S; Grätzel, M. Merocyanine Aggregation in Mesoporous Networks. *Journal of the American Chemical Society* **1996**, 118, 5420-5431.

32. Leclere, P; Surin, M; Viville, P; Lazzaroni, R; Kilbinger, A F M; Henze, O; Feast, W J; Cavallini, M; Biscarini, F; Schenning, A P H J; Meijer, E W. About Oligothiophene Self-Assembly: From Aggregation in Solution to Solid-State Nanostructures. *Chemistry of Materials* **2004**, 16, 4452-4466.

33. Dautel, O J; Wantz, G; Almairac, R; Flot, D; Hirsch, L; Lere-Porte, J-P; Parneix, J-P; Serein-Spirau, F; Vignau, L; Moreau, J J, E. Nanostructuring of Phenylenevinylenediimide-Bridged Silsesquioxane: From Electroluminescent Molecular J-Aggregates to Photoresponsive Polymeric H-Aggregates. *Journal of the American Chemical Society* **2006**, 128, 4892-4901.

34. Da Como, E; Loi, M A; Murgia, M; Zamboni, R; Muccini, M. J-Aggregation in  $\alpha$ -Sexithiophene Submonolayer Films on Silicon Dioxide. *Journal of the American Chemical Society* **2006**, 128, 4277-4281.
35. Garcia-Ortega, H; Bourdelande, J L; Crusats, J; El-Hachemi, Z; Ribo, J M. Excited Triplet States in Aggregates and Monomers of Water Soluble Meso-Aryl Substituted Porphyrins. *Journal of Physical Chemistry B* **2004**, 108, 4631-4639.
36. Mishra, A; Behera, R K; Behera, P K; Mishra, B K; Behera, G B. Cyanines During the 1990s: A Review. *Chemical Reviews* **2000**, 100, 1973-2011.
37. Wang, Z-S; Hara, K; Dan-Oh, Y; Kasada, C; Shinpo, A; Suga, S; Arakawa, H; Sugihara, H. Photophysical and (Photo)electrochemical Properties of a Coumarin Dye. *Journal of Physical Chemistry B* **2005**, 109, 3907-3914.
38. Sayama, K; Tsukagoshi, S; Hara, K; Ogha, Y; Shinpo, A; Abe, Y; Suga, S; Arakawa, H. Photoelectrochemical Properties of J Aggregates of Benzothiazole Merocyanine Dyes on a Nanostructured TiO<sub>2</sub> Film. *Journal of Physical Chemistry B* **2002**, 106, 1363-1371.
39. De Angelis, F; Tilocca, A; Selloni, A. Time-Dependent DFT Study of [Fe(CN)<sub>6</sub>]<sup>4-</sup> Sensitization of TiO<sub>2</sub> Nanoparticles. *Journal of the American Chemical Society* **2004**, 126, 15024-15025.
40. Wang, C; Mohny, B K; Williams, R D; Petrov, V; Hupp, J T; Walker, G C. Solvent Control of Vibronic Coupling Upon Intervalence Charge Transfer Excitation of (CN)<sub>5</sub>FeCNRu(NH<sub>3</sub>)<sub>5</sub><sup>-</sup> as Revealed by Resonance Raman and Near-Infrared Absorption Spectroscopies. *Journal of the American Chemical Society* **1998**, 120, 5848-5849.
41. Bae, E; Choi, W. Effect of the Anchoring Group (Carboxylate vs Phosphonate) in Ru-Complex-Sensitized TiO<sub>2</sub> on Hydrogen Production Under Visible Light. *Journal of Physical Chemistry B* **2006**, 110, 14792-14799.
42. Stromberg, J R; Wnuk, J D; Pinlac, R A F; Meyer, G J. Multielectron Transfer at Heme-Functionalized Nanocrystalline TiO<sub>2</sub>: Reductive Dechlorination of DDT and CCl<sub>4</sub> Forms Stable Carbene Compounds. *Nano Letters* **2006**, 6, 1284-1286.
43. Roddick-Lanzilotta, A D; McQuillan, A J. An *In Situ* Infrared Spectroscopic Study of Glutamic Acid and of Aspartic Acid Adsorbed on TiO<sub>2</sub>: Implications for the Biocompatibility of Titanium. *Journal of Colloid and Interface Science* **2000**, 227, 48-54.
44. Grätzel, M. Solar Energy Conversion by Dye-Sensitized Photovoltaic Cells. *Inorganic Chemistry* **2005**, 44, 6841-6851.
45. Zaki, M I; Hasan, M A; Al-Sagheer, F A; Pasupulety, L. *In Situ* FTIR Spectra of Pyridine Adsorbed on SiO<sub>2</sub>-Al<sub>2</sub>O<sub>3</sub>, TiO<sub>2</sub>, ZrO<sub>2</sub> and CeO<sub>2</sub>: General Considerations for the Identification of Acid Sites on Surfaces of Finely Divided Metal Oxides. *Colloids and Surfaces A: Physicochemical and Engineering Aspects* **2001**, 190, 261-274.
46. Watson, D F; Marton, A; Stux, A M; Meyer, G J. Insights into Dye-Sensitization of Planar TiO<sub>2</sub>: Evidence for Involvement of a Protonated Surface State. *Journal of Physical Chemistry B* **2003**, 107, 10971-10973.
47. Watson, D F; Marton, A; Stux, A M; Meyer, G J. Influence of Surface Protonation on the Sensitization Efficiency of Porphyrin-Derivatized TiO<sub>2</sub>. *Journal of Physical Chemistry B* **2004**, 108, 11680-11688.
48. Zaban, A; Ferrere, S; Sprague, J; Gregg, B A. pH-Dependent Redox Potential Induced in a Sensitizing Dye by Adsorption onto TiO<sub>2</sub>. *Journal of Physical Chemistry B* **1997**, 101, 55-57.
49. Shklover, V; Nazeeruddin, M-K; Zakeeruddin, S M; Barbe, C; Kay, A; Haibach, T; Steurer, W; Hermann, R; Nissen, H-U; Grätzel, M. Structure of Nanocrystalline TiO<sub>2</sub> Powders and Precursor to their

- Highly Efficient Photosensitizer. *Chemistry of Materials* **1997**, 9, 430-439.
50. Johansson, E M J; Edvinsson, T; Odelius, M; Hagberg, D P; Sun, L; Hagfeldt, A; Siegbahn, H; Rensmo, H. Electronic and Molecular Surface Structure of a Polyene-Diphenylaniline Dye Adsorbed from Solution onto Nanoporous TiO<sub>2</sub>. *Journal of Physical Chemistry C* **2007**, 111, 8580-8586.
51. Eiden-Assmann, S; Widoniak, J; Maret, G. Synthesis and Characterization of Porous and Nonporous Monodisperse Colloidal TiO<sub>2</sub> Particles. *Chemistry of Materials* **2004**, 16, 6-11.
52. Nazeeruddin, M K; Kay, A R, I; ; Humphry-Baker, R; Muller, E; Liska, P; Vlachopoulos, N; Grätzel, M. Conversion of Light to Electricity by Cis-X<sub>2</sub>Bis(2,2'-Bipyridyl-4, 4'-Dicarboxylate)Ruthenium(II) Charge-Transfer Sensitizers (X=Cl<sup>-</sup>, Br<sup>-</sup>, I<sup>-</sup>, CN<sup>-</sup>, and SCN<sup>-</sup>) on Nanocrystalline TiO<sub>2</sub> Electrodes. *Journal of the American Chemical Society* **1993**, 115, 6382-6390.
53. Mills, A; Lepre, A; Elliott, N; Bhopal, S; Parkin, I P; O'Neill, S A. Characterisation of the Photocatalyst Pilkington ActivTM: a Reference Film Photocatalyst. *Journal of Photochemistry and Photobiology A: Chemistry* **2003**, 160, 213-224.
54. Nakade, S; Saito, Y; Kubo, W; Kitamura, T; Wada, Y; Yanagida, S. Influence of TiO<sub>2</sub> Nanoparticle Size on Electron Diffusion and Recombination in Dye-Sensitized TiO<sub>2</sub> Solar Cells. *Journal of Physical Chemistry B* **2003**, 107, 8607-8611.
55. Zhang, D; Ito, S; Wada, Y; Kitamura, T; Yanagida, S. Nanocrystalline TiO<sub>2</sub> Electrodes Prepared by Water-Medium Screen Printing Technique. *Chemistry Letters* **2001**, 10, 1042-1043.
56. Berger, T; Sterrer, M; Diwald, O; Knozinger, E; Panayotov, D; Thompson, T L; Yates, J T J. Light-Induced Charge Separation in Anatase TiO<sub>2</sub> Particles. *Journal of Physical Chemistry B* **2005**, 109, 6061-6068.
57. Lee, D; Omolade, D; Cohen, R E; Rubner, M F. pH-Dependent Structure and Properties of TiO<sub>2</sub>/SiO<sub>2</sub> Nanoparticle Multilayer Thin Films. *Chemistry of Materials* **2007**, 19, 1427-1433.
58. Zhang, H; Banfield, J F. Kinetics of Crystallization and Crystal Growth of Nanocrystalline Anatase in Nanometer-Sized Amorphous Titania. *Chemistry of Materials* **2002**, 14, 4145-4154.
59. Scolan, E; Magnenet, C; Massiot, D; Sanchez, C. Surface and Bulk Characterisation of Titanium-Oxo Clusters and Nanosized Titania Particles Through <sup>17</sup>O Solid State NMR. *Journal of Materials Chemistry* **1999**, 9, 2467-2474.
60. Aylward, G; Findlay, T. *SI Chemical Data*. 3rd ed, John Wiley & Sons Inc: Queensland, Australia, **1994**.
61. Atkins, P W. *Physical Chemistry*. 5<sup>th</sup> ed, Oxford University Press: Somerset, England, **1994**.
62. Campbell, W M; Officer, D L; Jolley, K. Unpublished results from our laboratories. **2007**.
63. Rochford, J; Chu, D; Hagfeldt, A; Galoppini, E. Tetrachelate Porphyrin Chromophores for Metal Oxide Semiconductor Sensitization: Effect of the Spacer Length and Anchoring Group Position. *Journal of the American Chemical Society* **2007**, 129, 4655-4665.
64. Zhang, Z; Nakashima, K; Lal Verma, A; Yoneyama, M; Iriyama, K; Ozaki, Y. Molecular Orientation and Aggregation in Mixed Langmuir-Blodgett Films of 5-(4-N-Octadecylpyridyl)-10,15,20-tri-*p*-tolylporphyrin and Stearic Acid Studied by Ultraviolet-Visible, Fluorescence and Infrared Spectroscopies. *Langmuir* **1998**, 14, 1177-1182.
65. Ernstorfer, R; Gundlach, L; Felber, S; Storek, W; Eichberger, R; Willig, F. Role of Molecular Anchor Groups in Molecule-to-Semiconductor Electron Transfer. *Journal of Physical Chemistry B* **2006**, 110, 25383-25391.
66. Tahir, M N; Theato, P; Oberle, P; Melnyk, G; Faiss, S; Kolb, U; Janshoff, A; Stepputat, M; Tremel,

W. Facile Synthesis and Characterization of Functionalized, Monocrystalline Rutile TiO<sub>2</sub> Nanorods. *Langmuir* **2006**, *22*, 5209-5212.

67. Parala, H; Devi, A; Bhakta, R; Fischer, R A. Synthesis of Nano-Scale TiO<sub>2</sub> Particles by a Nonhydrolytic Approach. *Journal of Materials Chemistry* **2002**, *12*, 1625-1627.

68. Hagberg, D P; Edvinsson, T; Marinado, T; Boschloo, G K; Hagfeldt, A; Sun, L. A Novel Organic Chromophore for Dye-Sensitised Nanostructured Solar Cells. *Chemical Communications* **2006**, 2245-2247.

69. Sahyun, M R V; Serpone, N. Photophysics of All-*trans*-retinoic acid (ATRA) Chemisorbed to Nanoparticulate TiO<sub>2</sub>: Evidence for TiO<sub>2</sub>\* to ATRA Energy Transfer and Reverse Electron Transfer Sensitisation. *Journal of Photochemistry and Photobiology A: Chemistry* **1998**, *115*, 231-238.

70. Tan, S; Zhai, J; Fang, H; Jiu, T; Ge, J; Li, Y; Jiang, L; Zhu, D. Novel Carboxylated Oligothiophenes as Sensitisers in Photoelectric Conversion Systems. *Chemistry - A European Journal* **2005**, *11*, 6272-6276.

71. Ishibashi, T-A; Uetsuka, H; Onishi, H. An Ordered Retinoate Monolayer Prepared on Rutile TiO<sub>2</sub>(110). *Journal of Physical Chemistry B* **2004**, *108*, 17166-17170.

72. Smolenyak, P E; Peterson, R A; Dunphy, D R; Mendes, S; Nebesny, K W; O'Brian, D F; Saavedra, S S; Armstrong, N R. Formation and Spectroelectrochemical Characterisation of Multilayer and Submonolayer Thin Films of 2,3,9,10,16,17,23,24-Octa(2-benzyloxyethoxy)Phthalocyaninato Copper (CuPc(OC<sub>2</sub>OBz)). *Journal of Porphyrins and Phthalocyanines* **1999**, *3*, 620-633.

73. Gauch, E; Hoppe, H; Strahle, J. Syntheses and Structures of Di- and Trinuclear Heterometallic Complexes with Nitrido Bridges Between Rhenium and Titanium. *Journal of Organometallic Chemistry* **2000**, 593-594, 175-179.

74. Horiuchi, T; Miura, H; Uchida, S. Highly Efficient Metal-Free Organic Dyes for Dye-Sensitized Solar Cells. *Journal of Photochemistry and Photobiology A: Chemistry* **2004**, *164*, 29-32.

75. Liang, M; Xu, W; Cai, F; Chen, P; Peng, B; Chen, J; Li, Z. New Triphenylamine-Based Organic Dyes for Efficient Dye-Sensitized Solar Cells. *Journal of Physical Chemistry C* **2007**, *111*, 4465-4472.

76. Hu, J-S; Guo, Y-G; Liang, H-P; Wan, L-J; Jiang, L. Three-Dimensional Self-Organization of Supramolecular Self-Assembled Porphyrin Hollow Hexagonal Nanoprisms. *Journal of the American Chemical Society* **2005**, *127*, 17090-17095.

77. Cambridge University, *Cambridge Crystal Database, version 5.28*, November, **2006**.

78. Nyquist, R A; Kagel, R O. Infrared Spectra of Inorganic Compounds (3800 to 45 cm<sup>-1</sup>). In *Handbook of Infrared and Raman Spectra of Inorganic Compounds and Organic Salts*, Academic Press Inc.: San Diego, **1997**; Vol. 4.

79. Soler-Illia, G J d A A; Rozes, L; Boggiano, M K; Sanchez, C; Turrin, C-O; Caminade, A-M; Majoral, J-P. New Mesotextured Hybrid Materials Made From Assemblies of Dendrimers and Titanium(IV)-Oxo-Organo Clusters. *Angewandte Chemie* **2000**, *39*, 4249-4254.

80. Choudhury, N R. Template Mediated Hybrid from Dendrimer. *Journal of Sol-Gel Science and Technology* **2004**, *31*, 37-45.

81. Silverstein, R M; Bassler, G C; Morrill, T C. *Spectrometric Identification of Organic Compounds*. 5<sup>th</sup> ed, John Wiley & Sons, Inc.: **1991**.

82. Pal, S K; Bhattacharaya, S; Batabyal, S K; Pradan, T K; Ganguly, T. Role of TiO<sub>2</sub> Nanoparticles on the Photoinduced Intramolecular Electron-Transfer Reaction Within a Novel Synthesized Donor-Acceptor System. *Journal of Photochemistry and Photobiology A: Chemistry* **2007**, *189*, 86-93.

83. Kakihana, M; Tomita, K; Petrykin, V; Tada, M; Sasaki, S; Nakamura, Y. Chelating of Titanium by Lactic Acid in the Water-Soluble Diammonium Tris(2-hydroxypropionato)titanate(IV). *Inorganic Chemistry Communications* **2004**, 43, 4546-4548.
84. Taratula, O; Rochford, J; Piotrowiak, P; Galoppini, E; Carlisle, R A; Meyer, G J. Pyrene-Terminated Phenylethyne Rigid Linkers Anchored to Metal Oxide Nanoparticles. *Journal of Physical Chemistry B* **2006**, 110, 15734-15741.
85. Grätzel, M. Mesoporous Oxide Junctions and Nanostructured Solar Cells. *Current Opinion in Colloid & Interface Science* **1999**, 4, 314-321.
86. Hidaka, H; Koikie, T; Kurihara, T; Serpone, N. Dynamics and Mechanistic Features in the Photocatalysed Oxidation of Disulfonated Anionic Surfactants on the Surface of UV-Irradiated Titania Nanoparticles. *New Journal of Chemistry* **2004**, 28, 1100-1106.
87. Concellon, A; Vazquez, P; Blanco, M; Caceres, C. Molybdophosphoric Acid Adsorption on Titania from Ethanol-Water Solutions. *Journal of Colloid and Interface Science* **1998**, 204, 256-267.
88. Edwards, J C; Thiel, C Y; Benac, B; Knifton, J F. Solid-State NMR and FT-IR Investigation of 12-Tungstophosphoric Acid on TiO<sub>2</sub>. *Catalysis Letters* **1998**, 51, 77-83.
89. Fiurasek, P; Reven, L. Phosphonic and Sulfonic Acid-Functionalised Gold Nanoparticles: A Solid-State NMR Study. *Langmuir* **2007**, 23, 2857-2866.
90. Sandhyarani, N; Resmi, M R; Unnikrishnan, R; Vidyasagar, K; Ma, S; Antony, M P; Selvam, G P; Visalakshi, V; Chandrakumar, N; Pandian, K; Tao, Y-T; Pradeep, T. Monolayer-Protected Cluster Superlattices: Structural, Spectroscopic, Calorimetric, and Conductivity Studies. *Chemistry of Materials* **2000**, 12, 104-113.
91. Kohlmann, O; Steinmetz, W E; Mao, X-A; Wuelfing, P; Templeton, A C; Murray, R W; Johnson, C S J. NMR Diffusion, Relaxation, and Spectroscopic Studies of Water Soluble, Monolayer-Protected Gold Nanoclusters. *Journal of Physical Chemistry B* **2001**, 105, 8801-8809.

## 7. *CONCLUSIONS*

### 7.1. *Overview*

The work described in the different Chapters of this thesis was diverse in content, but are related through the theme of nanostructured and functionalised titania. The production of inverse opaline titania and various titania substrates in Chapters 3 and 4 were geared towards use as either Grätzel cell electrodes or surfaces for the functionalisation by probe dyes. The functionalisation of ITO glass in Chapter 5 contributed towards the self-assembly of titania nanoparticle arrays upon ITO-coated electrodes. In Chapter 6, dye adsorption upon both dry and solvated titania surfaces was studied, which gives a contribution towards understanding of the behaviour of carboxylic acid sensitiser dyes within Grätzel cells. Overall, this study includes some preliminary work necessary towards the formation and sensitisation of self-assembled nanoparticle arrays of titania upon a substrate.

### 7.2. *Key Findings*

The key findings of Chapter 3 include that titania was nanostructured in the form of inverse opals to give the ideal ‘honeycomb’, ‘basement’ layers of rings and ‘grape-like’ morphologies. Similar structures, such as ‘skeletal’ inverse opals, titania rings and hollow spheres have been reported.<sup>1-3</sup> Inverse opaline titania was tested for performance within Grätzel cells, but gave power conversion efficiencies that were on par with flat and dense titania films. The low efficiency of Grätzel cells using the inverse opals is likely to be due to the fragility, non-uniform coverage and lesser amount of titania, compared to screen-printed and nanocrystalline Dyesol electrodes. Titania inverse opals were difficult to reproduce by the technique used in this study.

In Chapter 4, a variety of nanostructured titania substrates were produced for use in dye binding studies and include screen-printed Dyesol and Degussa P25 titania, in addition to sol-gel materials. Sintered aggregated titania substrates and nanoparticulate dispersible titania was produced using methods adapted from the literature.

It was found in Chapter 5 that ITO-coated glass could be functionalised by amines and carboxylic acids, as has already been reported in the literature.<sup>4</sup> Ferrocenyl derivatives of small, aromatic molecules were used to estimate surface coverage by UV-Vis spectroscopy and gave approximate monolayer coverage. In this work, ITO glass was functionalised with the amine **5.4** to give surface coverage values comparable to that of linear alkylamines on ITO.<sup>5, 6</sup> The detection of the functionalised surface was complicated by the small quantities deposited onto ITO and the loss of adsorbed material through diffusion off the surface during spectroscopic and voltammetric measurements.

The significant findings of Chapter 6 include that dyes bound to titania *via* carboxylic and malonic acid groups show a difference in aggregation behaviour upon solvated and dry surfaces. In general, the adsorption of probe dyes on a dry sintered surface gave a blue shift of UV-Vis absorbance, while an acidic solvated amorphous surface produced a red UV-Vis shift. This indicates that solvation favours the formation of J-aggregates, where there is a 'head to tail' packing of dye. However, the difference between the two titania surfaces may be the cause of the divergent behaviour of adsorbed dye. The issue of dye binding to titania is not fully resolved, as UV-Vis and fluorescence spectroscopy were the only methods that could be successfully applied to both dry and solvated samples. ATR-FTIR spectroscopy was used on dry samples of sol-gel titania and gave evidence for the binding of probe dyes as a carboxylate species with pseudo-ester character. Solution-phase <sup>1</sup>H-NMR spectroscopy was used to demonstrate the intimate association of probe dyes solvated sol-gel titania. While signal broadening was observed, there was no significant shift in <sup>1</sup>H-NMR signals that would correspond to the formation of a carboxylate species, which indicates that probe dyes are bound in a form that resembles the free species. The evidence indicates that in a solvated environment the binding mode may be an electrostatic or pseudo-ester linkage, while after the loss of solvent carboxylate binding becomes the dominant mode.

### 7.3. Discussion

In short, the production of titania inverse opals was found to be difficult, a variety of titania substrates was produced and ITO glass was functionalised with small amines and acids. The binding of dyes *via* carboxylic acids to titania was investigated using solution-phase techniques, which was made possible through the use of dispersed sol-gel titania. The study of dye binding to dispersed sol-gel titania complements the body of work available in the literature on the binding of dyes to dry sintered titania surfaces and may be a better model for the solvated titania electrodes within working Grätzel cells. To the best of my knowledge, no other study has been published on the binding of carboxylic acids to dispersed sol-gel titania using  $^1\text{H-NMR}$  spectroscopy.

Towards application in Grätzel cells, electrodes of titania inverse opals were formed with the objective of testing a wide range of bulky dyes, including large porphyrinic arrays. Ideally, the macroporous nature of the inverse opals would have permitted large porphyrinic arrays access throughout the electrode. The use of inverse opaline titania within Grätzel cells has been previously reported, but have been tested for efficiency with only a single dye, such as the 'N719' ('Ruthenium535') ruthenium coordination compound.<sup>7, 8</sup> However, the fragile and non-uniform nature of titania inverse opals formed in this work precluded the meaningful testing of dyes for Grätzel cell efficiency. The difficulty in reproducing inverse opals of titania for use as Grätzel cell electrodes led to the investigation of self-assembled arrays of sensitised titania nanoparticles.

Work towards the self-assembly of titania nanoparticles began with the functionalisation of ITO-coated glass with small, molecular species bound *via* electrostatic interactions. In addition, the adsorption of amines and carboxylic acids to ITO by electrostatic means was studied as the functionalisation of ITO through the formation of covalent bonds<sup>9, 10</sup> and the production of layered particle assemblies using involving polyelectrolytes<sup>11-13</sup> has been documented.

Following the functionalisation of ITO glass, the next phase of the work towards self-assembled, structured and functionalised titania electrodes for Grätzel cells was to study the binding of potential linkers and sensitiser dyes to titania. The binding of probe dyes *via* carboxylic groups to titania was studied using two different surfaces: dry aggregated

crystalline titania and acidic dispersed sol-gel titania. This was done as while the electrodes used for solar cell testing are aggregated and crystalline titania, dispersed sol-gel titania may be used as a crude approximation of the solvated titania surface in a working Grätzel cell. In addition, the use of dispersed sol-gel titania permitted the use of solution-phase spectroscopy to study adsorbed dye.

The adsorption of carboxylic acid probe dyes to titania was investigated using a range of spectroscopic techniques. Through the established techniques of  $^1\text{H-NMR}$  spin-spin relaxation and diffusion experiments, the intimate binding of probe dyes to sol-gel titania was confirmed, as has been done for systems such as thiols on dispersed gold nanoparticles.<sup>14</sup> Data from UV-Vis studies of probe dyes on crystalline titania lend support for equilibrium dye binding, as reported for larger coordination compound dyes.<sup>15</sup> Differences in binding were found for dry, crystalline titania and for dispersed amorphous sol-gel titania. The UV-Vis spectra for adsorbed dyes displayed peak shifts that indicate H-aggregates of dye on dry, crystalline titania, on dispersed sol-gel titania the UV-Vis shifts correspond to the formation of J-aggregates. However, the UV-Vis shifts could be due to the difference between the two titania surfaces, rather than dye aggregation.

Results from ATR-FTIR and  $^1\text{H-NMR}$  spectroscopy of dye adsorbed on sol-gel titania indicate that the binding mode of the carboxylic acid group is dependent on the presence of solvent. ATR-FTIR studies show that in dry samples the carbonyl  $\nu(\text{C=O})$  stretch is absent or greatly reduced, which implies that carboxylate binding dominates. This is supported by the carboxylate binding of species such as mercaptosuccinic acid upon dry, crystalline titania<sup>16</sup> and of glutamic acid on a solvated, amorphous titania film.<sup>17</sup> Modelling of sodium formate on titania also supports carboxylate binding on both dry and hydrated surfaces.<sup>18</sup> In contrast, after dye adsorption onto dispersed sol-gel titania, no significant shift in line position was observed. The  $^1\text{H-NMR}$  spectra of probe dyes adsorbed to sol-gel titania display line broadening, which has been observed for the binding of carboxyalkylphosphonic acids to titania powder.<sup>19</sup> The lack of a change in  $^1\text{H-NMR}$  signal position indicates that dye is bound in a form resembling the free dye. This indicates that dye is bound through electrostatic attraction or a pseudo-ester linkage, as opposed to a carboxylate species, when in a solvated environment. Support for either electrostatic or covalent binding is given by computational studies on

the binding of formic acid on titania, which show that the favoured binding mode is by hydrogen-bonding on dry anatase or as a pseudo-ester on either a rutile or a hydrated anatase surface.<sup>18</sup> That both carboxylate and pseudo-ester binding are available modes for titania nanoparticles smaller than 6 nm has been illustrated by a study of all-*trans*-retinoic acid, though simple adsorption is deemed likely only for particles greater than 50 nm in size.<sup>20</sup>

This work makes a contribution towards the self-assembly of dye-sensitised titania nanoparticle arrays for use within Grätzel cells. For use as a substrate for titania arrays, amine and carboxylic acid species were bound to ITO glass *via* electrostatic interactions. This route for surface functionalisation proved to be difficult to reproduce, indicating that other linker species, such as covalently-bound molecules, should be investigated. The binding mode of carboxylic acid groups to titania was studied and knowledge was gained regarding differences in dye binding between dry crystalline titania and dispersed sol-gel titania. Of note is that while the adsorption of carboxyalkylphosphonic acids to titania has been investigated with <sup>13</sup>C-NMR spectroscopy,<sup>19</sup> this work appears to be the first report of solution-state <sup>1</sup>H-NMR studies on the binding of carboxylic acids to dispersed sol-gel titania. As carboxylic acid species may be used to sensitise<sup>21, 22</sup> and perhaps link titania surfaces, this work goes a small way towards the development of self-assembled, dye-sensitised, titania nanoparticle electrodes.

#### **7.4. Future Directions**

Further work is required with computer modelling to provide simulated spectra for comparison with experimental FTIR data. The use of calculated spectra would greatly aid the assignment of dye vibrational modes following adsorption upon titania surfaces.

Surface-sensitive techniques, such as UV photoelectron spectroscopy (UV-PS) and X-ray absorption near-edge spectroscopy (XANES) could be applied to examine functionalised ITO and titania surfaces. As the oxidation number for the oxygen atoms of the carboxylic acid group are not expected to change on binding to titania, X-ray photoelectron spectroscopy (XPS) would not be as useful as UV-PS, though XPS has

been used to distinguish between nitric oxide, nitrogen dioxide and nitrous oxide adsorbed on a zinc oxide surface.<sup>23</sup> UV-PS may give information on the bonding modes of adsorbed species, while XANES has been used to determine the coordination number of surface titanium atoms in sol-gel titania.<sup>20</sup>

In terms of the self-assembly of titania nanoparticle arrays using small, molecular linkers, this work indicates that the use of ITO glass functionalised *via* covalent bonds or the use of polyelectrolyte layers may give films that are more robust and easier to reproduce.

## 7.5. References

1. Dong, W; Bongard, H J; Marlow, F. New Type of Inverse Opals: Titania With Skeleton Structure. *Chemistry of Materials* **2003**, 15, 568-574.
2. Sun, F; Yu, J C; Wang, X. Construction of Size-Controllable Hierarchical Nanoporous TiO<sub>2</sub> Ring Arrays and Their Modifications. *Chemistry of Materials* **2006**, 18, 3774-3779.
3. Cheng, X; Chen, M; Wu, L; Gu, G. Novel and Facile Method for the Preparation of Monodispersed Titania Hollow Spheres. *Langmuir* **2006**, 22, 3858-3863.
4. Zotti, G; Schiavon, G; Zecchin, S; Berlin, A; Pagani, G. Adsorption of Ferrocene Compounds on Indium-Tin-Oxide Electrodes. Enhancement of Adsorption by Decomposition of Ferrocenium Molecules by Oxygen. *Langmuir* **1998**, 14, 1728-1733.
5. Vercelli, B; Zotti, G; Zecchin, S. Adsorption of Hexylferrocene Phosphonic Acid on Indium-Tin Oxide Electrodes. Evidence of Strong Interchain Interactions in Ferrocene Self-Assembled Monolayers. *Langmuir* **2003**, 19, 9351-9356.
6. Oh, S-Y; Yun, Y-J; Hyung, K-H; Han, S-H. Self-Assembled Monolayers of Diamine Molecules and Phosphomolybdic Acid on an ITO Surface. *New Journal of Chemistry* **2004**, 28, 495-501.
7. Nishimura, S; Abrams, N; Lewis, B; Halaoui, L I; Mallouk, T E; Benkstein, K D; van de Lagemaat, J; Frank, A J. Standing Wave Enhancement of Red Absorbance and Photocurrent in Dye-Sensitized Titanium Dioxide Photoelectrodes Coupled to Photonic Crystals. *Journal of the American Chemical Society* **2003**, 125, 6306-6310.
8. Huisman, C L; Schoonman, J; Goossens, A. The Application of Inverse Titania Opals in Nanostructured Solar Cells. *Solar Energy Materials & Solar Cells* **2005**, 85, 115-124.
9. Doron, A; Katz, E; Willner, I. Organization of Au Colloids as Monolayer Films onto ITO Glass Surfaces: Application of the Metal Colloid Films as Base Interfaces to Construct Redox-Active Monolayers. *Langmuir* **1996**, 11, 1313-1317.
10. Cossement, D; Plumier, F; Delhalle, J; Hevesi, L; Mekhalif, Z. Electrochemical Deposition of Polypyrrole Films on Organosilane-Modified ITO Substrates. *Synthetic Metals* **2003**, 138, 529-536.
11. Ding, B; Kim, J; Kimura, E; Shiratori, S. Layer-by-Layer Structured Films of TiO<sub>2</sub> Nanoparticles and Poly(acrylic acid) on Electrospun Nanofibres. *Nanotechnology* **2004**, 15, 913-917.
12. Sakai, N; Prasad, G K; Ebina, Y; Takada, K; Sasaki, T. Layer-by-Layer Assembled TiO<sub>2</sub> Nanoparticle/PEDOT-PSS Composite Films for Switching of Electric Conductivity in Response to Ultraviolet and Visible Light. *Chemistry of Materials* **2006**, 18, 3596-3598.
13. Liu, Z; Zhang, X; Nishimoto, S; Jin, M; Tryk, D A; Murakami, T; Fujishima, A. Anatase TiO<sub>2</sub> Nanoparticles on Rutile TiO<sub>2</sub> Nanorods: A Heterogeneous Nanostructures *via* Layer-by-Layer Assembly. *Langmuir* **2007**, 23, 10916-10919.
14. Kohlmann, O; Steinmetz, W E; Mao, X-A; Wuelfing, P; Templeton, A C; Murray, R W; Johnson, C S J. NMR Diffusion, Relaxation, and Spectroscopic Studies of Water Soluble, Monolayer-Protected Gold Nanoclusters. *Journal of Physical Chemistry B* **2001**, 105, 8801-8809.
15. Nazeeruddin, M K; Humphry-Baker, R; Liska, P; Grätzel, M. Investigation of Sensitizer Adsorption and the Influence of Protons on Current and Voltage of a Dye-Sensitized Nanocrystalline TiO<sub>2</sub> Solar Cell. *Journal of Physical Chemistry B* **2003**, 107, 8981-8987.
16. Angelome, P C; Aldabe-Bilmes, S; Calvo, M E; Crepaldi, E; Grosso, D; Sanchez, C; Soler-Illia, G J A A. Hybrid Non-Silica Mesoporous Thin Films. *New Journal of Chemistry* **2005**, 29, 59-63.

17. Roddick-Lanzilotta, A D; McQuillan, A J. An *In Situ* Infrared Spectroscopic Study of Glutamic Acid and of Aspartic Acid Adsorbed on TiO<sub>2</sub>: Implications for the Biocompatibility of Titanium. *Journal of Colloid and Interface Science* **2000**, 227, 48-54.
18. Vittadini, A; Selloni, A; Rotzinger, F P; Grätzel, M. Formic Acid Adsorption on Dry and Hydrated TiO<sub>2</sub> Anatase (110) Surfaces by DFT Calculations. *Journal of Physical Chemistry B* **2000**, 104, 1300-1306.
19. Pawsey, S; Yach, K; Reven, L. Self-Assembly of Carboxyalkylphosphonic Acids on Metal Oxide Powders. *Langmuir* **2002**, 18, 5205-5212.
20. Zhang, Q-L; Du, L-C; Weng, Y-X; Wang, L; Chen, H-Y; Li, J-Q. Particle-Size-Dependent Distribution of Carboxylate Adsorption Sites on TiO<sub>2</sub> Nanoparticle Surfaces: Insights into the Surface Modification of Nanostructured Materials. *Journal of Physical Chemistry B* **2004**, 108, 15077-15083.
21. Galoppini, E. Linkers for Anchoring Sensitizers to Semiconductor Nanoparticles. *Coordination Chemistry Reviews* **2004**, 248, 1283-1297.
22. Nazeeruddin, M K; Humphry-Baker, R; Officer, D L; Campbell, W M; Burrell, A K; Grätzel, M. Application of Metalloporphyrins in Nanocrystalline Dye-Sensitized Solar Cells for Conversion of Sunlight into Electricity. *Langmuir* **2004**, 20, 6514-6517.
23. Chen, X; Burda, C. Photoelectron Spectroscopic Investigation of Nitrogen-Doped Titania Nanoparticles. *Journal of Physical Chemistry B* **2004**, 108, 15446-15449.

## 8. SUPPLEMENTARY DATA

### 8.1. Chapter 4

**Table 8.1.** Analysis of the TiO<sub>2</sub>, water, solvent and acid content of sol-gel titania.

Batch of native sol-gel titania	060120	060606a	060711
<b>Residual Solvents:</b>	Methanol, water.	Acetonitrile, water.	Acetonitrile, water.
<b>Wt/wt % loss on sintering (ramped to 490 C, 20 min)</b>	53.9; 52.5.	52.9; 52.9.	52.6; 52.4.
<b>Wt/wt % water by Karl-Fischer titration</b>	15.7; 15.2.	12.4; 13.2.	13.4; 13.3.
<b>Wt/wt % due to residual H<sub>2</sub>O and hydrochloric acid/solvent.</b>	37 to 39	40	39

The error in sintering experiments to find the dry weight of titania from two measurements of 10 g samples with a 0.5 mg error gives an uncertainty of  $\pm 0.01\%$ . The uncertainty in Karl-Fischer measurements includes a 0.02 mg error in weighing the mass of dry samples on a 5 decimal place balance. For 10 mg samples the error is then  $\pm 0.2\%$ . As the error of Karl-Fischer titration measurements is  $\pm 0.3\%$ , a conservative estimate of uncertainty for the percent of water in sol-gel titania is then  $\pm 0.5\%$ .

### 8.2. Chapter 6

**Table 8.2.** Experimental extinction coefficients of probe dyes in tetrahydrofuran.

Dye	Experimental extinction coefficient
4-methoxybenzylidenemalonic acid (6.1)	27,000
Cinnamylidenemalonic acid (6.2)	29,800
Ter(thienylenevinylene)malonic acid (6.3)	25,900
Ter(thienylenevinylene)cynoacetic acid (6.4)	27,400
8,15-dicyanoter(thienylenevinylene)-malonic acid (6.5)	18,300
Ter(thienylenevinylene)rhodanine acetic acid (6.6)	34,300
Ter(thienyl)vinylenemalonic acid	14,900
Ter(thienyl)vinylencyanoacetic acid	20,800

**Table 8.3.** Theoretical ratios of dye to titania, using estimated surface area for non-sintered native sol-gel titania 2 nm in diameter, with a surface area of 12.57 nm<sup>2</sup> per particle and a molar mass of 10847 g mol<sup>-1</sup>.

Dye	Rectangular footprint of the dye (x 10 <sup>-19</sup> m <sup>2</sup> )	Dye molecules per TiO <sub>2</sub> particle	m(dye)/m(TiO <sub>2</sub> )
6.1	3.8 - 4.5	28 - 33	0.57 - 0.67
6.2	4.0 - 4.8	26 - 31	0.52 - 0.63
6.3	4.8 - 9.8	13 - 26	0.47 - 0.99
6.6	8.5 - 1.0	13 - 15	0.60 - 0.70

**Table 8.4.** Theoretical ratios of dye to titania, using estimated surface area for non-sintered native sol-gel titania 3 nm in diameter, with a surface area of 28.27 nm<sup>2</sup> per particle and a molar mass of 36607 g mol<sup>-1</sup>.

Dye	Rectangular footprint of the dye (x 10 <sup>-19</sup> m <sup>2</sup> )	Dye molecules per TiO <sub>2</sub> particle	m(dye)/m(TiO <sub>2</sub> )
6.1	3.8 - 4.5	63 - 74	0.38 - 0.45
6.2	4.0 - 4.8	59 - 71	0.35 - 0.42
6.3	4.8 - 9.8	29 - 59	0.31 - 0.67
6.6	8.5 - 1.0	28 - 33	0.38 - 0.45

**Table 8.5.** Theoretical ratios of dye to titania, using estimated surface area for non-sintered native sol-gel titania 4 nm in diameter, with a surface area of 50.27 nm<sup>2</sup> per particle and a molar mass of 86771 g mol<sup>-1</sup>.

Dye	Rectangular footprint of the dye (x 10 <sup>-19</sup> m <sup>2</sup> )	Dye molecules per TiO <sub>2</sub> particle	m(dye)/m(TiO <sub>2</sub> )
6.1	3.8 - 4.5	112 - 132	0.29 - 0.34
6.2	4.0 - 4.8	104 - 126	0.26 - 0.32
6.3	4.8 - 9.8	52 - 105	0.24 - 0.50
6.6	8.5 - 1.0	50 - 59	0.29 - 0.34

**Table 8.6.** The amount of dye required for monolayer coverage of sintered Dyesol titania, using the footprint areas shown in Table 8.3.

Dye	Screen-printed transparent Dyesol titania. Surface area = 82.5 m <sup>2</sup> g <sup>-1</sup>		Pre-formed opaque Dyesol titania plates. Surface area = 60.0 m <sup>2</sup> g <sup>-1</sup>	
	n(dye) / m(TiO <sub>2</sub> ) (x 10 <sup>-4</sup> mol g <sup>-1</sup> )	m(dye) / m(TiO <sub>2</sub> )	n(dye) / m(TiO <sub>2</sub> ) (x 10 <sup>-4</sup> mol g <sup>-1</sup> )	m(dye) / m(TiO <sub>2</sub> )
<b>6.1</b>	3.0 - 3.6	0.07 - 0.08	2.2 - 2.6	0.05 - 0.06
<b>6.2</b>	2.9 - 3.4	0.06 - 0.07	2.1 - 2.5	0.05 - 0.06
<b>6.3</b>	1.4 - 2.9	0.06 - 0.12	1.0 - 2.1	0.04 - 0.09
<b>6.6</b>	1.3 - 1.6	0.07 - 0.08	1.0 - 1.2	0.05 - 0.06

**Table 8.7.** The amount of dye required for monolayer coverage of sintered sol-gel titania, using the footprint areas shown in Table 8.3.

Dye	'Native' sintered sol-gel titania 187.2 m <sup>2</sup> g <sup>-1</sup>		Tape-cast sol-gel titania 37.5 m <sup>2</sup> g <sup>-1</sup>	
	n(dye) / m(TiO <sub>2</sub> ) (x 10 <sup>-4</sup> mol g <sup>-1</sup> )	m(dye) / m(TiO <sub>2</sub> )	n(dye) / m(TiO <sub>2</sub> ) (x 10 <sup>-4</sup> mol g <sup>-1</sup> )	m(dye) / m(TiO <sub>2</sub> )
<b>6.1</b>	6.9 - 8.2	0.15 - 0.18	1.4 - 1.6	0.03 - 0.04
<b>6.2</b>	6.5 - 7.8	0.14 - 0.17	1.3 - 1.6	0.03 - 0.03
<b>6.3</b>	3.2 - 6.5	0.13 - 0.27	0.6 - 1.3	0.03 - 0.05
<b>6.6</b>	3.1 - 3.7	0.16 - 0.18	0.6 - 0.7	0.03 - 0.04

**Table 8.8.** UV-Vis absorption of dyes on sintered titania.

Dye	On sintered STA paste (nm)	On sintered sol-gel (nm)
<b>6.3</b>	425	436
<b>6.4</b>	432	430
<b>6.5</b>	475	460

**Table 8.9.** If the surface area of sintered ‘native’ sol-gel titania is  $187 \text{ m}^2 \text{ g}^{-1}$ , if the footprint area of **6.1** is  $4.5 \times 10^{-19}$ , a monolayer dye loading is  $6.9 \times 10^{-4} \text{ mol g}^{-1}$ . Supposing that the sintered material was still composed of discrete spheres, then the mole ratio between dye and titania spheres is given by  $n(\text{dye}) : n(\text{TiO}_2)$ . The percentage dye loading of sintered titania over that of native sol-gel titania gives an indication of the degree of particle aggregation introduced by sintering.

Titania grain size	Dye molecules per TiO <sub>2</sub> particle	Sintered loading / Non-sintered loading (%)
2 nm spheres	7	25
3 nm spheres	25	36
4 nm spheres	60	48

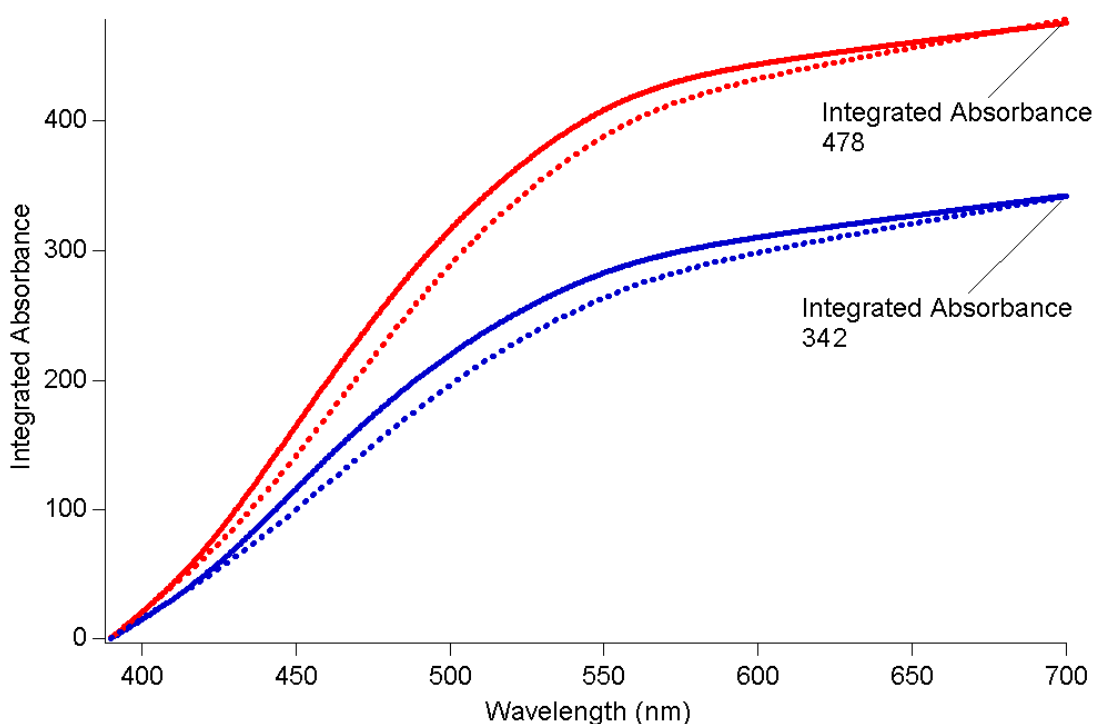


**Figure 8.1.** The integrated area of the UV-Vis absorption of sintered Dyesol titania dyed with **6.5**. The red shift in dye absorbance is due to rearrangement of dye on titania due to the loss of solvent, rather than to a decrease in the amount of dye present. The integrated region was 390 to 700 nm. Data is shown for samples immersed in a 0.2 mM solution of **6.5** in tetrahydrofuran for: a) 3 minutes, wet (—) and dried (.....); b) 6 minutes, wet (—) and dried (.....).

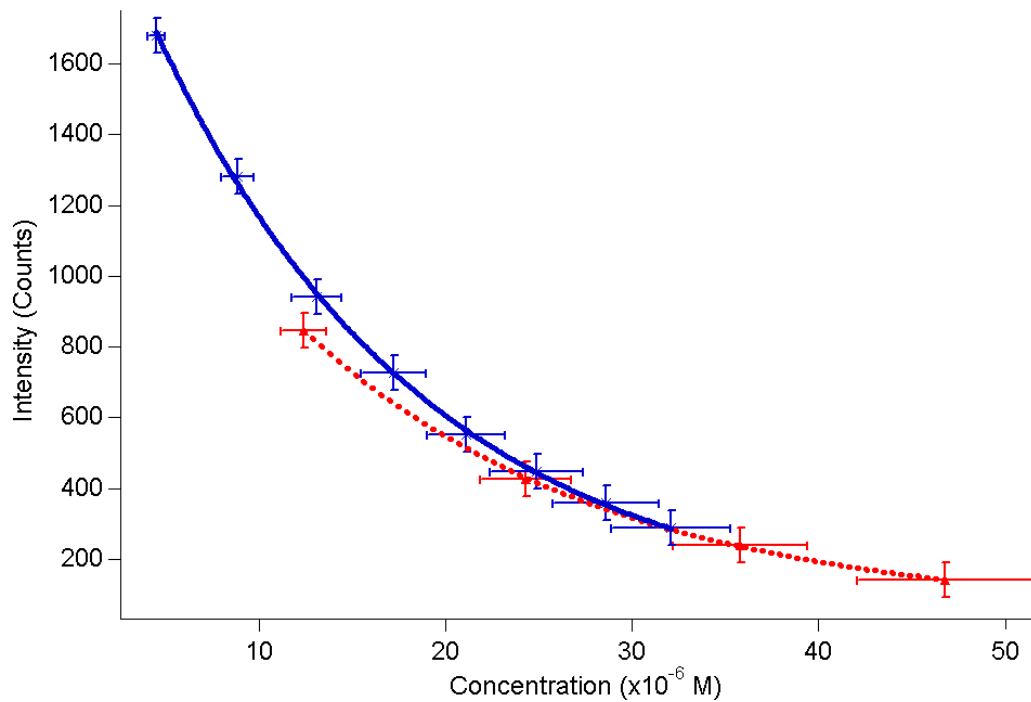


**Figure 8.2.** The fluorescence intensity of **6.4**, in methanol, normalised to absorbance. Two sets of data are displayed. The error bars are for conservative uncertainties of  $\pm 50$  counts of intensity and  $\pm 10\%$  of concentration.